NASA SP-248

HOLOGRAPHIC INSTRUMENTATION APPLICATIONS

A conference held at
AMES RESEARCH CENTER
MOFFETT FIELD, CALIFORNIA
January 13-14, 1970

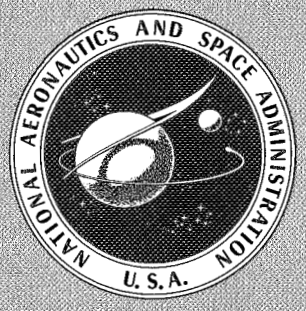

NATIONAL AERONAUTICS AND SPACE ADMINISTRATION

NASA SP–248

HOLOGRAPHIC

INSTRUMENTATION APPLICATIONS

A conference held at
Ames Research Center
Moffett Field, California
January 13-14, 1970

Edited by BORIS RAGENT
AND
RICHARD M. BROWN

Prepared by NASA Ames Research Center

Scientific and Technical Information Division
OFFICE OF TECHNOLOGY UTILIZATION 1970
NATIONAL AERONAUTICS AND SPACE ADMINISTRATION
Washington, D.C.

For sale by the Clearinghouse for Federal Scientific and Technical Information, Springfield, Virginia 22151
CFSTI price $3.00
Library of Congress Catalog Card Number 70-608767

CONTENTS

FOREWORD

The Conference on Holographic Instrumentation Applications was held on January 13 and 14, 1970, at Ames Research Center, Moffett Field, California. It was sponsored by the Measurement Sciences Branch of the Instrumentation Division. Special thanks are due to the Instrumentation and Data Processing Branch of the Office of Advanced Research and Technology, NASA Headquarters, for its approval and encouragement of this conference.

The purpose of the conference was to bring together people interested in the development of holographic instrumentation, and to provide an opportunity to discuss current trends and future possibilities. The conference was motivated by a desire to exchange information and stimulate further coordination among NASA personnel about the work being done under NASA auspices in the application of holography to problems of mutual interest. Of particular interest was the dissemination of the knowledge and techniques being developed under contract.

The conference was arranged in three consecutive sessions. The first was a general report by a representative of each of the participating centers as to its interest, direction, and effort in the development of holographic instrumentation. The second session heard reports from eight NASA contractors on their respective work. In the third session, individual NASA personnel presented detailed and specific reports on some of the topics that had been described in general terms in the earlier Center review session.

Of the 55 people attending the conference, 42 were from NASA and 10 were from NASA contractors. Representatives from most of NASA's research centers attended, indicating both a widespread interest in the subject and the importance of this type of conference in establishing lines of communication.

The work of many people went into the preparations for this conference. Richard Brown of Ames Research Center was the coordinator and responsible for all arrangements. The session chairmen, Benjamin Beam, Murray Gardner, William Gunter, and Mr. Brown, took on the burden of providing smooth operations during the sessions. Their jobs were made challenging by the ever-present dilemma facing all session chairman: when to cut off the stimulating discussions that follow the papers in order to maintain some sort of schedule.

Thanks are due to the speakers and participants for these proceedings. The presented papers were of a generally high standard, which is reflected in the written versions.

Finally, thanks are due to a number of Ames Research Center people who helped in the arrangement of the multitude of details that surround any conference. I would particularly like to extend my thanks to Sharon King for her cheerful acceptance of the extra burdens thrust upon her in preparation for the conference and in the arrangement of these proceedings.

Boris Ragent
Conference Chairman
March, 1970

INTRODUCTION

WOLFGANG MENZEL
NASA HEADQUARTERS

I would like to express my appreciation and that of the Office of Advanced Research and Technology to Dr. Mark, Mr. Dimeff, Dr. Ragent, Mr. Brown, and other members of Ames Research Center for their initiative and efforts in organizing and hosting this conference. It took a great deal of work to make all the arrangements necessary to ensure the success of this technical conference—the first of its kind in NASA.

As you know, holography, now already more than 20 years old, was only introduced to wider circles when lasers became available as laboratory tools. Since then, we have seen a fast-growing interest in holography, which has resulted in the publication of more than 800 papers. This scientific interest has been accompanied by a quest for useful applications, especially since early investigations suggested spectacular developments, for example, three-dimensional representations of still scenes, movies, and even television displays.

As a result of this interest, NASA began supporting efforts to find and develop techniques that use the unique characteristics of holography. Of specific interest to NASA was the use of holographic techniques in flow field investigations such as those conducted in wind tunnels, ballistic ranges, and other aerodynamic research facilities.

Aside from flow visualization, other applications of holography to measurement problems such as nondestructive testing, the analysis of stress and vibrational behavior of panels and structures, and the recording of small, high-speed particles are all of immediate interest to NASA.

In addition, interest in the use of holographic techniques for data storage, retrieval, and display has led us into the search for new recording media with the unique characteristics required for these applications. Developments in holographic microscopy will also undoubtedly be of great importance, for example, in improving integrated circuit inspection techniques, especially with regard to large-scale-integration reliability.

In a different area, acoustic holography has aroused increasing interest. Applications of acoustic holography are envisioned in nondestructive testing because of the propagation of sound through solids, but there may also be important medical diagnostic uses. Despite the great progress made in optical holography with the advent of the laser, there has not yet been a corresponding development in acoustic holography, although powerful coherent sound sources are readily available.

This is only a minor summary of the many approaches toward application of holographic techniques presently of interest to NASA. Undoubtedly in the following reviews and papers by NASA personnel and representatives of our contractors, we will hear about many more facets from recent work that have potential application to measurement problems.

I hope the conference will give a good picture of the state of holographic developments and applications to instrumentation problems, and that it will provide an opportunity to identify trends and recognize promising areas as a means of guiding future efforts. It is hoped that industry representatives will volunteer suggestions and opinions that will help us in defining future courses of action.

1 REVIEW OF HOLOGRAPHIC INSTRUMENTATION AT AMES RESEARCH CENTER

Boris Ragent
Ames Research Center

The interest in holography at Ames has involved investigation of its applications to measurement and data-recording problems in low-density flow visualization, vibration mapping, particle sizing, contouring, and panel flutter. In-house efforts have been concerned with the design of a holographic system utilizing active servostabilization for vibration compensation application to a noisy wind tunnel environment. A double-exposure holographic system has also been employed. Initial test results are encouraging, but inconclusive. Contracts with the University of Arkansas and TRW Systems have been employed to investigate the limitations and possible extensions of the capabilities of holography to measurement problems.

Work in holography at Ames Research Center has been directed toward evaluating the capabilities of holography for the solution of measurement problems of interest to the center and toward implementation of primary areas of application. The initial interest in this technique was for potential applications to flow-visualization problems and quantitative measurement of density and density derivatives, especially in low-density hypersonic flow test facilities. Other problem areas of interest, which have not yet received much attention, involve nondestructive testing techniques for measurements of large and small deflection contours of test members under dynamic loads, vibration measurements, panel flutter measurements, quality control, fatigue analysis, particle sizing, and precise measurement of motion (both linear and angular).

The in-house investigation of the application of holography to flow-visualization problems has been complemented and extended by work performed under a contract with TRW Systems Group of TRW, Incorporated, and a grant to the Graduate Institute of Technology of the University of Arkansas.

AMES' ACTIVITIES IN FLOW VISUALIZATION

The principal apparent advantages of holography over conventional optical techniques involve: (1) the possibility of recording three-dimensional flow field data; and (2) the lack of requirements for large, high-quality optical components. The principal limitations on this technique are: (a) the lack of sensitivity in low-density flow fields; (b) time-varying distortions introduced by gaseous boundary layers on walls, windows, etc., in the optical paths and their deleterious effects on time-averaged or multiple-exposure holography; (c) mechanical vibration effects in the test facility or its environment; (d) the amount of light required for large facilities; and (e) the required light source coherence lengths (or beam purity), especially in the case of pulsed holography.

The well-known feature of all optical measurements of gaseous flow fields—that is, the relatively small mutual interaction between visible light and most gasses—remains the most troublesome difficulty in the application of holography, as it is for more conventional techniques. For example, for a 1-cm path in air, a change in pressure of 1 atm at STP will produce an interferometric fringe shift of 4 to 5 fringes at the red wavelengths. For typical experimental situations involving large density changes in the flow fields, and hence shifts of many fringes—that is, in situations where the holographic signals are large and relatively good spatial resolution from holographic interferometry obtains—the model sizes required for testing are usually large enough that this good spatial resolution is not required. Unfortunately, however, where density changes in flow fields are small, resolution is correspondingly poor; but now model sizes are usually small and the requirements for good spatial resolution are more important. Thus, often in just those cases of the greatest practical interest, where the highest spatial resolution is required, optical techniques become more and more difficult.

For such practical cases, it is necessary to attempt to develop holographic techniques for subfringe interferometry. Several attempts to increase the sensitivity of measurements to flow field variations have been tried, for example: (1) fringe biasing, that is, the addition of external optical delay to move the entire fringe pattern to regions where changes in gaseous optical path length produce the greatest intensity changes in that portion of the fringe being investigated; (2) multiple-pass interferometry; (3) higher-order interferometry, and other techniques discussed later. None of these has yet proven to be completely applicable for routine use.

Early experiments at Ames involved interferograms made from double-exposure holograms of a free jet. A sample of this interferogram is shown in figure 1.1. A second crude feasibility type of experiment utilized a small two-dimensional nozzle to produce expanding flows of air at Mach 3.5, using convenient laboratory supplies of air exhausting to the atmosphere. A typical interferogram made from these double-exposure holograms is shown in figure 1.2. Measurements from these interferograms showed excellent correlation with theory, as shown in figure 1.3, which is a plot of calculated and experimental pressure ratios in the nozzle as a function of centerline distance from the nozzle throat. Another typical experiment in which double-exposure holograms were used to produce an interferogram involved a projectile in free flight, in this case a .22-caliber bullet fired into air at room temperature and pressure. The typical interferogram (in this case taken by the TRW Systems Group, under contract to Ames) is shown in figure 1.4.

The early experiments mentioned above were conducted using conventional CW lasers or pulsed ruby lasers. For application to more realistic flow facilities, which have associated severe environmental vibration and strong acoustic fields, it is essential to consider stabilization techniques for long-term exposures, or very short interval pulse separation (or synchronization) for multiple-exposure holography. Both of these approaches have been considered for application to a forthcoming set of tests to be performed in the Ames 8-in. tunnel facility. This test facility ($M = 2.5 - 4$) operates in a very severe vibrational environment and acoustic field, both of which have frequency components extending out to about 1000 Hz. It is believed that such a facility will provide a proof test of the effective stabilization capabilities of our holographic system. We are designing a servo-stabilized, optical path length controlled system for use with a CW laser capable of stabilization at

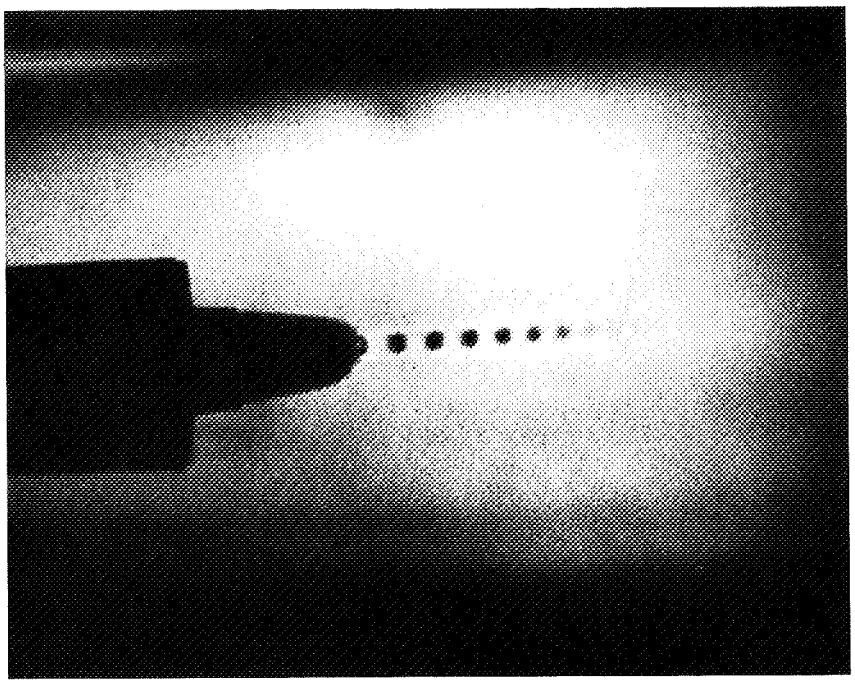

Figure 1.1 Interferogram of a free jet

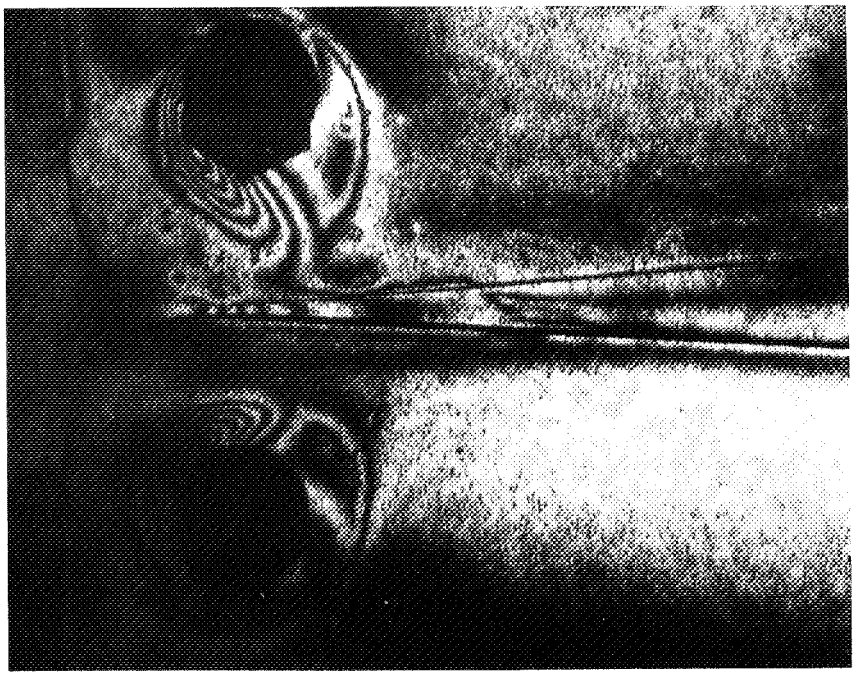

Figure 1.2 Interferogram of two-dimensional nozzle

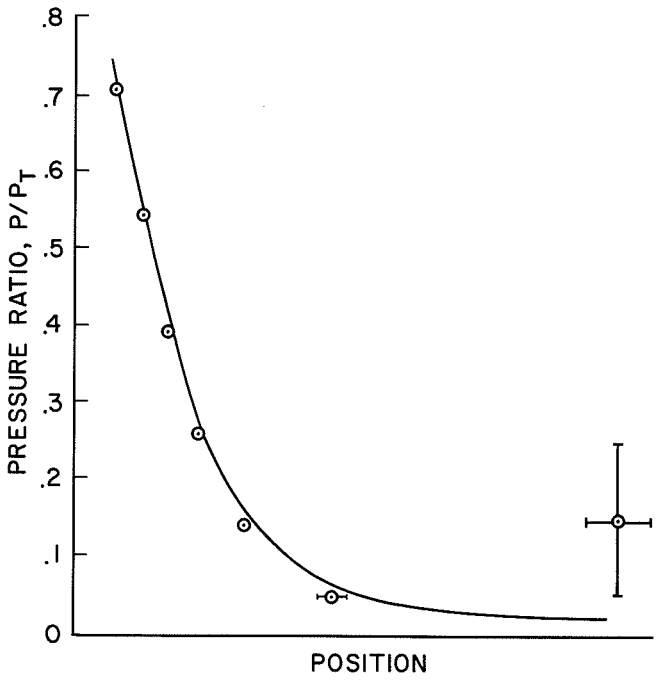

Figure 1.3 Plot of calculated and experimental pressure ratios for the nozzle in Fig. 1.2

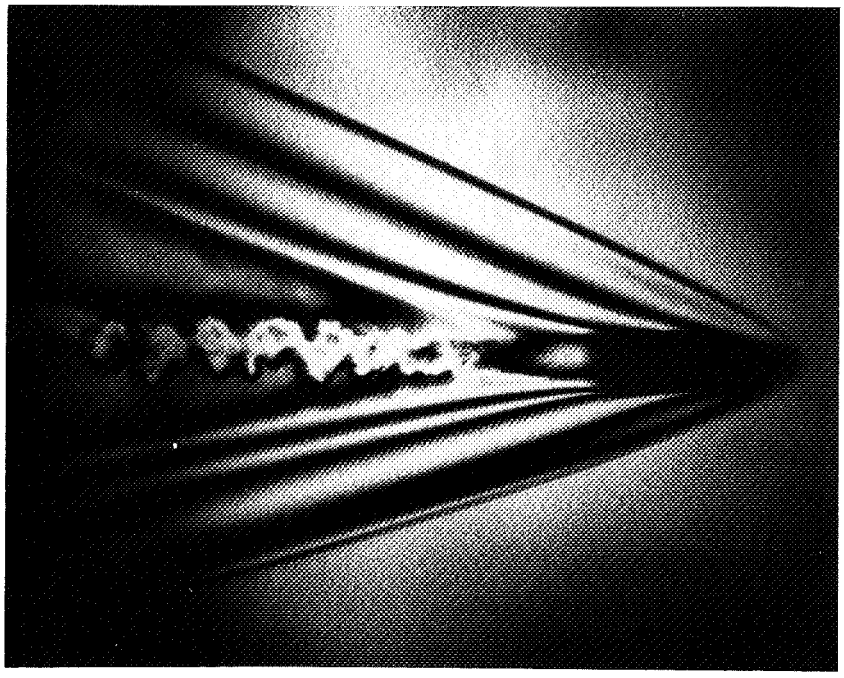

Figure 1.4 A .22-caliber bullet fired into air at room temperature (double exposure interferogram)

all frequencies of interest. The details of this system are discussed in detail in sections 17 and 19. This system is fairly standard except for the continuously adjustable beamsplitter and the fringe sampling and servostabilization device employed. Fringe stabilization to a small fraction of one fringe has been achieved experimentally in a bench-type setup out to frequencies of 500 Hz. Vibration isolation for the holographic system is afforded by the use of a massive structural steel support and independent suspension of this support.

ACTIVITIES OF CONTRACTORS

Ames' activities in holographic instrumentation have been strongly augmented by contracts with two groups outside of the center, the Graduate Institute of Technology of the University of Arkansas and TRW Systems Group. Both groups have been actively investigating many fields of holographic instrumentation; only a few of the highlights of their activities and their implications are discussed here.

The University of Arkansas

Some of the topics of interest considered, or under consideration, by this group, are listed below. Of course, in these activities and in those of the TRW Systems Group, as in all research type activities, not every investigation provided fruitful results.

1. Double reference beam holography
2. Investigations of recording media
   a. Film grain noise
   b. Unconventional image storage and processing
      (1) New photo-recording techniques
      (2) New processing techniques for silver halide emulsions
3. Subfringe enhancement techniques
4. Assorted topics
   a. Acoustic holography
   b. Analog transmission of holographic data
   c. Hologram aperture utilization

A very important and interesting development by Dr. G. J. Ballard, University of Arkansas, involved the use of separate reference beams for each of the two exposures in a double-exposure hologram intended to be used for interferometry (ref. 1). This technique allows for separation of the reconstructed scenes from each exposure, as well as for greater flexibility in the reconstructed interferogram presentation. Zero-order or finite fringe interferograms may be produced by varying the angle between the reconstructing beams, and the introduction of phase shifts into one of the reconstructing beams allows the fringes to be optimally displayed, especially for subfringe interferometry. Since each scene may be reconstructed independently, schlieren photographs may be made.

Another important set of investigations concerns the recording medium, the photographic plate. Consideration has been given, for example, to high-resolution, non-silver halide processes and various matrices, other than gelatin, for holding the photosensitive materials. The size and irregularity of the developed and background grains, inhomogeneities in the thickness of regions near developed grains, and large "macromolecules" in the gelatin cause scattering, phase errors, additional

noise, and degradation of the reconstructed images. Unfortunately, to date at least, none of the numerous candidate substitutes possesses the necessary sensitivity, resolution, and stability to qualify for holographic applications. Extensive measurements of the noise introduced by various photographic recording media have been compared with techniques of unconventional image storage and processing. For example, commercial color recording films have been tested as candidates for suitable phase hologram media, as have also new bleaching and "wash-off" relief methods of preparing photographic plates for "phase" holography.

Phase holography using holograms made by "bleaching" of the silver grains and wash-off relief processes increases the brightness of the reconstructed scene or the interferogram derived from multiple exposures. The brightness characteristics of such holograms have been studied as a function of the recording medium and the bleaching and wash-off relief process used. The brightness of the reconstruction is also affected by the recorded spatial frequency and the exposure received. All these variables interact in achieving a given holographic result. For example, effective emulsion speed may be increased for short exposures by using a treatment involving commercial laundry bleaches.

Subfringe interferometry is also a subject of great concern because of the interest in low-density flow measurements. With further development, the separate reference beam double-exposure technique discussed earlier is capable of resolving up to 1/60 of a fringe in environments that are not excessively noisy. A very clever device for improving the sensitivity of measurement to at least 1/300 of a fringe is described in Section 10.

A number of other topics have also been considered by the Arkansas group, including the simulation of transmission losses in relaying holograms from one location to another using communication links, and acoustical holography.

The TRW System Group

The group at TRW Systems has been very active in a number of areas. Some of the topics investigated in the past and under continuing investigation are listed below.

1. Improvements in holographic quality
2. Low-density chamber tests
3. Increases in interferometric sensitivity
   a. Ultraviolet interferometry
   b. High-order and multiple-pass interferometry
   c. Four-beam interferometry
4. Double-exposure schlieren system
5. Single pulse—double frequency ranging and contour studies
6. Assorted topics
   a. Comparison of holographic and conventional photography
   b. Gas cell phase shifters
   c. Location of finite fringes on test subject
   d. Studies of pulsed laser single-wavelength operation

A number of continuing small improvements in holographic technique have resulted in much improved picture quality. These include painting of back sides of hologram plates before exposure with flat black paint to prevent reflection from rear surfaces, obtaining better uniformity of scene lighting by paying more attention to diffusing techniques, improving coherence of lasers, and using better path-matching techniques to achieve higher brightness and contrast.

A technique attempted for measuring the subfringe interference patterns caused by very small phase disturbances used a gas cell phase shifter to produce a half-wavelength shift between successive double exposures. This should result in a dark field background for the reconstructed interferogram, except where small phase variations occur. Unfortunately, in a nonlaboratory environment it is extremely difficult to obtain complete cancellation due to ambient vibration levels, air currents, or other environmental perturbations.

One simple way of increasing the sensitivity of systems to small phase changes is to produce a greater number of fringes for a given phase change. This can be done by reducing the wavelength of the incident light used for holography, say, to ultraviolet wavelengths. The TRW group demonstrated the feasibility of this technique by means of second harmonic generation in a KDP crystal irradiated with red light for a Q-switched ruby laser. The output power was low but sufficient to demonstrate feasibility, and this technique may have some application for the future.

A most important series of experiments involved investigation of high-order and multiple-pass interferometry to increase sensitivity to small phase changes. Thus far, increased sensitivities by about a factor of 4 have resulted from higher-order interferometry. Multipass interferometry has many difficulties associated with wind tunnel application, chiefly involving the multiple passes through window boundary layers, but may find application to situations involving other types of test facilities, for example, ballistic ranges where each pass increases the sensitivity of the measurement. Of course, practical limitations occur due to resolution degrading effects, and some of these were investigated in the study. System aberrations limited the practical number of passes to about 10 in one experiment.

The accidental discovery of contour fringes in a single pulse hologram was attributed to the fact that the output of a typical pulsed laser used in holographic work often contained at least two wavelengths. This effect has now been investigated in some detail and has led to a technique for producing accurate contour measurements on irregular surfaces.

Comparisons of the light needed for producing a hologram of a scene and the amount of light necessary to produce a conventional photograph have shown that over distances of the order of a meter, the recording of a scene by holographic techniques is more economical (in light required) than conventional techniques.

Finally, another attempt to view very small phase shifts involves a new method that uses a "four-beam" interferometer and shows some promise of being capable of evolution into a device capable of self-alined subfringe interferometry (see Section 7).

REFERENCE

1. Ballard, G. J.: Double-Exposure Holographic Interferometry with Separate Reference Beams. J. Appl. Phys., vol. 39, Sept. 1968, p. 4846.

2 HOLOGRAPHY IN THE TEST AND EVALUATION DIVISION AT GODDARD SPACE FLIGHT CENTER

Michael W. Michalak
Goddard Space Flight Center

The Test and Evaluation (T & E) Division at GSFC has been involved in holography for a little over a year. Initial research efforts have been directed toward applying holography to thermal distortion analysis. These efforts have led to studies involving real-time and double-exposure holography, effects of vacuum on recording materials, contamination possibilities, and feasibility of multiple exposures. Real-time and double-exposure capabilities have been demonstrated. Tests indicate that vacuum (10^{-6} torr) has little or no effect on holographic image quality and that contamination due to plate outgassing is not significant. Research is being carried out to determine optimum parameters for multiple-exposure holography. Up to ten images have been recorded on a single plate.

Future application projects include vibration testing, three-dimensional data display, and optical processing of certain types of data.

The T&E Division of the Systems Reliability Directorate, Goddard Space Flight Center, has the mission of testing and evaluating the performance of unmanned spacecraft and their subsystems in simulated launch and space environments. Holography is being investigated as a new technique for application to testing by the division's Instrumentation Section.

In mid-1968, a task was established to investigate holography as a means of measuring small displacements in thermal and vacuum environments. Since that time, we have been formulating the techniques necessary, determining the materials needed, and gaining experience in the field. These efforts have been divided into two related areas: holography and holographic interferometry. We have been investigating two different types of holograms: transmission and white-light Bragg-Lippmann reflection types. We have also looked into three different types of recording media and tried some bleaching. At the present time, we are experimenting with density storage to use our plates to their fullest advantage. We have studied both real-time and double-exposure holographic interferometry. Now that a certain amount of experience has been gained, the conclusions drawn from these studies will point the way to more detailed research, eventually leading to the design and fabrication of an operational distortion-measurement system.

At first, we started making holograms on a laboratory bench using rather crude apparatus. New equipment and a granite slab soon put transmission holograms on a scientific rather than an artistic basis. An interesting technique also tried was local reference-beam holography, first described by Caulfield at Texas Instruments (ref. 1). This method utilizes the object itself as the reference beam. Illumination from the object is broken up into two parts. One part goes directly to the plate; the second part is focused to a very small image and used as a "point source" reference. We focused the object to about a 3.5-mm image and obtained a hologram. The holographic image was barely visible and noise was extremely high, but the technique may be worth investigating in more detail. Local reference-beam holography indicated the possibility of developing a holographic box camera, which would be most useful in an operational system.

Reflection holograms of the Bragg-Lippman type were tried, using both Kodak 649F and Agfa Gevaert 10E70 plates. The Kodak emulsions were about 16 μ thick as compared with 6 μ for Agfa The Agfa plates were unproductive, probably because of insufficient emulsion thickness. Fairly good results were obtained from the Kodak plates. Resolution was poor, since the reconstruction source was about 3 mm in diameter. This type of hologram would be useful for dissemination of holographic data where no coherent source is available for reconstruction.

The photographic fog on holographic plates is often detrimental to subsequent analysis of holographic images. Bleaching appears capable of reducing or eliminating this problem. A bleach using a 5 percent solution of mercuric chloride was tried, which reduces, but does not eliminate, the fog. The image brightness was found to be definitely improved, but other bleaches such as potassium ferrocyanide are reputed to be better. Further investigation into bleaching and phase holograms is expected to determine the optimum experimental parameters necessary to take full advantage of this technique.

There are many types of recording media available to the holographic engineer. Among these are silver halide emulsions, photochromics, and thermoplastics. These media were surveyed to determine whether or not a material other than silver halide emulsions would be practical in an operational holographic system. Thermoplastics may be written on by placing a set of static charges on the surface of the material. When the material is heated, deformations develop due to the forces exerted by the charges. Because of the complications involved in setting up the associated electronics, this medium was discarded as an alternative to silver halide emulsions.

Samples of several types of photochromics were obtained from American Cyanamid and Corning Glass. The samples were on squares of plastic film and in glass plates. They were activated by ultraviolet light and written on by bleaching with a laser beam. The activation time was about 15 min or more, and the bleaching time was between 5 and 10 min, depending on the strength of the bleaching source. Because of the long preparation and exposure time, this material was also discarded. Since this study, other materials, in single crystal form, have been shown to produce better results than the photochromics with which we experimented; notable examples are lithium niobate and barium sodium niobate. Also, researchers in England report exposure times of 1 to 6 min, using an argon laser and sensitized lead iodide layers evaporated onto a glass substrate (ref. 2). It seems only a matter of time before photochromic technology becomes competitive with silver halide emulsions in some types of holography.

There are several acceptable emulsions on the market today, but the two in common use at the time of this study were Kodak 649F and Agfa Gevaert 10E70. These films are comparable in resolution but the 10E70 is considerably faster than the Kodak film. Except for the Bragg-Lippmann type of holograms, for which the thicker 649F is best, we have used Agfa film almost exclusively.

The next problem was that of vacuum operation. Would prolonged exposure to hard vacuum (10^{-6}, 10^{-7} torr) cause film resolution to deteriorate enough to make holography difficult or impossible? Also, would material outgassing contaminate spacecraft components, in particular, optical components? Holograms were taken in a vacuum chamber at Goddard at ambient pressure, after a

48-hr soak at 10^{-6} torr, and again at ambient pressure. There was no noticeable difference among the three images, indicating that pressure is no barrier to high film resolution. To estimate contamination danger, an unexposed plate was subjected to 10^{-6} torr for 10 hr facing a magnesium fluoride-coated mirror. Ultraviolet reflectance measurements before and after pumpdown showed no measurable contamination of the mirror. These results confirmed that photographic plates could be used safely for holography at low pressures. As further proof, we made mass spectrometer runs of antihalation backed plates at 10^{-6} torr. There was no discernible difference in runs made with the chamber empty and with the plate in the chamber. Thus, we concluded that a holographic system can operate in a vacuum environment.

When planning a holographic system, the designer is often hindered by the necessity of removing a photographic plate after every exposure. The recording of more than one hologram per plate greatly reduces this problem, thus increasing the efficiency and flexibility of the system. Experimentation has led to the recording of ten holograms on a single plate. A rotation of the plate by 20° between exposures was used to spatially multiplex the images. To provide increased storage capability, both the front and back of the plate were used. Further research is being carried out to determine image quality as a function of plate angle and hologram density.

The second phase of our research in holography is to investigate specific techniques in holographic interferometry, namely, real-time and/or double-exposure methods. Work in real-time interferometry has been a feasibility study. Holograms of an object were recorded, processed, and replaced. It was found that by using our own plate holders, without micrometer adjustments, we could replace the plate to within five or ten fringes of exact superposition. A portable display unit then was constructed for a demonstration in which the hologram was recorded and replaced in one building. Then the setup was moved to another building, and the laser was realigned to produce the same set of fringes. Thus, a real-time holographic interferometry setup was shown to be experimentally feasible.

The second technique studied was double-exposure holography in which an image of the distorted object is superimposed on an image of the undistorted object. For analysis, this method appears superior to the real-time method. In most cases, the object distorts continuously, and measurements in the real-time method therefore are difficult to obtain. Furthermore, the analysis derived by Haines and Hildebrand makes use of the third dimension available to holographers to measure the distance from the object to the fringes; a two-dimensional picture of the real-time data would be ineffective in determining this parameter. A three-dimensional double-exposure sequence would have the advantage of retaining three-dimensionality in a form amenable to analysis.

For the future, we look to a more detailed investigation along the avenues generated by our previous studies. We will be doing research in holocameras, making use of local reference-beam holography or perhaps optical delay lines. Until photochromics are perfected, we will be using photographic emulsions and trying to take full advantage of density storage. We will be experimenting with bleaches to provide the best possible images for analysis and doing theoretical analysis of holographic interferometry as a basis for designing, building, and testing an effective instrument for measuring small distortions.

REFERENCES

1. Caulfield, H. J.: Information Retrieval From Local Reference Beam Holograms. Phys. Ltrs., vol. 27A, No. 5, July 15, 1968, pp. 319–320.
2. University of Warwick, Brit. J. Appl. Phys., Series 2, pp. 197–200, Feb. 1969.

3 REVIEW OF HOLOGRAPHIC INSTRUMENTATION AT JET PROPULSION LABORATORY

Robert V. Powell
Jet Propulsion Laboratory

JPL is investigating nondestructive testing techniques utilizing optical, acoustic, and microwave holography. Spray-particulate distribution measurements are being made to study the combustion process in liquid rocket engines. Measurement techniques are also being developed to study heat transfer in arc lamps.

JPL is developing holographic instrumentation techniques to measure mechanical vibrations and deformations of structures as a means of flaw detection. In the field of chemical propulsion, JPL is investigating nondestructive testing techniques utilizing optical, acoustic, and microwave holography to determine the void distribution in solid propellants. In the area of liquid propulsion, spray-particulate distribution measurements are being made to study the combustion process in liquid rocket engines. Measurement techniques are also being developed to study heat transfer to the anode of a high-powered xenon compact arc lamp. Most of these on-going activities are reported by their respective investigators in later sections.

Future plans for holographic instrumentation at JPL include optical processing of video imaging data and the development of spacecraft memories utilizing holographic techniques.

A comprehensive review, "Optics at the Jet Propulsion Laboratory," appeared in the special "Optics in NASA-1" issue of *Applied Optics*.

CURRENT HOLOGRAPHIC ACTIVITIES

As a first impression, the work at the separate centers appears to be highly redundant, considered from the holographic point of view. However, the work being reported is the result of the application of holographic techniques to many disciplines. From the applications point of view, there is considerably less evidence of redundancy. Funding for these activities, at least at JPL, has come largely from the discipline area where the holographic techniques are being applied. Certainly consideration should be given to this applications orientation in any effort to consolidate a holographic program within NASA.

Current JPL activities in holography may be summarized as follows:

1. Flaw detection in structures
2. Nondestructive testing of solid chemical propellants
3. Combustion studies in liquid propellants
4. Heat transfer studies in xenon arc lamps

To pursue the development of vibration analysis and flaw-detection techniques, a laboratory has been equipped and staffed, and the work is now in an exploratory phase. Some important applications of flaw-detection techniques under consideration are the inspection of solid propulsion system components, microcircuits, and structures.

Figure 3.1 shows an application of dual-exposure holography to nondestructive testing of a model of a solid propellant segment. Briefly, two exposures are made on the same film changing the stress (i.e., temperature or pressure between exposures). The interference bands then indicate the relative displacement in wavelengths resulting from the stress change. This observed displacement must then be compared to an expected normal displacement to complete the flaw detection.

Holography in propellant stress analysis is carried on in-house and out-of-house by contract. The work is oriented toward exploitation of the technique in nondestructive testing. Work is under way on two contracts, whose immediate objective is a feasibility demonstration of two dissimilar techniques, both based on holography. The first contract is with TRW Systems, Inc., to develop an acoustic-optical imaging technique suitable for the inspection of dielectric, highly attentuating materials such as solid propellants. In brief, the technique is similar to acoustical holography in that an image is constructed by using coherent light to process the information in an acoustic signal that has sampled a test specimen. It differs from holography in that the acoustic wavefronts contain only amplitude information and are projected from the first optical sideband of the laser beam as a two-dimensional image.

The second contract is with Electro-Physics Corporation, Folsom, California, for the development of a microwave holographic technique to inspect the same materials mentioned previously. This technique is true holography in that the hologram it produces contains both amplitude and phase information from the sampling signal. The microwave work is treated in greater detail in Section 12.

To ensure a high level of confidence in the reliability of the structural integrity of development as well as flight solid propellant motors, present motor modeling programs at JPL depend heavily on the use of photoelasticity. The extension of holography to photoelasticity has interesting applications, which we propose to investigate in-house. In the field of stress-freezing, it is believed that the use of holography will permit the analysis of the photoelastic pattern without physically slicing or destroying the model. This can be done by gating the focal plane to varying depths through the model and constructing a hologram that can be reconstructed for each gated position.

Figure 3.2 illustrates a unique two-beam pulsed ruby laser holocamera developed by the TRW Systems group under contract to JPL. The exciting thing about this development is that successful holograms of reacting sprays in an operating liquid propellant rocket engine can be made. Some obvious problems in the successful execution of such a design derive from the vibration, thermal, and corrosive environment encountered in typical rocket test stand operations. In figure 3.2 the laser is housed in the upper tube. The reference beam and scene beam derived from the laser beam by the beamsplitter and optics in the black box on the left travel through the smaller center tube and the cone-shaped section, respectively. The hologram is formed in the black box on the right.

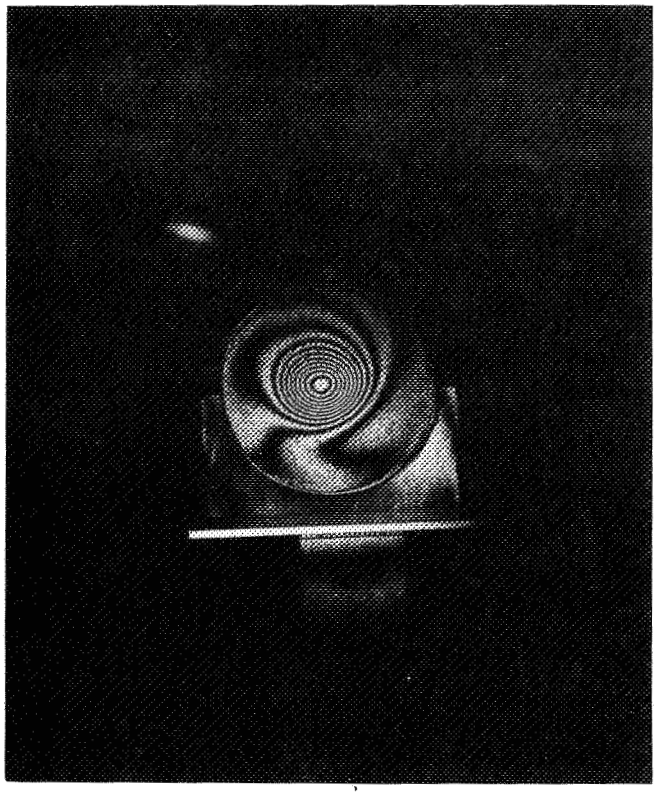

Figure 3.1 Double exposure holographic interferogram of a model of solid propellant under pressure stress

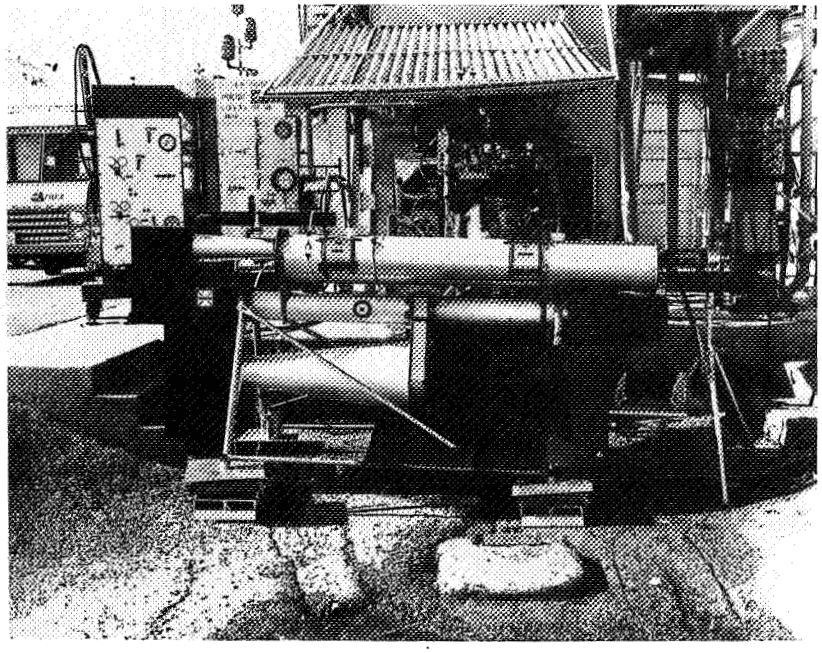

Figure 3.2 Ruby laser holocamera for rocket combustion studies

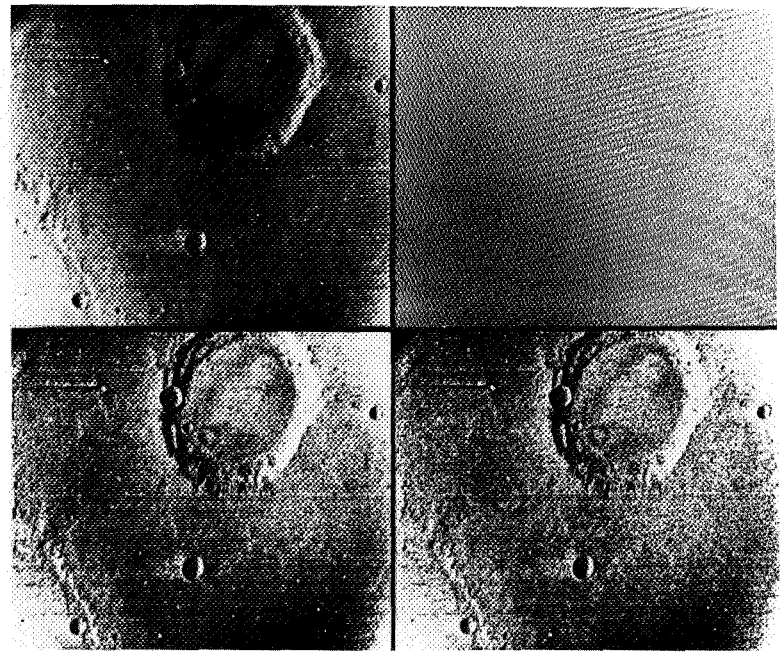

Figure 3.3 Computer-processed Mariner VI photographs; (a) photograph as received, (b) electronic noise to be removed, (c) scene with noise removed, (d) scene with high-frequency components emphasized

The camera mounted on the right permits laser photography for comparison purposes. More will be said about this unique holocamera design in Section 11.

I do not have an illustration of the heat transfer studies; however, you will find illustrations as well as a more detailed coverage of the subject in Section 18. Briefly, flash holograms of the hot gas paths around the outside surface of the anode will indicate which anode shapes are preferable in terms of turbulent flow in developmental arc lamps.

FUTURE HOLOGRAPHIC ACTIVITIES

In addition to an appropriate continuation of the efforts described, JPL would like to initiate an active development program in optical data processing using the coherent light techniques common to holography. Figure 3.3 illustrates some results of our present digital image-processing techniques as applied to Mariner VI. The upper left picture is that of the unprocessed picture data as received from Mars. The upper right picture is a map of the electronic noise in that picture as determined by Fourier transform techniques. The lower left picture is the result of subtracting the noise mask from the unprocessed picture. The improvement in the lower right picture over the noise-free picture, is largely the result of high frequency enhancement. Processing time may run as high as an hour per 600- by 600-element picture. If we are to handle the expected high volume of pictures anticipated from future planetary missions, some method (e.g., optical processing) must be developed to permit the required high processing rates.

JPL also is very interested in the possible application of holographic recording techniques to a memory with graceful degradation characteristics. Such a memory would have an important application to the 10- to 15-year outer planet missions.

4 REVIEW OF HOLOGRAPHIC INSTRUMENTATION AT MARSHALL SPACE FLIGHT CENTER

John R. Williams
NASA Marshall Space Flight Center

Investigations by this center into various areas of holographic technology include both basic and applied research. The areas presently under investigation are: (1) hypervelocity holography; (2) holographic nondestructive testing of honeycomb, epoxy joints, metal welds, etc.; (3) holographic stress analysis of solder joints and printed circuit boards; (4) lifetime predictions of materials under cyclic loads by optical correlation; (5) velocity and size distributions of particle fields; (6) holographic analysis of contaminate deposits on optical surfaces; and (7) testing of large optics by holographic interferometry.

A review of both past and planned future work is presented, as well as the on-going projects. Personnel, lab space, and equipment are briefly discussed.

Work in holography at Marshall Space Flight Center is primarily applied research combined with the basic investigations necessary to completely understand and analyze the specific application. The group conducting this research is in the Optical Physics Branch of the Space Sciences Laboratory (SSL). This group consists of three full-time professional people, one part-time professor, one technician, and seven co-op students. At present we have almost 3000 sq ft of laboratory space containing approximately $350,000 in equipment entirely devoted to various investigations in the field of holography and Fourier optics. Areas under investigation include hypervelocity holography, holographic nondestructive testing, holographic stress analysis, lifetime predictions of materials by optical correlation, particle field studies, holographic analysis of contaminate deposits, and testing large optics by holographic interferometry. In addition, this work has been complemented by work performed under contracts with GCO, Inc., and the University of Tennessee Space Institute. Some other areas of interest in which work is being initiated are image deconvolution, computer-generated holography, long-range large-object holography, quantitative analysis of holographic interferometry by computer, and holographic analysis of integrated circuits.

HYPERVELOCITY HOLOGRAPHY

MSFC's first funded effort in this area was concerned with producing high-quality holograms of projectiles traveling at hypervelocities. This effort is being conducted in conjunction with the Astrophysics Branch of SSL. The effects of impacting hypervelocity particles, namely meteors, are simulated by accelerating various-sized projectiles at known hypervelocities and studying the impact phenomena. By making holograms of the projectile, and thus adding the third dimension, a more meaningful description of the projectile integrity can be acquired. Also, by making a hologram at the instant of impact one can then measure the debris created and determine the projectile/target fragmentation.

The system used in the early stages of this effort was composed of a high-power pulsed ruby laser, a helium-neon laser for alinement, and a small light-gas gun. Figure 4.1 is a photograph of the ruby laser. The oscillator/amplifier head is shown on a granite slab with the control console off to the left. This laser originally produced a 50 nsec pulse with 750 MW of power and a coherence length of about 3 cm. Placing an aperture in the cavity and selecting a portion of the rod extended the coherence length to at least 3 ft, which was adequate for the first shots. Figure 4.2 is a photograph showing the light-gas gun used. This gun has a velocity capability of about 7 km/sec. Figure 4.3 is a photograph of the helium-neon laser used for alinement purposes. As can be seen in this photograph, the optical system used was an off-axis one, instead of an in-line configuration; even though the first holograms were backlit, new techniques being investigated in this lab indicate that frontlit holograms of hypervelocity projectiles are feasible. Figure 4.4 is a photograph of a holographic image of a hypervelocity projectile. Some details on this project were reported in the February issue of *Applied Optics*.

HOLOGRAPHIC NONDESTRUCTIVE TESTING

Holography promises to be an extremely useful technique in the area of nondestructive testing. Since holography allows us to compare two different wave fronts at two different instants in time, we can determine the effects of various loads on a particular subject. Both real-time and multiple-exposure holography are being used in this project, but for simplicity in photographing the results only multiple-exposure holograms are used in this paper. Figures 4.5 through 4.7 are examples. Figure 4.5 is a photograph of an image from a double-exposure hologram of an epoxy joint sample. The sample is the small metal strip shown C clamped to a larger steel block. There is a vertical epoxy weld just inside each C clamp. The one on the right is visible, while the one on the left, sandwiched between the metal strips, is not visible. It can be detected, however, by the irregular fringe pattern just to the right of the left C clamp. This type of fringe pattern is being used to determine the integrity of the joint. This type of joint is much more apparent in figure 4.6, also a double-exposure hologram. In both figures, the load applied was a 1° C heat change. Figure 4.7 is a double-exposure hologram of a honeycomb sample. Here again the load was a 1° C heat change. An improper bond can be seen by noting the irregular fringe pattern in the cross-markings. Even though this bond area is not void of cementing material it does indicate a nonuniformity between the skin and the honeycomb. This topic is presented in more detail in Section 14.

HOLOGRAPHIC STRESS ANALYSIS

With both manned and unmanned spaceflights increasing in complexity and duration, it is necessary that the components have longer and longer lifetimes. One problem that NASA has experienced along these lines is the failure of printed circuit boards. Since the individual solder joints are so small, they do not lend themselves to standard stress analysis. Therefore, one cannot measure or determine the stress introduced in the joint as it goes through the required number of thermal cycles. The printed circuit board may be inspected with a microscope, but since cracks develop from the inside and proceed outward to the surface of the board, only a go/no-go decision can be made. No information is obtained that would aid in determining the lifetime of the solder joint and thus the board's expected lifetime. Efforts are being made at MSFC to measure the stress in the solder joints by holographic interferometry. By using double-exposure holography with temperature as the load, one obtains an interferogram where the fringe spacing is indicative of the

Figure 4.1 Pulsed ruby laser system

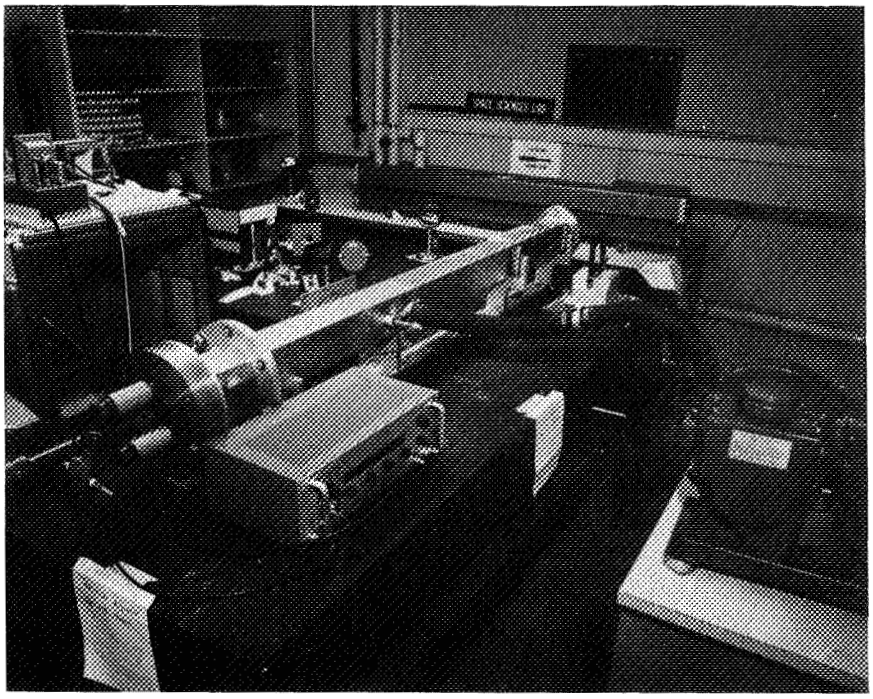

Figure 4.2 Light-gas gun

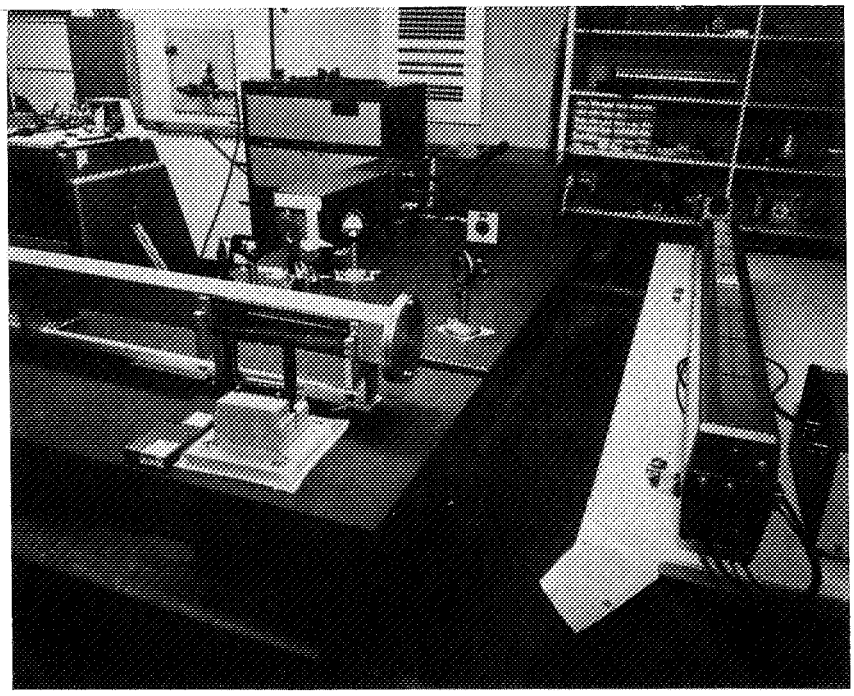

Figure 4.3 Helium-neon alinèment laser and optical configuration

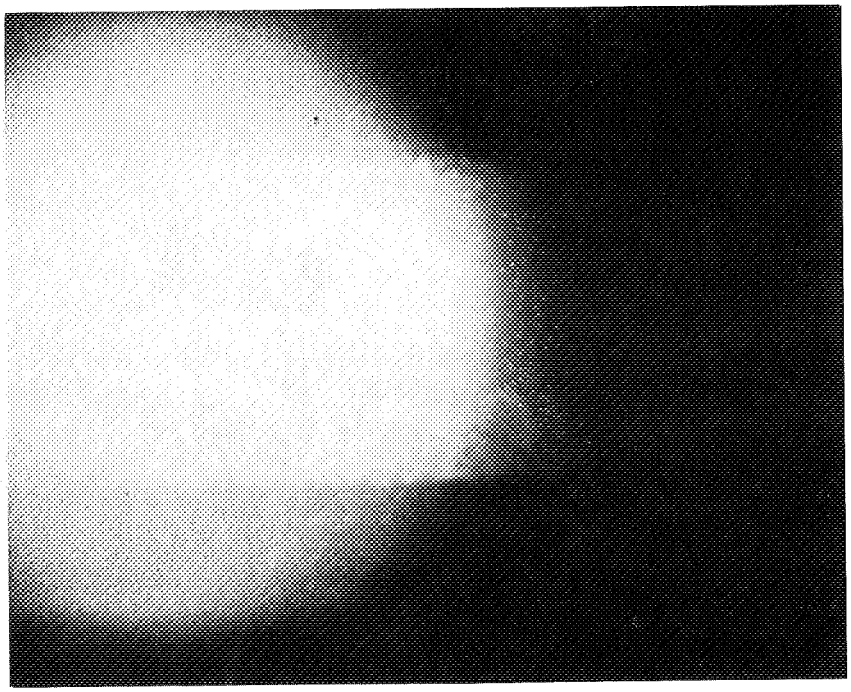

Figure 4.4 Holographic image of hypervelocity projectile

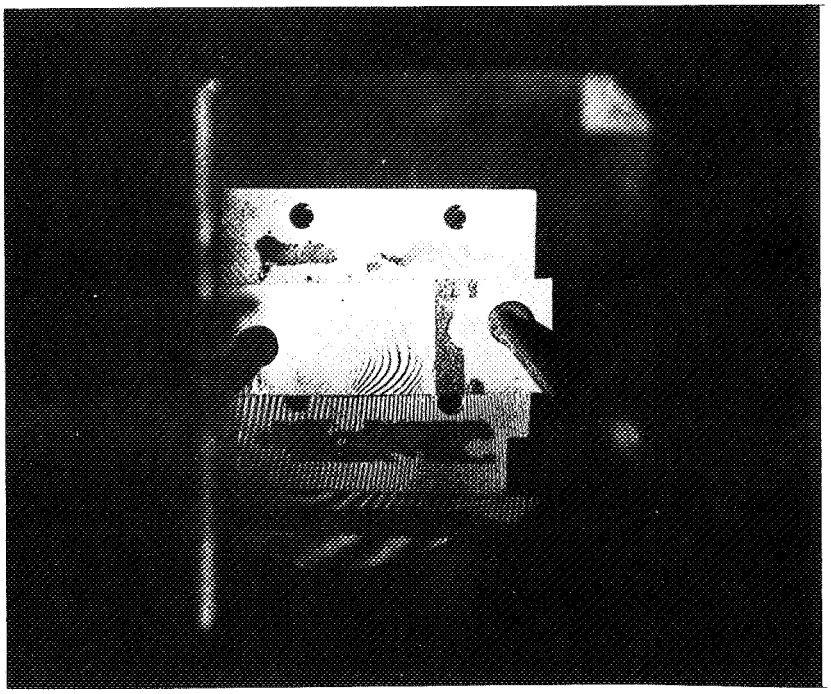

Figure 4.5 Double-exposure holographic image of epoxy joint

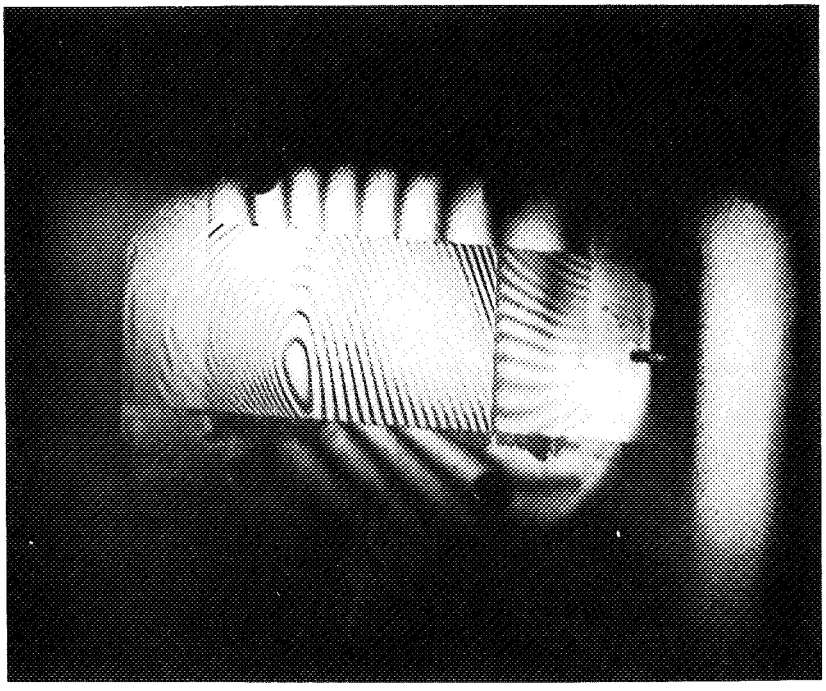

Figure 4.6 Double-exposure holographic image of epoxy weld

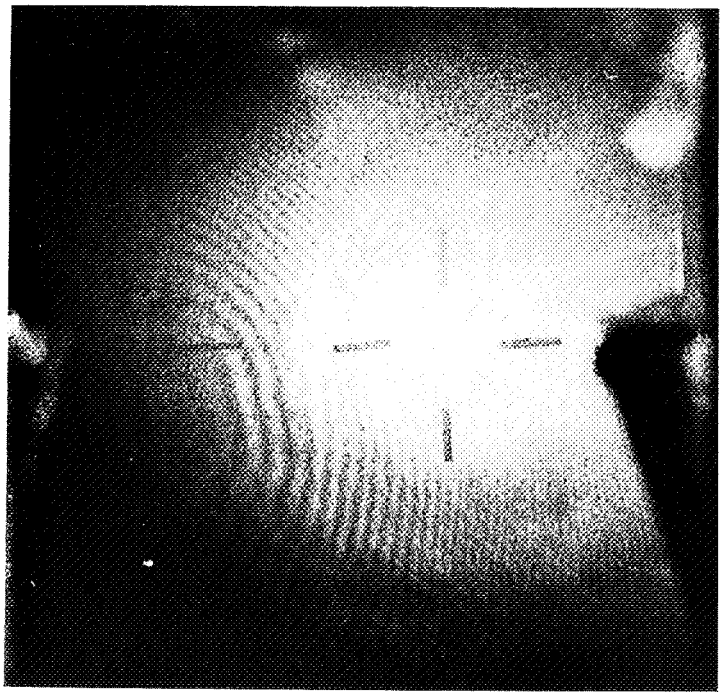

Figure 4.7 Double-exposure holographic image of honeycomb skin

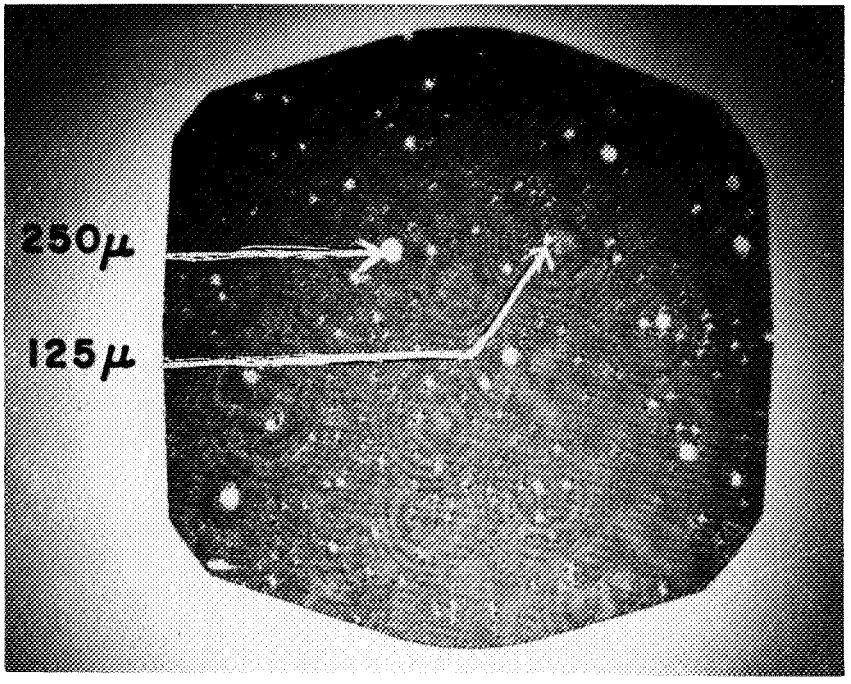

Figure 4.8 Holographic image of paint spray particles

physical movement. If the relative movement of each constituent of the joint is known, then the stress introduced can be determined. To facilitate fringe measurement, both a metalograph and simple lenses have been used to magnify the joint.

LIFETIME PREDICTIONS OF MATERIALS BY OPTICAL CORRELATION

As indicated in the previous section the ability to accurately predict lifetimes of such important components as printed circuit boards is vitally needed. The results from this effort are continually compared with the results from the previous effort using holographic interferometry.

As you are aware, the hologram can be used as a complex filter as well as a three-dimensional imaging technique. In this technique, a Fourier transform hologram, or matched filter, is made of the printed circuit board in an "unloaded" state. The hologram is developed and placed back in its original position. When the board is reilluminated and is unchanged, a correlation spot is produced, which can be monitored with a photomultiplier. This correlation spot is monitored in this manner as the printed circuit board is allowed to undergo a small, 1° C temperature cycle. As the board changes temperature and the surface changes, then it no longer correlates as well with the hologram so the intensity of the correlation spot decreases. In this manner, both temporary and permanent surface changes can be monitored. This work is presented in more detail in Section 15.

PARTICLE FIELD STUDIES

This area of holography has not received as concentrated an effort as the rest of the projects being conducted. Two specific problems provided the impetus for this work. One was the need to know particle size and velocity of particles emanating from a rocket nozzle, and the other was the need to know the sizes of particles exhausting from a smokestack. Since other locations such as Jet Propulsion Laboratory and Arnold Engineering Development Center were producing information similar to engine plume particle content, a large effort was not initiated in this area. The problem of particle content in smokestacks and similar combustion devices was, and is, of vital interest in the field of air pollution. An effort was initiated to study particle fields with the problem of air pollution as the application.

Various types of particle fields have been holographed, and figure 4.8 is an early holographic image of a paint spray. In this effort, as with most areas of holography, one is interested in attainable resolution and magnification. Since, from a medical standpoint, one needs information not only about the large particles but also about the very small ones, it is necessary to be able to consistently detect particles of 5 μ and less. An effort is continuing along these lines with resolution and magnification the main points of interest.

HOLOGRAPHIC ANALYSIS OF CONTAMINATE DEPOSITS

Space Sciences Laboratory has been given the primary responsibility to study the possible problem of contamination of optical surfaces in space, and many new, as well as traditional, methods are being employed. One of these is the application of holographic interferometry to the study of optical surfaces. Since there is considerable probability that waste dumps, engine exhaust, outgassed material, etc., will collect on orbiting optical equipment, the ability to study this deposition real-time both in the lab and in orbit is needed. Since holography permits the use of interferometric

systems without requiring extremely high quality optics, holograms can be made of an optical flat while it is under vacuum. The flat can then be used as a reference for future surface inspection. Once the hologram is made, developed, and replaced in its original position, the flat can be monitored through the hologram. So long as the flat remains clean, no apparent change is seen, but fringes begin to form when a material sample is heated and forced to outgas and plate out on the flat. These fringes contain information about both the film thickness and uniformity. Various experimental setups have been used in this effort and will be presented in greater detail in Section 14.

TESTING LARGE OPTICS BY HOLOGRAPHIC INTERFEROMETRY

In preparations for orbiting a diffraction-limited mirror as large as 3 m in diameter, numerous problems arise. MSFC has been applying holographic interferometry in this area in an effort to help evaluate some of these problems. Since most of these problems are manifested as a surface change, the ability to monitor such a surface, very accurately, is a step in the right direction. Either double-exposure or real-time holographic interferometry can constitute a technique for such detection.

Several different mirrors have been used in this effort; the largest has a 16-in. diameter with the center 10 in. illuminated. Figures 4.9 through 4.11 are holographic images of double-exposure holograms from the 16-in. mirror. Figure 4.9 had a rotation of about 100 μrad between exposures. Figure 4.10 had the temperature of one corner increased about 0.1° C, while figure 4.11 had the temperature decreased by gaseous freon. These tests had the mirror illuminated with a 10-in. piece of diffused glass. This provides the square background seen in the mirror. An experimental system is being developed whereby the mirror surface can be altered by known amounts so that the accuracy and reliability of this technique can be determined. It is planned to incorporate an optical transfer function system along with the holographic interferometer as part of the surface monitoring effort.

LARGE-OBJECT HOLOGRAPHY

In several of the efforts described previously, the need for a large-object, high-speed holography capability arose. This has been satisfied by the pulsed ruby laser shown in figure 4.12. This laser produces a 50-nsec 1-J pulse, with a coherence length of at least 3 m. It is being used in several of the projects where its particular capabilities can contribute. Figures 4.13 and 4.14 are holographic images made some time ago with this laser. They represent moderate coherence characteristics. Figure 4.15 is a hologram of a 6-ft mannequin in an Apollo flight suit. Because of the camera's limited field of view, this photograph does not adequately show that the entire man, from head to toe, is in the hologram. More recently, large-area bleached holograms of considerably higher quality have been made, but photographs of these are not yet available.

NEW AND PLANNED MSFC ACTIVITIES

Several efforts in holography and Fourier optics have just been initiated or are planned for future study. Some of these are image deconvolution, computer-generated holography, large-distance holography, quantitative analysis of holographic interferometry by computer, and holographic analysis of integrated circuits.

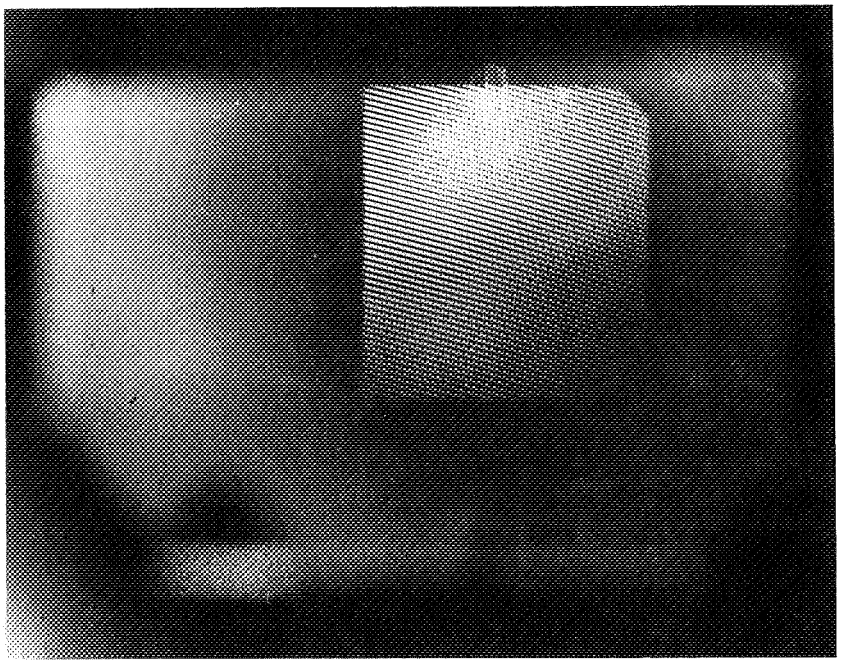

Figure 4.9 Double-exposure holographic image of physically moved mirror

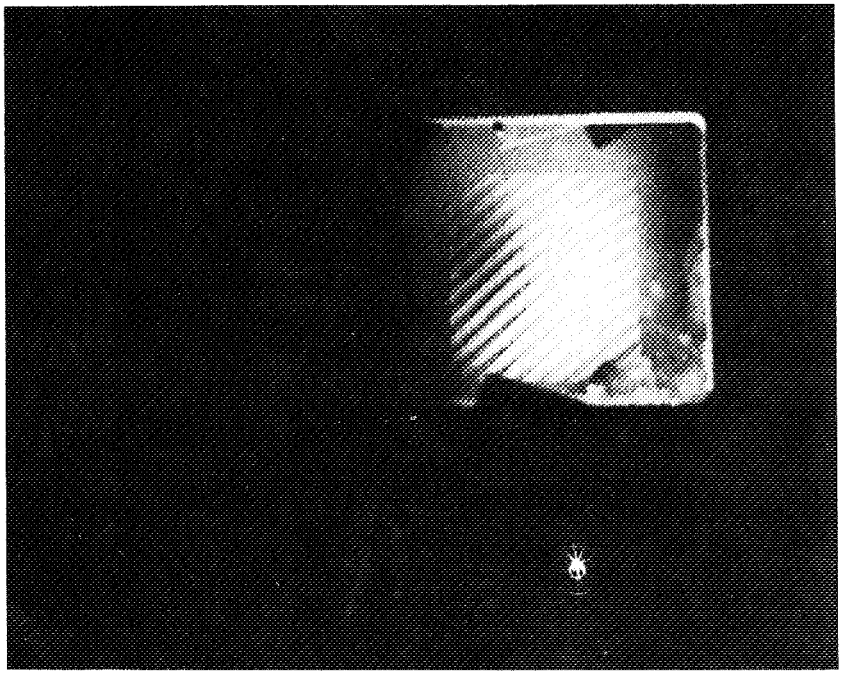

Figure 4.10 Double-exposure holographic image of a mirror with 0.1° C temperature change

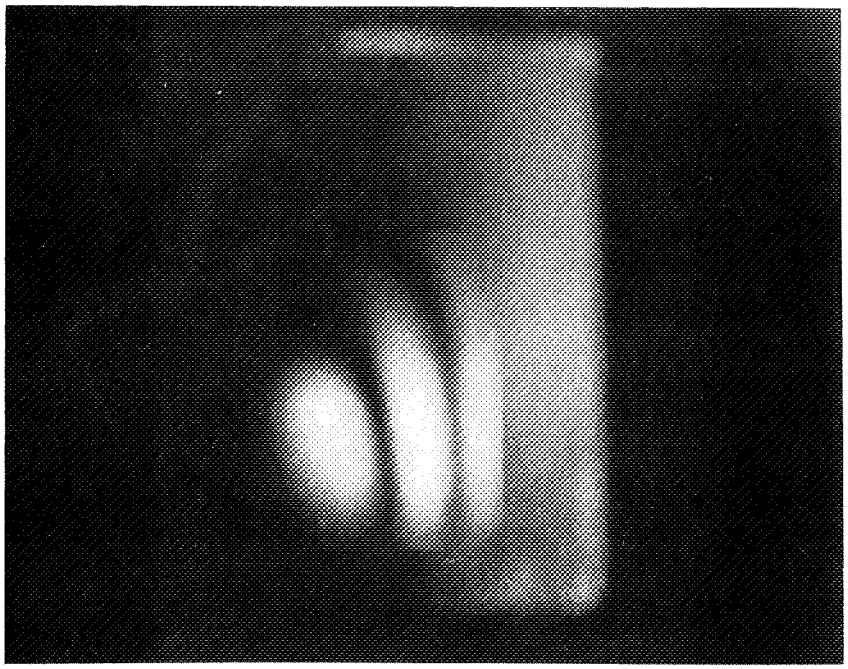

Figure 4.11 Double-exposure holographic image of a mirror with extremely small temperature change

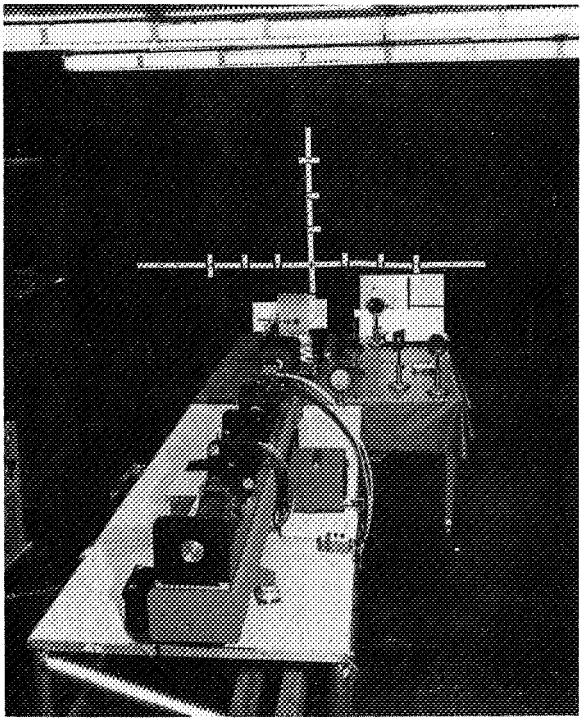

Figure 4.12 Ultracoherent pulsed ruby laser system

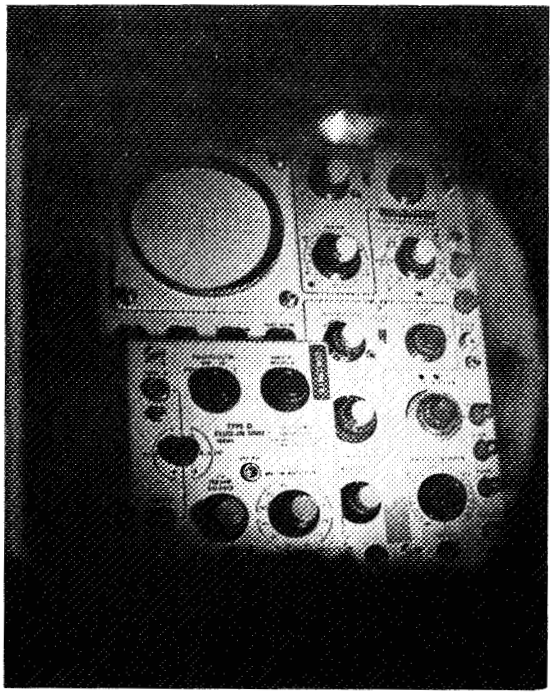

Figure 4.13 Holographic image of oscilloscope

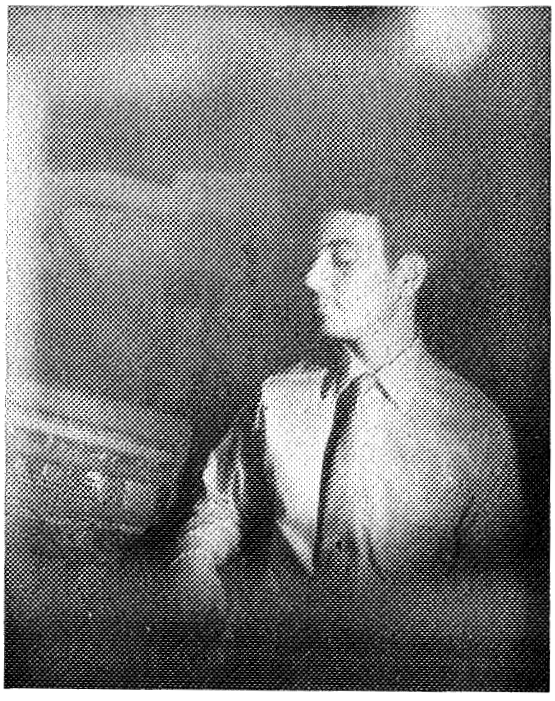

Figure 4.14 Holographic image of a person

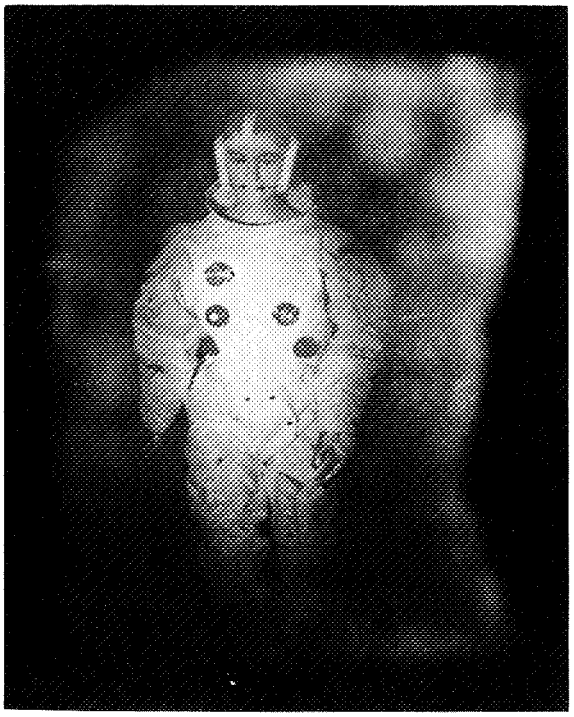

Figure 4.15 Holographic image of a 6-ft mannequin wearing an Apollo suit

Work has just started in the area of image deconvolution. Studies have been conducted in various types of optical filtering primarily to gain experience and experimental expertise. The problem presently addressed is concerned with X-ray negatives. Since X-ray devices do not possess true point sources, their negatives, in the final analysis, are not truly focused. Filtering techniques are being investigated to compensate for this condition.

In most optical filtering systems, a very accurate filter is needed if the goal is a pattern recognition. If a very accurate filter is used, scanning of other shapes or sizes requires a very large number of filters. The ability to form and erase such filters electronically would be an extremely important contribution. Thus, an interest exists in computer-generated holograms.

The value of radar and long-range photography has been well established. It is not unreasonable to consider their advantages combined with the added capability of holography. Numerous applications await the system that can produce true holograms over large distances.

Holographic interferometry appears to be one of the most promising areas of holography. A systematic approach to quantitative fringe analysis, therefore, is not unrealistic. An effort has been initiated at MSFC to perform controlled experiments and tie the mathematical model of these results, where applicable, with standard interferometry. There are many instances in holographic interferometry, as in normal interferometry, where the computer can aid in the analysis.

Primarily because of MSFC's experience in applying holographic interferometry and optical correlation to printed circuit boards, an expansion of this effort to include integrated circuits is being considered. In many respects the integrated circuit would be much easier to work with since it is man-drawn and more defined than the typical solder joint.

These are a few of the areas being considered at MSFC. Many small studies are being conducted along with the large projects to maintain a well-defined, up-to-date capability in the field. A few of these "small" studies are magnification, resolution, developing techniques, bleaching techniques, and improved technology procedures.

CONTRACT ACTIVITIES

At present there are two contracts from MSFC on holography. One is with GCO, Inc., while the other is with the University of Tennessee Space Institute. The contract to GCO is on holographic techniques for the analysis of steady-state and transient vibrations. A report on this effort is included in this publication as Section 6. The contract with the Space Institute is for the development of optical data-processing techniques applicable to detection and study of meteor trails. This effort has been in progress since September 1969.

5 REVIEW OF HOLOGRAPHIC INSTRUMENTATION AT LANGLEY RESEARCH CENTER

Joseph H. Goad – presented by Don M. Robinson
Langley Research Center

During the past four years, a small program has been carried out at Langley Research Center to examine potential holographic instrumentation application areas. Initial experimental results have been obtained in applications involving interferometric flow visualization, dynamic particle sizing, interferometric measurement of displacements by surface contouring or vibration mapping and nondestructive testing. Results of each application will be summarized. One problem area in applying the above techniques to dynamic events is the availability of a pulsed laser with a highly coherent output, a subnanosecond pulse duration, the ability to be synchronized or slaved to the event, and a good pulse-to-pulse reliability. Areas of interest are outlined in which holography could possibly provide more meaningful or unobtainable data.

During the past four years, a small program has been carried out at Langley to examine application areas where holographic instrumentation may have potential. These include display holograms, holographic interferometry for such uses as flow visualization, surface contouring, measurements of displacements, vibration mapping and other nondestructive testing techniques, and dynamic particle sizing. Initial experimental results indicate that some of these areas are promising for a near-term facility application (for example, a flow visualization technique to be described and a particle sizing effort). Most of these areas of interest have been reported previously by various investigators; consequently, Langley's main objective for the holographic effort is to evaluate such techniques for application in areas where this emerging technology may alleviate existing measurement problems. To determine the applicability of holographic techniques to a given situation, one of three questions must be satisfied: (1) Can holography provide data more readily than other means? (2) Can data with higher accuracy be obtained? (3) Can data be obtained that are not accessible by other means?

FLOW VISUALIZATION

Approximately 40 percent of the work effort at Langley is in the field of aerodynamics. One of the most valuable techniques for obtaining performance data in wind tunnel facilities is flow visualization. Classically, the techniques of shadowgraph photography, schlieren, and interferometry have provided valuable data. Many times, however, these conventional techniques fail to yield the desired quality or quantity of data.

Holographic interferometry has received attention at Langley as a means of alleviating some of the problems with conventional systems. One technique applied at a Langley wind tunnel facility is a real-time flow visualization system using holographic moiré patterns. The system uses a moiré principle in which a very fine system of fringes is magnified to produce real-time visible

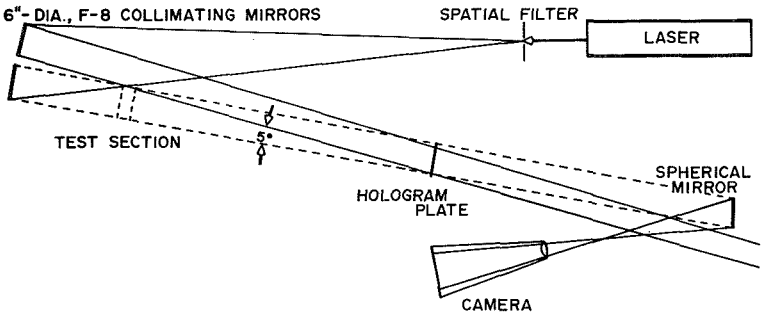

Figure 5.1 Holographic moiré interferometer system

interferometric-type fringes that can easily be recorded. These moiré fringes are produced by superimposing two sets of straight-line interference patterns, or grids. Figure 5.1 is a diagram of the experimental setup used to record these fringes. This arrangement is similar to an interferometer in that the two coherent beams are superimposed, thus producing an interference pattern. The first set of fringes is recorded on a photographic plate with no disturbance in either beam. This hologram is then replaced in its original position, and a second set of live straight-line fringes from this system is superimposed upon the first set. If the hologram now is rotated slightly, a magnified set of fringes, called moiré fringes, results. A disturbance in either of the beams causes the moiré fringes to be displaced as in an interferometer, indicating the real-time flow or disturbance. Figure 5.2 illustrates interferometric data obtained with this system. Interferograms of a burning candle are shown for an infinite fringe setting and for a finite fringe setting of the system. This system is easier to set up and adjust than a conventional interferometer and does not require high precision optics. Other advantages of this system are real-time observation of the flow for rapid interpretation and real-time photography of the flow. The technique will be applied for flow visualization where interferometry is desired but difficult to set up.

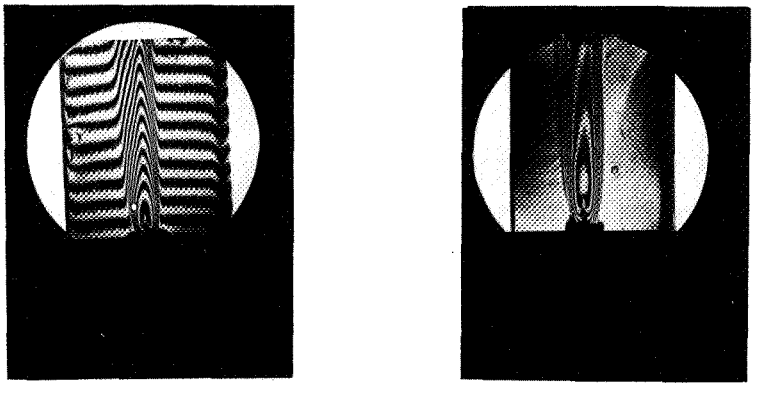

Figure 5.2 Real-time flow visualization using holographic moiré patterns

SMALL PARTICLE HOLOGRAPHY

Another in-house effort has been the investigation of the use of single-beam, far-field holography as an imaging technique. To date, experimental work has confirmed theory developed on small particle imaging and magnification, and a theoretical investigation has been made to determine the available reconstruction resolution by measuring the number of fringes on the hologram.

The final goal of this work is the holographic reconstruction of particles 50 μ in diameter having velocities of up to 20 km/sec. The intended application here is in a small-particle accelerator being constructed for use in simulated micrometeoroid impact. A record of the particle will provide data for accurate velocity measurements and particle integrity data. If a sufficiently coherent pulsed laser is available, particle sizing will be possible.

A holographic approach to the photography of these particles was tried because of the problems that are encountered with conventional photographic techniques. One of the most significant problems is the limited depth of focus in a conventional imaging system. This can be a serious problem if the exact position of the particles is unknown, as is the case for the simulated micrometeoroid impact. This uncertainty of exact particle location is, in fact, one of the main reasons for using holography to photograph these particles, since depth of focus can be increased.

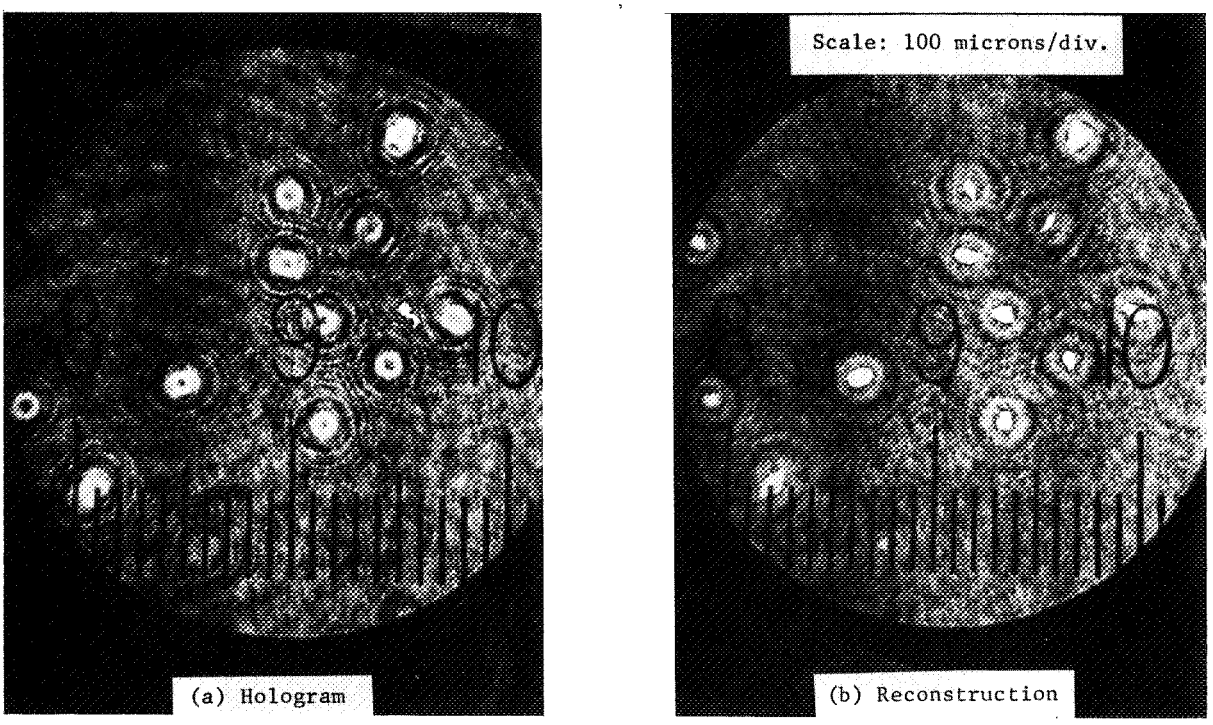

Figure 5.3 Hologram and reconstruction of 100- to 150-μ-diameter particles in a single plane. z is about 1.5 cm. Magnification is 33X. The scale is superimposed on the photograph to indicate size

To demonstrate laboratory feasibility of the holographic approach, experiments were conducted in two phases. The first phase consisted of hologramming objects from 250 μ down to 25 μ in size under static conditions, and the second phase simulated dynamic conditions in which accelerated particles were hologrammed using a Q-switched ruby laser. Figure 5.3 shows an example of a hologram and reconstruction taken with a helium-neon laser of some granular particles on a microscope slide. The reticle spacing shown in the figure is 100 μ per division from which size information can be obtained. Similar results were obtained with other object distributions using both a helium-neon and a Q-switched ruby laser. An example of some data gathered in the dynamic phase of the experiment is shown in figure 5.4. This fiberlike object was holographed with a Q-switched ruby laser and reconstructed with a helium-neon laser using a TV vidicon/monitor type readout. It was intended in this experiment to measure the size of individual particles (approximately 100-μ mean diameter), which were shot by a 220-caliber rifle/sabot type accelerator to a velocity of about 2.5 km/sec. However, due to the grouping of the particles as they passed through the test chamber, the distribution was generally of the shape shown in figure 5.4. Individual particles have been measured, however, in an experiment in which a 2.5-km/sec projectile impacted a target and the particle spray was holographed by this technique.

Figure 5.5 is a diagram of the proposed system to construct holograms of particles accelerated to hypervelocities. The particle is detected by a reflected-light technique at the velocity-measuring stations. This detection provides information so that the velocity calculator can provide Q-switch laser synchronization with the particle arrival at the holography station. One problem area in applying the above technique is the availability of a pulsed laser with a highly coherent output, a subnanosecond pulse duration, the ability to be synchronized or slaved to the event, and a good

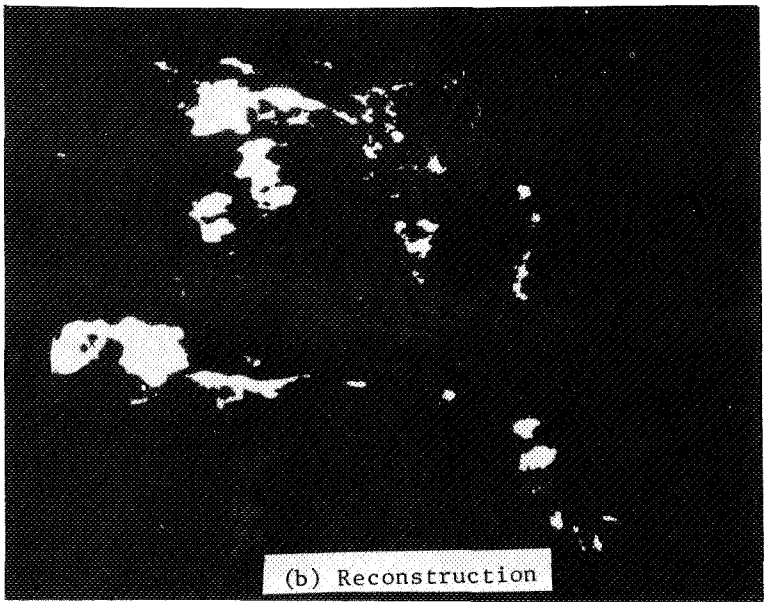

Figure 5.4 TV reconstruction of "object" moving through chamber at about 2.5 km/sec. Fiberlike character of the reconstruction indicates the object may be grease or cotton strands. Magnification is 35X

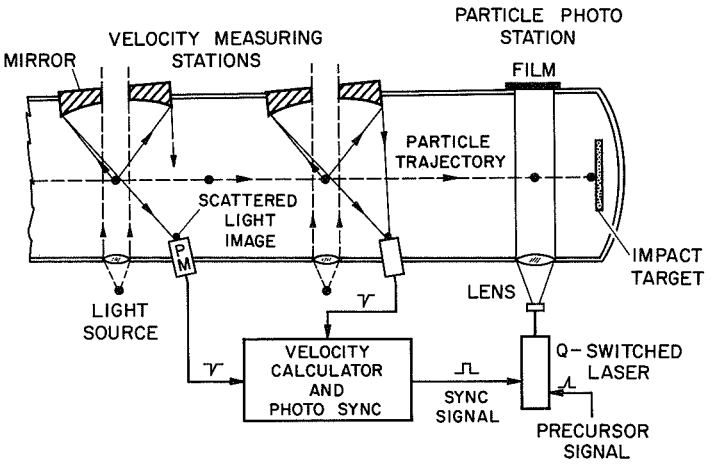

Figure 5.5 Proposed system for measuring the velocity and holographing hypervelocity mil-size particles

pulse-to-pulse reliability. Two possible laser configurations are the mode-locked ruby laser and the reversed pumped Raman laser. The Raman laser appears to be the best candidate from the standpoint of reliability and synchronization. A mode-locked ruby laser uses a saturable dye, which introduces a timing uncertainty in synchronization. The synchronization of the Raman laser depends on the switching of the ruby pump source, which can be controlled with a Pockels cell. A reversed pumped H_2 Raman laser compresses the nominal 20-nsec pump source duration to an output pulse in the order of 0.3 nsec. For a 50-μ particle accelerated to 20 km/sec, a pulse duration of 0.3 nsec will produce about a 6-μ particle movement during exposure. Construction of a far-field hologram with 10 percent particle motion should provide a reconstruction containing sufficient information to increase our knowledge of micrometeoroid impact phenomena.

SURFACE CONTOURING, NONDESTRUCTIVE TESTING, AND VIBRATION MAPPING

Several applications in structural analysis and dynamic loads have generated a need for holographic surface contouring, nondestructive testing, and vibration mapping. Very precise

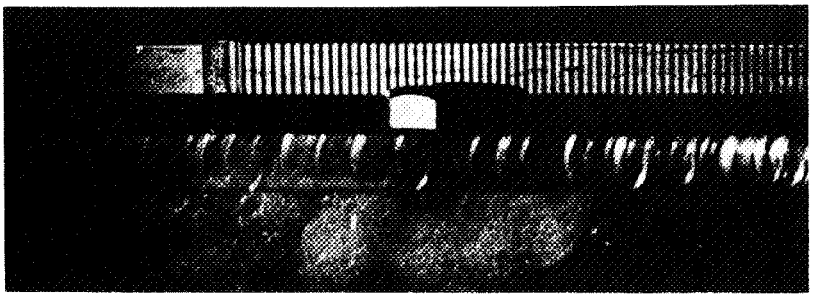

Figure 5.6 Uniform angular deflection of metal bar

measurements are needed to validate many static and dynamic mechanical structure theories. Measurements with holographic techniques provide the required accuracy for an experimental versus theoretical evaluation. Figure 5.6 is a surface contour of a simply loaded beam taken by a double-exposure technique. Each fringe indicates a one-half wavelength deflection from the undeflected position. Distortion of a C clamp compressing a metal ring is shown in figure 5.7. Surface contouring has also been used to determine base plate distortion of a small vacuum chamber.

A contract (NAS1-8361) with TRW Systems was initiated by Langley to establish the feasibility and usefulness of holography as a research tool to advance the state of the art in experimental dynamic mechanics. The contract covered three task areas where theoretical data could be compared with data obtained from holographic techniques:

1. High-frequency vibrations of beams and plates
2. Transient response of a cantilever beam
3. Transverse wave propagation in a beam

Experimental techniques used in this research contract were time-average holography, stored-beam holography, and stored-beam holography combined with a high-speed motion picture camera. The vibration studies extended structural dynamic data to frequencies virtually unexplored until now. In all cases, the data obtained show good agreement between theoretical and experimental response. This agreement serves to illustrate the high accuracy obtainable by holographic techniques. An example of some results from this contract where holography provides data unobtainable by other techniques is illustrated in figure 5.8. This particular interferogram shows a simply supported metal

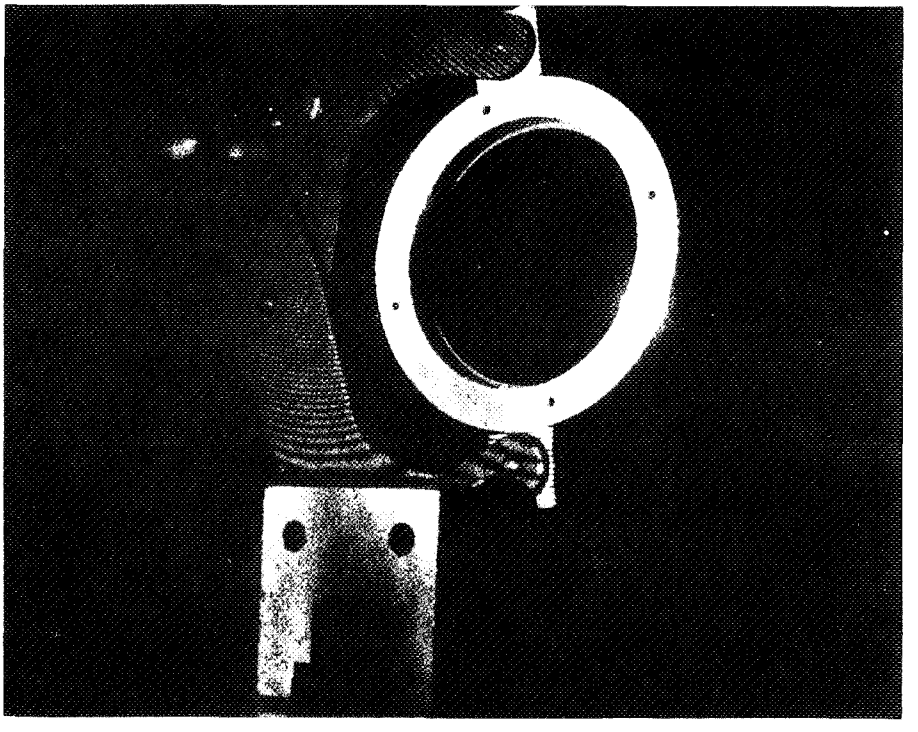

Figure 5.7 Distortion of C clamp compressing metal ring

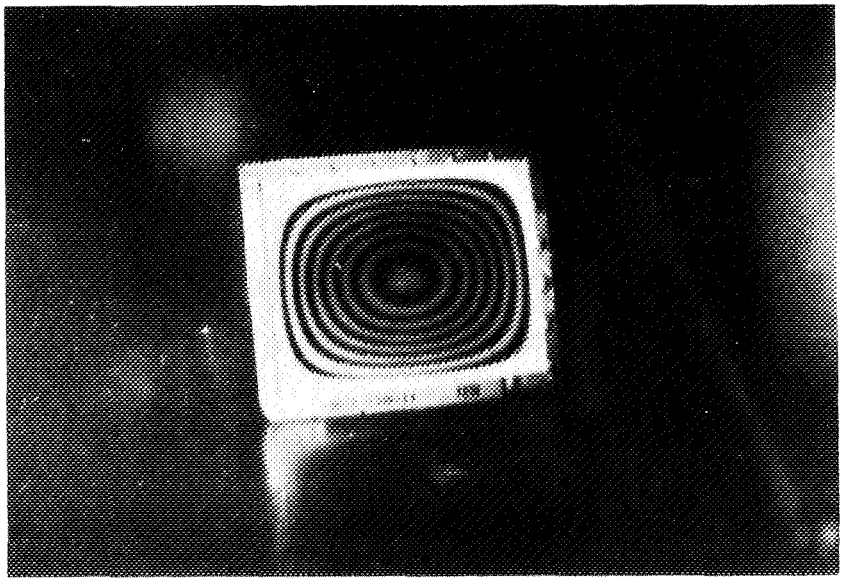

Figure 5.8 Holographic mode shape of 8- X 10-in. plate

plate vibrating in the fundamental mode. From the fringes, the displacement of the plate can be measured and compared to the results indicated by theory. The agreement between theory and experiment is shown in figure 5.9

Some in-house work has also been conducted that is related to the above techniques for determining contour maps of various vibrating surfaces. Figure 5.10 is an example of the use of a time-average approach to holograph a headphone diaphragm vibrating at various frequencies; different modal patterns of a vibrating 35-mm film can are illustrated in figure 5.11.

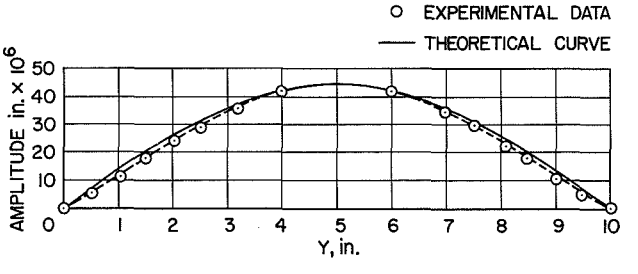

Figure 5.9 Calculated and experimental mode shape (first mode)

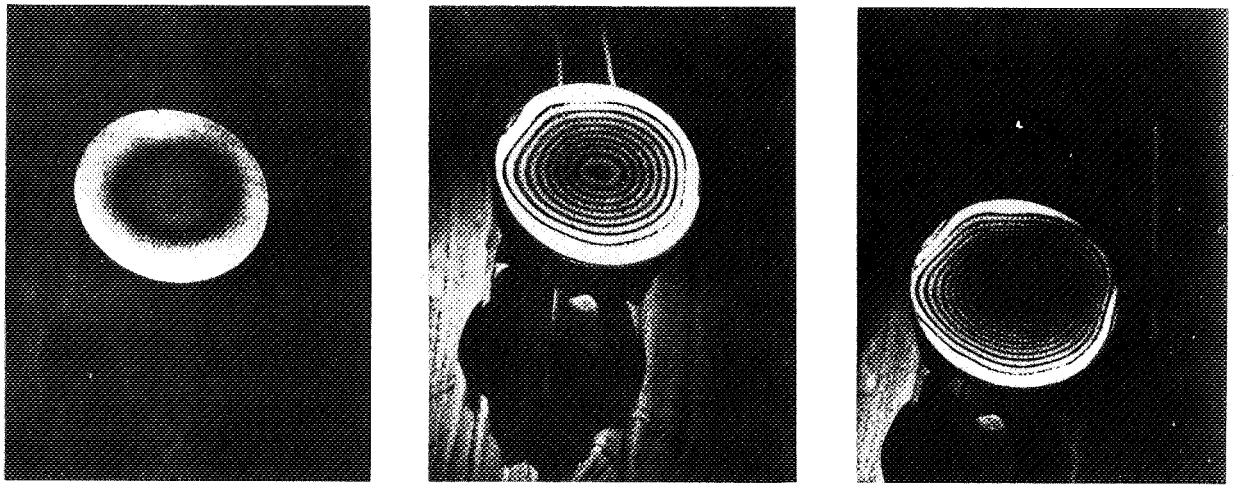

Figure 5.10 Interferograms of vibrating headphone diaphragm

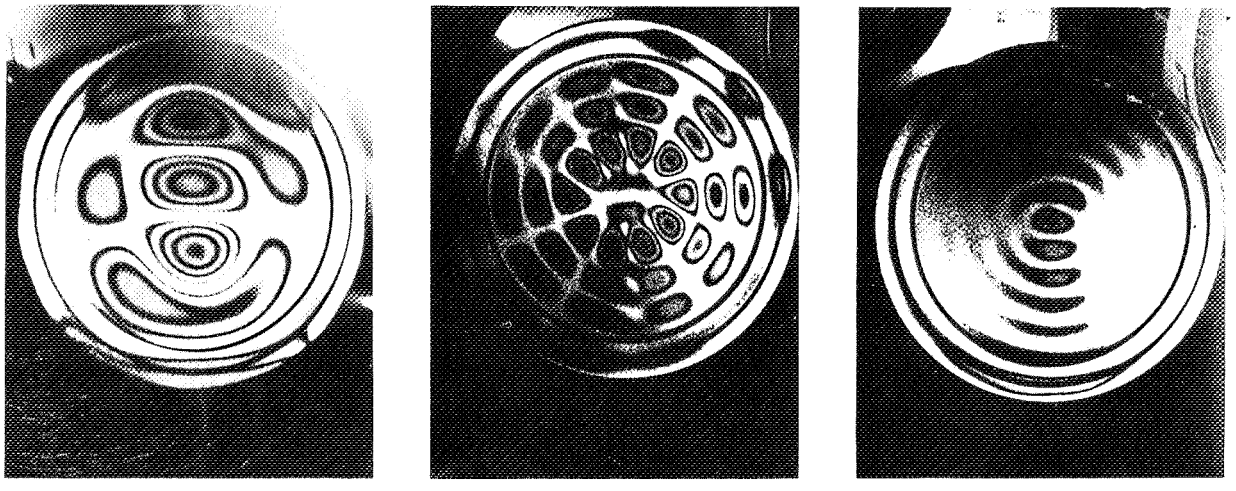

Figure 5.11 Interferograms of resonating 35-mm film can

6 HOLOGRAPHIC TECHNIQUES FOR THE ANALYSIS OF STEADY-STATE AND TRANSIENT VIBRATIONS

Charles F. Jacobson and Peter A. Hubbard
GCO, Inc.

GCO has investigated the use of holography as a tool for the analysis of vibration and shock. Steady-state vibrations have been investigated using both time-average and real-time holographic interferometry. Techniques have been developed for determining the phase of the mechanical vibrations using modulated reference or reconstruction wavefronts as well as strobed illumination in a real-time holographic interferometer. For situations such as shock, flutter, and transient phenomena, where sinusoidal single-frequency analysis is not possible, techniques for the instantaneous observation of interference fringes have been developed. Specifically, real-time fringes were photographed with a high-speed motion-picture camera.

Holography is proving to be a valuable tool for structural engineering. Through holographic interferometry, very small displacements and deformations can be measured, and vibration characteristics can be determined. There are three types of holographic interferometry:

1. Time-average holographic interferometry of sinusoidally vibrating objects (such as sonar transducers), where the interference is approximately between the peak displacement positions of the image.
2. Real-time holographic interferometry, where the interference is between the image and the object.
3. Double-exposure holographic interferometry, where the interference is between two slightly displaced images.

TIME-AVERAGE HOLOGRAPHY

Consider first time-average holography. Powell and Stetson (refs. 1 and 2) demonstrated the potential of holography as a tool for interferometric measurement by their dramatic experiments with a vibrating can. Nodes and antinodes were clearly indicated. The fringes of constant phase difference could be used to calculate the amplitude of vibration as follows.

Figure 6.1 is a two-dimensional representation of the recording geometry for holographic interferometry of a vibrating object, a sonar transducer in this case.

The active face of the transducer defines the principal plane of the XY axes. Its amplitude distribution is assumed to be normal to the planar surface, and the instantaneous displacement is given by:

$$\text{displacement} = m(x,y) \sin \omega_0 t$$

where

ω_0 = acoustic frequency

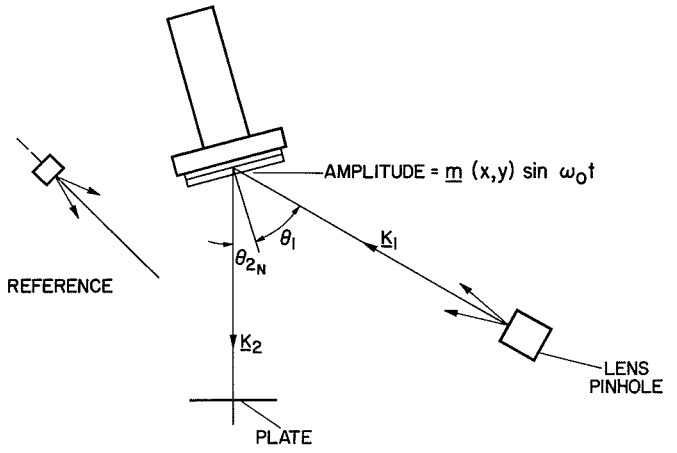

Figure 6.1 Geometry of holographic interferometry for vibration analysis

The transducer is illuminated from the right with a spherical wavefront from a laser. The propagation vector k_1, from the pinhole to the point (x,y) on the face of the transducer, makes an angle θ_1 with respect to the normal to the transducer. The observer looks at point (x,y) at an angle θ_2 with respect to the normal. It can be shown that, if the reconstructed-image intensity of the undriven transducer is represented by $|G|^2$, then with continuous-wave laser illumination and steady-state vibration, the reconstructed-image intensity of the vibrating transducer is given by

$$|G_v|^2 = J_0^2(k\Delta)|G|^2$$

where the term J_0 is the zero-order Bessel function of the first kind, and where the argument $(k\Delta)$ of the zero-order Bessel function is

$$k\Delta = (2\pi/\lambda)[m(x,y)(\cos\theta_1 + \cos\theta_2)]$$

Note that Δ is the optical-path difference between peak and zero displacement.

Dark fringes occur at the roots of $J_0^2(k\Delta)$. (It is helpful to consider that the static image is modulated by a characteristic function, such as this one in the case of time-average holography.) From the geometry, $\cos\theta_1$ and $\cos\theta_2$ can be calculated. With a table of the roots of the zero-order Bessel function, one can solve for $m(x,y)$.

If the i^{th} root of J_0 is denoted as p_i, then

$$m_i = \frac{p_i\lambda}{2\pi(\cos\theta_1 + \cos\theta_2)}$$

Because of the two cosine terms, which we call the obliquity factor, the fringes observed for the general case are fringes of constant phase difference. In other words, the fringes observed depend on the direction of the illumination beam, the observation direction, and the orientation of the transducer.

Figure 6.2 shows the reconstructed image of a square plate in several vibrational modes. Figure 6.3 shows the amplitudes of vibration for one case. Note that the phase is reversed on opposite sides of the nodes. The value of displacement was obtained easily from the values of the argument of J_0 at its various roots, the first dark fringe corresponding to the first root of J_0 and so on.

REAL-TIME HOLOGRAPHIC INTERFEROMETRY

In real-time holographic interferometry, a hologram is made of the object in its static position. After development, the hologram is replaced in its original recording position, and the interference between the holographic reconstructed image and the illuminated object is observed. Now the experimenter drives the object acoustically while observing the interference fringes. At resonances the static fringes tend to wash out, and the observer notes a dim fringe system characteristic of the modes of vibration. Under ideal circumstances the real-time characteristic function is

$$1 + \cos \phi_\epsilon \, J_0(k\Delta)$$

where the term $\cos \phi_\epsilon$ describes the static fringe system without vibration. Note that the fringe visibility decreases rapidly for increasing $(k\Delta)$.

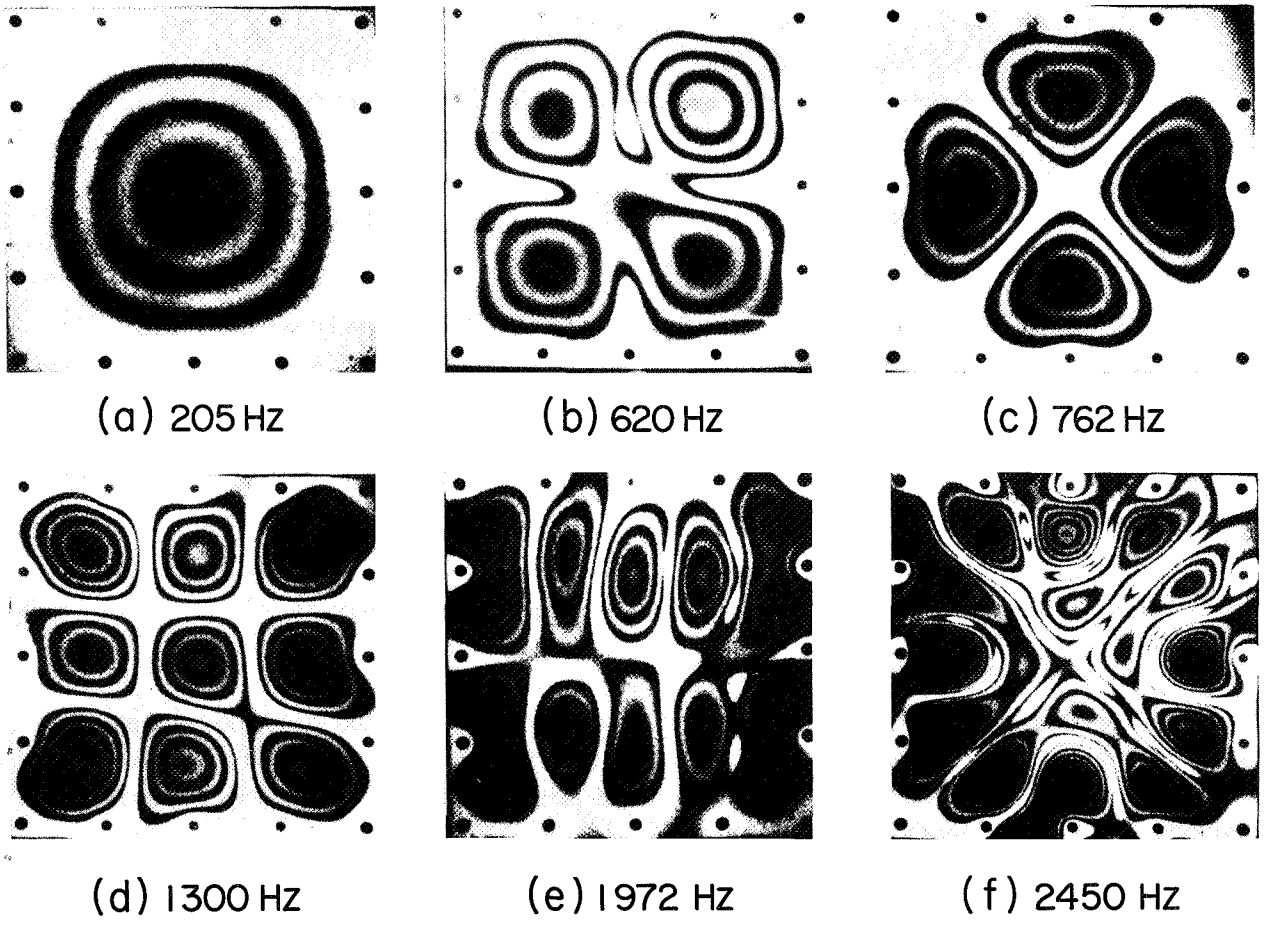

Figure 6.2 Time-average holographic fringe patterns of square aluminum plate in several vibrational modes

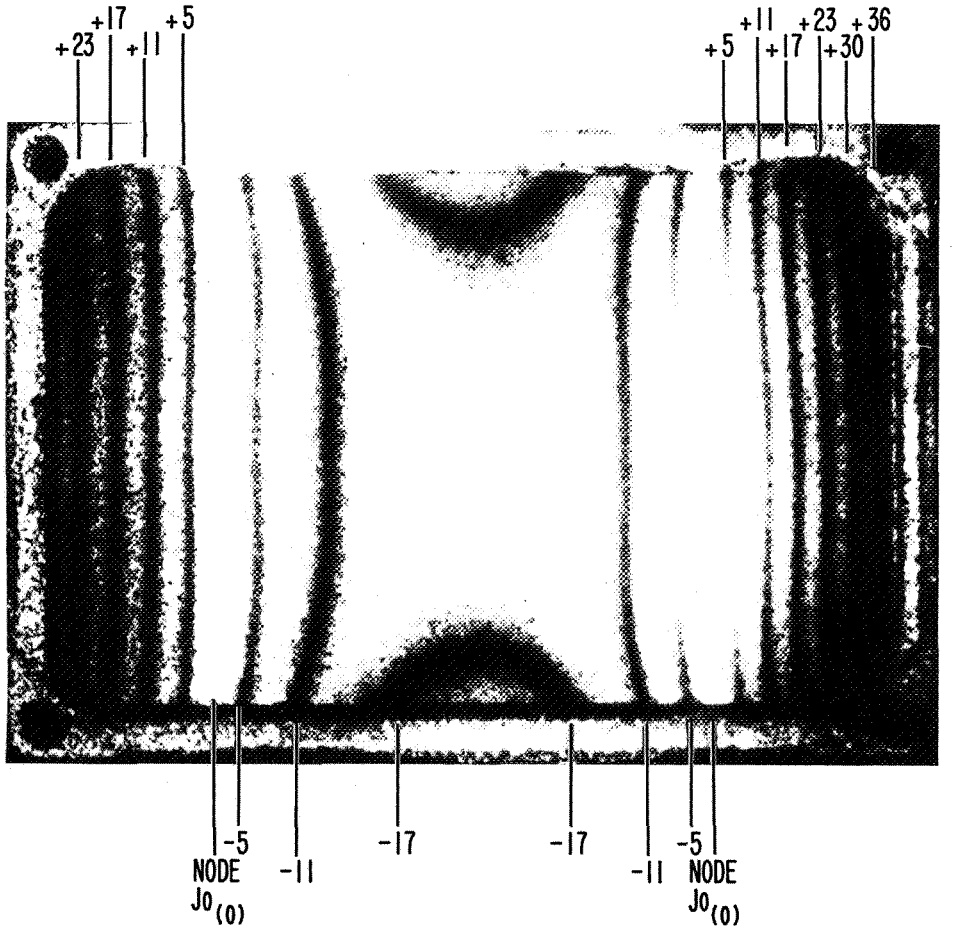

Figure 6.3 Dark fringes on this time-average holographic interferogram of a sonar transducer are amplitude-displacement contours, in μin.

This real-time method is useful for quickly finding resonances of the object. After the experimenter determines resonance frequencies by real-time interference, he can record a time-average hologram at each resonance for amplitude measurement.

As with many observed phenomena with poor visibility, the visibility or detectability of real-time vibration fringes is enhanced by dither of either frequency or amplitude.

STROBE HOLOGRAPHIC INTERFEROMETRY

The technique of strobe holographic interferometry offers the ability to measure phase and amplitude in real time. Ennos and Archbold (ref. 3) described a novel system using mechanical strobing. Johnson and Schienkov[1] achieved very nice results by shuttering a CW He-Ne laser with a Pockels cell while recording the hologram.

[1] Unpublished report from Office of Naval Research, Code 468, Oct. 1968, by C. Johnson and P. Schienkov.

At GCO, a Pockels-cell modulator was used with an argon laser, which gave sufficient light for real-time observation. If optimum conditions are achieved (fringe visibility of 1), the characteristic function is

$$(\omega\Delta t/2\pi)[1 + \cos(\phi_\epsilon - k\Delta \sin \omega_0 t)]$$

where $\omega\Delta t/2\pi$ = duty cycle of strobe, and ϕ_ϵ describes the static real-time fringe system. If strobing coincides with the vibration peak, the characteristic function reduces to

$$(\omega\Delta t/2\pi)[1 + \cos(\phi_\epsilon \pm k\Delta)]$$

This peak can be found by observation. Fringe contrast can be very good.

Figure 6.4 is a block diagram of the system. An argon laser with wavelength-selecting prism and coherence-extending etalon was used. A horizontal Glan air prism increased the degree of linear polarization. The light was modulated to vertical polarization with a Pockels-cell modulator driven by a high-power pulse generator. A vertically alined Glan air prism passed only vertically polarized light. The pulse generator was synchronized to an audio oscillator with a variable-phase output. The fixed-phase output was amplified to drive the object.

Examples of strobed, real-time holographic interferometric fringes of a vibrating aluminum panel are shown in figure 6.5.

PHASE MEASUREMENTS

Phases of vibration of the antinodes on several vibrating plates were measured holographically with the shuttered argon laser system. The peak displacement at each antinode was maximized using the phase-shift control on the oscillator (Hewlett-Packard model 203). The error of measurement is estimated to be less than ±5°.

On all panels except a round one, the peak maximum displacements of the antinodes were either in phase or 180° out of phase. The exception is illustrated in figures 6.6 and 6.7.

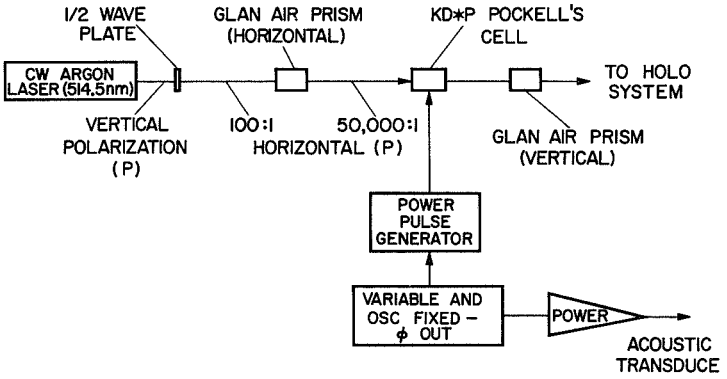

Figure 6.4 Shuttered-laser system for strobed real-time holographic interferometry of vibrating objects

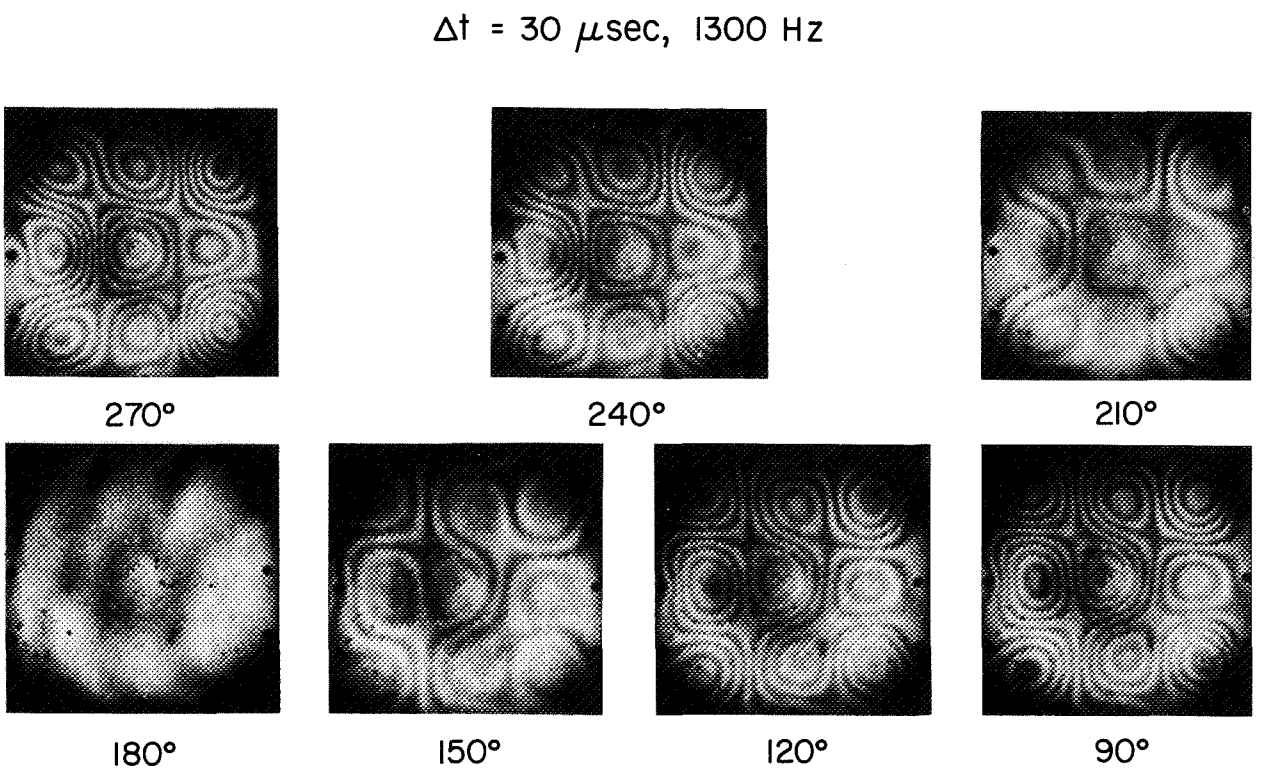

Figure 6.5 Strobed real-time holographic interferometric fringes of vibrating panel

Shown in figure 6.6 are photos of real-time hologram reconstructions of a circular plate vibrating at 670 Hz in a (1,1) mode. The measured phase difference between the two antinode peaks is 205° (instead of 180°). This same plate had a second (1,1) mode at 700 Hz, as shown in figure 6.7, with two antinodes also vibrating 205° out of phase with each other. However, the fringe system in figure 6.7 is angularly displaced by 90° relative to the system in figure 6.8.

Figures 6.6(e) and 6.7(e) are photographs of the plate with no vibration. The four static fringes were obtained by very slightly tilting the top of the plate-holding fixture back away from the observer. Before the tilting, two or three circular fringes were roughly centered on the disc. The tilt shifted the fringes down and somewhat to the left.

These static fringes can be used to resolve the 180° phase ambiguity that occurs with more than one antinode. Note in particular in figure 6.6(e) the fringe that arches over from 10 o'clock to 4 o'clock. In (a) and (b) this fringe is not too greatly changed, but it is pushed down by the top right antinode, indicating that the top right antinode has moved away from the observer while the bottom left antinode has moved toward the observer. In figure 6.6(c) and (d) this same fringe swings up and around the top right antinode, indicating that this antinode is now closer to the observer (i.e., in the direction of its position before tilting). Similar observations can be made about figure 6.7.

We believe that the existence of a (1,1) mode at two distinct frequencies is due to anisotropic physical properties of the aluminum plate induced during the rolling processes. The phenomenon of

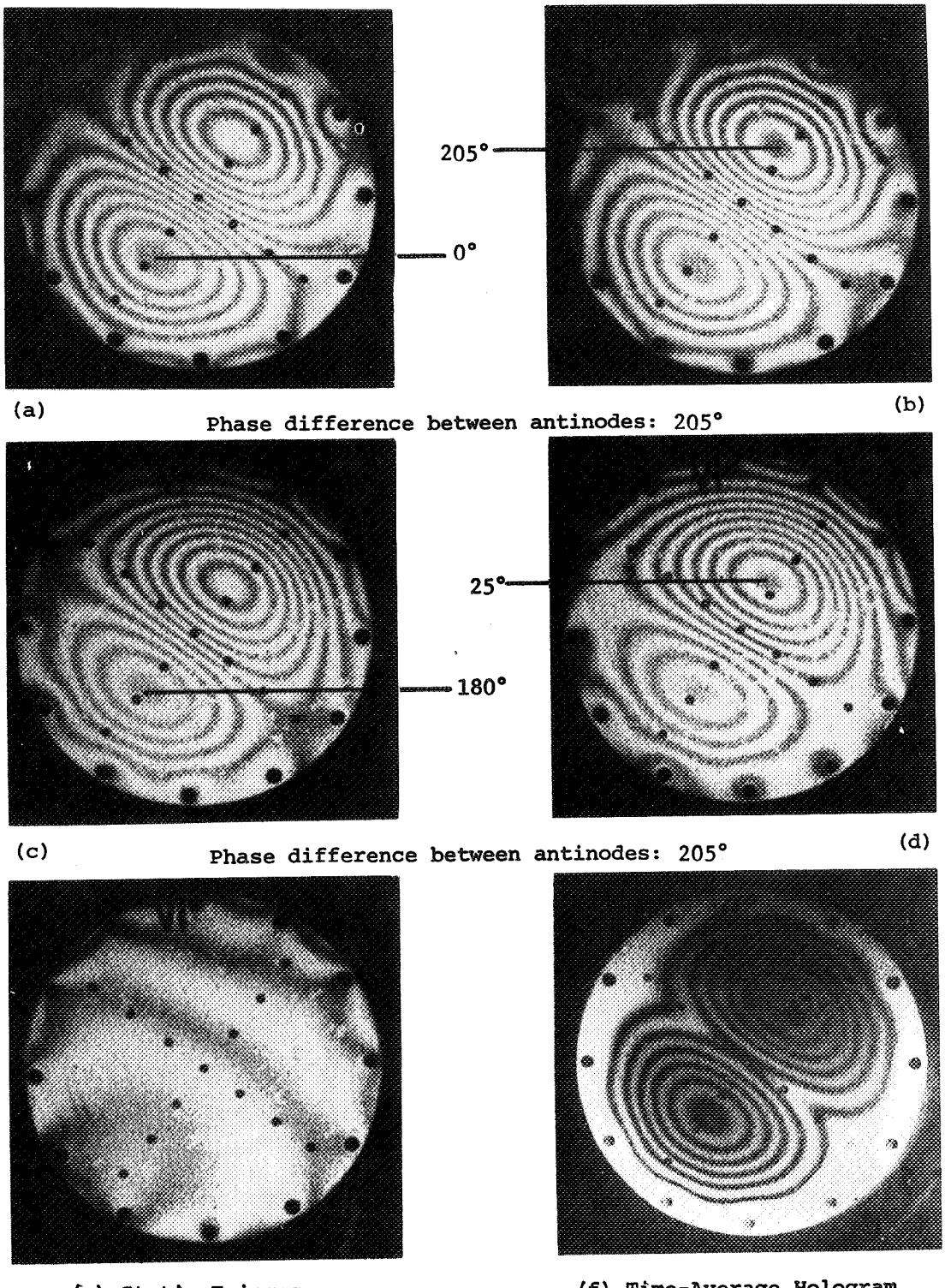

Figure 6.6 Real-time holographic interferometric phase measurement of vibrating plate (phase measured at antinode peaks)

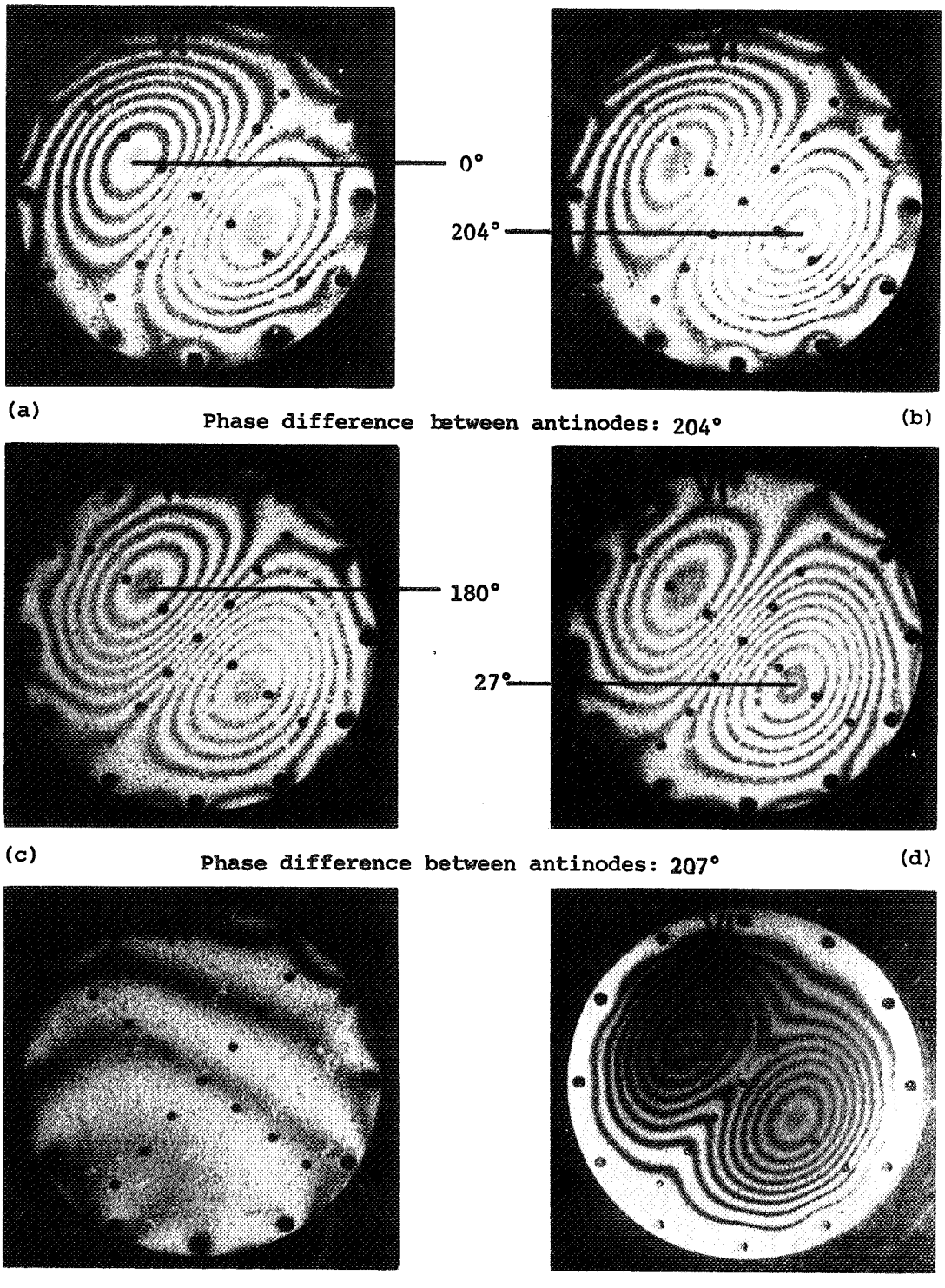

Figure 6.7 Real-time holographic interferometric phase measurement of vibrating plate (phase measured at antinode peaks)

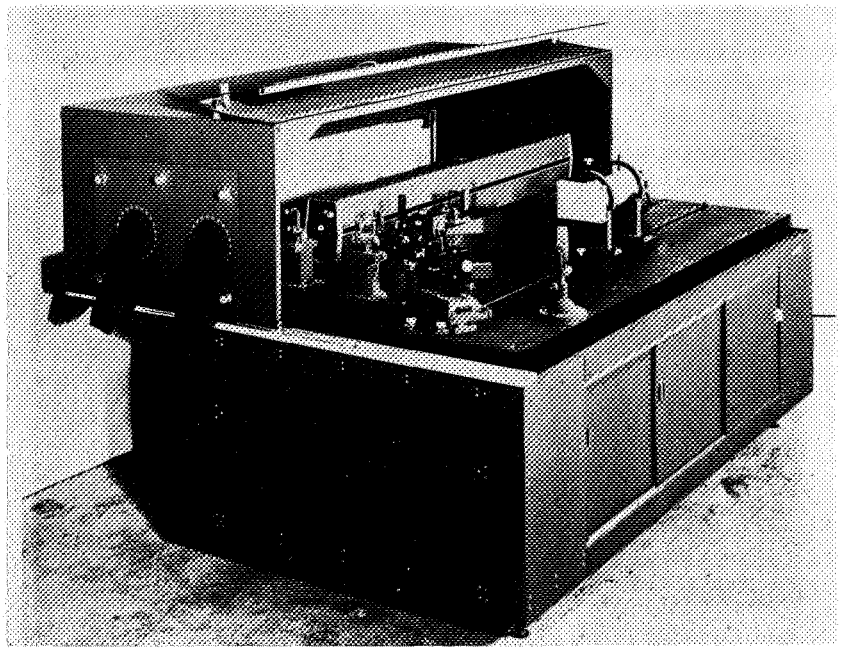

Figure 6.8 Holographic transducer analyzer

adjacent antinodes not being 180° out of phase may be due to a nonlinear effect. Figures 6.6(f) and 6.7(f), time-average reconstructions of these two modes, show more clearly the absence of a node between the two antinodes and indicate the presence of a fundamental component.

INSTRUMENTATION

To facilitate fringe interpretation, GCO has demonstrated and instrumented a technique for making $\cos \theta_1$ and $\cos \theta_2$ approximately equal and their sum equal to 2. The requirements for a holographic vibration analyzer are:

1. Versatility
2. Operating simplicity
3. Ability to operate in a normal environment
4. Isolation from seismic disturbances
5. Fixed setup to allow for comparison experiments—several years apart if necessary

Figures 6.8 and 6.9 show the holographic transducer analyzer built for the USN Underwater Sound Laboratory. A light-tight hood allows operation in a lighted room; it opens easily to allow general access, and the end panel may be removed for observation and for photography of reconstructions.

Figure 6.8 shows schematically the layout of components on the holographic vibration analyzer. The laser shown is a Spectra-Physics Model 125. For more power, an argon laser can be used. A variable attenuator denoted as A is useful for adjusting fringe visibility. A large beamsplitter (BS_2) in the object beam allows us to virtually superimpose the observation and illumination points, making θ_1 and θ_2 equal at every point on the object. Although this use of the beamsplitter appears to make inefficient use of the laser light, when a special retroreflective coating is used on the

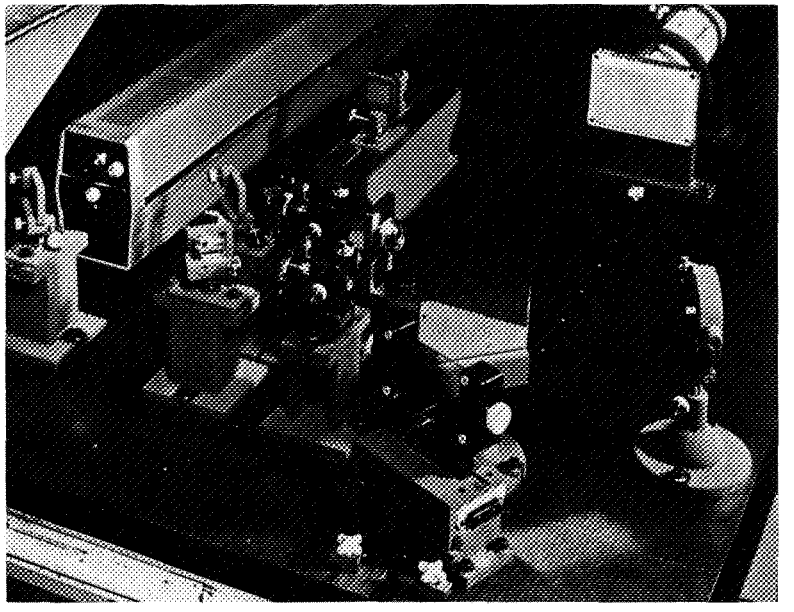

Figure 6.9 Optical components of holographic vibration analyzer

transducer face, the light efficiency is actually increased by more than 35 times over direct illumination of an object painted flat white. If a flat object is located at least 3 times its maximum dimension from the plate, then the error in assuming $\cos\theta_1 + \cos\theta_2$ constant (and equal to 2) is less than 2 percent (if the object is assumed to be vibrating normal to its surface).

All the components are mounted on a cast-Meehanite surface plate that has been "normalized" for maximum stability. The surface plate is mounted on a pneumatic isolation system, which provides isolation from seismic vibrations. The surface plate is 4 ft by 8 ft by 6 in. thick, with a ribbed structure, and weighs about 3000 lb without components. The load capacity is 2000 lb. All components have been designed to be interferometrically stable, and all except the transducer and the optical rail with mirror M_2 are bolted in place. Because the components are fixed in place it is possible to test an object, put it into service, bring it back years later, and retest it for comparison.

HIGH-SPEED HOLOGRAPHIC INTERFEROMETRY FOR SHOCK, FLUTTER, AND TRANSIENT PHENOMENA

Determination of the optimum system for high-speed holographic interferometry presents more of a problem. The major decision is which type of laser to use. The following discussion deals with this question and shows why we decided to use a shuttered, CW laser with real-time holographic interferometry.

How much data is required? In some classes of shock tests a simple double-exposure hologram or a single frame of real-time holographic interferometric data would provide sufficient information to analyze the event. Generally, however, multiple frames of holographic interferometric data are needed, possibly hundreds or even thousands, depending on the experiment. Therefore, high-speed photography of real-time holographic interferometry is desirable.

We estimated that in a normal system, a photographic film with an ASA speed of over 1 million would be needed. The fastest available is Kodak 2485 with a speed of only 10,000.

The system for steady-state analysis uses a CW helium-neon or argon laser. Strobing or high-speed photography would be achieved by shuttering. Thus only a fraction of the laser power output would be used. A pulsed laser would be preferable, if one were available with appropriate capabilities. One can consider recording a sequence of high-speed holograms, which offers the advantages that the stability of the holographic system and environment is not critical and that fringe visibility is very good. But to be useful, each hologram would have to be a double exposure of two different but undetermined positions and would require about 1 J/pulse. Therefore, the real-time approach seemed best.

The original static object position is the reference for all measurements and interferometric data. A laser was needed that could be pulsed at least 10 kHz (100 kHz desirable) with an energy of 10 μJ/pulse, pulse length less than 1 μsec, pulse jitter 0.5 percent of prf, light coherence length of 1 m or longer, and visible radiation. Since no such laser is available, we looked at possible ways to improve the light economics, using CW lasers.

Investigations of improved reflection efficiency of the object revealed that the 3-M Company's Scotchlite is very well suited. This material is very directive—approximately 3° between 3 dB points. Therefore, to use it properly, we must use a beamsplitter, which discards much of the light. Even so, the efficiency of this reflective coating is so great that a net overall improvement by a factor of 35 was realized.[2]

Consider next the hologram. The optimum exposure for an amplitude hologram results in a density of 0.6—an intensity transmission of only 25 percent. Bleaching a real-time hologram provides two benefits: (1) a much brighter reconstructed image, and (2) a higher transmissivity of the object beam. To implement the use of the bleached emulsion, we used a technique similar to Pennington and Harper's (ref. 4) except that we exposed, developed, bleached, and reconstructed in-place in a liquid gate. This processing technique eliminates the concern over residual stress in the emulsion. The procedure was to soak the hologram plate in a prehardener, expose in prehardener, develop in D-19, fix, wash, bleach using Kodak Etchbleach-2, and rinse and reconstruct in water. The transmissivity of the bleached (phase) hologram was at least 75 percent, so object brightness was increased by a factor of 3; and the reconstructed-image intensity also improved by a factor of 2.5. No specific attempt was made to optimize the process.

Finally, at some sacrifice of fringe visibility we concentrated the reference-reconstructing beam by means of a longer focal-length lens in the reference beam, thereby further increasing the brightness of the reconstructed image.

---

[2]Private communication with Verne Costich at Spectra-Physics indicates theoretical improvement of nearly four times by the use of a beamsplitter with high polarization sensitivity. A beamsplitter with high reflectance for polarization in the plane of incidence and high transmittance for polarization perpendicular to plane of incidence (or vice versa) could be used with a quarter-wave plate to decrease the light-intensity loss in the beamsplitter from 75 percent to less than 10 percent.

The system used is shown schematically in figure 6.10. It is a standard holographic system except for the use of a liquid gate for a plateholder and a high-speed camera. The camera was a Hi-Cam camera with an f/2.8 lens and a 400-ft reel of 16-mm film.

Several runs were made at various speeds from 1000 to 5000 FPS. Kodak 2485 film, with a rated ASA speed of 10,000, was tried first, but this film has a very high contrast and is quite grainy and noisy. We then tried Kodak 2484, which nominally has a maximum ASA speed of 2000. It worked quite well. We estimate that our fastest exposure was at an effective ASA speed of 6000, and while the image is somewhat thin, it is usable. Our best results were obtained using Accufine developer at room temperature. The laser was operating at 514.5 nm with an output power of 250 mW.

Figure 6.11 shows 20 sequential frames of data from one high-speed sequence. The first frame is just before impact; the second frame is at or just following impact. Notice that the vibrations build up rapidly and that by the fifteenth frame they are changing too rapidly to follow in detail. The frame rate was 5000 FPS, and the shutter speed 20 μsec. The 20 frames represent a time span of 4 msec. The object is a thin-walled cylinder 27-in. high, 18-in. diameter, with a 0.020-in.-thick wall.

Consider now what is the best one can do today. Using the previous data as a reference, we can consider the following improvements:

1.	More powerful laser	
	a. CW gas, 2.5 W	10X
	b. Pulsed solid state	?
2.	Smaller area (1 sq ft)	4X
3.	Improved technique	
	a. Higher diffraction efficiency	2X
	b. Miscellaneous: higher efficiency object-illumination optics	3X
	Total improvement	240X
	(equivalent to framing rate of 1.2×10^6 FPS)	

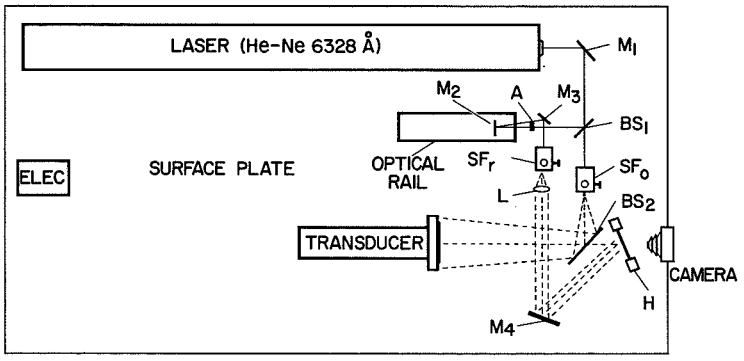

Figure 6.10 Optical layout for high-speed photography of real-time holographic interferometry

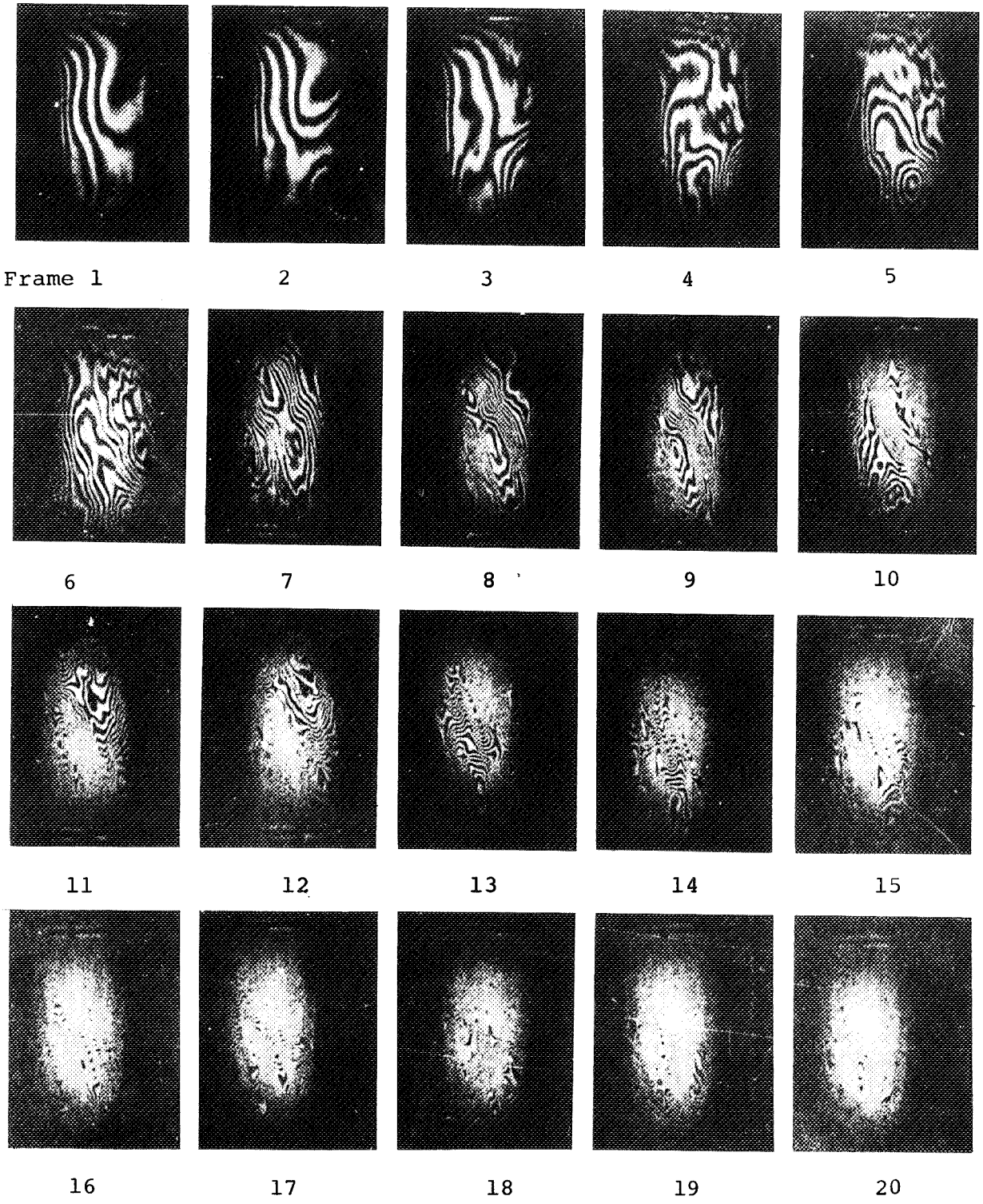

Figure 6.11 Real-time holographic interferograms of cylinder photographed by high-speed camera (5000 FPS) after shock event

Let us now look at requirements. The maximum frame rate may be determined by the rate of change of phase shift in the real-time holographic interferometer if we want a complete histogram. The instantaneous phase is given by

$$\phi(t) = 2\pi(\cos\theta_1 + \cos\theta_2)\frac{m(x,y,z)}{\lambda}\sin(\omega t)$$

The instantaneous frequency (f) is given by

$$f = \frac{1}{2\pi}\cdot\frac{d\phi}{dt}$$

and the frame rate (FPS) must be at least twice the maximum frequency ($2f_{max}$). Therefore,

$$FPS = 8\pi\frac{m}{\lambda}f_0$$

For example, consider the following cases. Assume a highest frequency component of 200 Hz.

Normalized amplitude (m/λ)	*Camera speed* (FPS)
5	2.5×10^4
50	2.5×10^5
2000	10×10^6

However, in other cases it may be sufficient to sample at a slower rate, if the shutter time is short enough to stop the fringes. For example, if one were interested in vibration-amplitude distributions or mode shapes under a random excitation then one would only have to sample at several times the maximum expected acoustic frequency. For the examples given, the shutter times would have to be as follows:

Normalized amplitude (m/λ)	*Shutter speed* (μsec)
5	40
50	4
2000	0.1

By extrapolation, it would be state of the art to decrease exposure to 83 nsec—a decrease by a factor of 240 from the exposure used to make the high-speed motion picture at 5000 FPS.

LIMITS

Our best estimate of the limits of performance, based on current state of the art, are as follows:

Displacement accuracy:	λ/40 (visual) λ/400 (densiometric)
Maximum amplitude:	500 λ (0.25 mm)
Minimum amplitude:	λ/40
Maximum area:	250 sq ft
Minimum shutter time:	83 nsec

CONCLUSIONS

Several new techniques—including strobing, phase measurement, and high-speed motion-picture photography—have been developed for the application of holographic interferometry to vibration analysis. They allow the analysis of both steady-state and nonsteady-state vibrations. In many cases,

it is well within the state of the art to do vibration analysis on engineering objects by using CW gas lasers and real-time holographic interferometric techniques.

Data reduction of the holographic information for complex three-dimensional objects needs further attention.

ACKNOWLEDGMENTS

We acknowledge the helpful comments and encouragement given by Dr. Helmut G. Lackner of Marshall Space Flight Center, Huntsville, Alabama. We also thank Dr. Don Neumann and Dr. Edwin Champagne of GCO, Inc., and Duane Gifford, who did much of the experimental work. This work was sponsored by NASA-MSFC under contract NAS 8-21369.

REFERENCES

1. Powell, R. L.; and Stetson, K. A.: Interferometric vibration analysis by wavefront reconstruction. J. Opt. Soc. Am., vol. 55, no. 12, Dec. 1965, pp. 1593–8.
2. Stetson, K. A.; and Powell, R. L.: Hologram Interferometry. *Ibid.*, vol. 56, no. 9, Sept. 1966, pp. 1161–6.
3. Ennos, A. E.; and Archbold, E.: *Laser Focus*, vol. 4, 1968, pp. 58–9.
4. Pennington, K. S.; and Harper, W. B.: 1969 Spring Meeting, Optical Society of America, San Diego, California, March 1969.

7 HOLOGRAPHIC INSTRUMENTATION STUDIES

L. O. Heflinger and R. E. Brooks
TRW Systems Group

This program is an investigation of holographic techniques applicable to NASA's instrumentation needs. A number of interferometric and schlieren systems have been devised, analyzed, and tested in the quest for a system sensitive enough to enable flow visualization at reentry simulation pressures. Some of the systems are described, such as subfringe interferometry, high-order interferometry, multipass interferometry, and double-exposure schlieren.

Techniques have been developed for improving the usefulness of pulsed ruby lasers for front-lighted holography and interferometry. The production of pulsed ruby holographic contour maps, achieved by two-frequency operation of the pulsed ruby laser, is briefly described.

A number of interferometric and schlieren systems have been examined in the quest for a system that would make visible aerodynamic flows in very low-density gases, such as those used for reentry simulation. The magnitude of the optical perturbations created by such flows is less than 1/100 wave. Combinations of systems have not been experimentally explored, but the reader will observe that some of the techniques outlined are compatible in principle with others, yielding the possibility that a combination system could yield a gain in sensitivity equal to the product of the sensitivity increases achieved by each individual system.

Several other experiments were performed relating to the use of pulsed lasers for front-lighted holography and holographic interferometry. One promising outcome of these experiments is a technique for producing contour maps via front-lighted pulsed ruby laser holograms.

FLOW VISUALIZATION TECHNIQUES

Restrictions Set by the Intended Application

The goal of visualizing aerodynamic flows where the optical phase perturbation is less than 1/100 wave, together with the goal that a useful system be applicable to large test facilities, restricts the search to systems that are self-compensating. Thus, consideration is not given to systems requiring 1/100-wave flatness of the windows and optical components, but only to systems that somehow have a built-in insensitivity to window imperfections, etc. However, this does not exclude systems that require conventional high quality optics such as quarter-wave windows.

One of the most favorable applications for high-sensitivity systems is the ballistic range. This application permits double exposures to be made with only 100 μsec separation, thus eliminating many problems of stability and vibration. The addition of counterflow to the ballistic range complicates the problem with a turbulent boundary layer at the windows. A technique for circumventing this turbulence is described below. The most difficult application is to the steady-state wind

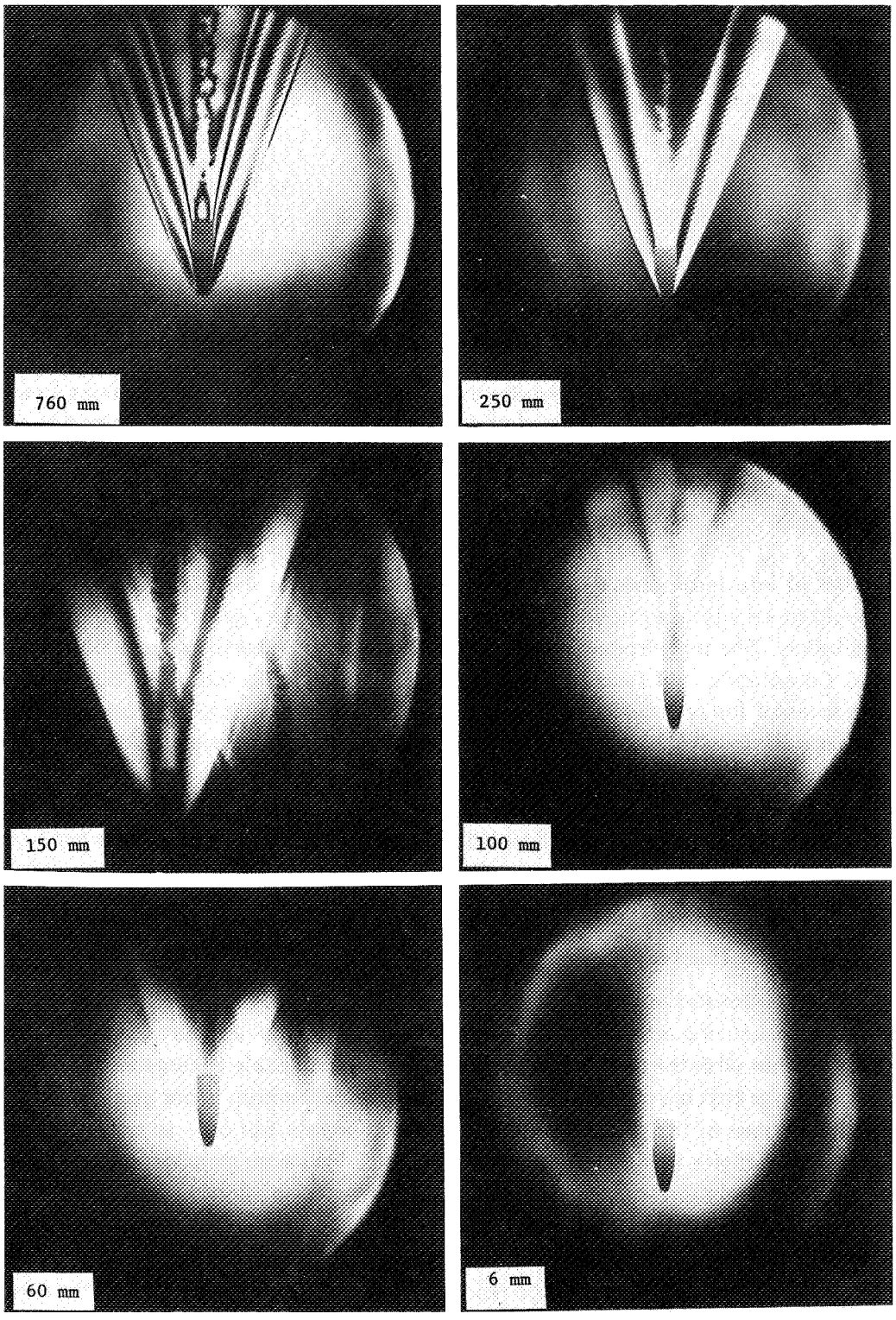

Figure 7.1 Double-exposure holographic interferograms at various chamber pressures

tunnels where vibration poses a major problem. Full self-compensation in such applications probably requires the ability to make adjustments during the readout process that compensate for vibrational displacements during the sampling exposures.

Figure 7.1 illustrates the need for high-sensitivity systems as the operating pressures are reduced. Straightforward double-exposure holographic interferograms are shown of a Mach 3 bullet in flight with various operating pressures in the flight chamber. The first picture shows operation at atmospheric pressure where an adequate number of fringes are available for even quantitative flow analysis. As the pressure is reduced, the number of fringes diminish until in the 6-mm Hg shot only a faint residual of a portion of the shock front is visible. The desired region of operation for certain simulations is nearly two orders of magnitude below the 6-mm shot. Thus, great gains in sensitivity over standard holographic interferometry are required.

The Capability of Holography for 1/100-Wave Fidelity

A basic question is whether holography is capable of reproducing waves with 1/100-wave accuracy. It is obvious from stored-beam or live-fringe holographic interferometry that a hologram is capable of fractional wavelength accuracy. A simple experiment can illustrate local wave fidelity far in excess of 1/100 wave in the reproduction of optical waves by a hologram.

Consider as subject for a hologram two points A and B, shown in figure 7.2. Point B is very dim compared to A and is displaced from A by a small angle. A reference beam is tacitly assumed.

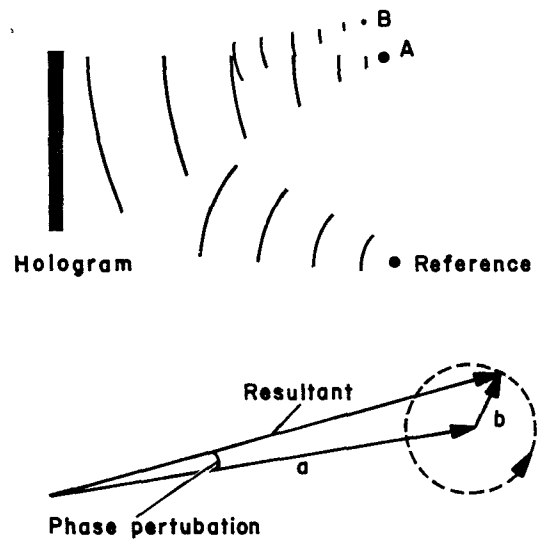

Figure 7.2 Configurations involved in an experimental measurement of a holographic wave front reconstruction fidelity

If one represents the electric field *at the hologram* from the point A by the phasor a and that from B by b in the figure, then the total subject field at the hologram is represented by the vector sum of these. Because of the small angular difference between points A and B, the small phasor b rotates slowly relative to a as one moves across the hologram, the resultant oscillating slightly in phase and amplitude relative to a. The magnitude of this phase perturbation caused by the point B is $\sqrt{I_B/I_A}$ rad and the relative fluctuation in amplitude is $\sqrt{I_B/I_A}$. Detailed consideration of the experimental results leads to the conclusion that the phase perturbation is at least as significant as the amplitude perturbation in forming the reconstructed image. Thus, the reconstructed image of point B is evidence of the hologram's ability to detect phases of $\sqrt{I_B/I_A}$ rad. Holograms were made with various intensity ratios between the two subject points B and A. Upon reconstruction, point B was still visible when its intensity was 10^{-6} that of point A, for which

the corresponding amplitude of the phase modulation was only 1/6000 wave. When the intensity of B was 10^{-7} that of A, its reconstruction was not visible to the unaided eye but could be made visible by the use of a telescope that increases the area of the hologram sampled.

We conclude from this simple experiment that holograms are easily capable of detecting 1/100-wave phase-shift information when the information is appropriately presented and when the sampling area is as large as the observer's eye pupil.[1]

Subfringe Interferometry

The principle of subfringe interferometry is simply to shift the phase of the subject beam 180° between the exposures of a regular double-exposure holographic interferogram.[2] The reconstruction reproduces the algebraic sum of the two exposing waves, and therefore should be a completely dark field except where the subject perturbation has upset the exact 180° relation. Thus, small subject perturbations make themselves visible as brightenings on the dark background.

The 6-mm shot of figure 7.1 is a sort of accidental subfringe interferogram in that some extraneous air current or motion created a near 180° phase shift in the portion of the scene where the shock is faintly visible.

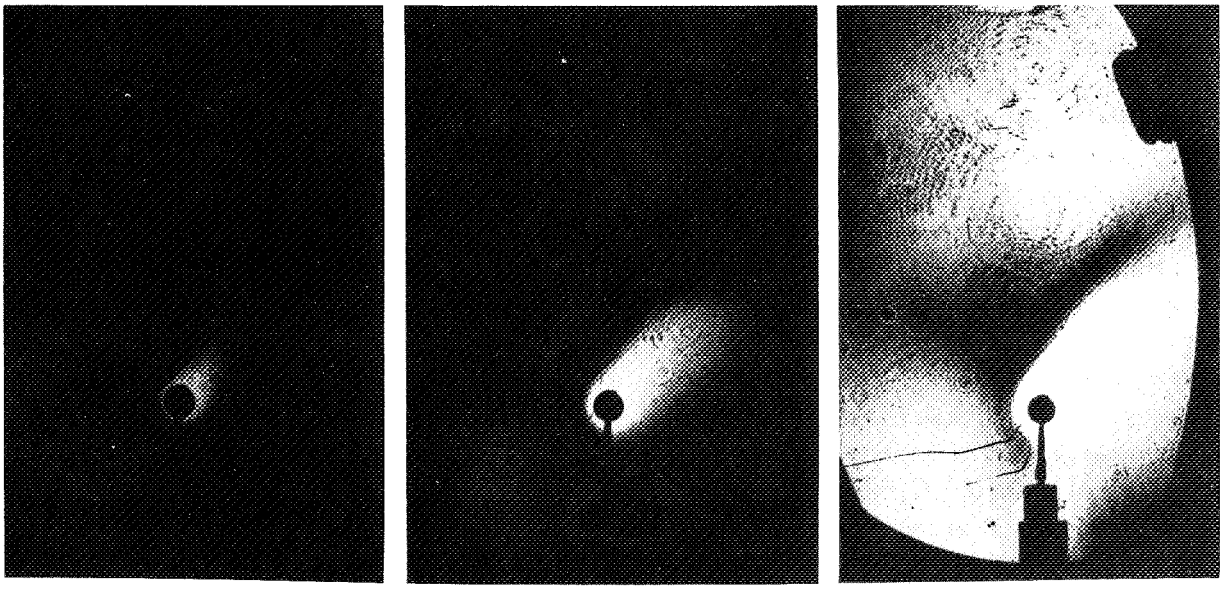

Figure 7.3 Subfringe interferogram of air surrounding a heated resistor. Path change at resistor is 1/3 wavelength, and copy exposures of 1, 5, and 20 sec show range of brightness of the holographic image

Figure 7.3 is an example of subfringe interferometry. The subject is a heated resistor, which creates a 1/3-wave change in optical path length in the air adjacent to the resistor. In the copy

[1] This experiment is also of interest in that it shows the dynamic range of hologram recording. The limit of 10^{-6} was the same whether subject A was a point source or a sizable ground glass. Note that the reconstruction output is not necessarily linear over this entire range.

[2] Detailed analysis shows that a phase shift slightly different from 180° produces maximum sensitivity, but this refinement will not be included here.

photographs, three different exposures were used to show the brightness range in the holographic reconstruction. It is estimated that perturbations at least as small as 1/10 wave are visible.

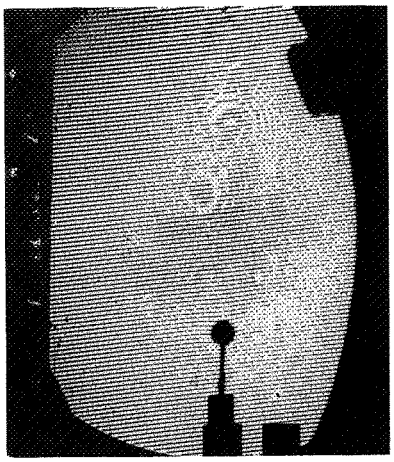

Figure 7.4 Finite fringe holographic interferogram of heated resistor

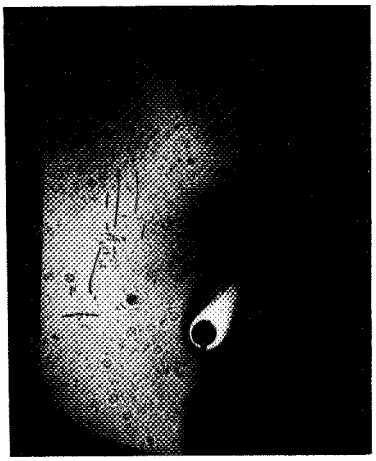

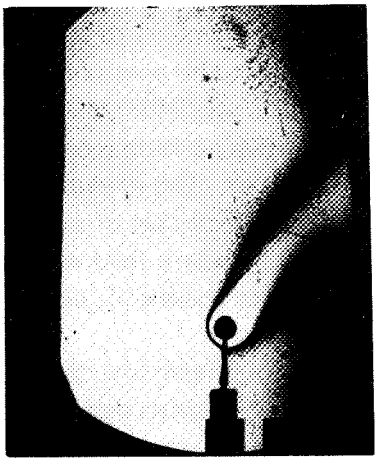

Figure 7.5 Subfringe interferogram of same heated resistor with slightly different background phase shift. Copy exposures are in ratio 1:4

For comparison, figure 7.4 shows the same subject viewed by a finite-fringe holographic interferogram. Examination shows 1/3-wave shift at the resistor.

Figure 7.5 shows another subfringe interferogram taken under nominally the same conditions. This photo shows two significant properties of subfringe interferometry. The first is the sharpness in terms of phase of the black interference fringe. The phase shift required to move from one side of the fringe to the other is less than 1/6 wave. This narrowing of the dark null stems from the high contrast of the holographic recording medium. A truly linear film characteristic would exhibit a broader null. This is a desirable effect, for it increases the phase sensitivity of subfringe interferometry. This null sharpening effect is expected to occur only when no diffuser is used in the subject beam, as is the case in the above pictures.

The second important property shown by figure 7.5 is the experimental difficulty of obtaining precise 180° phase shifts. The ultimate sensitivity of the system can be no better than the precision of the 180° phase shift. Moreover, nearly precise equality of the two exposures is also required for high sensitivity. This latter requirement is particularly difficult to satisfy with pulsed lasers. Figures 7.3 through 7.5 were made with a gas laser where exposure equality is easy to achieve but vibration and air currents make the phase shift uncertain.

Figure 7.6 shows another instructive and useful property of subfringe interferograms made without a diffusing screen; in this case, subject and reference were both collimated beams. Such a subfringe interferogram is essentially a diffraction grating wherever the subject phase shift has upset the 180° conditions. Where the subject is absent, the exposure is a uniform grey and thus does not diffract. Thus, by simply holding the hologram so it diffracts light from the overhead white lights, as shown in figure 7.6, one may observe the subject phase shifts.

Four-Beam Interferometry

An interferometer has been devised that theoretically reduces the phase shift and exposure equality requirements to second-order effects. By eliminating the precision required of these settings, the interferometer should be capable of more sensitive performance than the subfringe interferometer. The readout presentation appears similar to that of subfringe interferometry, namely, a dark field with brightening where subject phase shift exists.

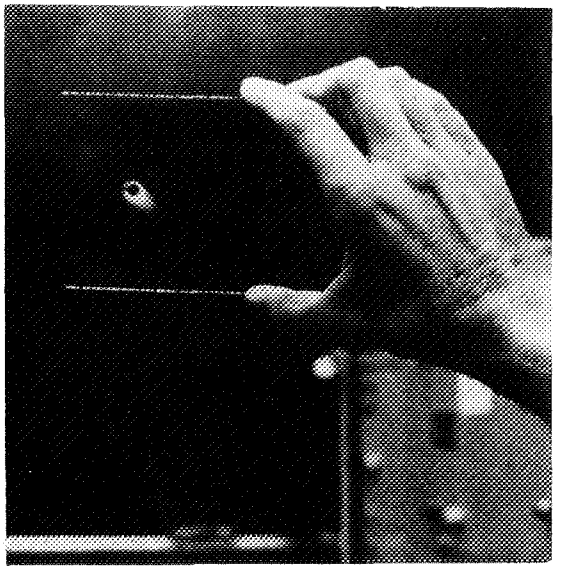

Figure 7.6 Readout of subfringe interferogram with overhead white lights

This four-beam interferometer is shown in figure 7.7. It consists essentially of subject and reference beams separated by a large angle. Both subject and reference beams are each composed of two beams, separated by the same small angle. At the hologram on the first exposure, these four beams produce a grating of fine fringes, intensity modulated at a low spatial frequency corresponding to the small angle. On the second exposure in the absence of a subject perturbation, a similar pattern of fine fringes is produced, but due to the 180° phase shift, the low-frequency intensity modulation is complementary to the intensity pattern of the first exposure in the sense that $\cos^2$ is complementary to $\sin^2$. Thus, in the absence of a subject perturbation, the two exposures result in nothing more than a uniformly exposed ($\sin^2 + \cos^2 = 1$), high-frequency grating.

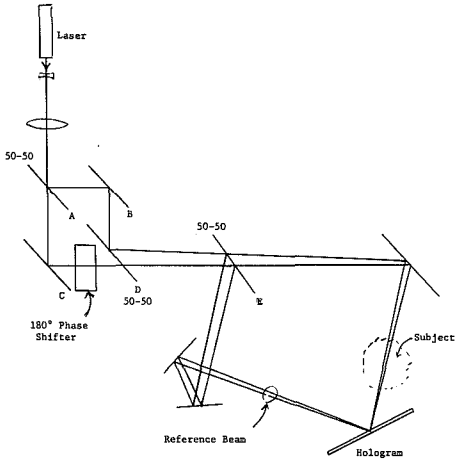

Figure 7.7 Four-beam interferometer

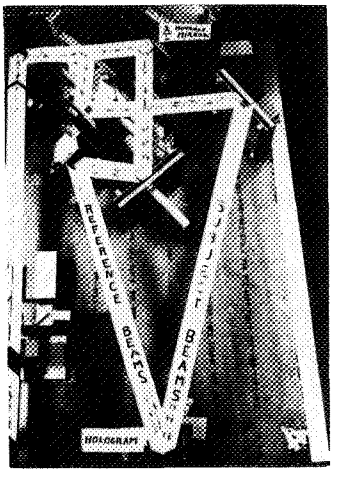

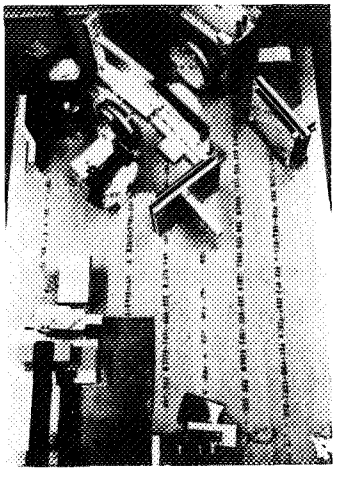

Figure 7.8 Test setup for four-beam interferometer

However, in regions where the subject perturbation has disturbed the phase on the second exposure, the resulting high-frequency grating produced by the two exposures will be phase-

modulated at the low spatial frequency with the peak-to-peak amplitude of the phase modulation equal to the subject phase perturbation. The intensity of the grating is still uniform.

The resulting hologram is illuminated with a single beam for readout. The high-frequency grating strongly diffracts light into what we shall call the primary order. Where the subject has introduced the phase modulation, side orders of diffracted light will appear at the small angle away from the primary order. The light of one of these side orders is selected by an aperture and constitutes the viewing light.

Figure 7.8 shows the experimental assembly with 6-in.-diameter optics used to test the concept, and figure 7.9 shows the readout of one of the holograms. The subject again is the heated resistor, but this time the perturbation at the surface of the resistor is only 1/6 wave. While the 1/6 wave is easily visible, it is far short of what we ultimately expect of the system.

Note the similarity between the structure of the hologram in this four-beam interferometer and the structure of the hologram in the tests used to see if holograms were basically capable of 1/100-wave sensitivity. Those tests were performed so as to bear a close relation to the four-beam interferometer and hence show the potential performance of the four-beam interferometer when all the practical problems are conquered. Readout of the sensitivity test holograms in the configuration of the four-beam readout yielded the same limits mentioned in the direct viewing tests above.

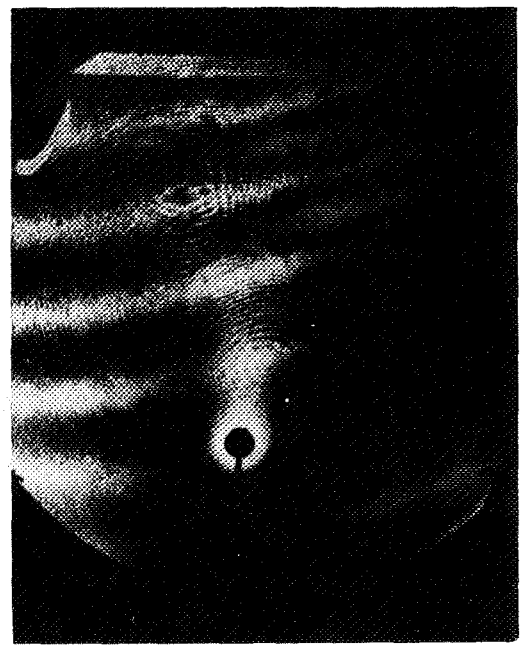

Figure 7.9 Readout of a four-beam interferogram. Phase shift due to resistor is 1/6 wavelength.

One practical problem evident in figure 7.9 is imperfect optics and alinement, which create the horizontal banding. In the absence of alinement to within 1/8 wave or so, it can be shown that the four-beam arrangement is not superior to the subfringe arrangement. Present optics do not permit such alinement.

Doubled Ruby Holographic Interferograms

A technique yielding a factor of 2 gain in sensitivity is simply to shorten the wavelength of light by running the output of the pulsed ruby laser through a doubling crystal. (See ref. 1 for a more complete description.) Figure 7.10 shows an interferogram made in this way. An interesting property is that two interferograms can be obtained simultaneously—one red and one in the near ultraviolet—by letting both the direct and doubled light fall on the hologram. These can be read out individually from the hologram. This technique may be applicable to the study of dispersive media.

Multipass Holographic Interferometer

Figure 7.11 shows a multipass holographic interferometer. To understand the operation of this interferometer, begin with the subject light passing to the right through the small lens. This subject arm light is brought to focus by the small lens, passes through the aperture, and is recollimated by the larger lens. The light then passes into the subject cavity th ɔugh the partial mirror where it undergoes many reflections and passes through the subject many times. On each reflection at the partial mirror, a fraction of the light exits the cavity and is brought to a focus at the aperture plate by the larger lens. However, because there is a small angle between the partial mirror and the end mirror, these focus spots are displaced at the aperture plate. The arrangement is adjusted so that as the pass number increases, the spots first move farther away from the entrance aperture, then they turn around and move closer to the entrance aperture with a selected pass—and only that one—falling back through the aperture. This selected pass is then recollimated by the small lens and used as the subject beam for a double-exposure holographic interferogram. In the arrangement shown, the reference beam for the hologram is displaced at a very small angle from the subject beam, permitting the use of high-speed films to compensate for the small fraction of light returning from the selected pass. The beamsplitter and reference arm mirrors achieve this small reference angle conveniently.

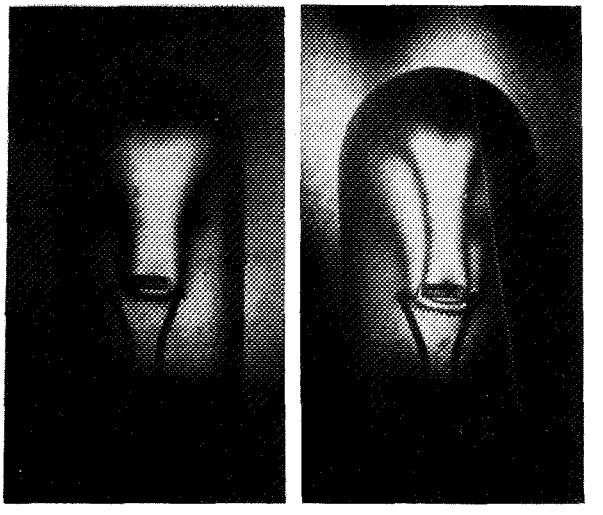

Figure 7.10 Simultaneous red and ultraviolet interferograms of heated filling gas of a lamp

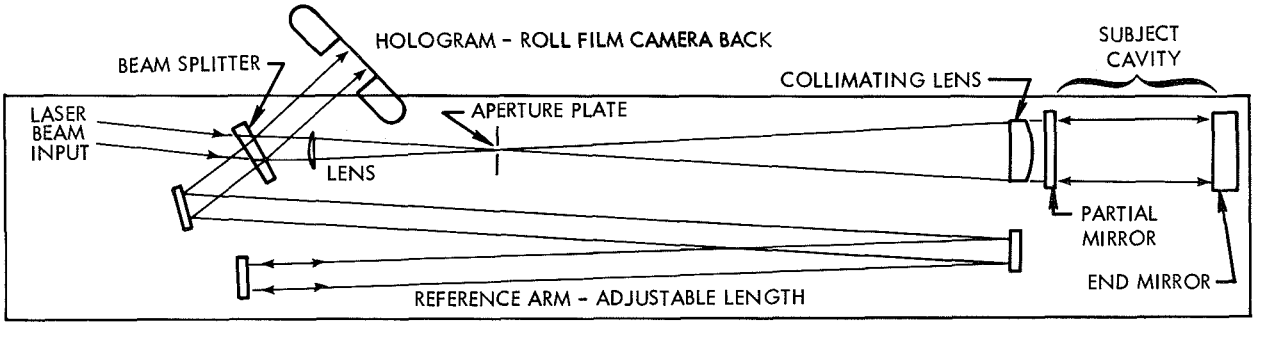

Figure 7.11 Multipass holographic interferometer

Note that because this is really a double-exposure holographic interferometer, it has self-compensation for imperfect optics. The optical quality is determined by the requirement that only the desired pass fall through the aperture, which still sets fair demands on quality. Figure 7.12 shows the quality of the optics used in the experiment. The photograph was made with 20 passes by adjusting the reference arm for zero offset.

Figure 7.13 shows the heated resistor at different temperature rises with 10 passes. A finger is shown in (f) and finite fringe presentations at 10 passes are shown in (g) and (h). The ultimate sensitivity of this technique is related to the required resolution at the subject because the beam walks sideways as it passes back and forth between the mirrors.

Another scheme utilizing coherence sorting rather than spatial sorting of the desired pass has been devised that does not suffer this resolution restriction. This scheme has not been tested.

High-Order Interferometry

Still another approach to increased phase sensitivity utilizes the fact that readout of a hologram in the nth order yields n times the phase sensitivity of first-order readout.

Figure 7.14 illustrates the basic principle. For example, a 1/10-wave phase shift will shift the position of the fringe lines by 1/10 d. Readout in the first order shown in (a) will yield just a 1/10-wave shift in the readout wave, whereas readout in the nth order shown in (b) will have a phase shift of n x 1/10 wave.

In order to use this principle in a self-compensating system so that perfect optics are not required, the following scheme has been devised and tried. The arrangement consists of equal strength collimated subject and reference beams impinging on the hologram at a very small angle. A first hologram is made of the empty scene with a very heavy exposure. Thus, the developed hologram consists of a grating of very narrow clear lines at the nulls of the interference pattern. A second hologram is made on a second photographic plate with the subject present. A kinematic jig is used to secure reproducibility of plate positions. A double-exposed contact print is made with one exposure from each of the developed holograms. The contact print is then illuminated with a collimated beam and read out in the nth order.

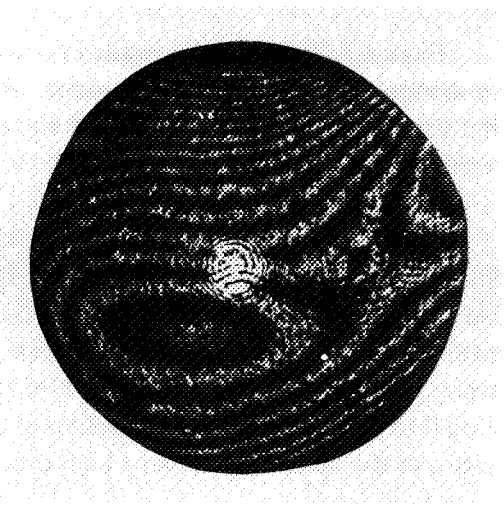

Figure 7.12 Interferogram showing optical quality of multipass interferometer

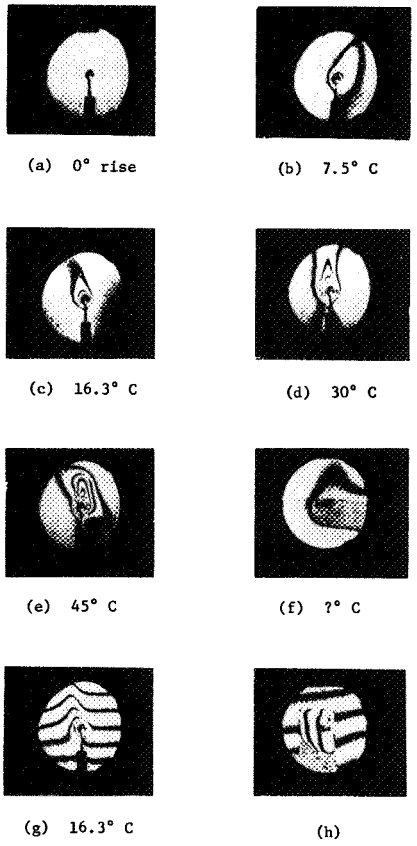

Figure 7.13 Examples of 10-pass operation of multipass interferometer

Figure 7.15 shows the result in which the subject is a wedge that entirely fills the scene. Readouts of first through fourth order show the expected increase in the number of fringe lines.

The results are not particularly encouraging. While in accompanying experiments light has been detected at the 100th order of special holographic gratings, the complexities of the process and the strong dependence on nonlinear emulsion properties (Kodalith plate was used) pose substantial difficulties in the actual use of very high orders.

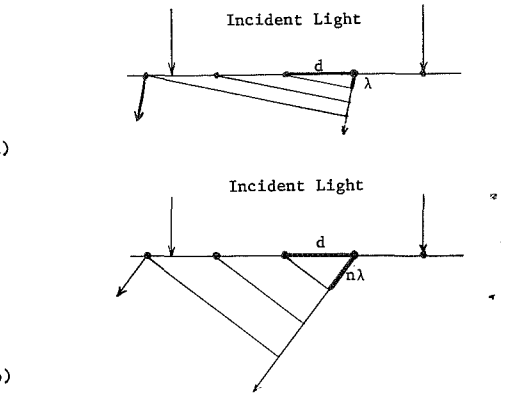

Figure 7.14 Principle of high-order interferometry

Double-Exposure Holographic Schlieren

Figure 7.6 illustrates a technique for double-exposure holographic schlieren that has been devised and given a cursory test. This double-exposure schlieren is self-compensating for optical imperfections in the subject path, in contrast to the more familiar single-exposure holographic recording of a schlieren output beam. Like the latter, the double-exposure technique permits adjustment of the knife edge during readout.

The recording steps are shown in figure 7.16 (a) with the subject and reference beams incident on the hologram. Note that were it to pass on through the hologram, the reference beam would converge to a point. The first exposure is shown by the solid lines. For the second exposure, the

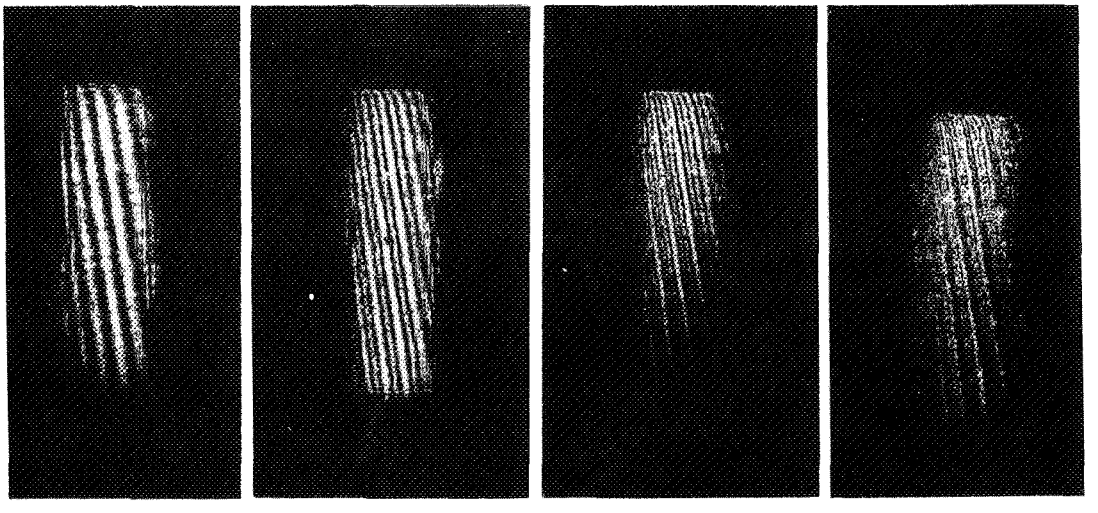

Figure 7.15 Readout of high-order interferogram in orders 1 through 4

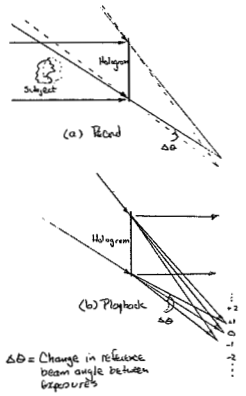

Figure 7.16 Process of double-exposure schlieren

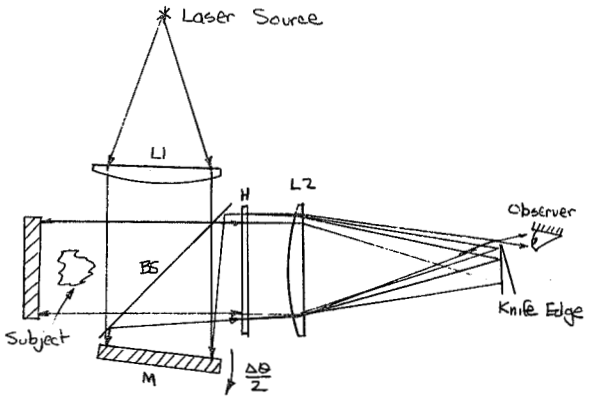

Figure 7.17 Configuration used for low-angle double-exposure schlieren tests

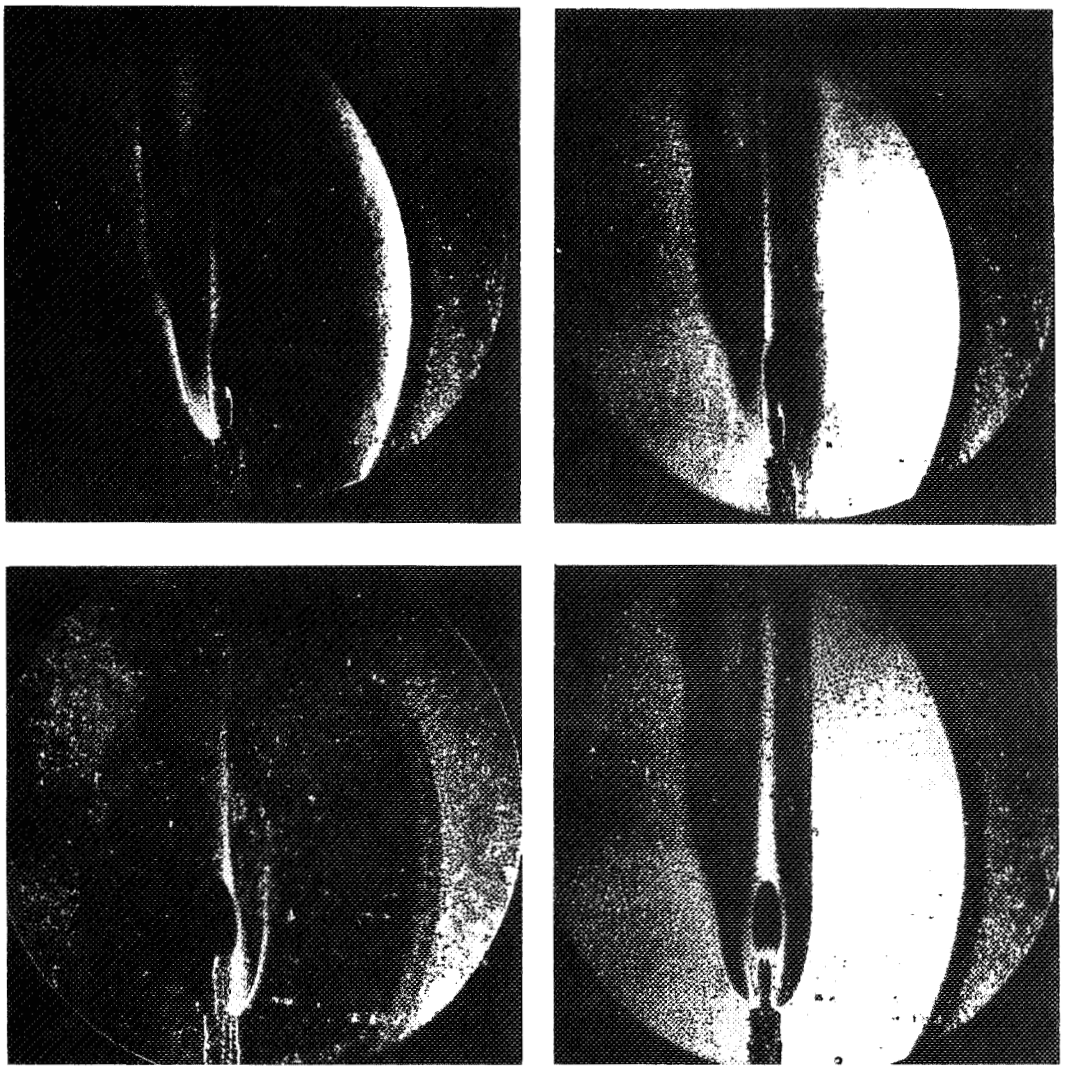

Figure 7.18 Double-exposure schlieren readout

subject perturbation is introduced and the reference beam direction is changed by a small angle as shown by the dotted lines.

After development the plate is read out as shown in figure 7.16 (b). The readout light source is focused to a point at 0 duplicating the reference beam; this also reconstructs the subject beam, but the reconstructed subject beam is not used. Reconstructed beams appear at the reference beam offset angle from the reconstruction beam. These beams arise from nonlinearities of the recording plate and carry the information about the subject perturbation in the manner of a conventional schlieren beam. One of these beams is used for schlieren viewing by inserting a knife edge at its focus.

Analysis indicates that it is only the subject perturbation that affects the readout beam. Thus, even the recording reference beams need not be perfect, so long as the imperfections are the same for the two exposures. This suggests the technique may be useful where recordings are made with imperfect pulsed lasers.

Because the technique depends on the nonlinear behavior of the emulsion, it was first tried in the narrow-angle configuration shown in figure 7.17. The readout is shown in figure 7.18 for different knife-edge settings. The upper and lower left-hand pictures show the expected schlieren asymmetry for the knife edge on opposite sides of the beam. However, there is much extraneous darkening of unknown origin in these pictures. It may be due to motion of the candle flame during exposure. This cursory test should not be regarded as an evaluation of the technique's potential.

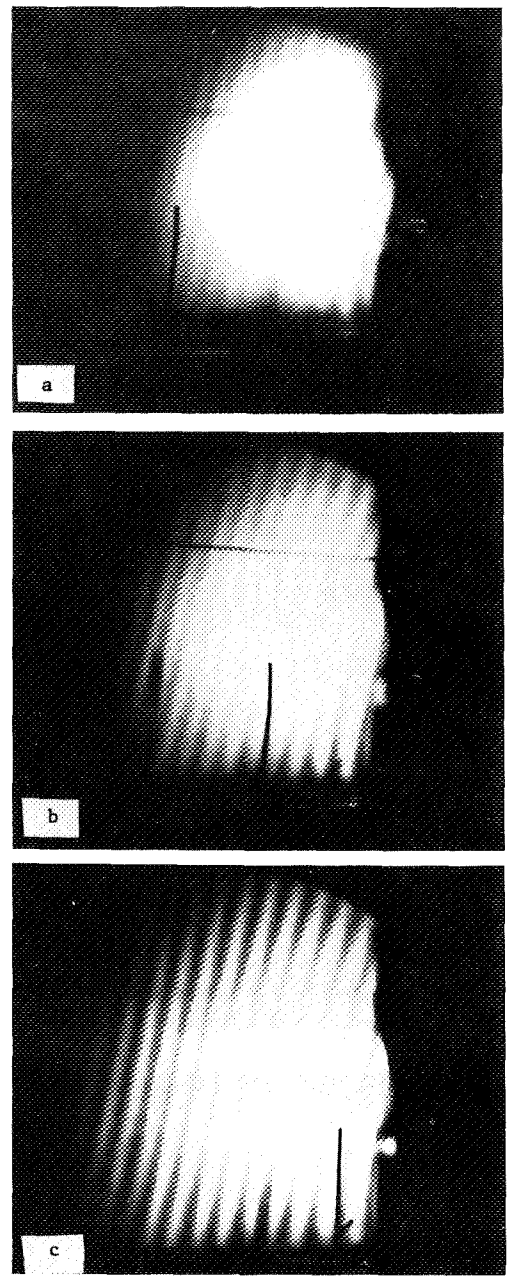

Figure 7.19 Test of placement of finite fringes

Finite Fringes in Three-Dimensional Interferometry

One of the most useful techniques in classical interferometry for the detection of small phase shifts is the finite-fringe technique wherein the subject causes a displacement of the background fringe grid. Because of the three-dimensional nature of holographic interferograms in which a ground glass is used behind the object, simple attempts to produce finite fringes usually result in the fringe grid appearing in some plane other than that of the subject. Thus, when the hologram is photographed, either the subject or fringe grid is out of focus.

To overcome this problem, a formula was derived that describes how the ground glass itself may be given a slight rotation about a specified point so that the finite-fringe grid will appear in the same plane as the subject. To verify the concept, a gas laser was used to make a hologram of three vertical wires spaced 1 in. apart in depth. Figure 7.19 shows three photographs of the holographic image with the camera focused successively on each wire. The fringes are located in the plane of the closest wire (c) and are progressively out of focus in (b) and (a).

An interesting possibility stemming from the three-dimensional nature of diffuse holographic interferograms is to develop a precision fringe-position measuring system operating directly on the holographic image. Because neither the diffuser nor the hologram is in the plane of the subject, the quality of the fringes at the subject should be very high and free from imperfections arising from dust, etc. Moreover, because the background fringes arise from the rotation of a rigid body and not from optical perfection, they can be extremely straight, permitting the detection of minute departures due to subject perturbations. The sensitivity possible should be set by the well-behaved statistics of laser granularity; the resolution, which sets the area over which one can average; and the permitted angular viewing aperture, which is set by the nature of the subject itself.

Viewing through Turbulent Boundary Layers

Another potential application of diffusely illuminated three-dimensional holographic interferograms is exemplified by viewing through turbulent boundary layers on the windows of tunnels. Essentially, the ground glass used to illuminate the subject provides light traversing the subject from many different directions. If the subject possesses sufficient axial symmetry that the interference patterns for different directions are effectively the same, then the interference patterns appear to

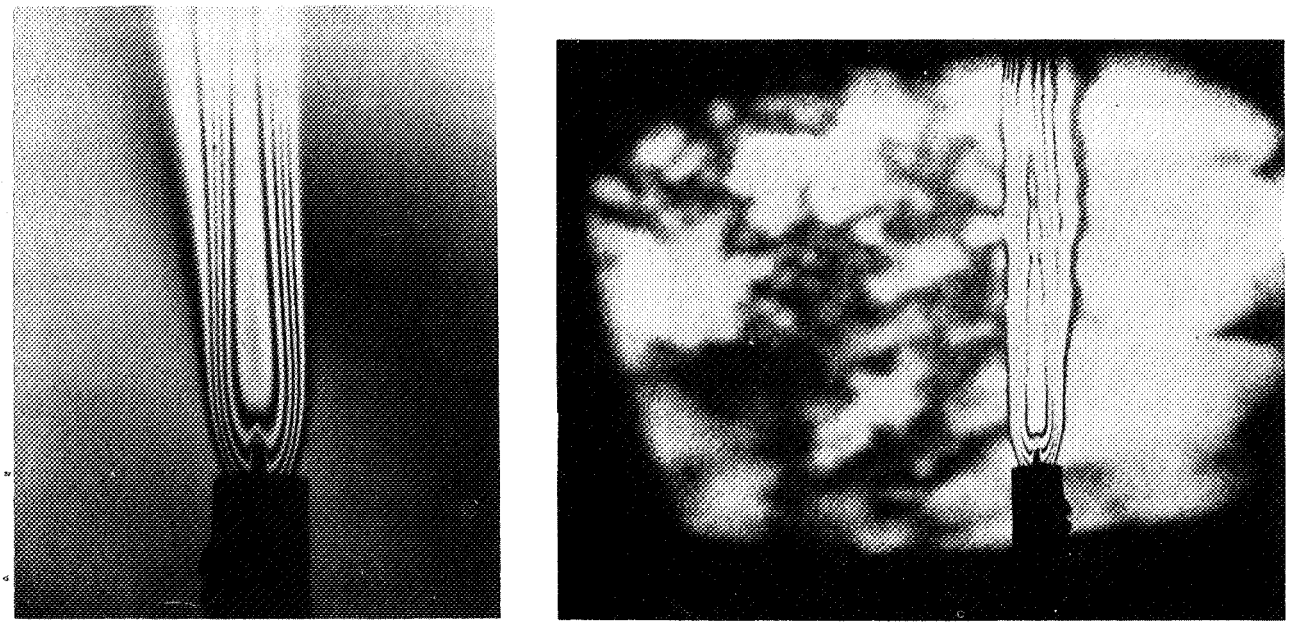

Figure 7.20 Interferogram of candle flame viewed through turbulent boundary layer with (a) wide aperture, and (b) narrow aperture showing boundary layer

focus at the center plane of the subject when viewed with a large-aperture lens. However, contributions from the boundary layer turbulence affect each direction of view in a different way. If a sufficiently large aperture is used so that a large sample of the random boundary layer is averaged, a true view of the subject interferogram is obtained. The effect of the turbulence is to reduce the contrast of the subject fringes but it does not displace them.

For a boundary layer giving a gaussian variation in boundary layer optical phase shift, the subject fringe visibility $(I_{max} - I_{min})/(I_{max} + I_{min})$ is given by $e^{-\sigma^2/2}$, where σ is the rms fluctuation of the boundary layer optical path in radians. The interpretation of this formula is that the technique is useful when the boundary fluctuations create less than one wave of optical path excursion, while for greater excursions the fringe contrast is too low to be useful.

Figure 7.20(a) shows an interferogram of a candle flame copied with a large-angle aperture ($\sim$f/4) so the boundary layer is averaged out and copied at a small aperture, figure 7.20 (b), f/45, so the boundary layer shows. For this hologram the boundary layer was created by a heat gun blowing through a plexiglas channel in front of the hologram.

FRONT-LIGHTED PULSED LASER HOLOGRAPHY AND HOLOGRAPHIC INTERFEROMETRY

Pulsed Laser Two-Frequency Contour Mapping

In the course of making front-lighted holograms, it was discovered that the ruby laser readily operates at two frequencies simultaneously. If operated with an output reflector consisting of a dielectric slab of proper thickness, this effect can be controlled and rendered useful for making range contour pictures (ref. 2).

Figure 7.21 (a) shows a range contour picture made from a single pulse of the ruby laser. The contour spacing of 23 mm is equal to the optical thickness of the resonant reflector. When the thickness of the reflector is decreased, the contour interval is shortened as is shown in figure 7.21(b)

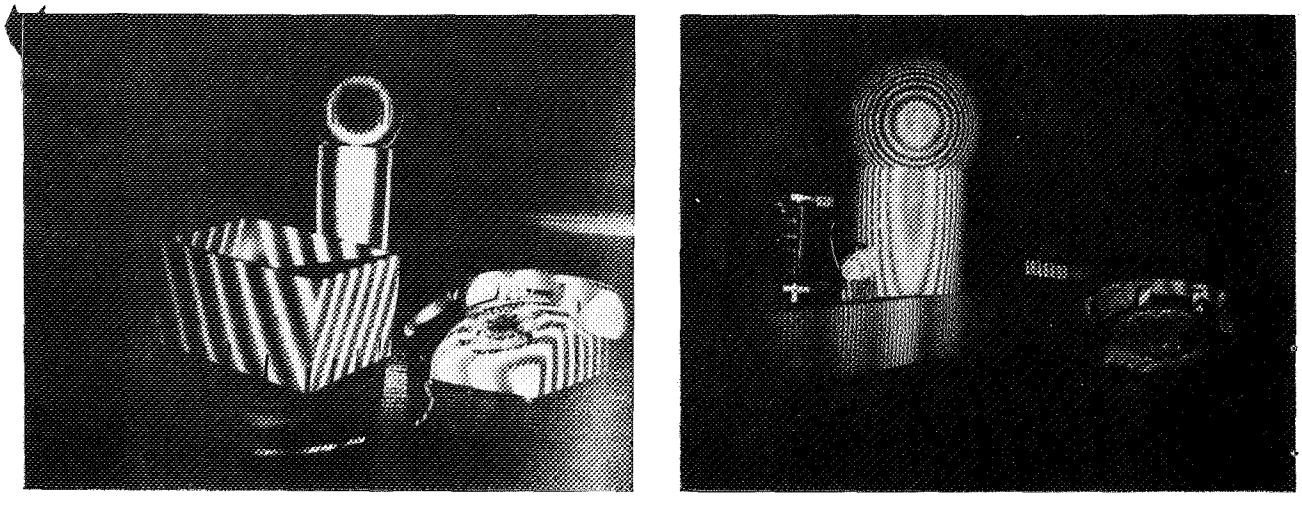

(a) (b)

Figure 7.21 Two-frequency pulsed ruby contour maps

where the contours are 8 mm. This technique appears to have application to such problems as the testing of large paraboloid antennas. Thus far, contours of about 1/2 cm and larger are producible.

One interpretation of the holographic image is that its intensity versus range is a pictorial presentation of the classical Michelson fringe visibility function and as such is useful in the study of the laser's spectral composition. Figure 7.22 illustrates a case in which more than two spectral components were operating, as revealed by the more complex intensity pattern.

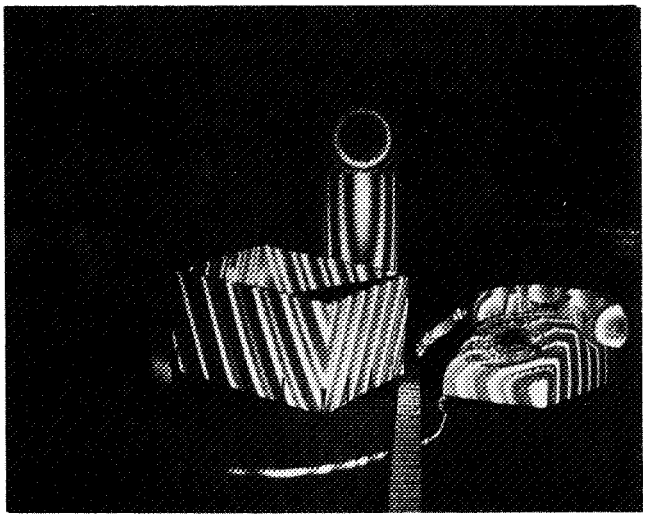

Figure 7.22 Multifrequency laser operation

Front-Lighted Pulsed Laser Interferometry

For unambiguous interpretation of holographic interferograms, the laser must operate at the same (single) frequency for each pulse. Otherwise, where optical path variations occur over the subject, the fringe pattern is created by both physical changes between pulses and optical path contours, since the production of two frequency contours is independent of whether the frequencies occur simultaneously or sequentially. This is a particularly severe requirement for front-illuminated subjects because of the large possible optical path variations.

Figure 7.23 shows single-frequency operation produced by the well-known dye cell Q-switching technique. The sloping 1.5- by 2-ft card would readily reveal multifrequency operation as contouring. Figure 7.24 shows double-exposure interferograms made with the same laser conditions as in figure 7.23. In figure 7.24 (a), one observes a basic 8-mm contour pattern distorted by the sagging of the cardboard between the two exposures. In figure 7.24 (b), the two frequencies produced on the successive exposures are much closer together but not necessarily identical, resulting in coarse contours distorted by the card sag. From such a picture, it is not possible to quantitatively unravel how the displacement fringes have been altered by the unknown frequency shift. The point to be emphasized here is that one should use care in the interpretation of front-lighted pulsed interferograms.

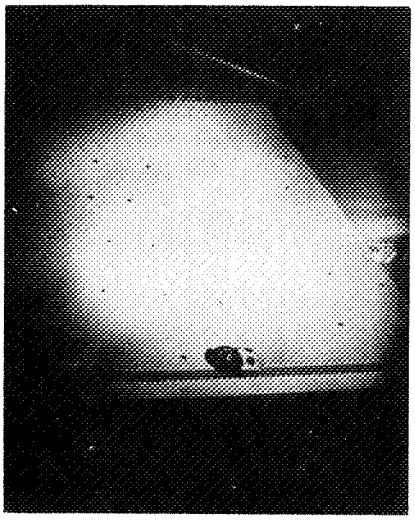

Figure 7.23 Single-frequency laser operation

ACKNOWLEDGMENT

R. F. Wuerker has been coinvestigator on several of the experiments

described in this report. In particular, he is largely responsible for the success of the techniques of doubled ruby interferometry, viewing through turbulent boundary layers, and pulsed laser contouring. Moreover, he has made valuable contributions in discussions of many of the other techniques. This work was sponsored by NASA-Ames under contract NAS 2-4992.

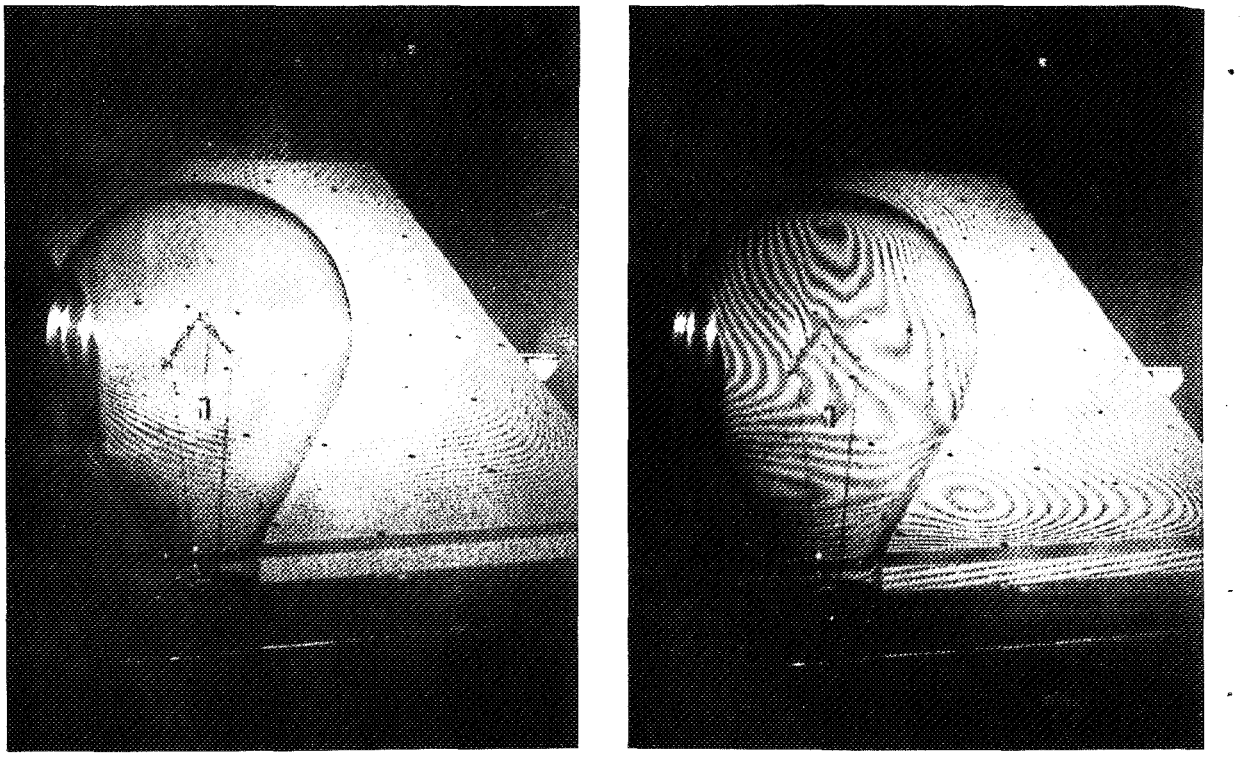

Figure 7.24 *Combination contour-displacement interferograms.*

REFERENCES

1. Wuerker, R. F.; Heflinger, L. O.; and Briones, R. A.: Holographic Interferometry with Ultraviolet Light. Appl. Phys. Ltrs., vol. 12, no. 9, May 1968, pp. 302–3.
2. Heflinger, L. O.; and Wuerker, R. F.: Holographic Contouring Via Multifrequency Lasers. Appl. Phys. Ltrs., vol. 15, no. 1, July 1969, pp. 28–30.

8 INVESTIGATION OF OPTICAL MEMORY TECHNIQUES

Albert A. Friesem and Howard N. Roberts
Electro Optics Center
Radiation, Incorporated

An investigation is under way of the feasibility of using holographic techniques for a read/write optical memory, having no moving parts, which is capable of storing 10^{10} to 10^{12} bits. The emphasis is to evaluate various holographic techniques and determine what storage material is most suitable. Other components of the system such as the input array, output detector, deflection and scanning systems, and light sources are also being explored. The results of these investigations should enable NASA personnel to determine the requirements for the storage materials and to specify the performance bounds of the system.

A number of techniques exist for implementing medium- to large-scale bulk data-storage systems. Some of these techniques are highly developed (for example, disks and cores) and are in commercial use; others (ferrites, integrated circuits, thin films, etc.) are under development and hold promise for future use in applications requiring small, high-speed memories. However, if the storage requirement exceeds 10^9 or so bits, the storage density and the interconnection problem of these memories become limiting factors, and it appears that only memories using optical techniques are feasible.

It has been known for some time that vast quantities of data can be stored through optical storage techniques using photosensitive materials. For example, it is conceivable that 10^8 bits of information could be stored on a square centimeter of high-resolution film. However, using conventional optical techniques at these storage densities requires, among other things, great precision in the readout optics, storage material with virtually no surface defects, and great care in the handling of the stored data, since dust and scratches could easily obscure portions of the recorded data. Thus, these conventional optical storage techniques have found little practical use.

Holographic storage techniques, on the other hand, can have the high storage capabilities associated with conventional optical techniques without the problems stated above. The advantages to be gained from the use of holography in optical memories are:

1. Each hologram, if properly illuminated, will project a real image, which can be detected without the use of imaging optics. Each hologram can be considered as storing jointly an array of data and possessing the optical properties of a high-powered magnifying lens.
2. A large number of holograms can be stored in such a way that the real image from each hologram will appear in a prescribed position. For the case where each hologram is read out separately, only one detector array is required and the need for mechanical transport of the stored data is eliminated.

3. Image resolution can be as good as the diffraction limit imposed by the size of the hologram. The aberrations that occur with magnifying lenses can be avoided in hologram imaging.
4. Since information stored in the hologram is not localized but can be unfocused, diffused, and distributed, the hologram record is relatively insensitive to dust or scratches. Distribution of the stored data implies redundancy and, with it, tolerance in registering a hologram with the readout beam.
5. The form of the hologram need bear no relation to the form of the stored data. Thus, the data can be stored at high density while the readout can have a relatively low density to alleviate the readin/readout array problems.
6. The hologram may be formed on nonabsorbing material without the necessity of using schlieren imaging techniques.
7. Holograms may be superimposed unambiguously by forming them in thick media, thus increasing the capacity of the memory.
8. The information stored can be three dimensional; phase and color information can be stored as well.

These are compelling reasons to study the possibility of using holographic techniques for an optical memory. However, full use of these advantages requires a careful system design since various holographic parameters must be carefully controlled to realize optimum performance.

The presentation that follows is an overall view of the optical memory system under investigation. The various components of the system are considered, and their influence on the behavior of the optical memory is described.

INVESTIGATION OF SYSTEMS CONCEPTS

One of the objectives of this study is to investigate system concepts and approaches useful for implementing a workable configuration of a 10^{10}- to 10^{12}-bit read/write memory. Although the main emphasis is to study potential read/write materials and various holographic recording techniques, these studies can be guided by an investigation of the overall system requirements that affect available tradeoff parameters. The parameters associated with both the input and output interfaces of this data-storage and -retrieval system are not completely defined. We can, however, analyze some of the system components to see how they influence the overall system design.

Figure 8.1 is a block diagram of a possible optical memory system, whose basic components are (1) the input interface, including a data composer, which converts an input electrical signal to an optical signal; (2) a read/write storage material; (3) devices used to deflect the reference, signal, reconstructing, and erasing beams; and (4) the output interface, which includes a detector array used to convert the optical signal from the memory to an electrical signal.

The Input Interface

A holographic memory with a rapid data-access capability can be designed by using a block data-transfer (or paging) configuration. In this case, the memory input format is a planar array containing 10^4 to 10^6 bits. The input data, which may originate from a number of primary sensors, may conceivably be incompatible with such a block format. It therefore is necessary to consider a buffer that organizes and temporarily stores the information for forming the block input. This

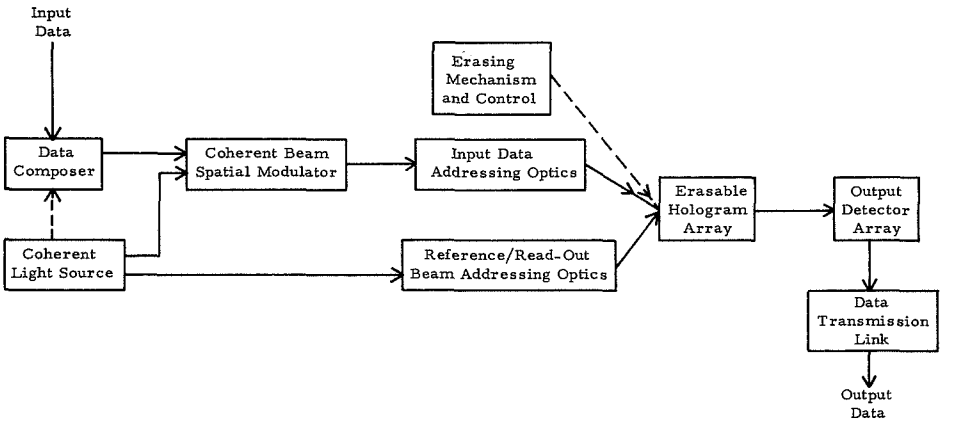

Figure 8.1 A system approach to the design of a high capacity erasable read/write holographic memory

information can then be rapidly transferred to the optical memory for storage. Since the characteristics of the incoming data are not known at this time, it is premature to discuss the details of the buffer store. For the moment, we shall assume that the input data originate with some sensor whose electrical output can be coupled to an x-y deflection system used to form the desired input to the optical memory.

The first step is to prepare the appropriate size data blocks for recording in the holographic storage subsystem. To do this, some means for spatially modulating a coherent beam of light with the information must be provided. The modulation can be in amplitude, phase, or polarization. In principle, continuous tone (analog) modulation is possible, but it is more likely that a binary (digital) coding will be used. We expect that in the final design the input format will be a planar array of bright and dark areas with the presence of a bright spot in a bit storage location indicating a "1" and the absence indicating a "0."

A number of materials can be used as a data composer component. Some possible configurations are described below.

Ferromagnetic materials. Curie point writing on thin ferromagnetic films (e.g., MnBi) is a candidate for spatially modulating light; a possible configuration is shown in figure 8.2(a). The data block is composed by scanning a focused light beam over the film surface. The light modulation is controlled by the data to be stored: a "1" would turn the beam on and a "0" would not. The intensity of the focused spot is adjusted to locally raise the temperature of the MnBi above the Curie temperature (360° C), altering the sense of the original magnetization of the material. Consequently, at these points, the polarization of a linearly polarized light beam transmitted through or reflected from the film is rotated relative to the remainder of the film. An analyzer is oriented to pass light from regions that were magnetically altered by the scanned light beam. The result is a spatially modulated light wave, which forms the block of data to be stored. The beam-scanning function can be accomplished with an x-y deflection device, and the beam modulation can be accomplished with standard optical and electronic hardware capable of 100 MHz bandwidths (electro-optic light modulators).

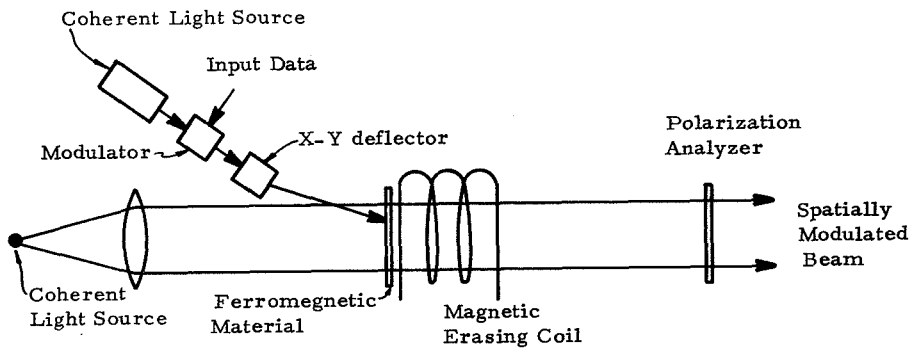

(a). Curie Point Writing on Thin Ferromagnetic Films.

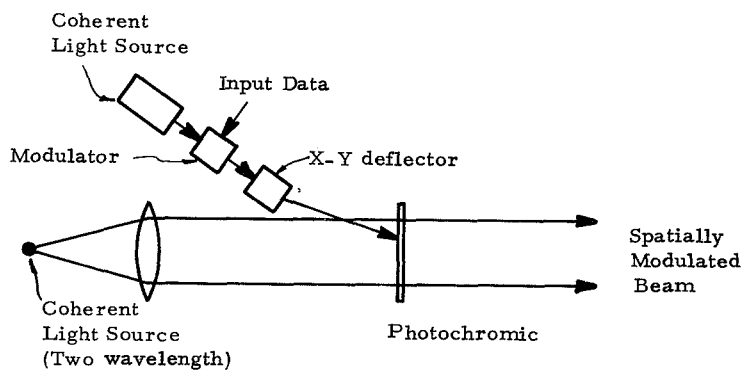

(b). Optical Density Variations Generated on a Photochromic.

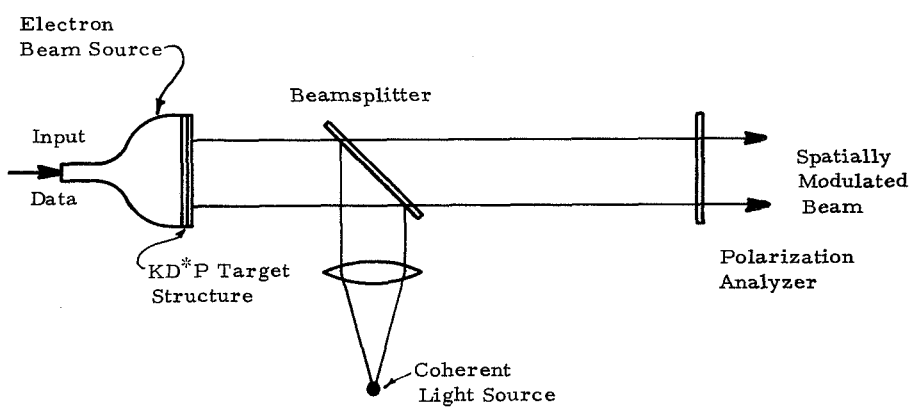

(c). Electron Beam Control of Polarization Rotation in KD*P.

Figure 8.2 Three possible schemes for composing data blocks and spatially modulating a coherent beam

The resolution of MnBi films can be as high as 1000 lines/mm, so that spot sizes could approach a few microns. Since the available input area will probably be 2 or 3 cm^2 for an input format of 10^6 bits, each bit will occupy a 25- x 25-μ region.

The MnBi film can be erased and used to prepare a subsequent block of data by applying a magnetic field of a few thousand Oersteds over the entire input area. Although localized erasure can be accomplished by applying a weaker field in the presence of a pulse of light at the position to be erased, we expect that block erasures will be used in the final design.

Photochromic materials. Photochromic materials change transmittance during an exposure and thus also can be used to form the data blocks for input to the hologram memory. Real time operation is then possible because this change in transmittance is concurrent with the exposure process so that no developing procedure is required. In addition, this change of transmittance can be reversed by illuminating the photochromic material with light of a different wavelength.

Figure 8.2(b) is an illustration of how such materials can be used as a data composer. The information is recorded on the photochromic material by a modulated scanning beam, which generates an array of transparent or opaque dots used as the input data to the optical memory. Since typical resolution values of photochromic materials are in excess of 3000 lines/mm, the expected 10^6-bit input array can be readily recorded in a 2- to 3-cm^2 area. The information stored in the data composer can be erased by illuminating the photochromic material with a uniform beam of a different wavelength; the data composition process can then be repeated.

KDP materials. The change in the indices of refraction of KDP or KD*P crystals as a function of the applied electric fields can be used to spatially modulate a beam. Figure 8.2(c) is a sketch of how such a device could be used in a data composer. The face of a cathode ray tube can be modified to permit a scanned electron beam to generate a pattern of charged spots, on the target layer, corresponding to all the "1"s in a binary data block. A thin layer of KDP or KD*P crystal is placed close to this charge pattern. The crystal orientation can be adjusted so that the changes induced in the refractive indices by the E field, due to the charge pattern, rotate the polarization of a light beam reflected from the KDP or KD*P. The electron beam, modulated by the incoming data, is scanned to generate charge deposits only in regions where a "1" is indicated. If the charge decay or "spreading" time constants are long compared to the interval required to write a data block and read it optically, this device performs as a spatial beam modulator when used with a polarization analyzer, as shown in figure 8.2(c). However, mosaics of KDP or KD*P crystals may be needed for successful implementation of this device.

Polarization rotation angles of a few degrees can be achieved in such a configuration. The charge decay and spreading effects place definite bounds on image persistence and resolution. These aspects must be examined in some detail to determine the usefulness of such a device in the system.

Comments. The schemes proposed for the input interface could have poor contrast, resulting in poor discrimination between "1" and "0." It is relatively easy to enhance the contrast by spatial frequency filtering if Fourier transform holograms are used; in fact, such enhancement is achieved

by using the nonlinearities of the recording film. Contrast enhancement is less easily obtained when Fresnel holograms are used, although the recording scheme can be modified to include it.

Other factors that must be examined in a more detailed evaluation of input interface systems include (1) the light efficiency of the modulating device and the power level required to modulate the beam; (2) the cycling rates and the total number of cycles possible; (3) the electrical drive level requirements (powers and voltages); (4) the hold times of a stored bit and required refreshing rates (if needed); (5) the optical dispersion effects if wavelength changes are used in the holographic storage scheme; and (6) the physical dimensions and the layout of optical and electrical components.

The Beam-Deflecting Functions

Laser beams must be deflected at several places in the system. The beam deflecting schemes may have to operate at several wavelengths and over a wide range of beam intensities. For either the data composer or the holographic storage media, the number of randomly accessible positions will be in the 10^4 to 10^6 range over a two-dimensional format. If the angular sensitivity of a thick holographic storage medium is used to increase the storage capacity of the memory, beams must arrive at each hologram location with several controllable incident angles.

Laser-beam-deflection techniques pertinent to this application will probably involve electro-optic or acousto-optic approaches or both. Both approaches require random access times of the order of 0.1 to 10 μsec for deflection to any one of 10^4 to 10^6 accessible positions in a two-dimensional format.

Electro-optical deflection schemes typically require an electronic driver capable of supplying a programmed set of high voltage (1 to 60 kV) pulses. Random access rates are limited primarily by heating effects in the crystals due to the power required to switch the crystals. Acousto-optic deflection schemes require radio frequency signals in the 15- to 150-MHz range at 1- to 5-W power levels. Random access rates are limited by the time required for an acoustic wave to propagate across the optical aperture of the device, and the ultimate resolution (number of resolvable positions that can be accessed) is limited by the aperture size or the permitted radio frequency drive bandwidth.

When acousto-optic deflectors are used for positioning both the reference and signal beams, the deleterious effect of frequency shifts introduced by the traveling acoustic waves must be eliminated. If a large enough frequency difference exists, the intersecting beams at the holographic storage location will not form a sharp hologram. However, if the required exposure time is a small fraction of the difference frequency period, a sharp hologram can be formed.

A beam-deflection system may also be required if, for example, a photochromic data-storage material is used, and the local erasing is accomplished by absorption of ultraviolet energy. There are electro-optic and acousto-optic materials that operate at ultraviolet wavelengths.

There are other problem areas of concern in studying beam-deflection devices for holographic optical memories. For example, it may be necessary to design deflection devices to accommodate

several laser wavelengths. For the electro-optic devices, some compensation can be made by changing the drive voltages. For acousto-optic devices using Bragg diffraction, more complex adjustments are necessary to compensate for the effects of wavelength variations. Also, more complex deflection devices will be needed to take advantage of the high angular and wavelength selectivity of thick storage materials. For example, a beam-translation device must be added to an x-y angular deflector to provide variation in angle of arrival at each hologram position.

Other parameters that must be considered are the stability and positional repeatability of the deflected beams, light efficiencies, power consumption, and thermal dissipation in the interacting material.

The Holographic Storage Format

For the optical memory under consideration, we have confined the investigation to two basic hologram formats: Fresnel and Fourier transform holograms. The latter has the advantage of requiring less space-bandwidth product for the recording medium, and it generates less aberration in the readout wavefront; to offset these advantages are the more severe effects of the film nonlinearities. Before discussing the properties of these basic holograms in detail, it is instructive to consider some possible configurations and determine their effect on other components of the system, especially the beam-deflection components. Figure 8.3(a) illustrates a scheme to store and retrieve near Fourier transform hologram arrays. An angularly deflected beam acts as both the reference and readout beam with appropriate shutters (not shown) permitting the desired mode of operation. The retrieved data are projected toward the input data array, but the beamsplitter directs a fraction of this energy toward an array of output detectors. A similar scheme for storing and retrieving diffusely illuminated (Fresnel) holograms is depicted in figure 8.3(b). Figure 8.3(c) shows a combination of translation (electro-optic) and angular (either electro-optic or acousto-optic) beam deflectors. This combination can produce changes in the angle of arrival of the reference or the readout beam at the hologram array for angularly sensitive storage. A multiple-wavelength-sensitive readin and readout can be accomplished with such an arrangement.

The Light Sources

One or more monochromatic light sources will be required to store and retrieve the blocks of data in the hologram memory. A separate source might be needed if an optical modulating scheme is used to compose data blocks. Another light source might be required for the erasing function. The data readout illumination will probably be derived from the source used to record the corresponding data block, but means of adjusting the power level of the readout beam may be needed.

The specific characteristics required of these light sources depend on other system parameters, such as the sensitivities and efficiencies of the page composer, the beam-deflecting devices, the hologram material, and the output detector. If wavelength selectivity is used for holographic storage on a thick medium, laser lines must be sufficiently spaced in wavelength to avoid intermodulation effects; an electrically tunable laser would be highly desirable. The degree of temporal and spatial coherence required to permit full use of the space-bandwidth product and dynamic range available from any storage material must also be considered. The choice of pulsed, CW, or hybrid modes of operation must also be considered. Several other factors are involved in determining a source

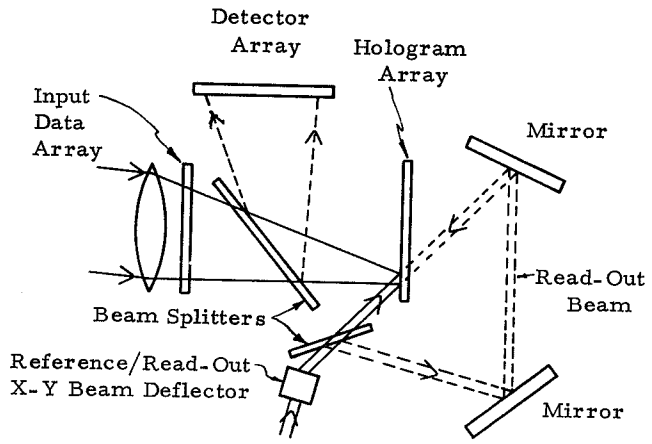

(a). Planar Fourier Transform Hologram Read-In/Read-Out Scheme.

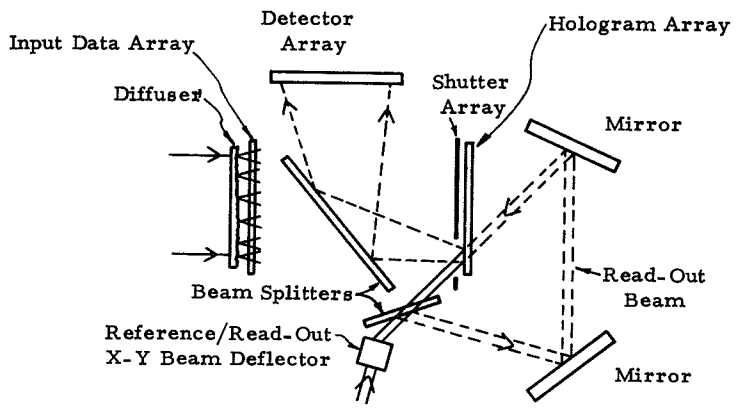

(b). Planar Fresnel Hologram Read-In/Read-Out Scheme.

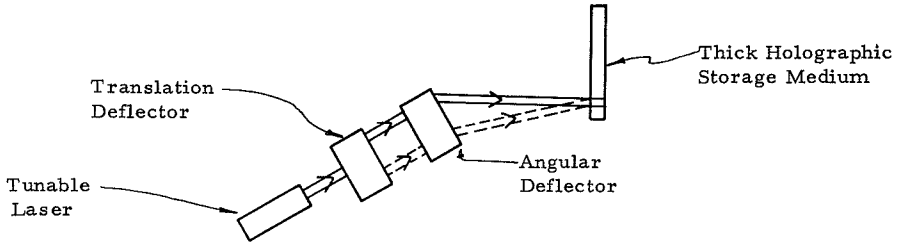

(c). Scheme for Generating Several Incident Angles at Each Storage Location at Several Wavelengths.

Figure 8.3 Possible deflection schemes for storing and retrieving holographic data

suitable for the optical system; these include the electrical (or chemical)-to-optical conversion efficiencies, and wavelength and intensity stability.

The Readout Detector

The readout function also influences the system design. The size of each stored block of data must be matched to the dimensions and resolution of the output detector (or detectors). The intensity of the beam projected from each hologram must be sufficient to permit positive detection at each bit location in the detector. The signal-to-noise ratio (S/N) in the projected image of each block of data must be consistent with permitted error rates. The detectors must respond to all wavelengths used for readout, and their read rates must be consistent with the capacity of any subsequent system such as a data-link computer. If in the readout the data array is erroneously displaced by a significant fraction of a bit dimension, a preread positioning code may have to be supplied in the image from each stored hologram to calibrate the absolute position of each image.

A typical vidicon will respond to about 10^{12} photons/sec/cm^2 with a S/N of about unity. Suppose that each bit is 0.1 mm x 0.1 and that 10^5 bit locations are distributed uniformly over the vidicon face with roughly half on and half off. Then each bit requires 10^8 photons/sec/bit to render it detectable at S/N = 1. With a 0.5 duty cycle, this calls for 5×10^{12} photons/sec/hologram. If $\lambda = 5000$ Å, the energy per photon is $E_p = 4 \times 10^{-19}$ J photon. Then the minimum required power level of the readout beam, for an assumed diffraction efficiency of 10^{-2}, is $P = 40 \times 10^{-6}$ (W/hologram).

Laboratory measurements indicate that this estimate is of the right order of magnitude. For a 10^5-bit image array and a more reasonable S/N, the readout beam power level should be closer to 1 mW. Lower diffraction efficiencies can be offset by increasing the incident laser power level or employing a more sensitive detecting device.

Other potential detectors include a vidicon with a silicon target, an array of photodiodes, or an array of phototransistors. The silicon-vidicon tube offers the prospect of a space-bandwidth product of 10^6, but it is limited to one readout channel and, therefore, to relatively low readout rates unless multiple electron beams are used. Planar arrays of photodiodes permit simultaneous interrogation of all output positions (multichannel outputs), thus offering the potential for much higher readout rates. Phototransistor arrays offer multichannel readout plus memory capabilities that can permit the array to function as an output buffer.

HOLOGRAPHIC STORAGE MATERIALS AND TECHNIQUES

Several kinds of materials are potential candidates for the erasable storage medium. These include photochromics, lithium niobate and similar crystals exhibiting refractive index changes in response to strong optical fields, photoplastics, and ferromagnetic materials. The required laser output power levels and wavelengths for readin and readout will be determined in part by the sensitivities of these materials and by their holographic diffraction efficiencies. The physical dimensions of the storage medium will be determined primarily by the resolution of the material (space-bandwidth products) and allowed geometrical factors (thickness). The recording linearity and the light-scattering property of the material will affect the S/N of the readout data. The useful life of

the entire system will be determined in part by the available number of write/read/erase cycles. The length of time the data can be stored in the material will affect the rate at which it must be retrieved and relayed to more permanent ground-based data-storage terminals. The effects of some of the above properties on the performance of the optical memory with conventional recording media are being examined; photochromics, lithium niobate crystals, and manganese bismuth also are being investigated.

The error rates that can be achieved with any holographic storage material must be established as a basis for determining the usable capacity of the system. We performed a theoretical analysis of the error rates in a holographic memory system with photographic film as the recording medium. To facilitate the study of this problem, it has been assumed that (1) the noise samples from the scattering of the granular structures of the film are statistically independent Gaussian random vectors; and (2) the noise is coherently additive. From such a model, the error rates have been calculated for a holographic system as a function of S/N and input data formats. We found that the storage capacity is limited by the S/N needed to achieve a certain error rate. For example, for an error rate of 8.6×10^{-7} and S/N of 100, the storage capacity is 3.5×10^5 bits/mm^2. Error-correction codes are being investigated as a means of improving these rates.

Two-Dimensional Recording Materials

Two-dimensional recording materials are simpler than three-dimensional materials in two respects: the analysis of their behavior, and their utilization in a system. For both reasons, a system based on storage in only two dimensions can be realized more readily in the near future.

The storage format in a two-dimensional medium is fairly straightforward. Each data block will likely be stored as a Fresnel or a Fourier transform hologram. The factors that should be determined for any particular system are the spatial extent of each hologram, the spatial-frequency range to be accommodated, and the number of overlapping holograms present on any region of the material. Also, the manner of division of the material into blocks corresponding to the various beam deflection positions must be examined. The format is determined by such factors as the dynamic range of the material and the capabilities of the record and deflection systems.

We are investigating holographic data storage in a series of experiments in which digital data are recorded (regularly and randomly spaced array of transparent dots in a black background) in both Fourier transform and Fresnel holograms. The holograms were recorded on conventional photosensitive emulsions and dichromated gelatin materials. The emphasis in the experiments is on determining (1) the best format of the digital data, (2) the effects of nonlinearities due to the recording media, and (3) the noise level in the reconstructed image.

We recorded Fresnel holograms with various reference-to-signal beam ratios to determine the effects of the nonlinearities in the recording material on the reconstructed image. The noise level, as well as its form, depends on the number of active elements in the digital data, the duty cycle, and the severity of the nonlinearity. It was observed that the noise due to the nonlinearity of the recording medium generally decreases as the number of active elements in the data increases. Using a vidicon and an oscilloscope, we estimated a S/N of 12 for the reconstructed image of a 1.6×10^5

array; this value is close to that predicted by theory. When the Fresnel holograms of the digital data are recorded on dichromated gelatin plate, the diffraction efficiency of the holograms is improved significantly. However, the noise level also increases as the diffraction efficiency of the hologram increases. No significant change in the noise level was noted when a jittered array was used in place of the regular array as an input signal for Fresnel holograms. For the Fourier transform type holograms, an improvement in the S/N was noted for the jittered array. This result is expected because such an array produces a more uniform spectrum, thus reducing the effects of the nonlinearity of the recording film.

An example of the effect of hologram aperture size on the S/N for Fresnel type holograms is shown in figure 8.4. The various photographs depict the reconstructed image of a binary signal of

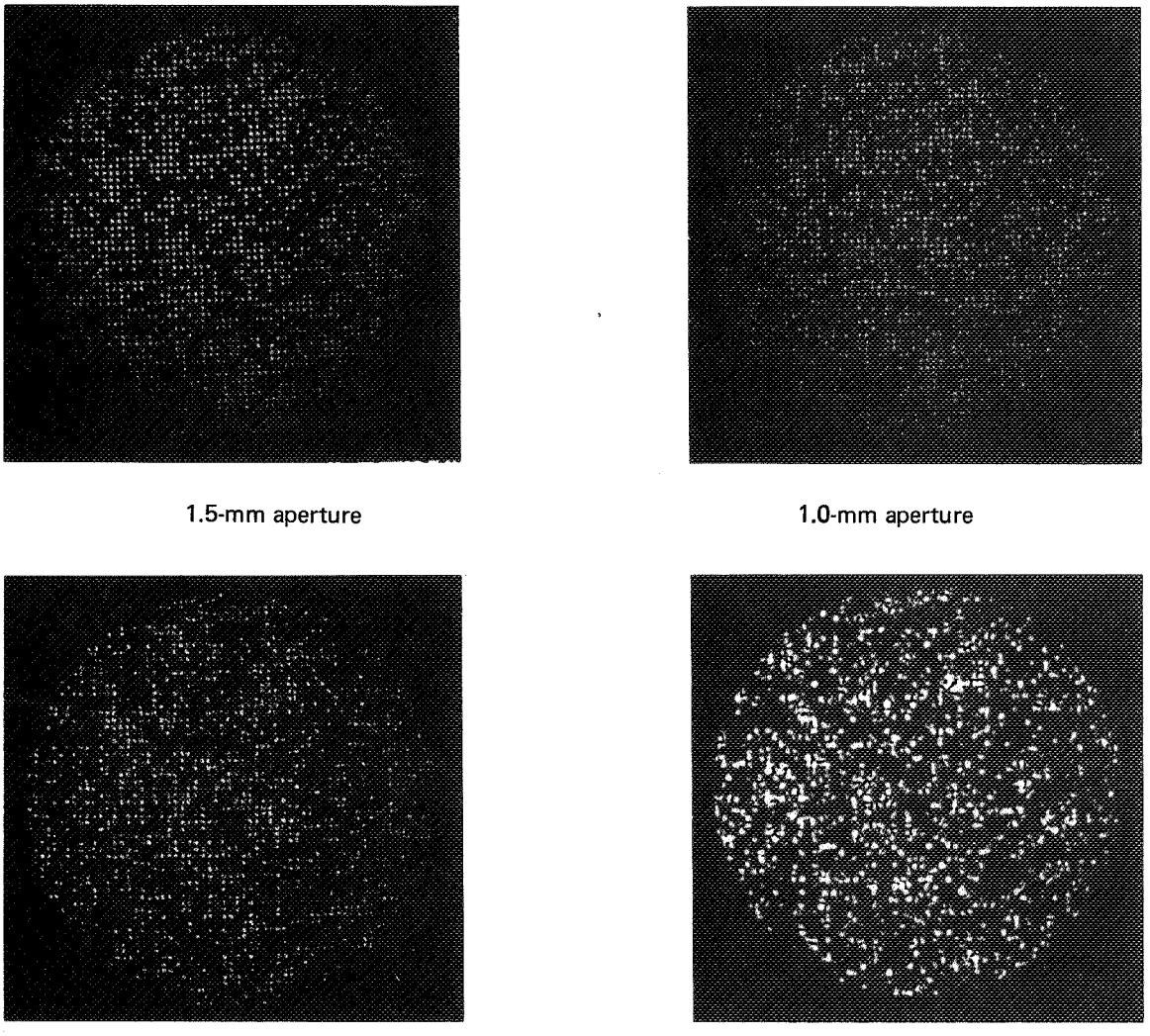

1.5-mm aperture

1.0-mm aperture

0.5-mm aperture

0.2-mm aperture

Figure 8.4 Magnified reconstructed images of 10^4 bits from a Fresnel type hologram showing the effect of aperture size on resolution and noise

10^4 bits, with four different hologram aperture sizes. As expected, the reconstructed image is best with a large aperture, but acceptable results are achieved with an aperture of only 0.5 mm. This aperture is approximately twice the theoretical value, which was found by using the following calculations. The minimum hologram aperture, A, required to resolve the bits equals $2\lambda z\nu$, where λ = 6328 Å; z, the distance between object and hologram, was 50 mm; and the spatial frequency, ν, was 4 lines/mm for the array of 10^4 bits. From these parameters, we find that the minimum hologram aperture is 0.24 mm. A redundancy of 2 or greater is required for a reasonable signal-to-noise level in the reconstructed image.

Three-Dimensional Recording Media

Holograms recorded in three-dimensional media have distinctive properties when compared with conventional planar holograms: (1) the inherent high angular and wavelength sensitivities provide high data storage capabilities, and (2) appropriate choice of thickness allows high diffraction efficiencies. The interference effects are recorded as surfaces within the recording medium forming, in effect, a three-dimensional grating. The diffraction process from such a structure is analogous to X-ray diffraction from crystals, and it is being studied in this context to determine the response of simple hologram gratings. These studies provide information about diffraction efficiency, as well as angular orientation and wavelength sensitivities of thick holograms.

A variety of three-dimensional recording media are under investigation, including thick photographic emulsions, lithium niobate crystals, and photochromic materials. The last two offer particular advantages in data storage because of their relatively high thicknesses and excellent resolution capabilities. For example, a 1-cm cube of photochromic glass or lithium niobate crystal with resolution elements of 1/3000 mm contains 27×10^{12} resolution cells. The major problem is how to effectively utilize all or most of these cells.

The wavelength or the direction of incidence of the readout beam may be varied with a corresponding change in diffraction intensity from a hologram. Both of these parameters therefore can be effectively used to construct a hologram that stores a great multiplicity of images, each stored uniformly throughout the recording medium and separately reconstructable.

An illustration of the excellent angular discrimination capabilities for photochromic materials is shown in figure 8.5, where three photographs depict a representative sample of the reconstructed images from a multiple-exposed hologram. One hundred relatively complex diffraction patterns were recorded in this hologram. The patterns resulted from the interference between the plane wave of the reference beam and complex waves from the signal beam. A sequence of 100 diffusely illuminated transparencies was used as objects, each having a bandwidth of approximately 150 lines/mm. Exposure times for each recording ranged from 2 to 3 min, and angular orientation (between reference beam and hologram) was changed by 4 min of arc to separate each recording. Finally, the reconstructed image of each recording was investigated. The three shown in figure 8.5 are the 61st, 62d, and 63d reconstructed images. There is very little, if any, interaction between recordings.

We performed an experiment to demonstrate the effectiveness of holographically storing a multiplicity of signals in thick material by means of wavelength variation. The illumination source

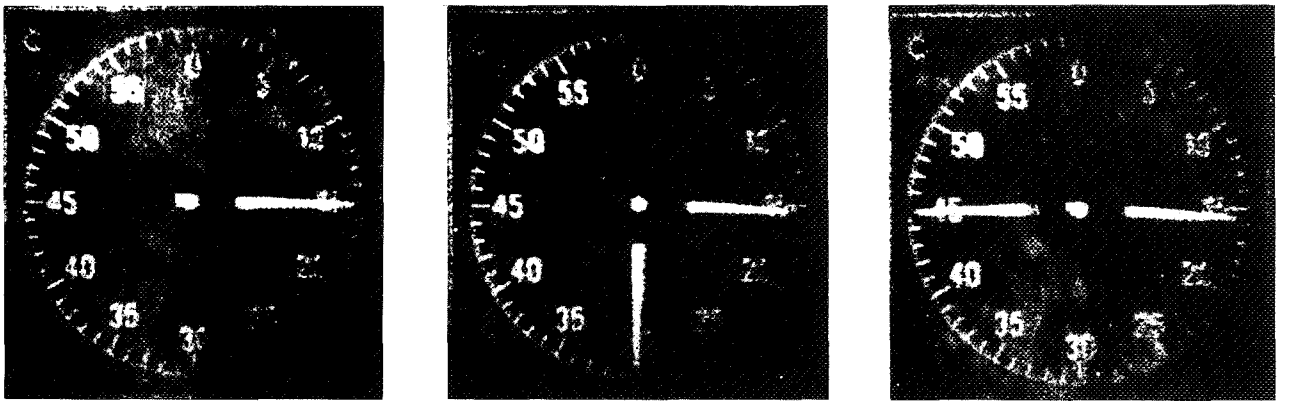

(a) Image from Sixty-First Recording

(b) Image from Sixty-Second Recording

(c) Image from Sixty-Third Recording

Figure 8.5 Reconstructed images from a multiple-exposure hologram of 100 recordings illustrating angular discrimination capabilities. Angular separation between each recorded image is 4 min of arc

was an argon laser with a wavelength selector that incorporates a convenient adjustment for obtaining five discrete wavelengths from the laser.

Figure 8.6 shows the five different 35-mm photographic transparencies that served as input signals. Each of the signals was diffusely illuminated with a different wavelength (λ_1 = 4579 Å, λ_2 = 4765 Å, λ_3 = 4880 Å, λ_4 = 4965 Å, λ_5 = 5145 Å) and holographically recorded in a silver halide photochormic glass ($\approx$ 1600 μ thick). Five superimposed recordings were made sequentially and arranged so that on reconstruction, each image was formed in the same location.

The composite hologram was then illuminated successively with five collinear reconstructing beams, each of a different wavelength (as in recording). Two examples of the reconstructed imagery are shown in figure 8.7. These images are of high quality and, if the recording and readout arrangements are identical, each can be observed only when it is illuminated by the same wavelength that was used in recording it. The ghost images and attendant detrimental effects are completely suppressed by the effect of the thick recording medium. For comparison, the same experimental setup was used to construct a similar composite hologram with relatively thin photographic plates (6 μ thick). As shown in the two photographs of figure 8.8, each reconstructed image contains four spurious images. These defocused images overlap the desired image, producing a relatively poor reconstruction.

ACKNOWLEDGMENTS

This work was sponsored by NASA-ERC under contract NAS12-2200. Other contributors to this program are A. Kozma, A. Vander Lugt, W. H. Lee and M. O. Greer. Additional sources of information are provided in the bibliography.

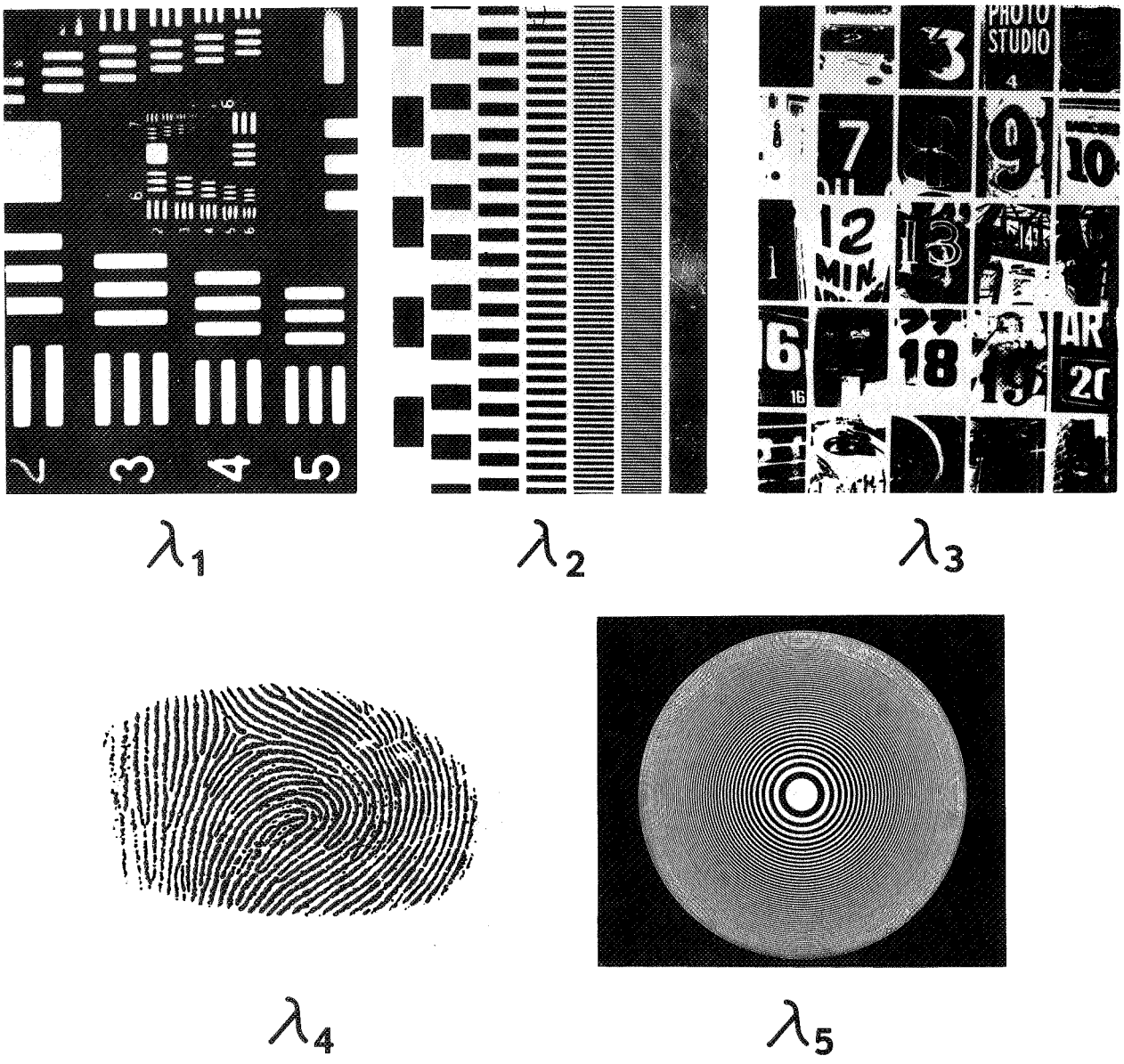

Figure 8.6 Original signals. Each signal was illuminated with a different wavelength, λ

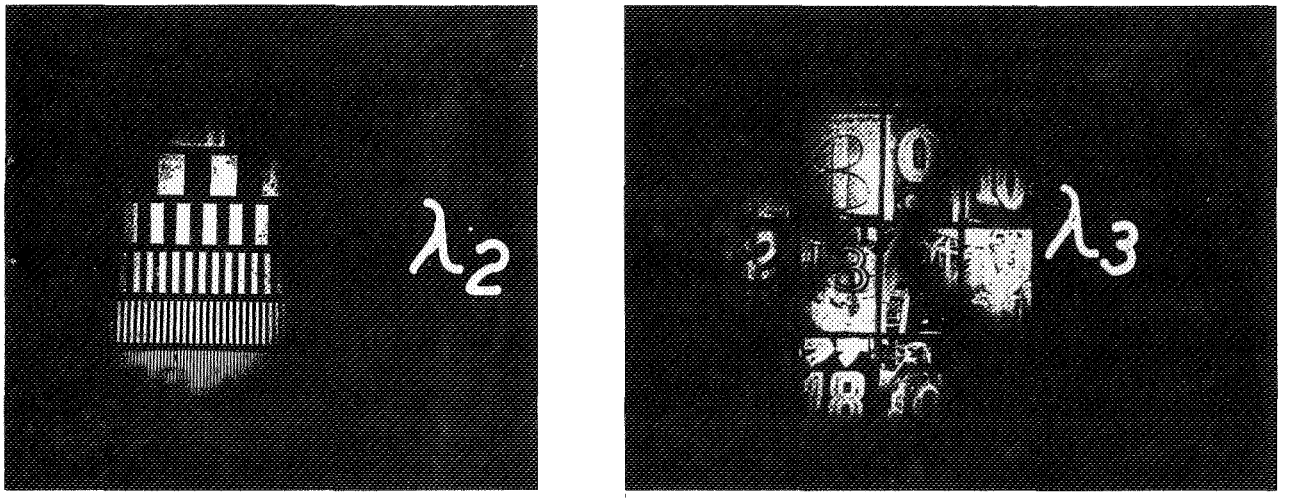

(a) Illumination wavelength λ_2 (b) Illumination wavelength λ_3

Figure 8.7 Reconstructed images from silver halide photochromic glass thickness $\approx$ 1600 μ

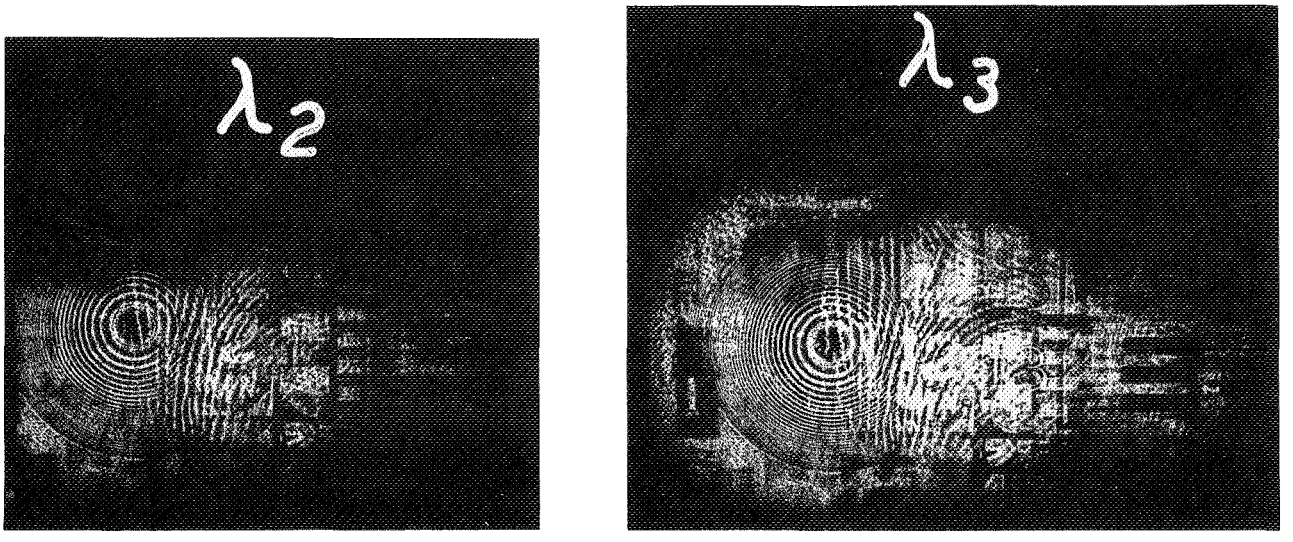

(a) Illumination wavelength λ_2 (b) Illumination wavelength λ_3

Figure 8.8 Reconstructed images from thin photographic emulsion

BIBLIOGRAPHY

Anderson, L. K.; Brojdo, S.; LaMacchia, J. T.; and Lin, L. H.: A High Capacity Semipermanent Optical Memory. IEEE J. Quant. Elect. QE-3, 6, 245 (1967).

Assour, J. M.; and Lohman, R. D.: A Photosensitive Readout Array for Optical Memories. Paper 3.6, IEEE sponsored International Electron Devices Meeting, Washington, D.C., Oct. 1969.

Crowell, M. H.; and LaBuda, E. L.: The Silicon Diode Array Camera Tube. Bell System Tech. J., vol. 48, no. 5, May–June 1969, pp. 1481–1528.

Friesem, A. A.; Kozma, A.; and Adams, G. F.: Recording Parameters of Spatially Modulated Coherent Wavefronts. Appl. Opt., vol. 6, no. 5, 1967, pp. 851–856.

Friesem, A. A.; and Walker, J. L.: Thick Absorption Recording Media in Holography. Appl. Opt., vol. 9, 1970, p.201.

Goodman, J. W.; and Knight, G. R.: Effects of Film Nonlinearities on Wavefront-Reconstruction Images of Diffuse Objects. J. Opt. Soc. Am., vol. 58, no. 9, 1968, pp. 1276 – 1283.

Gordon, E. I.: A Review of Acousto Optical Deflection and Modulation Devices. Proc. IEEE, vol. 54, no. 10, Oct. 1966, pp. 1391–1401.

Kogelnik, H.: Reconstructing Response and Efficiency of Hologram Gratings. Proceedings of the Symposium on Modern Optics, Polytechnic Institute of Brooklyn, March 1967, pp. 605–617 (Polytechnic Press, Brooklyn).

Kozma, A.: Analysis of the Film Nonlinearities in Hologram Recording. Opt. Acta, vol. 15, 1968, p. 527.

Kulcke, W.; Kosanke, K.; Max, E.; Habegger, M. A.; Harris, T. J.; and Fleisher, H.: Digital Light Deflectors. Proc. IEEE, vol. 54, no. 10, Oct. 1966, pp. 1419–1429.

Leith, E. N.; Kozma, A.; Upatnieks, J.; Marks, J.; and Massey, N.: Holographic Data Storage in Three-Dimensional Media. Appl. Opt., vol. 5, no. 8, 1966, pp. 1303–11.

Pinnow, D. A.; and Williamson, S. R.: Acousto-Optic Light Deflection: The Design and Operation of a Simple X-Y Deflection System. Paper WG20, Spring Meeting of the Optical Society of America, San Diego, March 1969.

Reynolds, J. L.; Tao, T. Y.; and Schools, R. S.: An Experimental Optical Memory System. NEREM Record, vol. 10, Nov. 1968, pp. 78–79.

Smits, F. M.; and Gallaher, L. E.: Design Considerations for a Semipermanent Optical Memory. Bell Systems Tech. J., vol. 46, no. 6, July–August 1967, pp. 1267–1278.

Van Heerden, P. J.: Theory of Optical Information Storage in Solids. Appl. Opt., vol. 2, no. 4, 1963, p. 393.

9 APPLICATIONS OF HOLOGRAPHY TO APPLIED MECHANICS

By Robert Aprahamian and David A. Evensen
TRW Systems Group

This paper summarizes the efforts of TRW Systems to demonstrate the applicability of continuous wave and pulsed holography to applied mechanics. Three specific areas are considered, namely, transverse vibrations of beams and plates, transient-transverse response of beams under impulsive loads, and transverse-wave propagation in beams resulting from impulsive loads.

Continuous-wave, time-average holographic interferometry was used extensively to determine the transverse vibrations of vibrating beams and plates at frequencies as high as 20 kHz. In addition, several selected modes as high as 100 kHz were recorded. A comparison is given of experimental and theoretical values of (1) mode number relative to frequency and (2) mode shapes.

The transient response of a cantilevered beam was recorded using stored-beam interferometry. A high-speed motion-picture camera placed behind the hologram was used to record the resulting motion of the fringes. Analysis of the images on the motion-picture film provided the transient response, which is compared with the analytically predicted response. The results show excellent correlation.

Holograms were made of transverse waves propagating in a long beam clamped on both ends. The transverse waves were introduced by striking the beam at its center with a ballistic pendulum. Three double-exposure, interferometric holograms are shown for the beam 12.5, 25, and 50 μsec after the ballistic impact.

The study of vibrating plates and beams is not new. Until recently, however, it has not been possible to make simultaneous measurements of the motion at all points of a vibrating structure. Devices such as strain gages or capacitive displacement sensors are limited to measurements at a single point; the Chladni sand technique can determine the location of nodes of vibration over a large area (ref. 1), but is limited in its applications.

In 1965, Powell and Stetson (ref. 2) first introduced vibration analysis by holographic interferometry, and it has since been applied by others (refs. 3, 4). Several types of holographic interferometry—double-exposure, time-average, and stored-beam—have been used to make measurements of the motion of vibrating objects.

The purpose of our investigations was to demonstrate the feasibility of the experimental technique in quantitatively studying the vibration modes of beams and plates. The results of the study show conclusively the high potential of holography (both continuous-wave and pulsed) to become a basic measurement technique in the study of problems in applied mechanics.

TRANSVERSE VIBRATIONS OF BEAMS AND PLATES

While it is well known that the Chladni sand patterns can be used to obtain the nodal lines of beams and plates (ref. 1), they cannot be used to obtain the mode shape; nor can they be used at

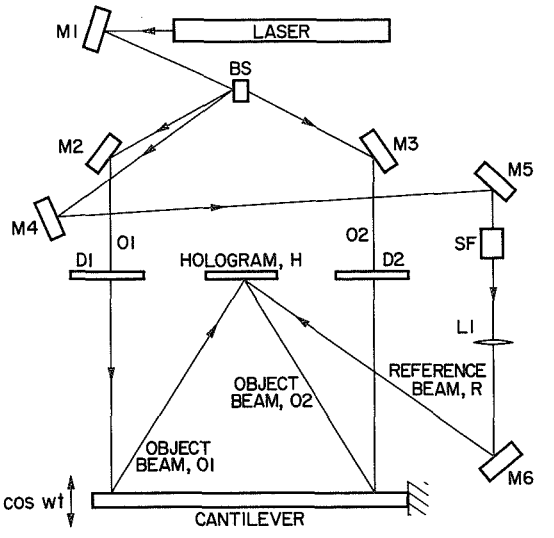

Figure 9.1 Apparatus used to make holograms of the cantilever beam

high frequencies where the amplitudes of motion are small. Holographic interferometry can solve both of these problems.

Figure 9.1 shows the experimental arrangement used to study the transverse vibrational modes of the cantilever beam. The cantilever, constructed of 6061-T6 aluminum, is 30-in. long, 1-in. wide and 1/4-in. thick. As is shown in the figure, the light emitted by the laser is directed to a beamsplitter, BS, by means of mirror M1. Three beams of light, designated as 01, 02, and R, are formed at the beamsplitter. Beams 01 and 02 are used to illuminate the cantilever specimen. They are directed by mirrors M2 and M3, respectively, through diffusers D1 and D2 onto the cantilever. The third beam of light, R, is due to internal reflections in the beamsplitter. It is weak in intensity compared with 01 and 02 and is ideal to use as a reference beam. Mirrors M4 and M5 direct it to a spatial filter, SF. The spatial filter consists of a 60X lens and a 6.8-μ pinhole. This light is then collimated by lens L1, and the collimated light is directed by mirror M6 to strike a high-resolution photographic plate, H.

The optical equipment and the cantilever beam were placed on a large granite table ($\sim$ 8000 lb) that was shock-isolated from laboratory surroundings. The test procedure was basically to excite the cantilever beam to resonance. When a resonant response was reached, a time-average hologram was made. It was excited by a piezoelectric crystal transducer driven by a standard oscillator-amplifier setup. The driving transducer was cemented to the tip of the beam, and a similar pick-up transducer was mounted near the root. The pick-up transducer, connected to an oscilloscope, monitored the response of the beam and detected the resonance condition.

Figure 9.2 shows a typical beam mode recorded in this fashion. The vertical white stripes identify nodal positions. The dark fringes can be interpreted to give amplitude information. The shape corresponding to this beam mode is plotted in figure 9.3. As shown in this figure, the mode shape

Figure 9.2 Fringe pattern from a time-average hologram of a cantilevered beam 30 in. long vibrating in its twenty-first mode (10, 121 Hz)

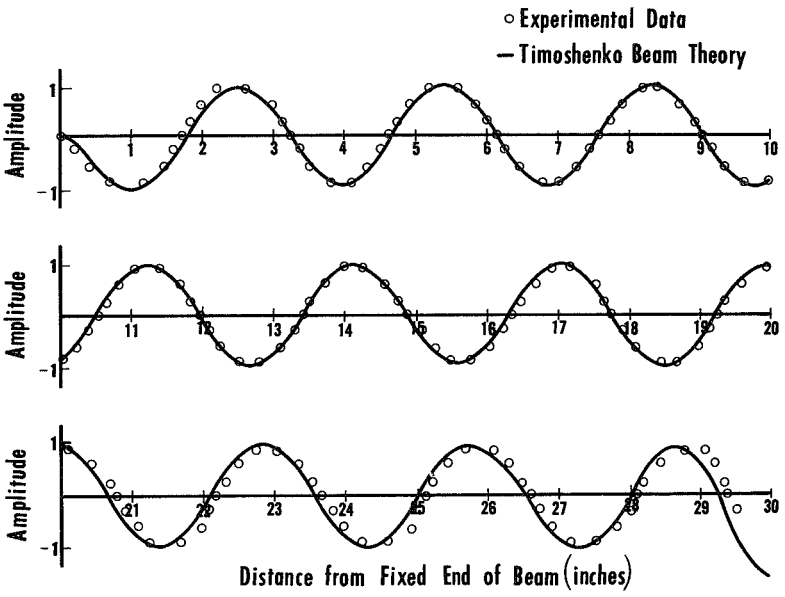

Figure 9.3 Comparison of experimental and calculated shapes for its twenty-first mode

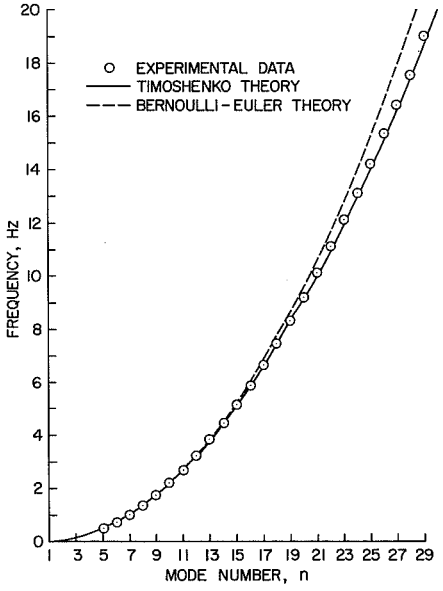

Figure 9.4 Mode number relative to natural frequency

predicted by the Timoshenko beam theory shows excellent agreement with the experimental results. The discrepancies near the free end of the beam and near the support are attributed to the presence of the two transducers. Figure 9.4 shows natural frequency relative to the mode number, n, as predicted by the Bernoulli-Euler and Timoshenko theories and the results of this study. It appears that the simple Bernoulli-Euler theory is valid to approximately the fifteenth mode. Above that, the more sophisticated Timoshenko theory, which includes rotatory inertia and shear, seems to be more accurate.

The vibration phenomenon may also be related to traveling waves in an infinitely long beam. We compared the wavelength needed to generate the standing-mode pattern with those predicted from the simple Bernoulli-Euler and Timoshenko theories; figure 9.5 shows the results. It is obvious that the Timoshenko theory should be used when the wavelength of the oscillation approaches five times the thickness of the beam.

Holography can be applied to the study of plates as well as beams. Figure 9.6 shows the experimental arrangement used to study the transverse vibration modes of a simply supported plate of aluminum 8-in. wide by 10-in. long by 1/16-in. thick. The plate had a fundamental vibration of 162 Hz. As is shown in figure 9.6, light from the laser is filtered and illuminates both a mirror and the vibrating panel. The mirror reflects the light to the hologram plane. Attached behind the simply supported plate is a small piezoelectric crystal used to vibrate the specimen. An oscillator provides a signal to control the frequency and magnitude of the vibration. This signal is monitored by an electronic counter to accurately determine the frequency.

The test procedure was somewhat different from the case of the cantilever beam. First, a hologram was made of the plate in the ambient state. Next, an observer looking through the stored-beam

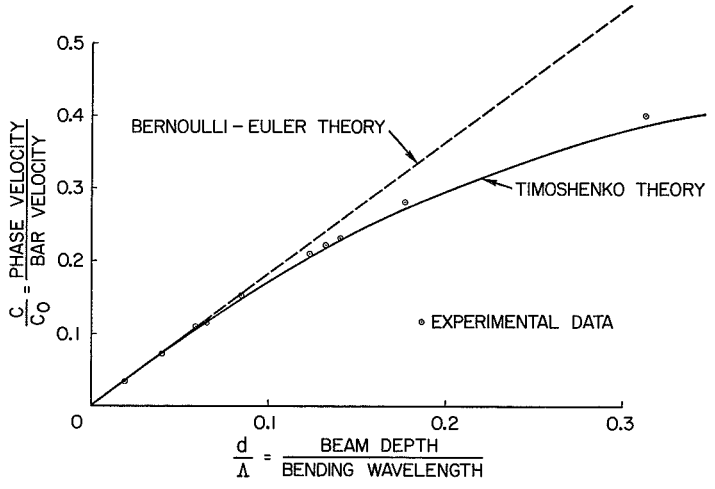

Figure 9.5 Phase velocity relative to wavelength

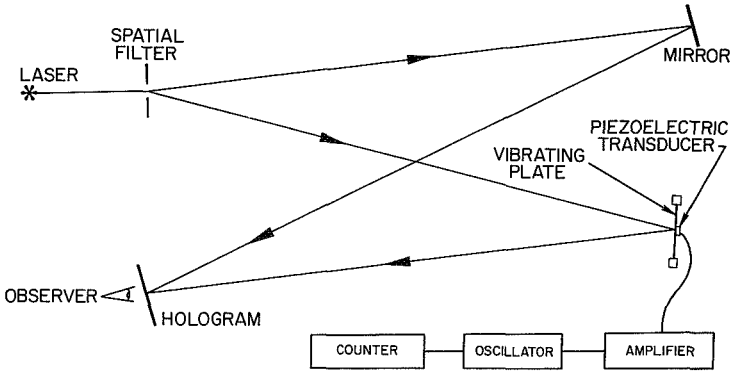

Figure 9.6 Apparatus used in the plate experiments

hologram adjusted the driving frequency of the crystal until a fringe pattern was seen that corresponded to a resonant mode. While the plate was oscillating in that mode, an unexposed plate was placed in front of the stored-beam plate and exposed to form time-average hologram. More than 100 modes were recorded using this technique with frequencies as high as 30 kHz. In addition, modes at frequencies as high as 76 kHz were recorded using time-average holograms. Figure 9.7 shows a typical holographic reconstruction of a plate mode. The data from the photographs are plotted in figure 9.8. Again, excellent agreement is shown. Figure 9.9 shows the modes identified

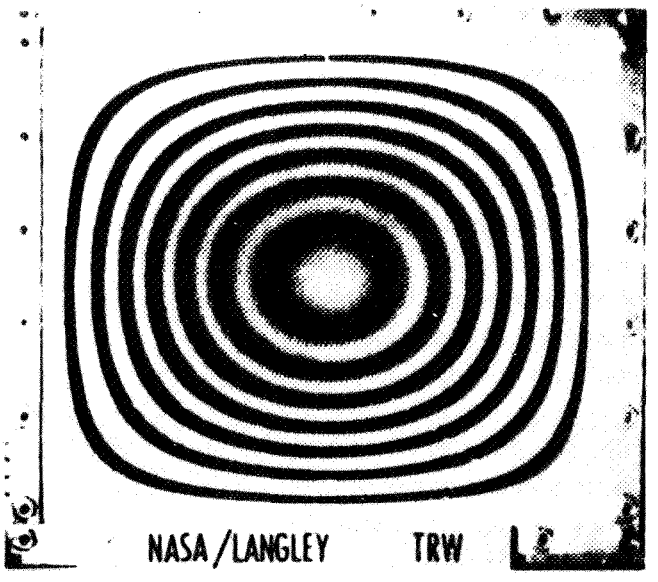

Figure 9.7 Holographic interferogram showing fundamental mode of a simply supported plate

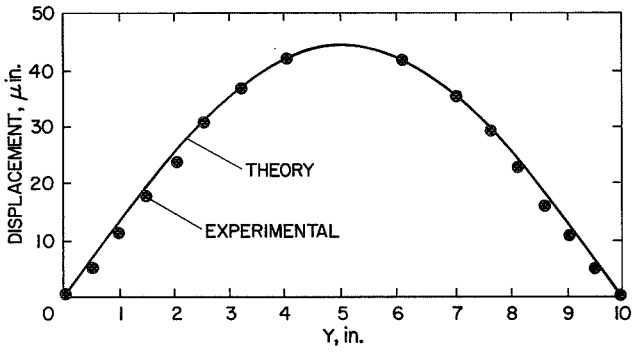

Figure 9.8 Calculated and experimental fundamental mode shape

by this technique. Figure 9.10 is a plot of the flexural-wave velocity C. This flexural velocity divided by the shear-wave velocity, C_s, is a linear function of the plate thickness, h, divided by mode wavelength, λ, as predicted by classical plate theory and Mindlin's plate theory that includes shear and rotatory inertia. Data obtained from our study are also plotted in figure 9.10. As is seen, classical plate theory may be used with $h/\lambda = 0.06$. Above that value, shear and rotatory inertia begin to be important.

TRANSIENT RESPONSE

The transient response of a cantilevered beam was determined using stored-beam, holographic interferometry techniques coupled with high-speed motion-picture photography. A stored-beam hologram was made of the cantilever beam. After the beam was struck at its tip by a ballistic pendulum, the holographically formed interference fringes were recorded with a high-speed camera. From an analysis of the motion of the fringes, the deflection-time history of the beam was determined. Comparison with theoretical predictions correlate very well.

The aluminum cantilever beam was 20-in. long, 1-in. wide, and 1/4-in. thick. Measurements of its response were made using the optical arrangement shown schematically in figure 9.11. In figure 9.11, light from a helium-neon laser (15 mW continuous-wave) is passed through a spatial filter, SF, and then

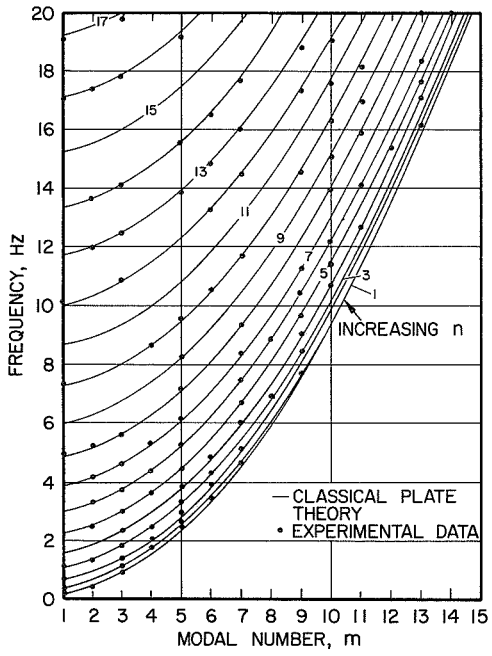

Figure 9.9 Plate resonant frequency relative to modal numbers m and n

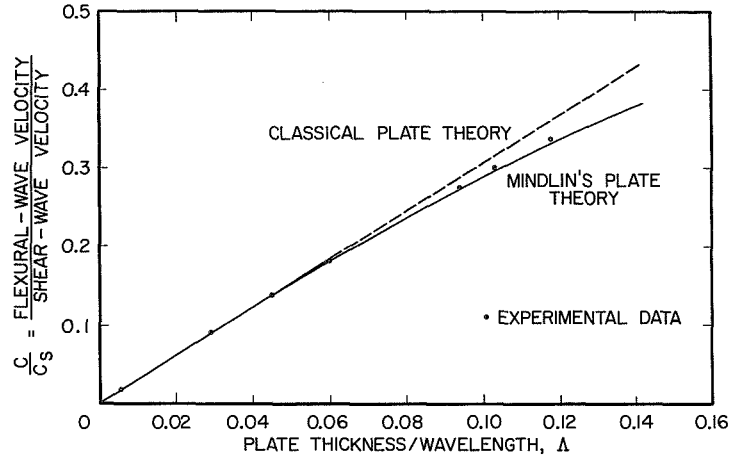

Figure 9.10 Experimental data of classical plate theory and Mindlin's plate theory

through a converging lens, L. The light is brought to a focus at mirror M; leaving the mirror, it expands and is passed through collimating lens CL. The light is split into two parts at the beamsplitter. The light reflected at point A by the beamsplitter is directed by mirror M_1 to the cantilever beam at point B. Since the cantilever is highly polished, it reflects the light back along its path to point A. A portion of the light passes through the beamsplitter and strikes the hologram at point H. This light forms the object beam for the hologram. At the same time, the light that originally was transmitted by the beamsplitter is reflected by mirror M_1' and is also directed to point H. This light constitutes the reference beam for the hologram. Distance A-M_1' was adjusted to be within 1 in. of the length A-M_1-B so that the path length difference between the object and reference beams would not exceed the coherence length of the laser.

The light paths just discussed were sufficient to illuminate a region nearly 2-in. long at the tip of the cantilever. Similar arrangements were made using mirrors (M2, M2'), (M3, M3'), and (M4,

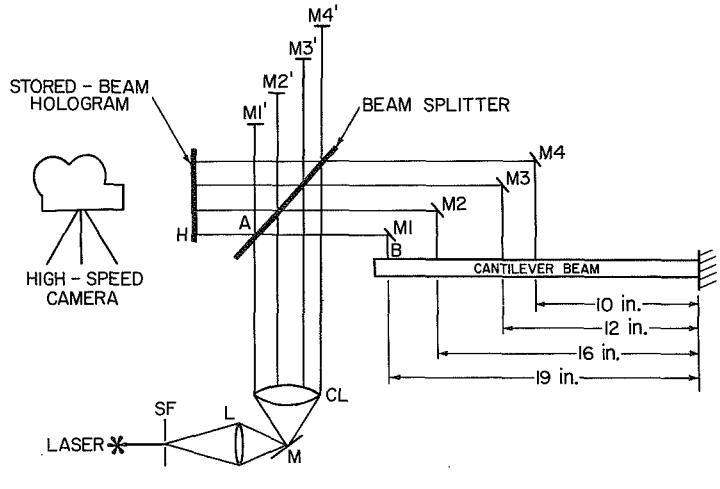

Figure 9.11 Optical arrangement for transient-response test

M4') to illuminate 1-in.-long regions of the beam at the respective distances of 16, 12, and 10 in. from the root. Stored-beam holograms that showed these four illuminated regions of the cantilever were made with this optical arrangement. This method of illumination was chosen because the laser output was insufficient to give a continuous view of the entire cantilever beam.

To excite the transient motion, a ballistic pendulum was used to impart an impulse to the beam. A small (0.016-g) steel ball was suspended on a 10-in. human hair to form the ballistic pendulum. The initial height of the ball was measured using a machinist's scale. A latch mechanism was used to release the ball without giving it an initial velocity. The pendulum ball struck a piezoelectric crystal that was mounted on the beam 0.5 in. from the tip. By monitoring the output of the transducer with an oscilloscope, the force-time history of the impulse was determined. The height to which the pendulum rebounded (after striking the beam) was recorded using a camera that had the shutter held open. The rebound height was determined from a scale that was photographed in the background of the photo.

A stored-beam hologram was made using the configuration of figure 9.11. A high-speed motion-picture camera was placed behind the stored-beam hologram. The camera was then set to run for about 1 sec, and after it reached full speed, the ball was allowed to fall and strike the beam. Approximately 1.5 sec later, the supply of film in the camera was exhausted and the test concluded.

Figure 9.12 shows the first five frames of the movie film that recorded the transient response of the cantilever beam. Frame 0 in figure 9.12 shows the interference fringe pattern just before the impact. The rectangular areas in figure 9.12 correspond to those portions of the beam that were illuminated in 1-in. squares located 10, 12, and 16 in., respectively, from the root and the 2-in. illuminated region at the tip of the beam. The left-most illuminated square corresponds to $x = 10$ in., and the right-most illuminated area corresponds to the 2-in. region at the tip. The small circular indentations visible in the figure were made in the beam surface to identify particular points.

Before impact, some fringes were evident in the picture (see frame 0) due to misalinement of the hologram. When the impulse was applied at the tip of the beam, the fringe pattern shifted in response to the beam motion. Frames 1 through 4 show that the fringes at the tip of the beam moved toward the right (i.e., off the tip of the beam), which indicated the beam had moved toward the movie camera. If the location (along the length of the beam) of two adjacent fringes is known, the transverse displacement of a point on the beam between the two fringes can be computed using interpolation. Such an interpolation procedure was applied near the tip of the beam to determine the transverse displacement corresponding to each frame of the movie film. Timing marks on the edge of the film made it possible to associate a time (from the initiation of impact) with each film frame. The data-reduction process is discussed in greater detail in reference 5.

A typical displacement-time history obtained in this fashion is shown in figure 9.13. The calculations, provided by J. S. Mixson of Langley, used the first ten Bernoulli-Euler beam modes of a 20-in. cantilever; the response was computed for a delta-function impulse applied at the tip of the beam. Data were scaled by the measured impulse imparted by the ball bearing to correspond with

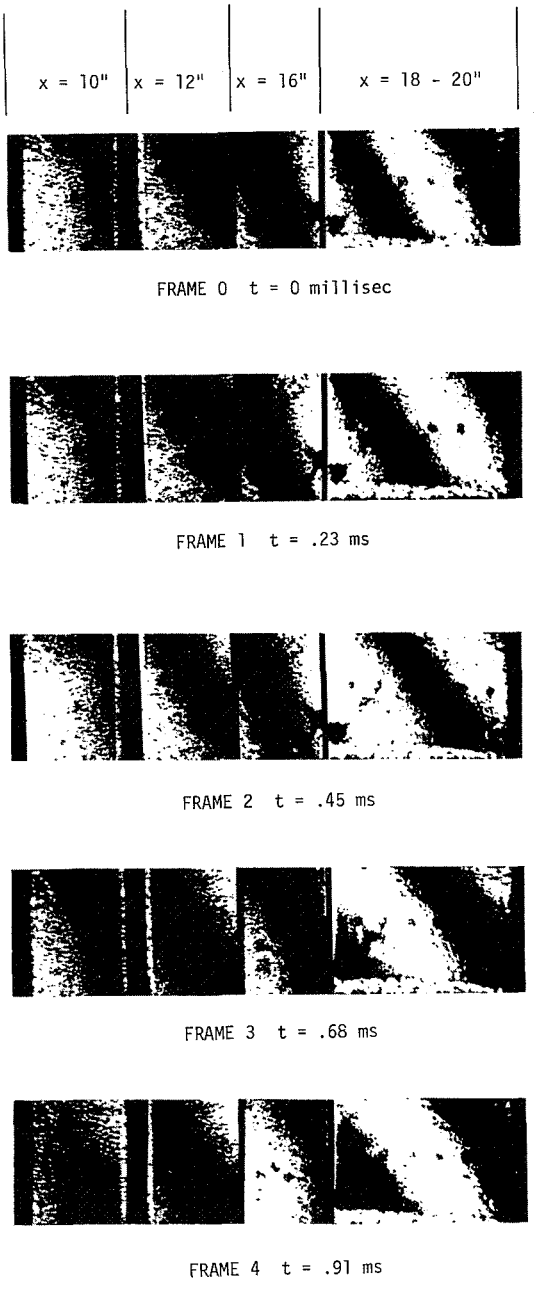

Figure 9.12 Photographs showing motion of the fringes just after ballistic impact

the analysis. Figure 9.13 shows the generally good agreement between theory and experiment for the transient response.

Although other areas on the cantilever (besides the tip region) were illuminated, they did not produce closely spaced, well-defined data points. This lack of resolution in the data for 10, 12, and 16 in. occurred because the illuminated areas contained only one fringe at a time (instead of two),

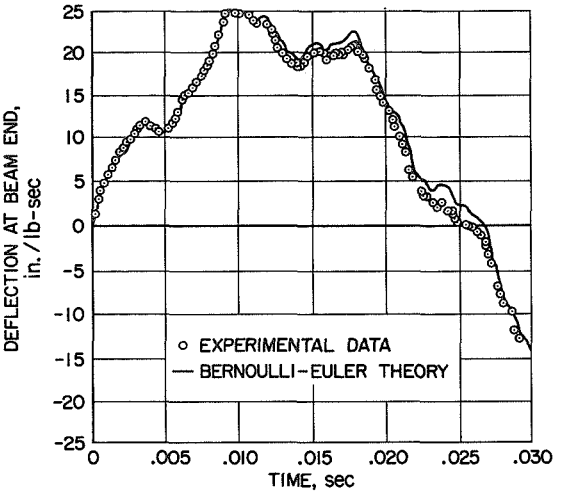

Figure 9.13 Comparison of theory and experiment for transient response of a cantilevered beam experiencing an impulse at its free end

which prevented interpolation between fringes. This difficulty in data reduction and other experimental considerations are discussed in reference 5.

TRANSVERSE-WAVE PROPAGATION

The propagation of transverse waves in beams was studied using double-exposure, pulsed holography techniques. The results show for the very first time the spatial nature of a bending wave in a beam.

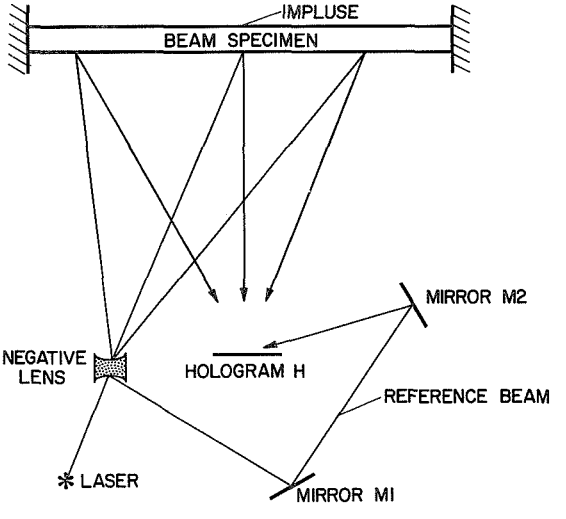

Figure 9.14 Apparatus for transverse-wave experiment

Transverse-wave propagation in a cantilever beam was recorded using double-pulsed holographic interferometry. The beam used in these tests was 0.25-in. thick, 1-in. wide, and 6-ft long. A ballistic pendulum was set up behind the beam; when the ball was released, it struck the beam at its center. Figure 9.14 shows the experimental arrangement. As shown in the figure, the light from the pulsed laser strikes the negative lens and expands to illuminate the beam. Reflected light from the first surface of the lens is directed by mirrors M1 and M2 to illuminate the hologram, H. Three separate tests were recorded using this technique. The state of deformation of the beam was recorded 12.5, 25, and 50 μsec after impact. Figure 9.15 shows the reconstructed image of three holograms obtained in this manner. At 12.5 μsec after impact, the beam acted as a plate; that is, it bulged at its center. Later a bending wave is seen to propagate down the beam. The deflection in relation to the distance from the struck center, as deduced from the hologram, is shown graphically in figure 9.16.

CONCLUSIONS

Holographic interferometry has been applied to study the transverse vibrations of beams and plates, to determine the transient response of a cantilever beam, and to determine the transverse deflection of a beam under impact. The vibration studies resulted in the determination of beam and plate modes at frequencies virtually unexplored until now. Photographs from time-average holograms have been presented which illustrate that the time-average holography technique described in this paper yields results even more descriptive than the well-known Chladni patterns. Both pure modes and compound modes can be detected with holography.

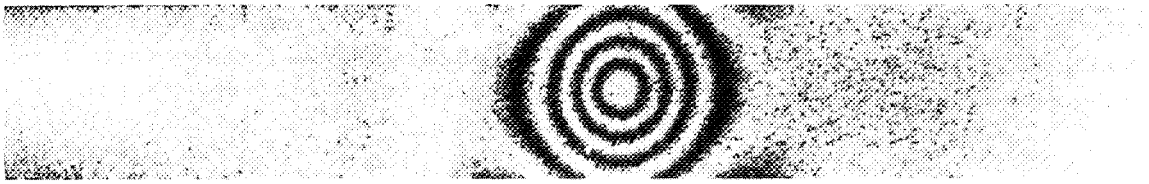

12.5 microseconds (after impact)

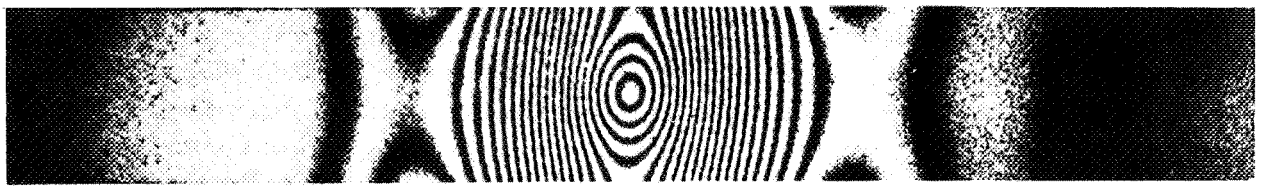

25.0 microseconds

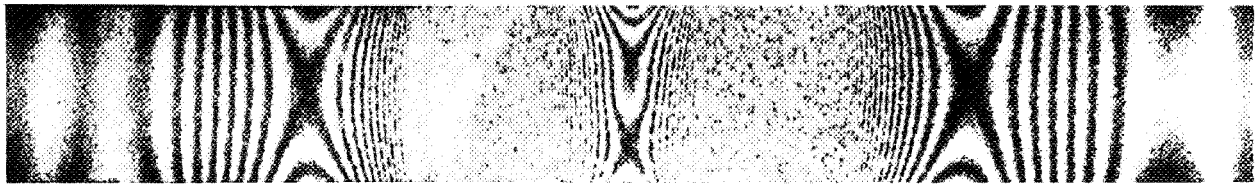

50.0 microseconds

Figure 9.15 Holographic interferograms of a bending wave in a clamped-clamped beam

The transient-response studies demonstrated the feasibility of using stored-beam holography to produce displacement-time histories. The close agreement between the theoretical and experimental responses indicates the accuracy of this new procedure. (Experience shows that it is advisable to illuminate enough of the structure to allow interpolation between adjacent interference fringes.)

The pulsed-holography technique applied to determining the transverse deflection of a beam under impact demonstrates the feasibility of pulsed holography to record transient events. No other technique is known by which the spatial deformation can be obtained under these conditions.

Based on these three tests, it is felt that holography has considerable potential in areas of applied mechanics that are still unexplored. For example, the techniques of holography can be adapted to the study of such problems as flutter and high-temperature effects on structures.

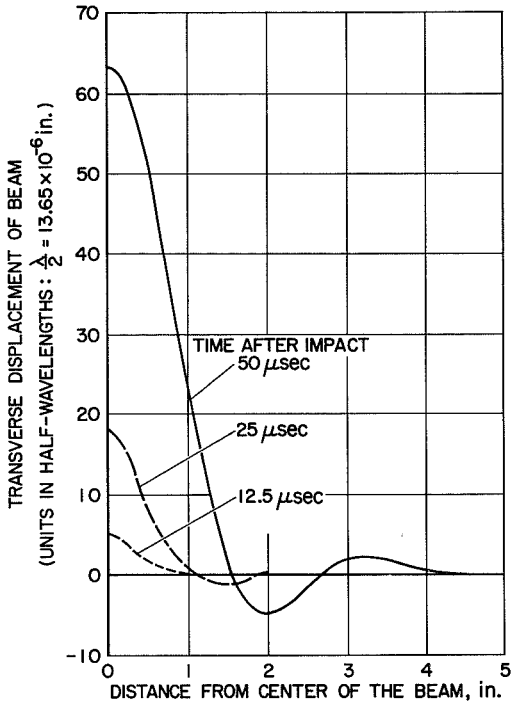

Figure 9.16 Transverse displacement of bending wave relative to position

ACKNOWLEDGMENTS

The authors wish to acknowledge the helpful advice and suggestions of several associates who contributed significantly to this work. R. F. Wuerker, R. E. Brooks, and L. O. Heflinger of the TRW Physical Research Center offered many useful suggestions concerning the technical details of holographic interferometry. J. E. Wright assisted in setting up and conducting the experiments and worked out many of the mechanical problems. J. S. Mixson of NASA Langley Research Center offered encouragement and support throughout the course of this study and contributed invaluable assistance concerning presentation of the results. In addition, he served as technical monitor and performed several analyses used in this report.

This work was supported by NASA Langley Research Center under contract NAS1-8361.

REFERENCES

1. Chladni, E.F.F.: Die Akustik. Leipzig: Breitkopf und Hartel. 1802.
2. Powell, R. L.; and Stetson, K. A.: Interferometric Vibration Analysis by Wavefront Reconstruction. J. Opt. Soc. Am., vol. 55, no. 12, Dec. 1965, pp. 1593–1598.
3. Monahan, M. A.; and Bromey, K.: Vibration Analysis by Holographic Interferometry. J. Acous. Soc. Am., vol. 44, no. 5, Nov. 1968, pp. 1225–1231.

4. Wabrasiewicz, B. M.; and Spicer, P.: Vibration Analysis by Stroboscopic Holography. Nature, vol. 217, no. 5134, March 23, 1968, pp. 1142–1143.
5. Aprahamian, R.; and Evensen, D. A.: Transient Response Determination using Holographic Techniques. Submitted to J. Exp. Mech.

10 INSTRUMENTAL HOLOGRAPHIC TECHNIQUES

G. S. Ballard and M. K. Testerman
University of Arkansas Graduate Institute of Technology
Little Rock

A method of dual-exposure holographic interferometry is described that uses a separate reference beam for each of the two exposures. The application of this method for the comparison of optical components and for the measurement of small phase deviations is discussed.

A number of photosensitive processes, other than the silver halide gelatin emulsion, are being investigated in this laboratory as to their possible application as a medium for hologram recording and data storage. This work and the associated spatial noise considerations are summarized, and several instruments built to aid in this investigation are described.

DUAL-EXPOSURE HOLOGRAPHIC INTERFEROMETRY WITH SEPARATE REFERENCE BEAMS

A variation of the dual-exposure method for recording holographic interferograms has been devised that retains the advantages of the typical double-exposure technique while offering the same flexibility of fringe presentation associated with real-time laboratory-type interferometers. The fringes obtained can be shifted for improved visibility, and finite fringe patterns can be obtained from a single hologram. This method can be used in recording interferograms of transient phenomena, for real-time interferometry, for comparing optical components, and as the basis of a technique for the quantitative measurement of small phase variations in an optical field. The method requires that each of the two hologram exposures be made with a separate reference beam.

A method for recording this type of hologram is shown in figure 10.1. Three collimated beams are formed, with R_1 and R_2 serving as the two separate reference beams. R_{obj} is the beam in which some test scene occurs; it is the beam that will be reconstructed, both with and without the test scene present, to obtain the interferogram.

To record a hologram of some test scene using this method, the test object is placed in the central beam, R_{obj}. A hologram of the scene is then recorded using beam R_1 as the reference. Beam R_2 is stopped and is not incident on the hologram recording plate during the first exposure. The dual exposure is completed by removing the test scene from beam R_{obj} and recording a hologram of R_{obj} using beam R_2 as the reference. During the second exposure, R_1 is stopped and is not incident on the hologram recording plate.

The only difference between this method and the well-known double-exposure technique is in the use of a different reference beam for each exposure, which allows two distinct holograms of R_{obj} to be formed in a single emulsion, one hologram with the object present and one without.

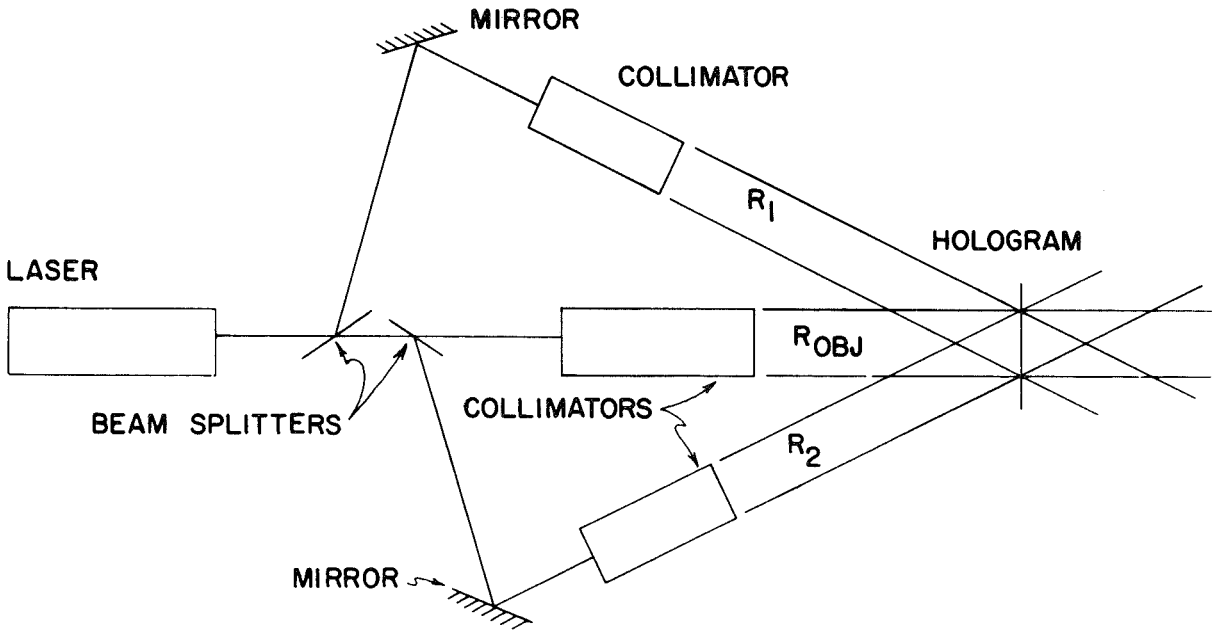

Figure 10.1 Recording a double-exposure hologram with separate reference beams

After processing, the hologram can be replaced in its original position. If it is illuminated with beam R_1 alone, the original test scene will be reconstructed. This reconstruction can be used for obtaining shadowgrams or schlieren photographs, or for any other purpose to which holograms may be suitable. If the hologram is reconstructed using only beam R_2, then R_{obj} without the test scene will be reconstructed. Illumination by both R_1 and R_2 simultaneously will result in reconstruction of R_{obj}, both with and without the test scene present. These reconstructions are coaxial, and, if mutually coherent, interference pattern due to the test object will be observed.

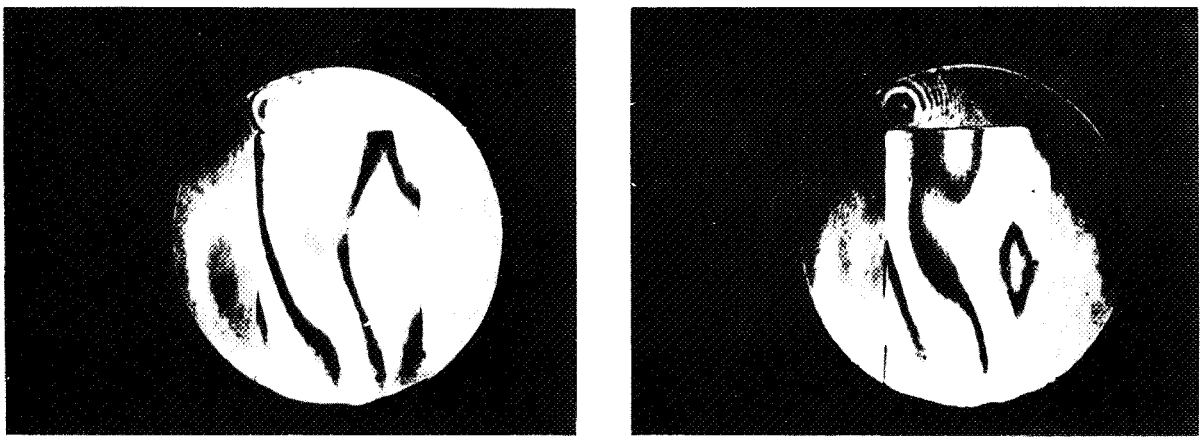

(a) (b)

Figure 10.2 Reconstruction of a holographic interferogram showing the effect of changing the phase in one reconstruction beam; (a) 0° phase shift, (b) 180° phase shift

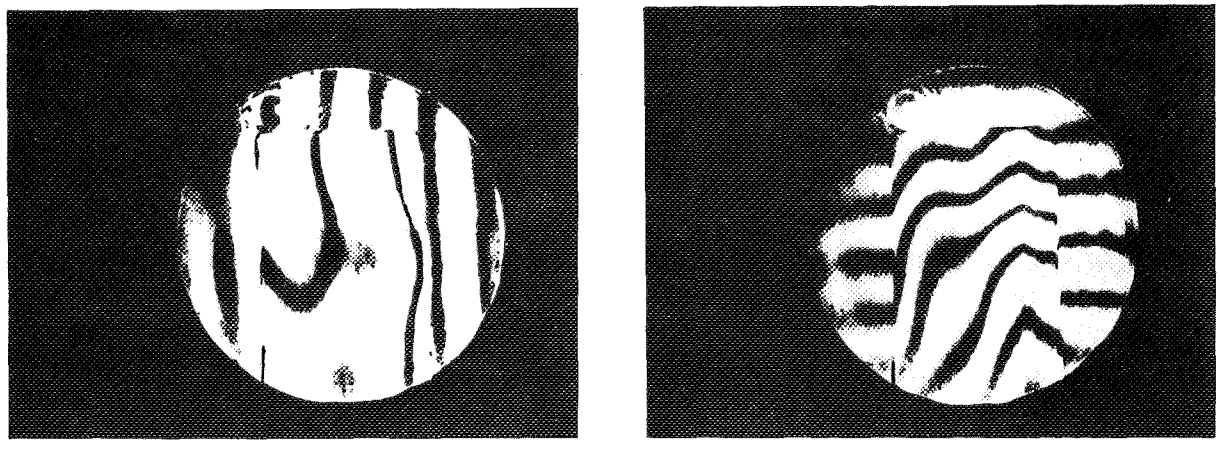

(a) (b)

Figure 10.3 Reconstruction of the hologram in figure 10.2 showing the effect of a change in the angle of the reconstruction beam; (a) small horizontal change, (b) small vertical change

A hologram was recorded using the above procedure with a microscope slide as the test object. Figure 10.2(a) shows the interference pattern of the object obtained when the hologram is reconstructed with both R_1 and R_2. In figure 10.2(b), the phase of R_2 has been shifted approximately 180° during reconstruction. This resulted in a corresponding phase shift in the beam reconstructed by R_2, but did not alter the phase of the beam reconstructed by R_1. The resulting change in the interferogram can be seen, and some portions of the fringe system are now shown to better advantage.

A finite fringe presentation can be obtained by altering the angle at which either R_1 or R_2 is incident on the hologram. The effect of a small horizontal change in the reconstructing angle of R_2 is shown in figure 10.3(a). In figure 10.3(b), a vertical change has been introduced. The result is the same as if one mirror in a laboratory-type interferometer were tilted slightly.

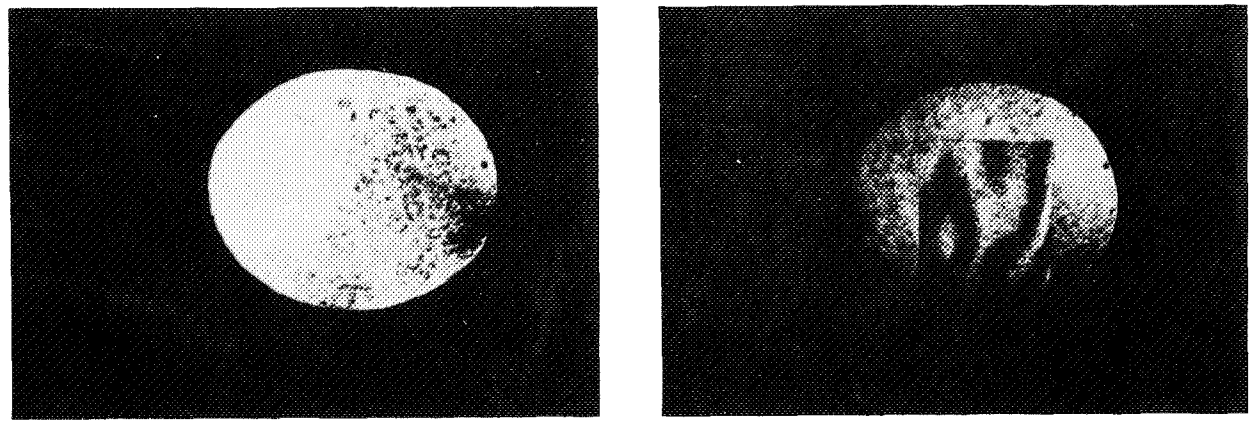

(a) (b)

Figure 10.4 Reconstruction of uniform field; (a) no object in reconstruction beam, (b) test object in reconstruction field

For real-time interferometry, a hologram is recorded with no object in R_{obj} for either exposure. Figure 10.4(a) is the uniform reconstruction of such a hologram. The placement of an object in either reconstructing beam will result in a phase alteration of not only that beam but also the beam it reconstructs. Figure 10.4(b) is identical to figure 10.4(a), except that the same slide used as an object in previous figures has been placed in R_2 during reconstruction.

In Figure 10.5 the object was placed in R_1 when a hologram was recorded and moved to R_2 during reconstruction. Thus, both reconstructing beams have been altered by equal magnitudes but in opposite directions: R_1 when the slide was removed and R_2 when the slide was added. The result is an interferogram with the number of fringes doubled.

For comparing different objects such as optical components, a hologram could be made using no object but with a "standard" in R_1 or R_2. Replacement of the standard with the component to be tested during the reconstruction will produce an interferogram showing the difference between the two components. For illustration, the hologram of figure 10.4(a) was reconstructed after the collimators used to form R_1 and R_2 were exchanged. In this case, the pattern of figure 10.6 actually shows the difference between the two collimator wavefronts with double sensitivity, as both reconstructing beams have been altered. If the wavefronts had been identical, no fringes would have been formed.

The double-exposure hologram with separate reference beams is the basis of a method for quantitatively measuring small phase variations in an optical field, whether the field exists in real time or is holographically stored. Figure 10.7 is a schematic of the technique now being investigated. This figure illustrates the reconstruction of a hologram recorded as in figure 10.1. A multiple-pass variable low-pressure chamber has been placed in R_2 just prior to collimation. As the pressure in this chamber is decreased, the optical pathlength of R_2 decreases, resulting in a continuously varying phase relationship between R_1 and R_2. The fringes in the reconstructed interference pattern will appear to move across the reconstructed scene. The output signal from each of the two

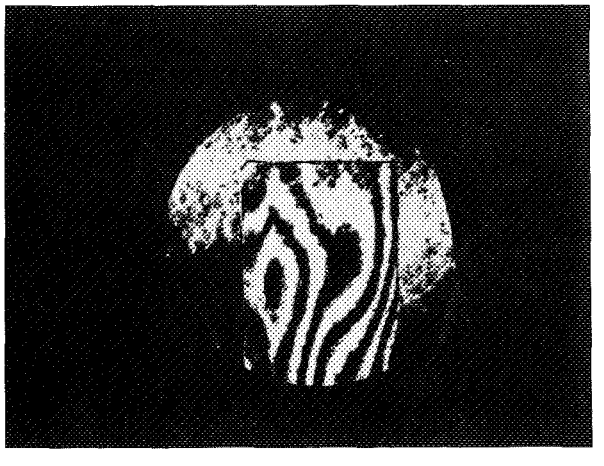

Figure 10.5 "Double-pass" interferogram

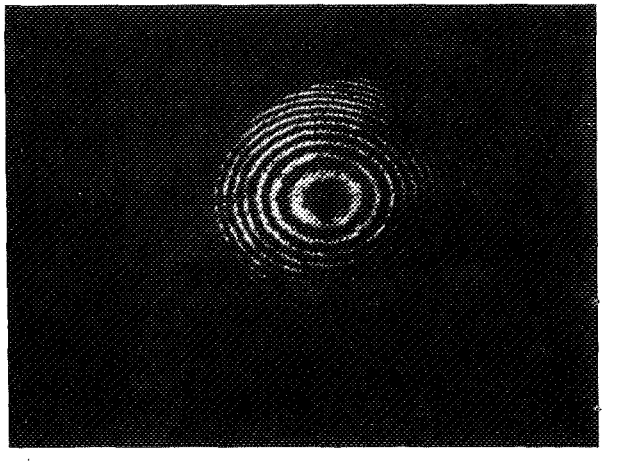

Figure 10.6 Interferogram showing difference in optical components

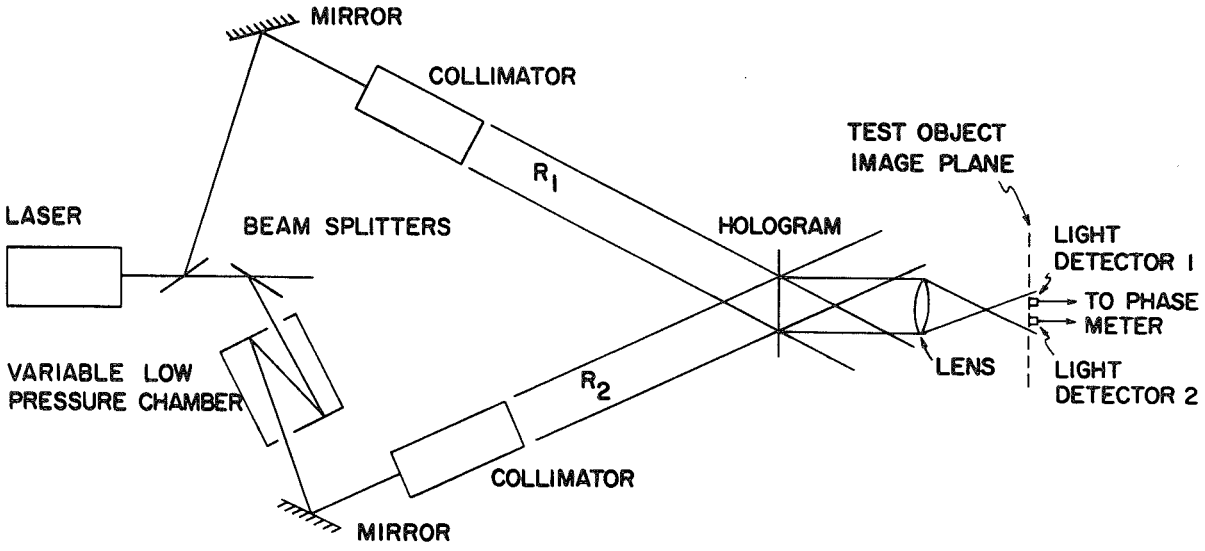

Figure 10.7 Method of measuring small phase deviations in a holographically recorded interferogram

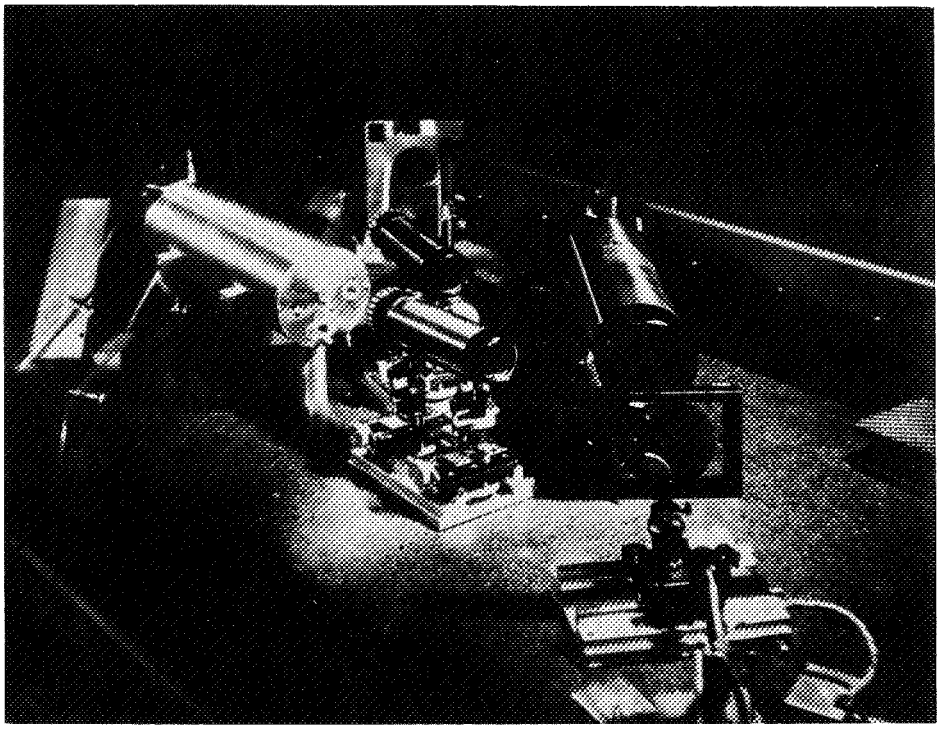

Figure 10.8 Hologram-recording and -reconstructing apparatus

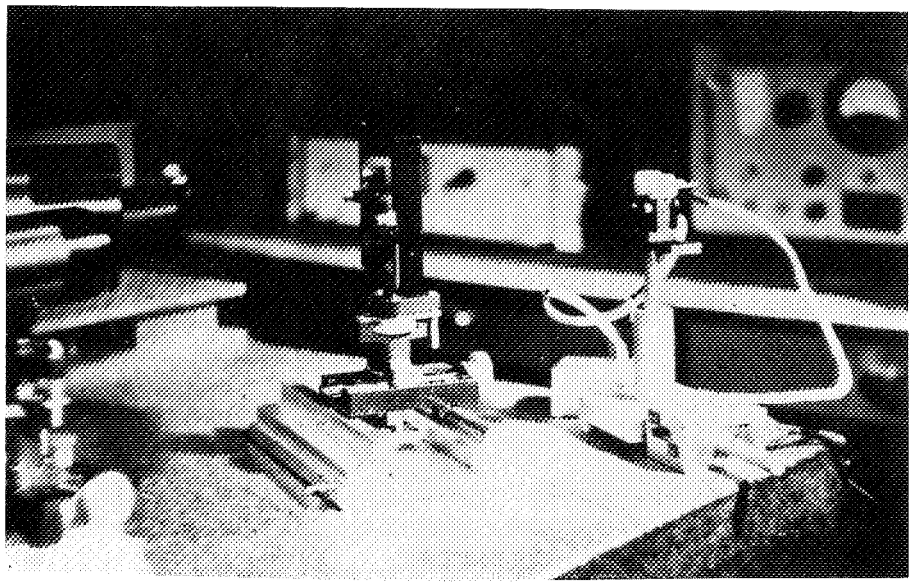

Figure 10.9 Film plate holder with detector in reconstructed beams

detectors shown in the figure will approximate a sine wave as alternate conditions of constructive and destructive interference are experienced. These electrical signals will vary in phase by an amount equal to the difference in optical phase between the two points in the reconstructed field at which the detectors are located. The frequency of the detector signals is determined by the rate at which the pressure inside the variable-pressure chamber is decreased.

If the two detector signals are introduced into an electronic phase meter, the optical phase relationship of the two points can be quantitatively read. A phase map of the entire field can be

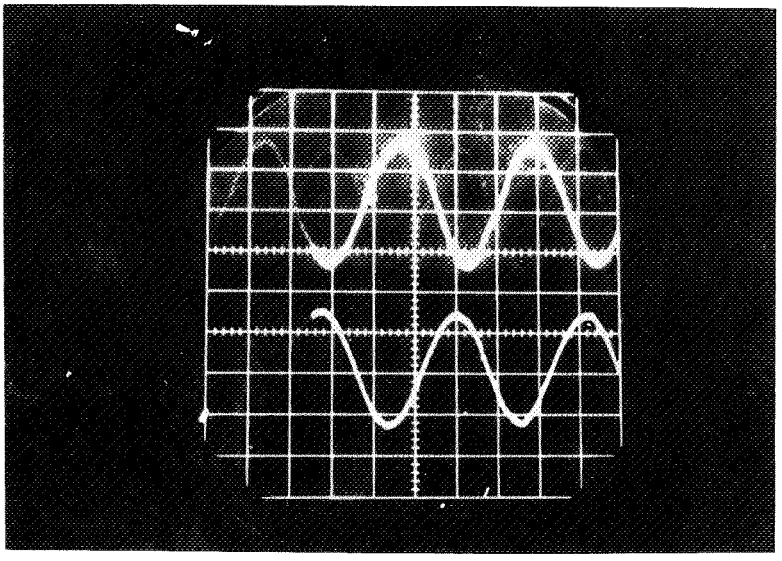

Figure 10.10 Signals produced when measuring phase shift

obtained by fixing one detector at some point in the field as a reference and moving the second detector throughout the reconstruction.

Figure 10.8 shows the actual experimental arrangement now being used. The three collimators, from left to right, form R_2, R_1, and R_{obj}. The large cylindrical object in the upper left of the figure is the phase-shift chamber. Figure 10.9 is another view showing a hologram in place with two detectors in the reconstructed beams. A typical output from the detectors is shown in figure 10.10. This figure illustrates the signals obtained when the detectors are placed at points in the reconstruction that are approximately 180° out of phase.

The detector signals have not yet been introduced into the phase meter, which requires a signal of at least 2 V for operation. This will be accomplished as soon as two matched amplifiers of sufficient gain and bandwidth are completed. It is hoped that the ultimate precision of the phase measurements will be limited by the precision of the phase meter, which is ±1°, thus providing optical path measurements down to 1/360 wavelength.

UNCONVENTIONAL PHOTOGRAPHIC STORAGE AND PROCESSING

In holography, the use of off-axis reference beams and the requirements of extreme stability during exposure make a high-speed/high-resolution recording medium very desirable. Unfortunately, high speed and high resolution are not compatible characteristics in a silver halide emulsion. High-resolution silver halides are notoriously slow, while fast emulsions suffer from poor resolution capabilities. The reason for this conflict is that silver halide emulsions are characterized by a poor photon efficiency, never greater than 1 percent and usually nearer 0.1 percent. To overcome this inefficiency, fast emulsions must have large grains, increasing the probability that enough photons will be absorbed by a grain to form the latent image. The presence of these large grains makes the recording of high spatial frequencies impossible. Conversely, high-resolution emulsions must have small grains, which reduces the probability that a grain will absorb a sufficient number of photons to form the latent image. Thus, the high-resolution emulsion is by necessity slow. The property

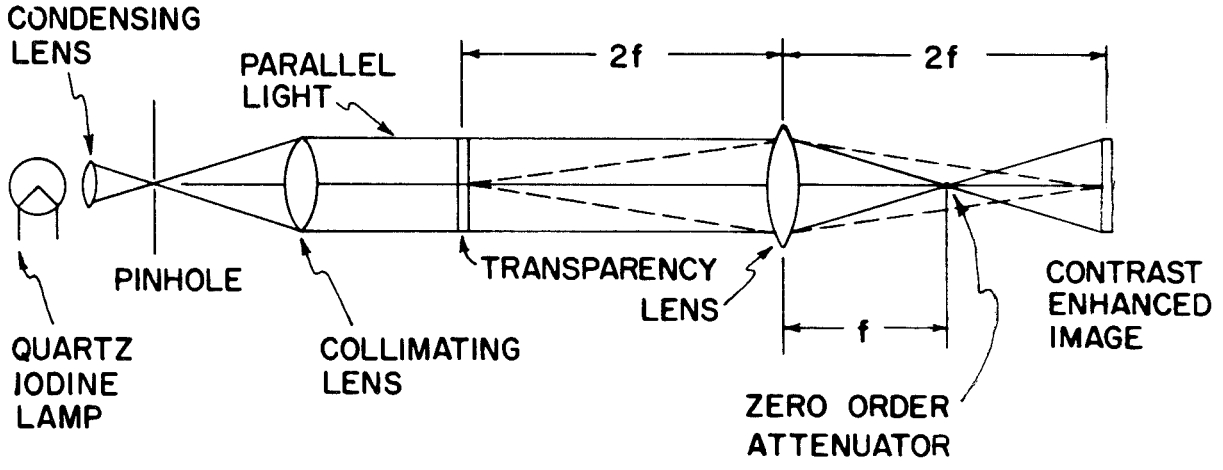

Figure 10.11 Contrast amplifier optical processor

that has made silver halides popular is not photon efficiency, but is an internal "gain" that aids image contrast. Upon development, a grain that has absorbed enough photons to form a latent image is completely reduced to metallic silver.

Many known photosensitive processes exhibit photon efficiencies approaching 1. These processes record photo information on a molecular scale. Thus, they would seem to be ideal for high-speed/high-resolution applications. These processes have not been popular because they lack the contrast gain of the silver halides. The purpose of our investigation is to determine the feasibility of using these processes for high-resolution/high-speed applications and achieving the contrast gain externally, if necessary.

Poor contrast is the result of information being recorded on an emulsion with only low optical density and with little difference in density between areas of the emulsion exposed to various light intensities. The effects of this lack of contrast are quite different, depending on whether the information recorded is a conventional image or a hologram.

For the case of a conventional image, light transmitted by the recording medium has a large dc bias superimposed on it. This bias is caused by the low overall density of the emulsion. One method of removing this bias is illustrated in figure 10.11. Due to the low optical density, most of the light incident on the emulsion is transmitted. A small portion of the incident light is diffracted by the information recorded in the emulsion. An attenuator, placed at the focal point of the imaging lens, will remove the large dc bias but will have no effect on the diffracted light. It is not desirable to remove all of the dc component, as part of this is fundamental to image formation; with no dc at all, a schlieren photograph would be obtained. It is desired to remove only that part of the dc associated with the low optical density of the emulsion. The image processed in this manner would

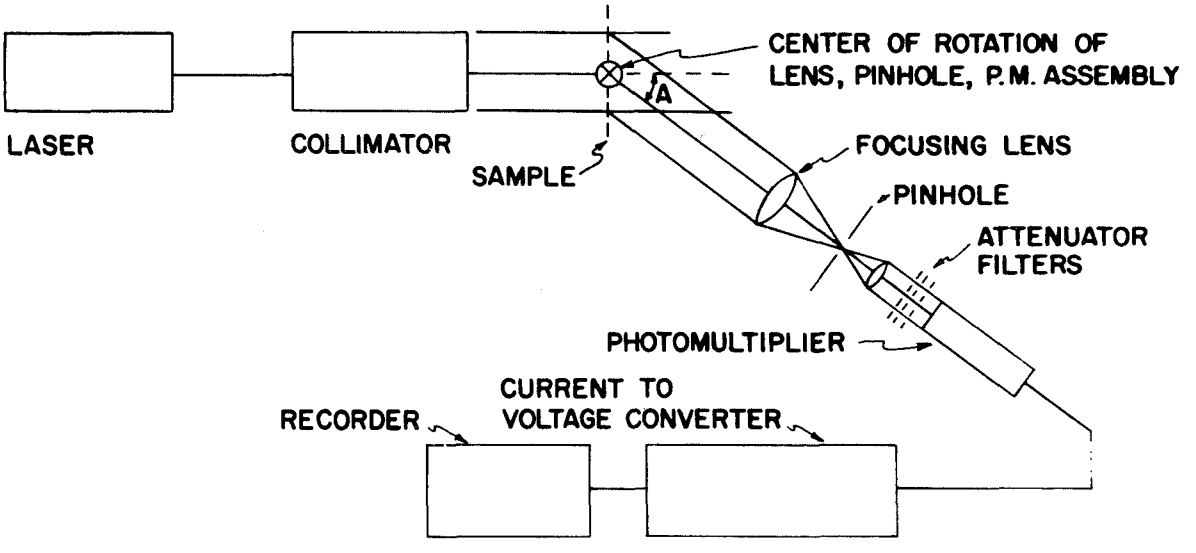

Figure 10.12 Schematic of a laser goniophotometer

exhibit the proper contrast, but would be very dim. Any low-contrast emulsion considered for use must possess extremely good noise characteristics, for scattering arising from any source within the emulsion will be amplified along with the recorded information and degrade the processed image.

For a low-contrast hologram, no contrast processing is necessary. In fact, linear recordings on present silver halide emulsions are low contrast, and pure-phase holograms exhibit no contrast at all. These low-contrast recordings reconstruct images possessing the proper contrast because the high dc bias is automatically removed from the image during reconstruction. Typically, the image is formed at an angle from the illuminating axis, while the bias light is transmitted straight through. Thus, the hologram recording geometry itself accomplishes the bias removal, without recourse to a processor similar to that required for a conventional image. Since the hologram may reconstruct a dim image, it is stil important that the emulsion exhibit low noise properties. Excessive light scattered by the emulsion can degrade the reconstructed image. The suitability of any high-resolution/high-speed low contrast recording medium depends on low noise characteristics, whether the information recorded is a hologram or a conventional image.

An instrument has been constructed that makes it possible to measure quantitatively the itensity of light scattered by an emulsion at angles from 0° through ±90°. Figure 10.12 is a schematic of this instrument. The main feature of the instrument is that the lens, pinhole, and detector are mounted as a unit on an arm that rotates about an axis passing through the sample being analyzed. Only light scattered at an angle A will be focused by the lens through the pinhole and then be detected. The entire spectrum is scanned as the lens-pinhole-detector assembly rotates from 0° to ±90°. This arrangement allows scattering at large angles to be measured using only a simple lens corrected for minimum spherical aberration, because problems of coma and curvature of field are avoided. Figure 10.13 shows the actual laboratory instrument. Figure 10.14 is a closeup of the

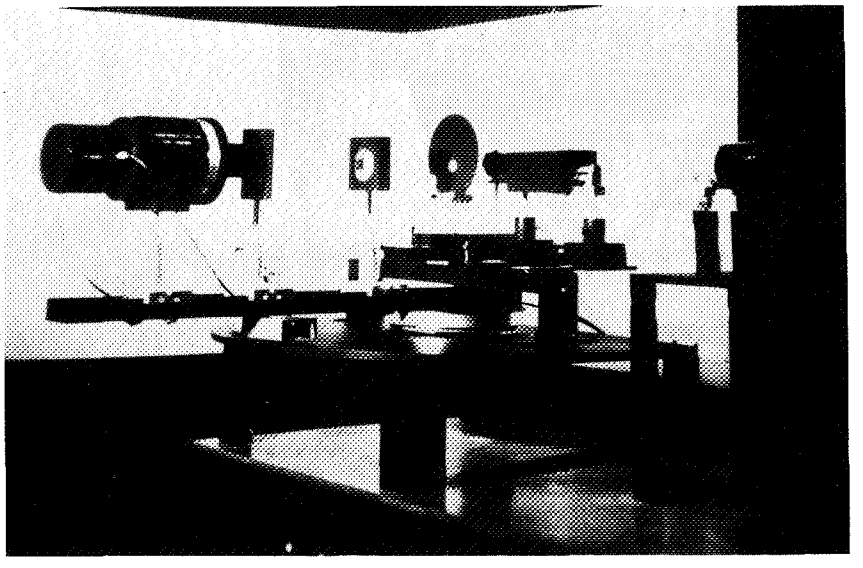

Figure 10.13 Instrument for obtaining light scattering data

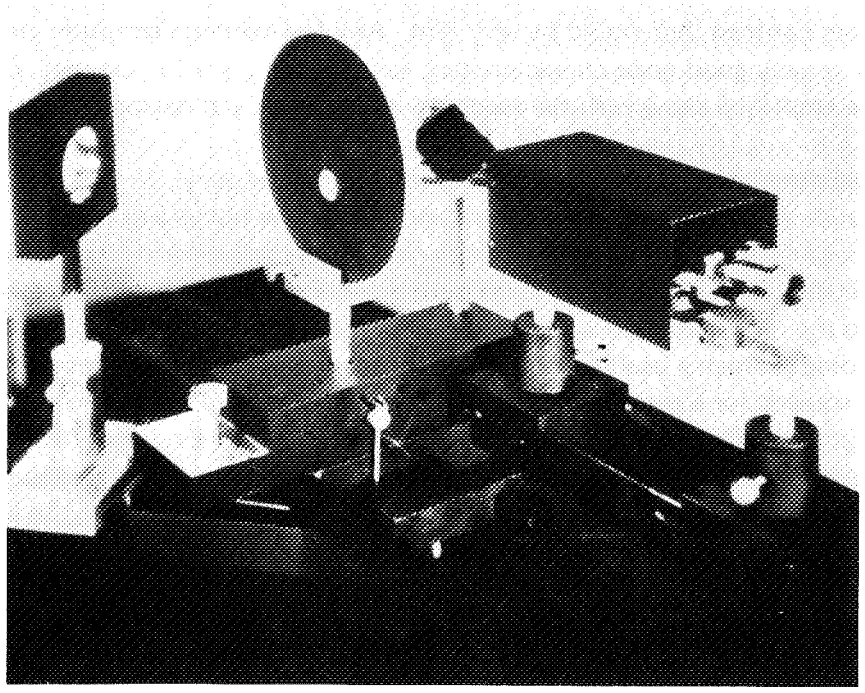

Figure 10.14 Collimator, sample holder, and focusing lens of laser goniophotometer

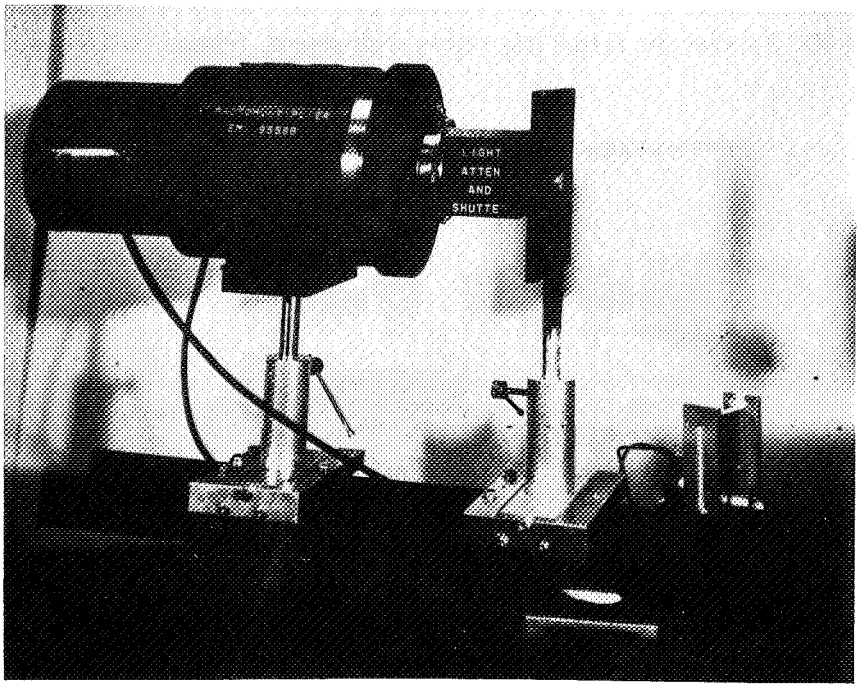

Figure 10.15 Drive motor, pinhole mount, and detector assembly of laser goniophotometer

collimator, sample holder, and focusing lens. Figure 10.15 shows the pinhole mount and detector, with provision for a shutter and suitable filters. The motor that powers the movable arm when a spectrum is obtained is also visible.

Two test emulsions have been chosen for preliminary work. These are a filtered gelatin emulsion and a polyacrylamide emulsion, to which ferric ammonium citrate has been added. The scattering spectrum of each of these emulsions has been run using the instrument just described; these spectra are shown in figure 10.16. No significance should be placed in the shape of these curves, as a considerable amount of instrumental noise was present. The sources of this noise are now being located and eliminated. What is significant is that there was no detectable difference between the scattering of the filtered gelatin emulsion and a plain, uncoated glass substrate. The polyacrylamide appeared to be more noisy at angles below 11°, but above this angle there was no detectable scattering. For comparison, Kodak 649-F and Agfa 10E70 emulsions were also run. They produced identical spectra, also plotted as the curve labeled "silver halide." These preliminary results indicate that the two test emulsions chosen do exhibit the required low noise characteristics.

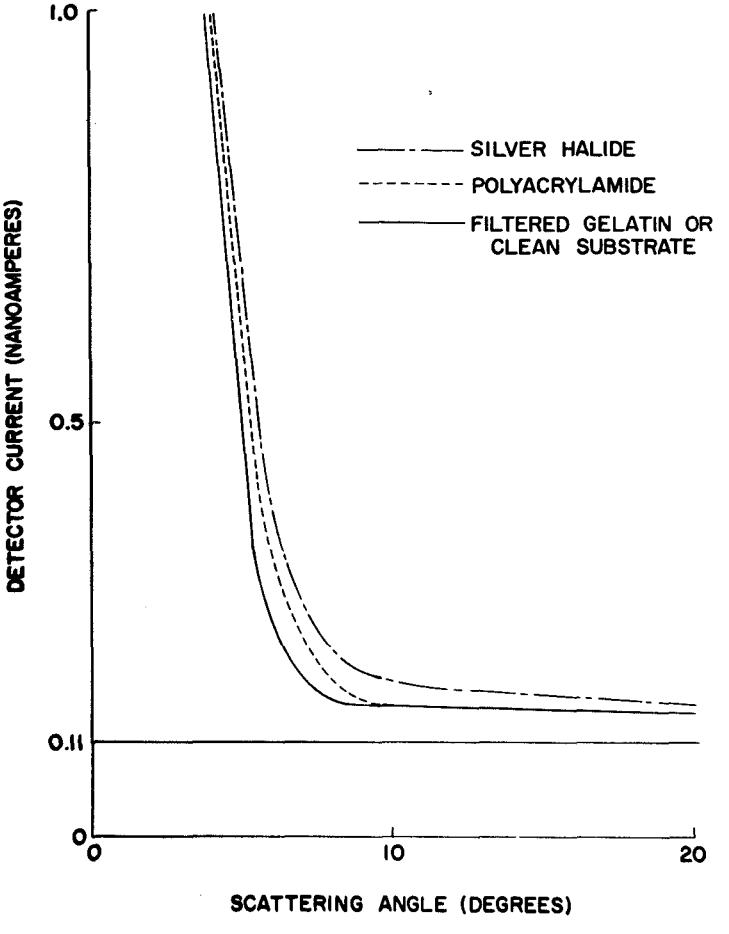

Figure 10.16 Light scattering spectrum

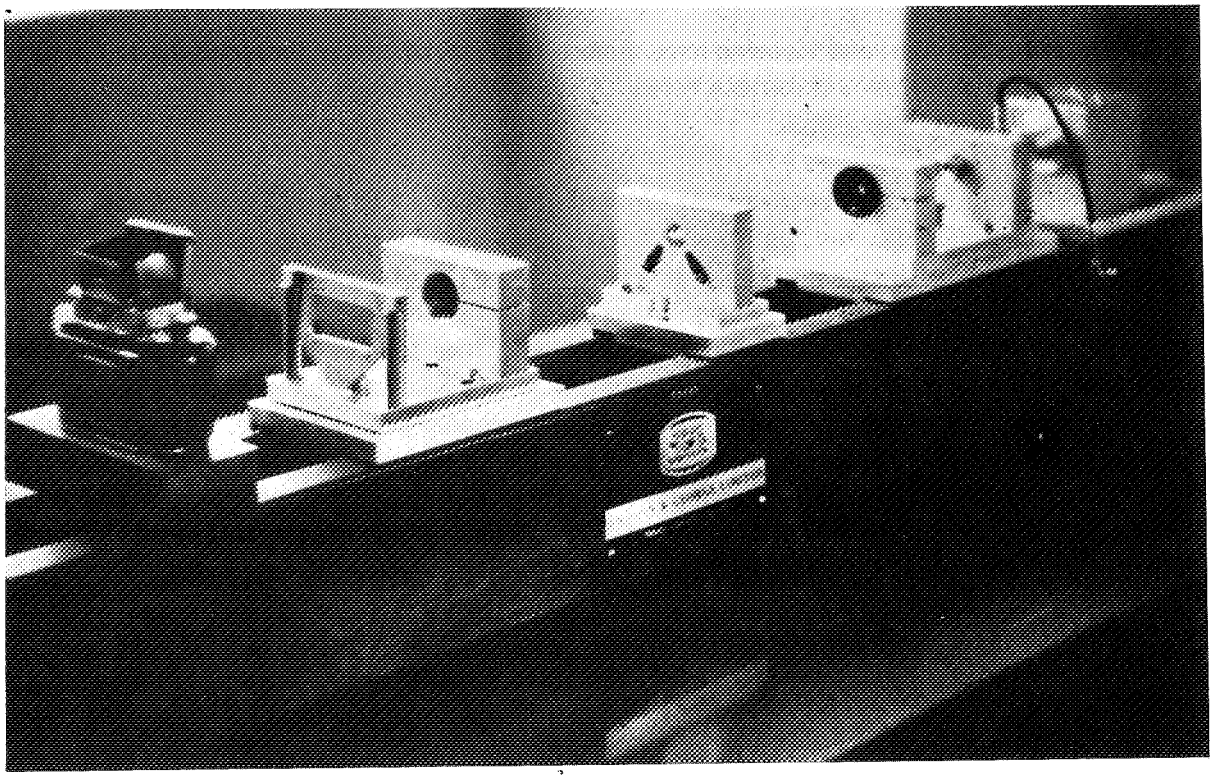

Figure 10.17 Optical processor for contrast amplification of conventional image

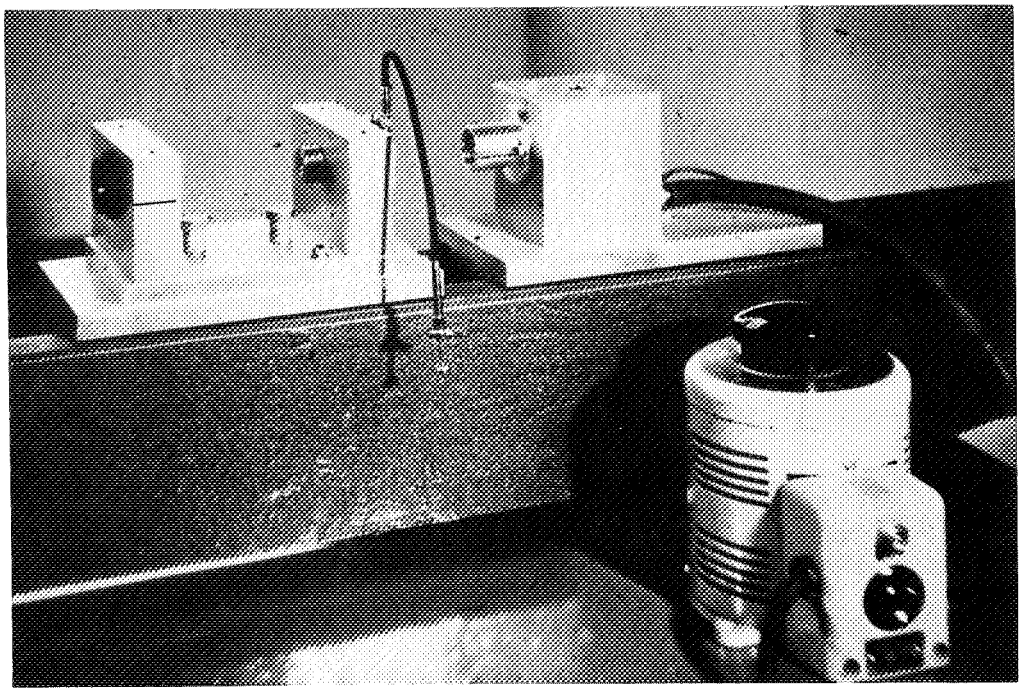

Figure 10.18 Light source, pinhole mount, and collimating lens of contrast amplifier optical processor

An instrument has been built, similar to that in figure 10.11, for contrast amplification of conventional images recorded on these materials, and is shown in figure 10.17. Figure 10.18 shows the lamp housing, pinhole mount, shutter, collimating lens, and autotransformer used to vary the intensity of the lamp. Figure 10.19 illustrates the focusing lens and zero-order attenuator. The attenuator is an accurately positioned photographic image of the pinhole. The instrument actually utilizes multiple pinholes rather than just one. This quasi-diffuse illumination should tend to minimize local imperfections in the optical system of the instrument.

The feasibility of utilizing these and other high-speed/high-resolution processes for recording both holograms and conventional images will be determined, using the instruments described as tools.

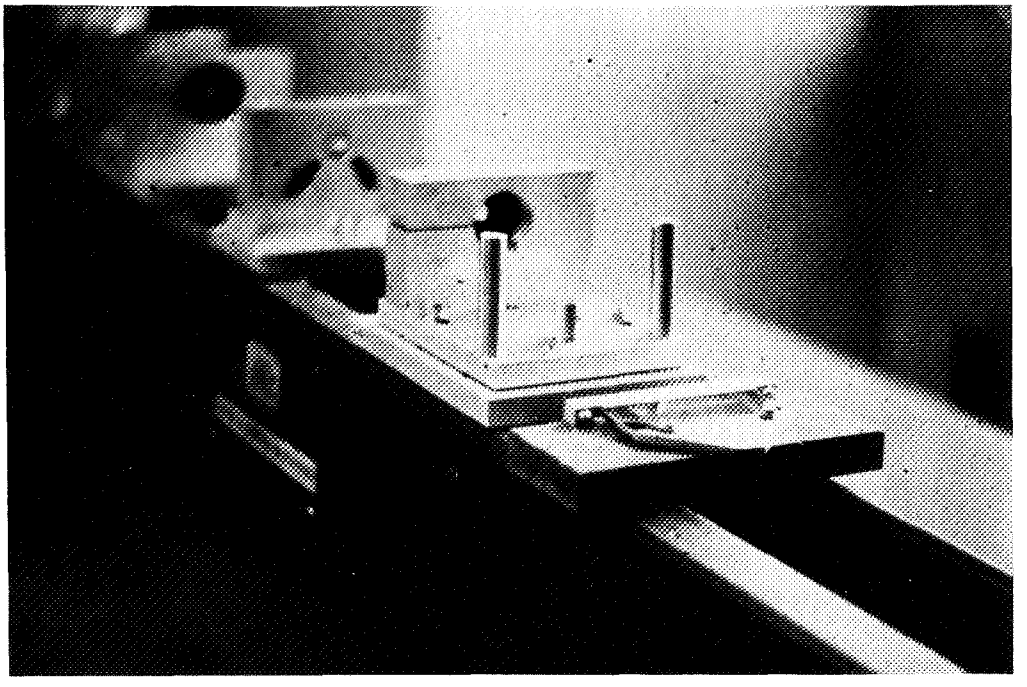

Figure 10.19 Focusing lens and zero-order attenuator used for contrast amplification

11 APPLYING HOLOGRAPHY TO REACTING-SPRAY STUDIES

Richard M. Clayton
Jet Propulsion Laboratory

and

Ralph F. Wuerker
TRW, Inc., Systems Group

Holographic techniques for studying liquid rocket combustion processes are discussed. Feasibility studies of the technique for recording reacting-spray particle-size information were implemented through JPL contracts with TRW Systems, which included the design and construction of a two-beam, pulsed ruby laser holocamera, and its operation at a JPL test facility. The resulting holocamera was used to record confined reacting sprays occurring inside 3- and 18-in.-diameter windowed rocket chambers, as well as unconfined (atmospheric pressure) sprays. The holographic apparatus is described, and some of the pertinent results are presented. It is concluded that holograms of reacting sprays are feasible, but that the technique needs further development if information elucidating spray-combination phenomena is to be obtained.

Conceptually, the liquid rocket combustion process is straightforward, requiring only that the reactants (fuel and oxidizer) be brought into intimate contact within the combustion chamber and that the chemical reaction be completed within the chamber, producing the high-temperature product gases for thrust production by a nozzle-expansion process. Complications arise, however, when it is also required that the reactions be completed in a minimum-sized combustor for flight propulsion applications.

For most of the contemporary liquid propellants, the primary heat release takes place in the gas phase and occurs very rapidly, assuming that the component reactants are well mixed. Thus, reaction times are rarely combustion-rate controlling, and the evaporation and mixing rates become the limiting processes. Closely associated with both of the latter are the fineness of the atomization and the degree of mixing achieved in the formation of the droplet sprays of liquid reactants. Therefore, if combustor size is restricted, optimization of these processes is necessary to yield high performance efficiency.

A number of injection schemes to perform atomization and mixing are possible, a few of which are depicted in figure 11.1. Of those illustrated, the impinging jet configurations have been shown to be the most effective for liquid rocket applications. An example of the spray produced by the so-called "unlike-impinging" element, flowing water, is shown in figure 11.2. Note that a field of spray is produced, having a definite spatial distribution of fluid mass and particle sizes.

A group of elements combined into an injector assembly forms the injection scheme for a typical conventional rocket engine. Figure 11.3 shows the composite spray (water) produced by the

47 elements of an 11-in.-diameter injector utilized for JPL combustion research; note the high number density of liquid particles that, under combustion conditions, must be evaporated and the vapors reacted before leaving the combustion chamber if high performance efficiency is to be achieved. For reference, the length of the chamber utilized with this engine is approximately 16 in., about the relative distance to the lower edge of the photograph.

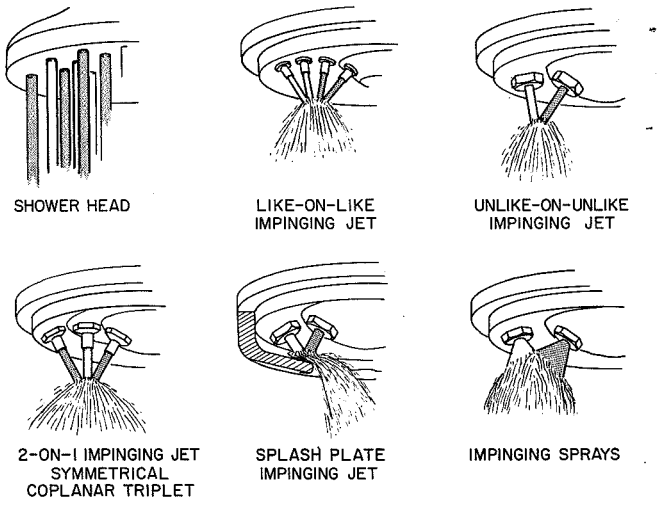

Figure 11.1 Typical rocket injector elements

As discussed above, combustion rates are closely related to the initial atomization processes and understanding these processes and characterizing the mass and particle distributions produced is basic to specifying engineering design criteria for injectors. Unfortunately, reacting sprays are very difficult to study because of severe combustion environments. Hence, most studies have utilized nonreactive fluids. Combustion results, however, do not always correlate well with the nonreactive results; therefore, the most obvious need is to correlate nonreacting- and reacting-spray properties.

To this end, holography appears to offer great potential because of the technique's ability to record a three-dimensional scene faithfully for later analysis. Therefore, a complete particle size and spatial distribution conceptually can be recorded at one instant using a high-power, pulsed-laser light source. Also, holography appears to have the resolution potential to record sizes down in the 10-μ range, which also is required for spray-combustion studies. Finally, the high light intensity of the

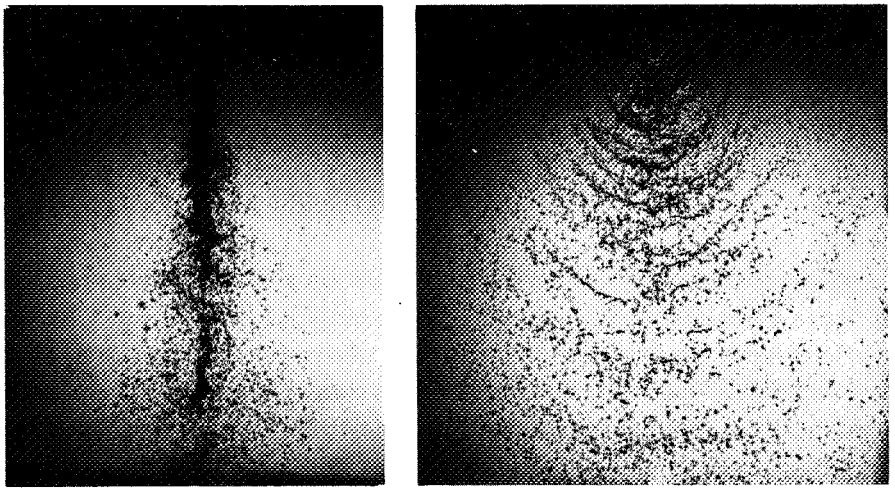

Figure 11.2 Orthogonal views of spray from a pair of impinging jets

laser seems well suited for penetrating the dense optical path through the combustion environment. Thus, a program was launched to test the application of this technique for studying reacting sprays.

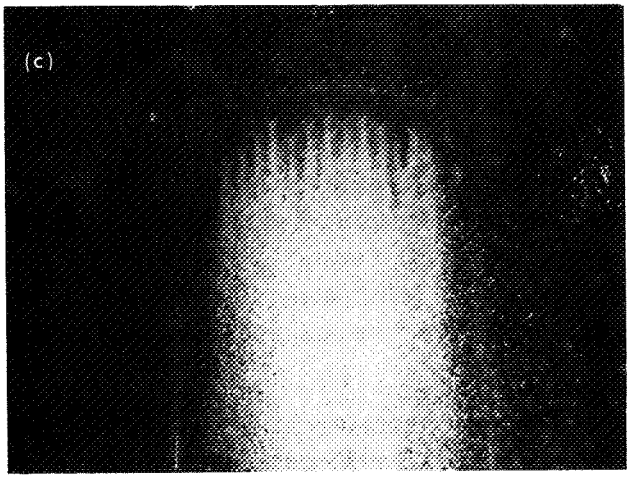

Figure 11.3 Spray from a composite 11-in.-dia injector

The program was implemented via two consecutive contracts with TRW Systems, which evolved into five phases of effort:

1. Design and fabrication of holographic apparatus suitable for operation at a JPL rocket test facility and for use with any of three JPL rocket combustion devices.
2. Producing holograms of nonreacting and reacting sprays in the open atmosphere.
3. Producing holograms of reacting sprays of single elements operating in a 3-in.-diameter combustor (transparent walls).
4. Producing holograms of the composite reacting sprays of the 11-in.-diameter injector (fig. 11.3), operating with an 18-in.-diameter combustion chamber (windowed walls).
5. Analyzing the holograms taken in (2), (3), and (4) for particle size and other combustion information.

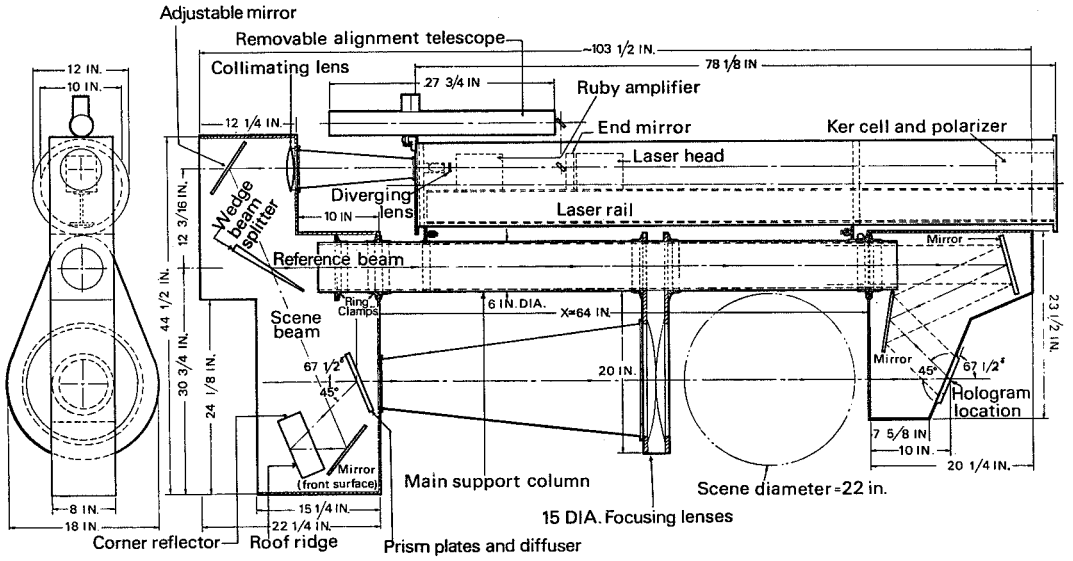

Figure 11.4 Schematic of the JPL pulsed ruby laser holocamera

HOLOGRAPHIC APPARATUS

As noted above, the holographic apparatus was required to function with three different combustion devices. The 18-in.-diameter combustor established the required scene volume dimensions. In addition, the equipment had to function in the environment of a liquid-rocket test stand, which imposed corrosive gases, high-temperature exhaust products, vibration, and random variations of climatic conditions on the camera. Further complications arose from the necessity of synchronizing the holographic operations with short-duration rocket firings (about 1 sec) from a control center located about 500 ft away. These requirements obviously took the holography technique "out of the laboratory." Ultimately, the holocamera shown in figure 11.4 was designed and fabricated. Figure 11.5 shows the equipment installed at the test stand, straddling the 18-in. engine.

Holocamera Design

The holocamera was built around a 6-in.-diameter, 6-ft-long aluminum pipe. An enclosure at one end contained a telescope, beamsplitter, and beam-directing components. At the other end was an enclosure containing the terminal optics, a shutter, and the hologram plate holders. The ruby laser illuminator was mounted on the top of the holocamera in a nitrogen-pressurized tube. This served to protect the laser components from the external environment. Mounted on the laser enclosure were an alinement telescope and a 1-mW helium-neon alinement laser.

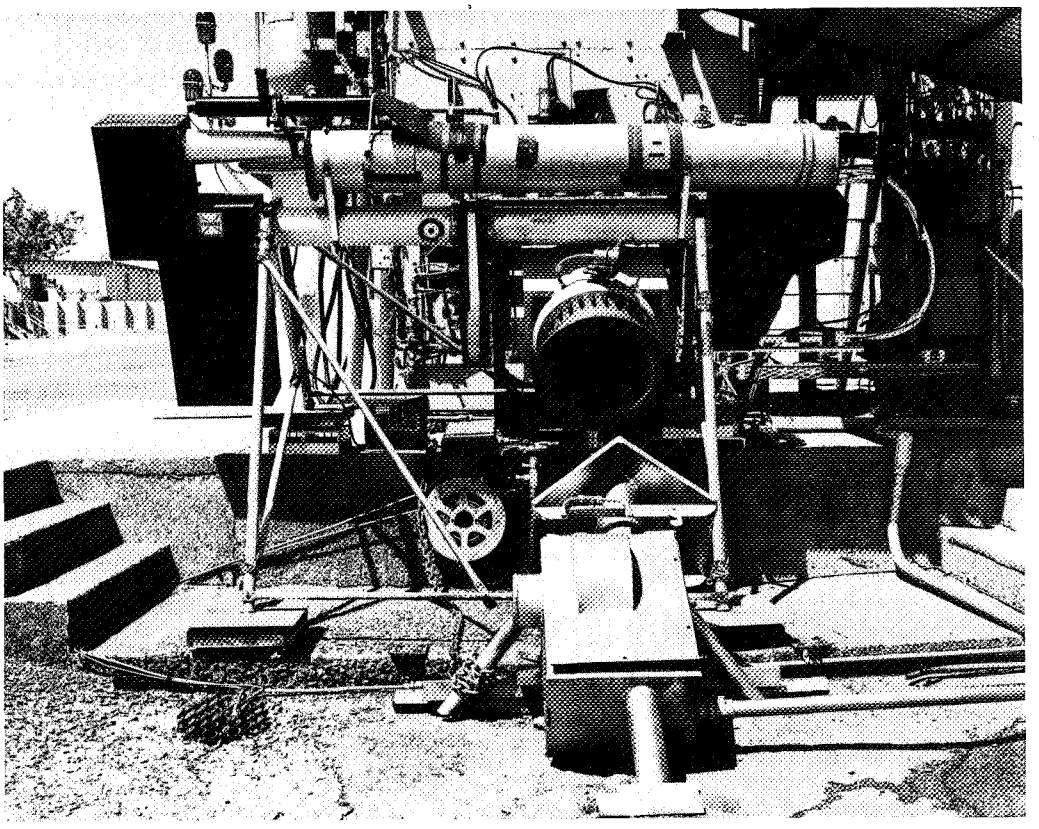

Figure 11.5 The laser holocamera straddling the 18-in.-dia engine

The ruby laser illuminator was from the Physical Electronics Laboratory of TRW Systems. It was a Kerr-cell Q-switched oscillator with a power amplifier stage. The ruby was 1/2-in. diameter by 3-3/4-in. long. The crystal was doped with 0.05 percent Cr^{+++} and cut with the "C" axis of the crystal at 60° to the optical axis. The oscillator cavity was 1.5-m long. The rear reflector was a dielectric mirror with a reflectance greater than 99 percent, while the output reflector was a 1/8-in.-thick sapphire resonant reflector. The Q-switch consisted of a nitrobenzene-filled Kerr cell and a calcite polarizer. The amplifier stage was used to boost the power emitted from the oscillator to a usable level. It consisted simply of a laser head containing a ruby similar to that used in the oscillator. The laser emitted a 50-nsec pulse of 694-nm light. The energy in the pulse was 1 to 3 J. Except for the long cavity length, the laser was quite conventional. No special precautions were taken to improve or control the coherence of the laser.

The light emitted by the laser was expanded to 5-in. diameter by a Galilean telescope and directed onto a glass wedge, which served as a beamsplitter. Six percent of the light was reflected from the first surface and became the reference beam, while about 88 percent of light was transmitted by the beamsplitter and became the scene beam.

The reference beam was directed down the center of the main support column onto a pair of mirrors at the far end of the holocamera and then onto the hologram plate at an angle of 45° to the scene beam. The hologram was canted so that its normal bisected the 45° reference-scene angle. This orientation was chosen so that the interference pattern would lie perpendicular to the surface of the hologram emulsion, thus minimizing the effects of emulsion shrinkage.

The light that passed through the beamsplitter was directed onto a pair of mirrors arranged as a roof reflector. These mirrors served to invert the light so that it could later be spatially matched to the reference beam. The light was then directed onto a "prism plate" that refracted the light by 45° into the scene-beam tunnel. A pair of large condensing lenses at the end of the tunnel focused the prism plate onto the hologram. To allow the reference beam room to impinge on the plate at 45°, it was necessary to set the hologram plate 10 in. away from the scene volume. Because of the added path, this caused some reduction in the resolution of the system.

A 4 X 5-in. focal plane shutter, taken from a 40-year-old Graflex camera, was adapted as the shutter in the holocamera. The maximum speed of the shutter was 50 msec. A cam and microswitch were added to fire the laser when the shutter was in the open position. The shutter was released by a solenoid actuated by the sequence timer that controlled the firing of the various combustion devices.

To further suppress ambient light, an 8 X 8-in. colored glass filter (Corning Glass CS-2-64), transparent at the ruby wavelength but opaque throughout the rest of the visible spectrum, and a sheet polarizer were mounted over the port nearest the hologram. For short periods of time, this was adequate; however, for long periods, there was enough light transmitted by the filter and the focal-plane shutter to fog the Agfa 8E75 plate. Fogging was eventually eliminated by the addition of a Harvard Electric capping shutter over the port.

Because the coherence of the laser was not very good, compensation techniques were necessary to make the hologram. The laser light has two coherence properties, spatial coherence and temporal coherence. To satisfy the spatial coherence condition, the 15-in. condensing lenses were used to image the prism plate diffusers onto the hologram. The light in the reference beam was directed to the hologram so that the scene and reference light at any point on the hologram could be traced back to the same ray leaving the Galilean telescope. In order to do this, an alinement procedure was established using the gas laser. Working in the dark so that the low-powered light was visible, a wire cross was inserted before the Galilean collimating lens. This threw a shadow of light into each beam. By use of the mirrors in the reference beam leg, the crosses were manipulated so that they were superimposed at the hologram plane. They were also adjusted by the use of neutral density filters and additional diffusers in the scene beam leg to give an intensity ratio of 1:1. This arrangement apparently yielded the best and brightest holograms.

The other compensating feature of the holocamera was its temporal matching property. This was realized by placing the optical elements so that the corresponding rays of scene and reference light traveled equal distances from the beamsplitter. Because of the 45° reference-to-scene beam angle, the length of the reference beam increased progressively from the top to the bottom of the hologram. To compensate for this change in length, the scene beam was directed into the back of the prism plate at the same angle. Because the prism plate is essentially a Fresnel prism, this arrangement provided good holograms even though the coherence length of the light was not great.

The prism plate was fabricated by machining a fine, precalculated sawtooth pattern in two pieces of plexiglas. These plates were mounted in the holocamera with their machined surfaces facing each other and were canted so that they would be imaged onto the hologram. Ground glass diffusers were mounted at the prism plate location to diffuse the light.

After a hologram was exposed, it was taken in a sealed cassette to a darkroom where it was developed. The developer was a 1:4 solution of Eastman Kodak HRP. After being developed and rinsed, the plate was fixed in a 1:4 solution of Eastman Rapid Fix. The plate was usually examined then by reconstructing the holographically recorded scene to see if it was acceptable. Afterwards, it would be washed and allowed to dry in still air.

When the holocamera was correctly adjusted, the reconstructions were as bright as those made with a gas laser, showing that the coherence of the ruby laser was adequate. Dull or foggy reconstructions indicated a mismatch in the scene-reference optical path. It was found that thick windows added to the scene path were sufficient to degrade the holograms if the reference beam was not compensated by the addition of an equivalent path length. Further details concerning this holocamera can be found in Wuerker et al. (ref. 1).

Holocamera Resolution Test

Because of the necessity of high resolution in the measurements of droplet sizes expected in the tests of rocket combustion, the holocamera was set up in the TRW laboratory for measurements of its resolution capabilities. The camera was arranged with a transparent resolution chart (USAF 1951 pattern) mounted in the test volume, 45 cm from the hologram. A 4 X 5-in. bellows-type

copy camera was mounted behind the hologram plate location and focused on the resolution chart. The normal, wooden plate holder was removed and replaced by one which could assure that a developed hologram could be replaced in the same position as it was recorded. Pictures were made of the test chart as illuminated by incoherent white light and by the laser light in the scene beam, as well as of the reconstruction of the test chart produced by the hologram (fig. 11.6). A high quality enlarging lens and Kodak S0243 film, with a resolution of at least 200 line pairs per mm (lp/mm) were used. The left photograph in figure 11.6 shows the resolution chart with the diffuser of the holocamera back-illuminated by a light bulb. The minimum resolvable spacing is 80 lp/mm, or a spatial period of 12.5 μ. The middle photograph is of the same chart using the emission from the ruby laser. This is a direct ruby laser photograph of the scene under identical conditions as before. An important difference between the two is the granular field, or speckle, which is due to the laser coherence and definitely limits the resolution of the photograph. The limiting resolution is now about 40 lp/mm, or a spacing of 25 μ. A difference of a factor of 2 in the resolution of a scene seems to be a rule of thumb for incoherent vs coherent illumination.

The right photograph in figure 11.6 shows the reconstruction of a hologram made under conditions identical to those above. It was developed in the regular manner, dried, and replaced in the holder. The photograph was taken by blocking the scene beam of the holocamera and using the reference beam to reconstruct the wavefront. The reconstruction can be read only to 20 lp/mm, a spacing of 50 μ. Thus the resolution of the reconstructed hologram is seen to be a factor of 4 poorer than a white light photograph, and a factor of 2 less than a directly illuminated photograph. Even under optimum conditions, this limits the positive identification of particles to those of 25 μ diameter or greater. Further details on these evaluations are described in Wuerker et al. (ref. 2).

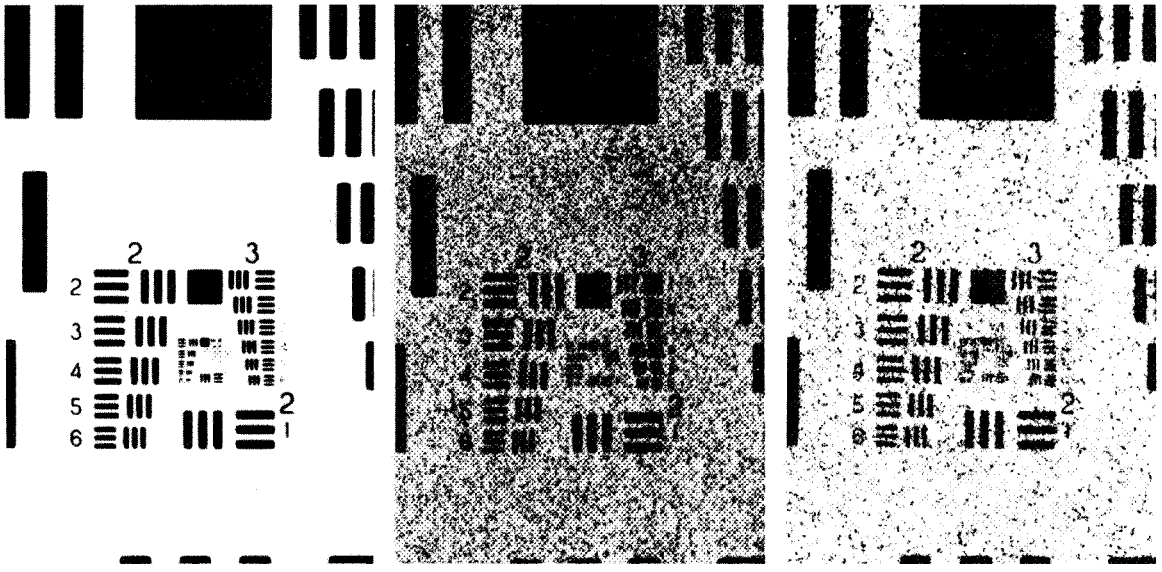

Figure 11.6 Three photographs of a 1951 resolution chart taken in the JPL 45° holocamera at 45-cm distance under identical conditions. Left picture is a photograph with white-light illumination, center picture is a photograph with ruby laser illumination, right picture is a photograph of a holographic reconstruction. The resolution was 80, 40, and 20 line pairs per mm, respectively

HOLOGRAPHIC RESULTS

Open-Atmosphere Sprays

Figure 11.7 shows a typical example of the reconstruction of the hologram of an open-atmosphere reacting spray. The two views were obtained by varying the angle of the copy camera and can be viewed stereoptically. Flow from the unlike-on-unlike impinging jets (jet diameter = 0.173 in.) is from right to left. The reactants are nitrogen tetroxide and a fuel blend of 50 percent hydrazine and 50 percent unsymmetrical dimethylhydrazine. The overall oxidizer-to-fuel ratio is 1.25:1 and the average velocity of the streams prior to impingement is ~123 fps. The sharply defined object extending across the scene is a steel bar supported in the plane of the impingement and contains 1/4-in.-diameter holes on 1-in. centers.

Comparison of the hologram reconstruction with the right-hand view of figure 11.2 (taken by backlighted flash photography) indicates an overall topological similarity between the nonreacting and reacting sprays, but the definition of individual spray particles is obviously reduced in the hologram reconstruction.

This lack of definition was observed in all the holograms and has yet to be satisfactorily explained. The effect seems to be more than the difference in optical resolution between incoherent and coherent illumination, expected as a result of the resolution tests described above, since microscopic examination of the holograms revealed that relatively few distinct drops of any size could be discerned. Rather, the regions of the spray where drops are expected gives the appearance of a fine, lacy pattern. A few particles were identified only in the periphery of the spray. It is not

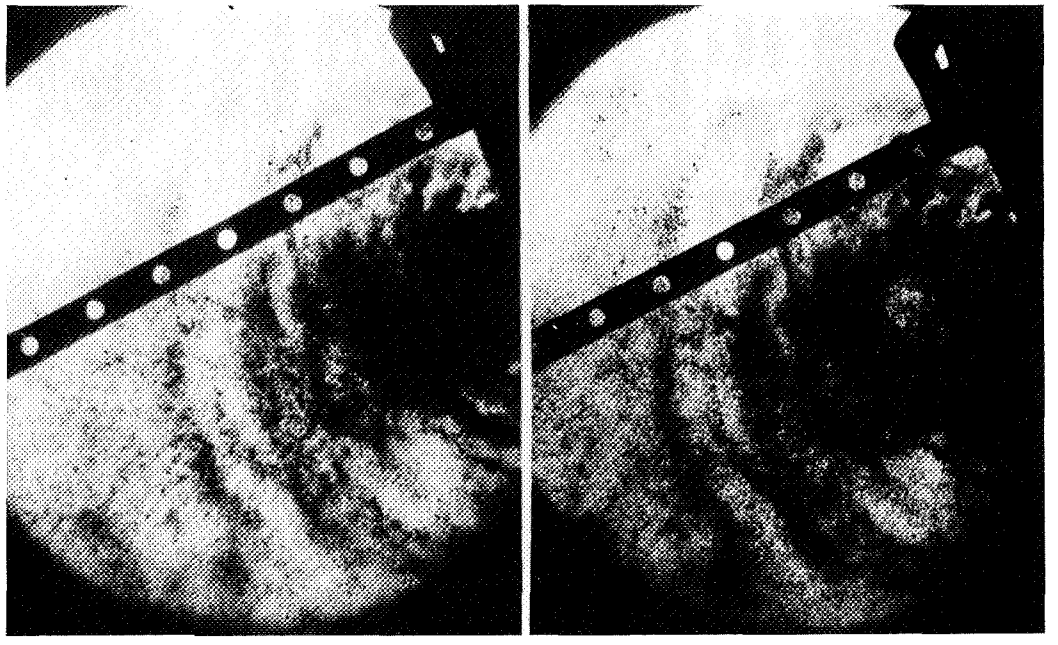

Figure 11.7 Stereo-photographs of the reconstruction of an open flame hologram

clear at this time whether this appearance of the reacting spray is real or reflects some limitation of the holographic technique for use with the temperature and density gradients encountered in such combustion fields.

Confined Sprays in the 3-in.-diameter Engine

For these experiments, a single unlike-impinging element was connected to a 3-in.-diameter acrylic combustion chamber. The jets were 0.099-in. in diameter and the fuel was unsymmetrical dimethylhydrazine with red fuming nitric acid oxidizer. The fuel:oxidizer mixture ratio was 40:1. The combustion chamber, 6-in. long and with 0.40-in.-thick walls, was fitted with an exhaust nozzle to produce approximately 100-psia chamber pressure. The entire engine was mounted within the scene volume of the holocamera (fig. 11.8).

Initial attempts to produce holograms of these firings failed because of the light absorption of the combustion field and the erosion of the acrylic chambers. The absorption effects were ultimately overcome by adjustments of the scene/reference intensity ratio; however, the erosion always degraded the holograms by introducing distortion and light diffusion. The marginality of these

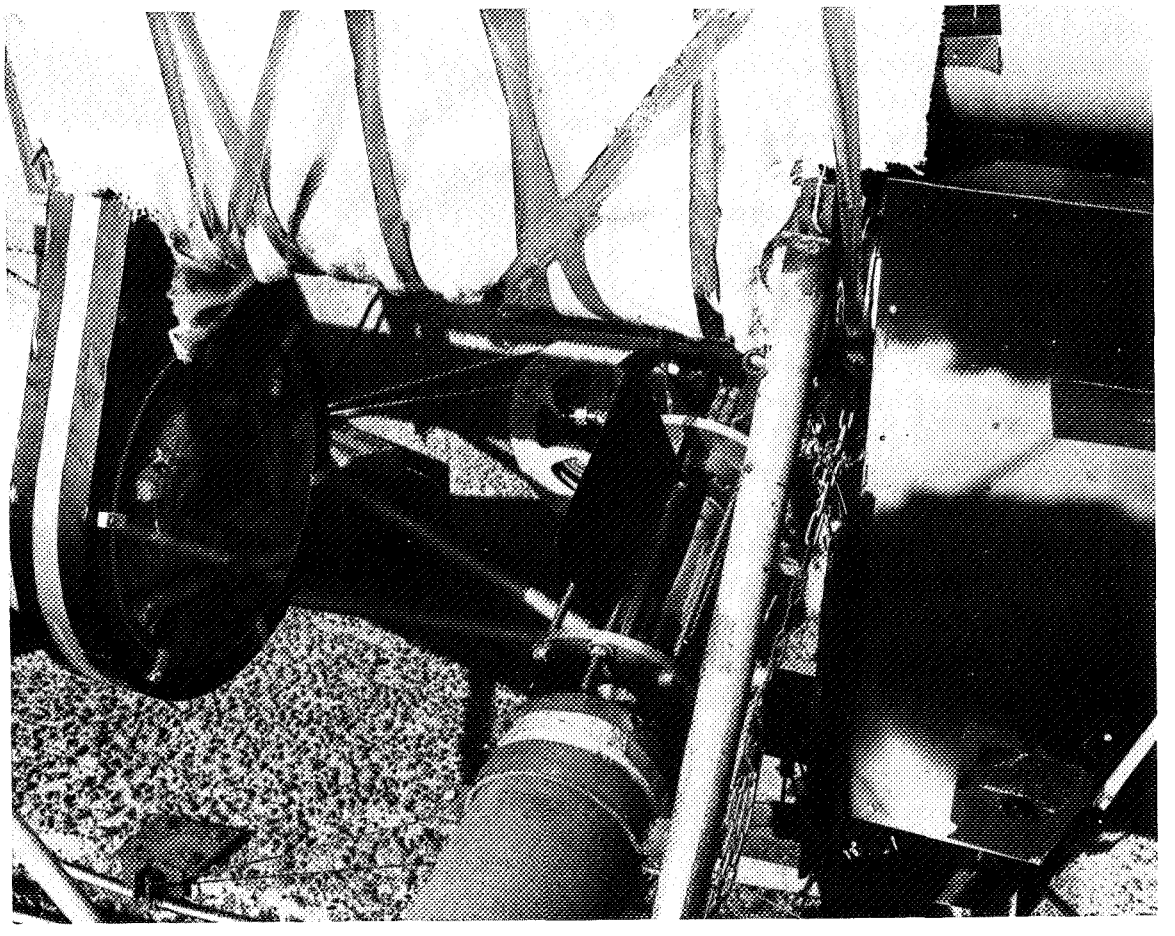

Figure 11.8 The 3-in. engine in the scene volume of the holocamera

chambers was suspected from the inception of the project, but it is felt that they at least served to test the applicability of the holographic technique.

Reconstruction photographs of one of the better holograms are shown in figure 11.9. The views differ by a change of focus of the copy camera, going from the near to the far wall of the chamber for the bottom to top views, respectively. The two center views correspond to best focus around the spray fan.

Microscopic examination of several holograms of the 3-in.-diameter engine firings failed to reveal any distinct drops of spray. The lacy structure noted previously for the atmospheric sprays was even more pronounced in these holograms. While the poor optical quality of the acrylic chambers undoubtedly degraded the clarity of the holograms, comparison of figure 11.9 with figure 11.7 (where no window effect is present) reveals a definite similarity in the gross appearance of the spray, suggesting that the appearance is not entirely the result of the acrylic.

Other attempts to obtain holograms of reacting sprays using improved windows and a different holocamera (ref. 3) have produced somewhat higher resolution results and even shown that a few particles can be observed under combustion conditions similar to those in the present experiments. However, it is the opinion of the senior author that these later results do not show a major difference from those reported herein. Thus, the question of the effective resolution of holography under combustion conditions remains.

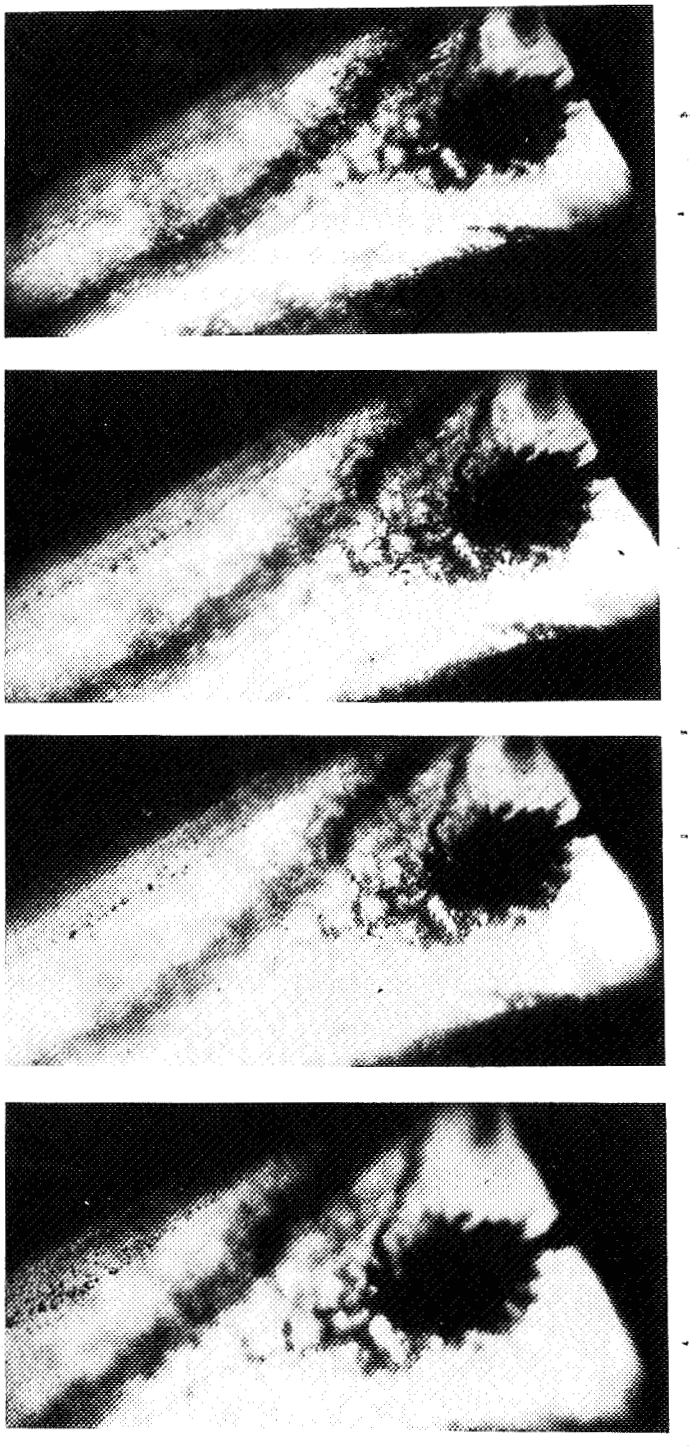

Figure 11.9 Four reconstructions of a hologram of a 3-in. engine firing; the copy camera was focused on different planes

Confined Sprays in the 18-in.-diameter Engine

The holographic arrangement for the 18-in. engine experiments is shown in figure 11.5. This engine utilized the injector shown in figure 11.3; and in view of the results of the atmospheric and 3-in. engine experiments, prospects for obtaining spray holograms of this complex combustion system clearly were marginal. However, a total of six reconstructable holograms were obtained after considerable efforts to isolate the holocamera from mechanical vibration imposed by the engine. The holograms were of relatively poor quality compared to the results previously shown, and certainly showed no particles, although the entire 18-in. distance across the combustor could be discerned. This certainly demonstrates the penetrating power of the pulsed ruby laser. No reproduction photographs are shown here because of the weak reconstructions.

HOLOGRAM ANALYSIS

After obtaining the holograms described above, a detailed evaluation of their combustion information content was made. The procedures employed in this evaluation are described in Wuerker et al. (ref. 2). The best of the atmospheric-spray holograms were chosen, and photographs of their reconstructions were examined by manually scanning them with a measuring microscope of 15X to 30X magnification. The overall results have been noted above concerning the absence of identifiable liquid particles in the region of the significant mass flux of the spray; however, droplet counts were possible in the peripheral regions. Interestingly enough, no drops of less than 100 μ were found.

It was determined that for those regions where droplets could be discerned, quantitative size distributions could be obtained from the miscroscope measurements. These limited samples yielded distributions reasonably close to those measured in nonreactive sprays, considering that it is probable that the smaller particle sizes were not visible. Whether this result adequately characterizes the reacting spray is doubtful, however, due to the small samples measured. But as the first step in testing the application of holography to spray studies, these results are encouraging.

REFERENCES

1. Wuerker, R. F.; Matthews, B. J.; and Briones, R. A.: Producing Holograms of Reacting Sprays in Liquid Propellant Rocket Engines. Final Report, JPL-952023 (NAS7-100), TRW Rep. 68-4712-2-024, 31 July 1968. NASA CR-97209, 1968.
2. Wuerker, R. F.; Matthews, B. J.; and Heckert, B. J.: Analysis of Holograms of Reacting Sprays. Final Report JPL 952357, TRW Rep. 12299-6001-RO-000, Jan. 1970.
3. Wuerker, R. F.; and Matthews, B. J.: Laser Holocamera Droplet Measuring Device. Final Report, Nov. 1968–July 1969, AFRPL-TR-69-204, Nov. 1969. (TRW-11709-6001-RO-00).

12 OPTICAL PROCESSING OF MICROWAVE SIGNALS FOR NONDESTRUCTIVE TESTING

Robert W. Cribbs
Electro-Physics Company

A research program is being conducted to analyze microwave nondestructive testing data with optical computers. The program objective is to scan large dielectric objects (for example, large solid propellant grains) with a microwave beam and produce a picture of any discontinuities within the structure. Resolution along the scanning direction is achieved by recording and processing a microwave hologram. Resolution along the microwave beam is achieved by a Fourier transform of a full waveguide band microwave sweep. This depth resolution is unlike the ordinary holographic depth perception in that this resolution is independent of the distance from the scanning plane to the object.

Past attempts at making microwave-reflection holograms and reconstructing them with laser light have yielded results unsuitable for nondestructive testing (NDT). If the types of microwave beams used are of the type used for light holograms, the main problem is that objects in the microwave hologram scene act as mirrors. With light illumination, most objects can be seen regardless of the angle at which the light strikes the object because the object is a diffuse reflector. With microwave illumination, most common objects can be seen (or recorded on a hologram) only if the angle of illumination equals the angle of observation. This fundamental problem also limits the usefulness of ultrasonic inspections.

The research effort described in this report is to make microwave holograms of the internal structure of large dielectric objects. Specifically, flaws in very large solid propellant grains should be detected and displayed in a concise, pictorial form. Since the flaw must be detected and measured independent of its shape or orientation, the "ideal mirror" problem must be overcome.

If useful microwave holograms are to be made, the concept of holography must be expanded to include both the formal techniques of light holography and the techniques of coherent optical processing. Very wide microwave bandwidths are used. There may be a general reluctance to call the several techniques described in this report "holograms." This reluctance will, I think, be temporary. With the swept-frequency lasers now available, the techniques described in this report can be applied to "generalized light holography" with spectacular results.

TECHNICAL APPROACH

The technical approach takes advantage of two recent advances: the achievement of high angular resolution with synthetic aperture radar, and the processing of full-band microwave signals for very high depth resolution. In ordinary holography, the lateral position of a point is recorded by

the lateral position of its interference pattern on the hologram. The distance between the hologram plane and the object is deduced from the position at which the object comes into focus. Most objects do not have sufficiently coarse surface texture to permit the eye to focus on microwave image. The achievement of depth resolution by generalized holographic techniques obviates the need for diffuse reflectors: the readout is a cross-sectional picture.

Figure 12.1 shows the types of display commonly used in NDT work. The A scan gives depth information under one point on the surface of the object being inspected. The B scan requires one scan of the transducer. The transducer transmits a narrow beam, so the lateral position of reflectors is determined by the lateral position of the transducer when the echo is received. C scans are made by gating the return echo at a single depth and making a series of scans. Two limitations of these scans are apparent. None of the scans gives information over the whole volume of the object being scanned. In addition the objects must have surfaces normal to the beam to be detected.

Figure 12.2 illustrates how one of these limitations can be overcome. The conventional narrow beam can be replaced by a broad beam and the transducer positioned to produce a beam striking the object normally. Curved surfaces produce a weak reflection. With the broad beam, this weak reflection is received over a large portion of the scan for spherical objects. If the broad-beam scan were processed the same way as the narrow beam, the display would be confusing and difficult to interpret. For example, all spherical objects would be detected and recorded at all positions of the scan.

CONVENTIONAL HOLOGRAPHY

Holographic processing provides a means of reconstructing the lateral position of spherical objects. The equipment required is shown in figure 12.3. The backward wave oscillator (BWO) generates a microwave signal at a single frequency. The BWO is on a table that scans past the scene. The microwave detector detects the interference between the transmitted and received microwave signal. This is amplified and used to modulate the intensity of a cathode ray tube (CRT). The y axis of the CRT is synchronized with the position of the table. The microwave equipment is shown in figure 12.4. For one-dimensional processing, the x axis is free running.

The CRT face is photographed to provide the hologram transparency required for the optical reconstruction. A one-dimensional pattern from two cylinders is shown in figure 12.5. The interference pattern causes the beam of the optical computer depicted in figure 12.6 to converge at the lateral position of the cylinders.

If the negative is placed directly in the laser beam, the image of the scene is superimposed on background light. (This background is called the "dc term" in optical computer work and is equivalent to the reference beam in holographic work.) The electrical signals from the detector swing positive and negative, whereas the photographic density recorded must be positive. In recording the hologram on film, therefore, an offset in light intensity must be added to the CRT display.

To separate the image from the background light produced by this offset, the film must be processed as shown in figure 12.7. Basically, the image is projected onto a grating and

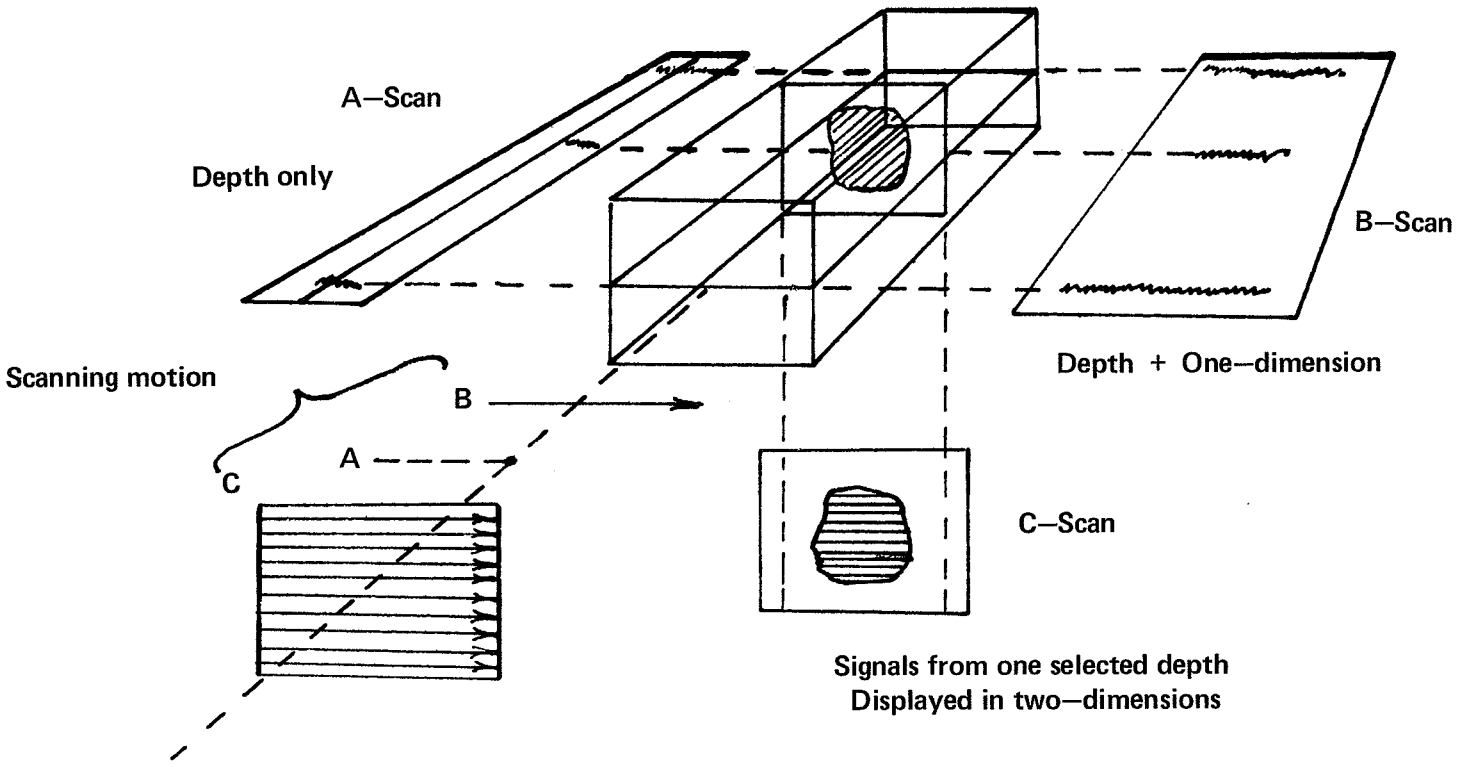

Figure 12.1 Narrow-beam scan modes used in NDT with instruments having depth resolution

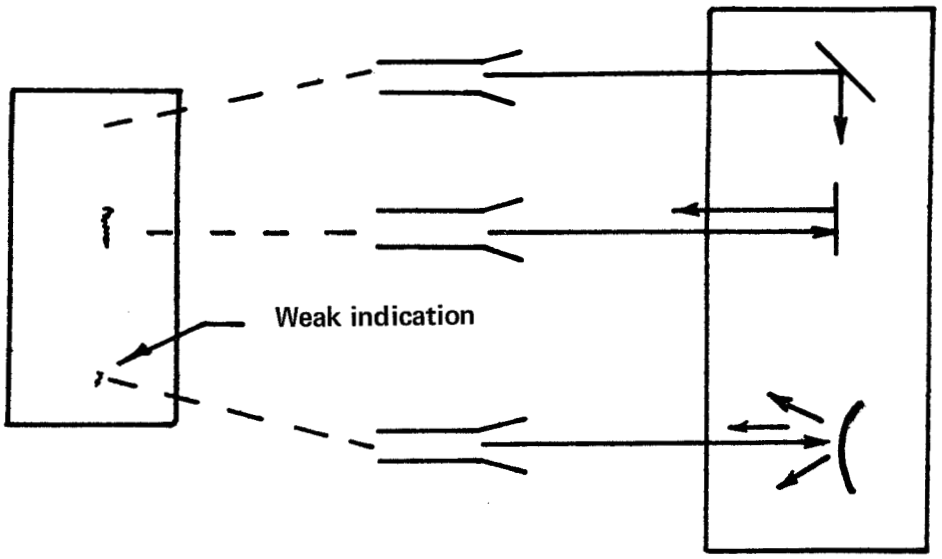

Narrow–beam B–Scan

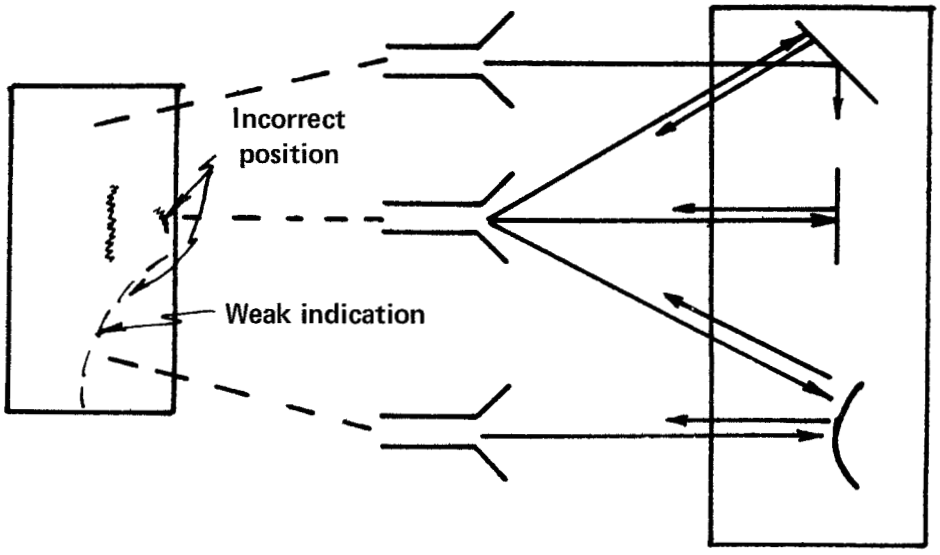

Wide–beam B–Scan

Figure 12.2 Narrow/wide-beam comparison

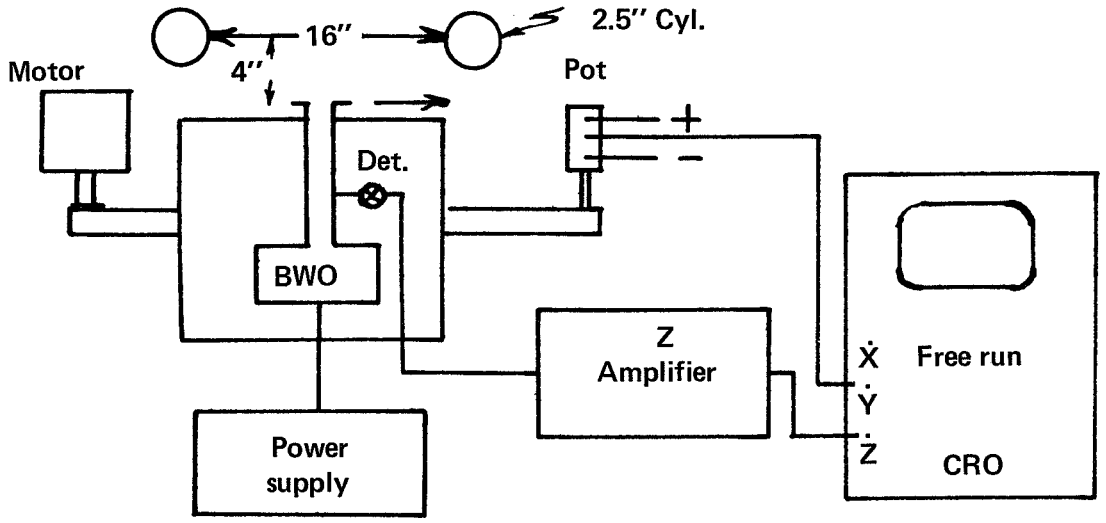

Recording one–dimensional hologram

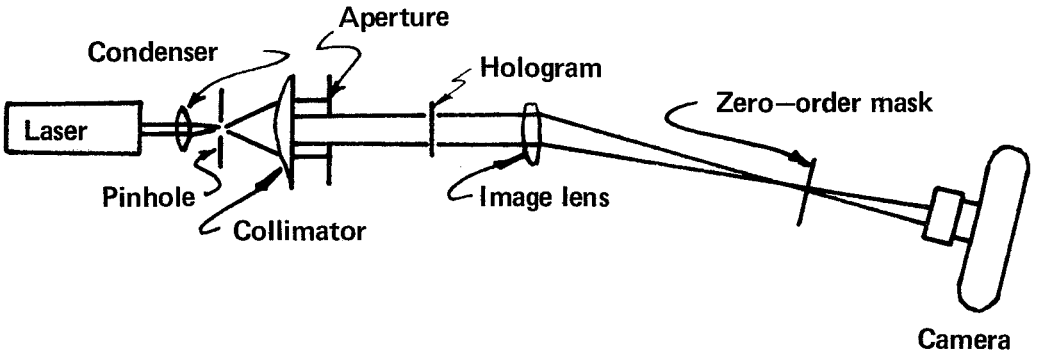

Reconstructing one–dimensional holographic image

Figure 12.3 One-dimensional hologram equipment

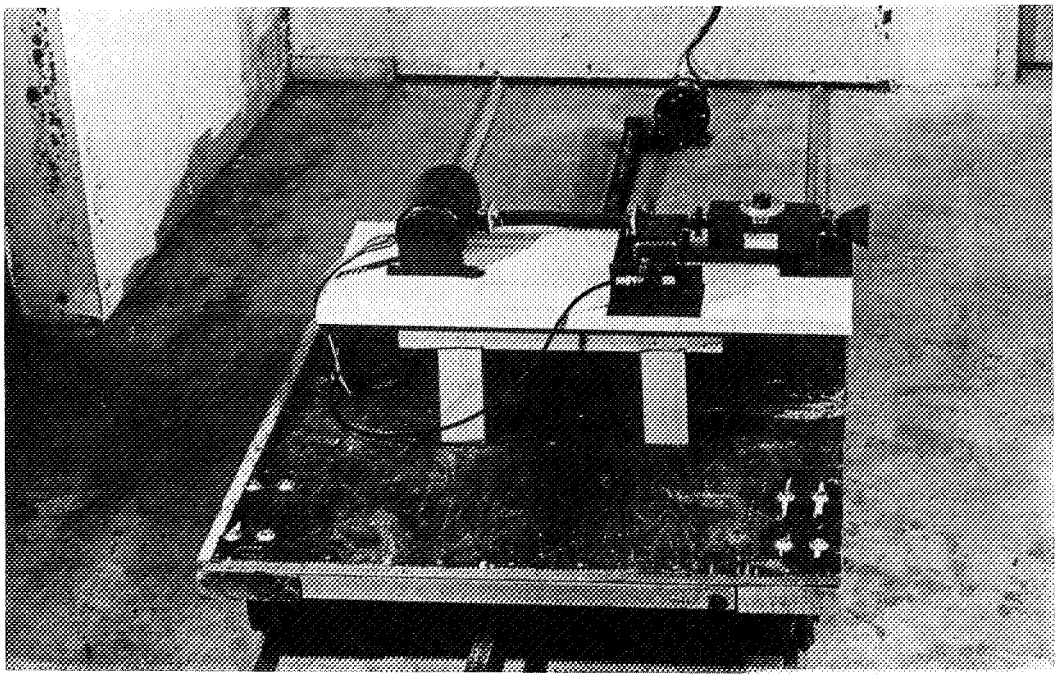

Figure 12.4 Microwave equipment

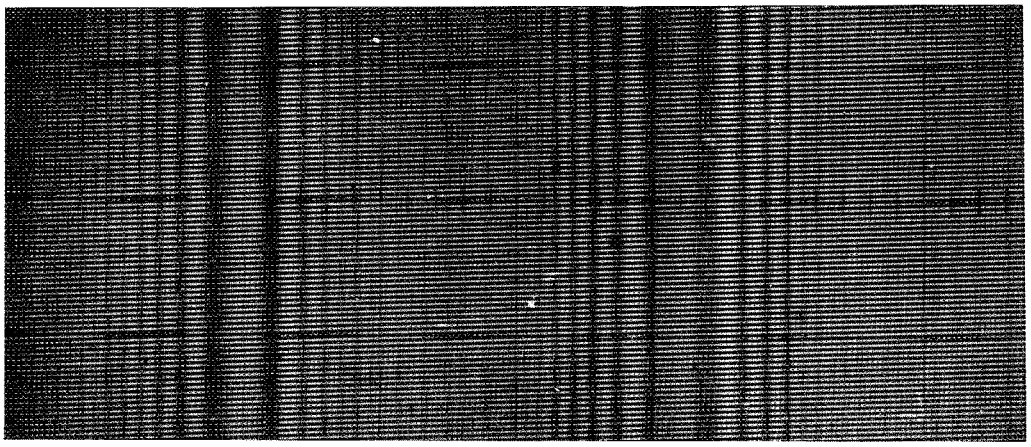

Figure 12.5 One-dimensional hologram

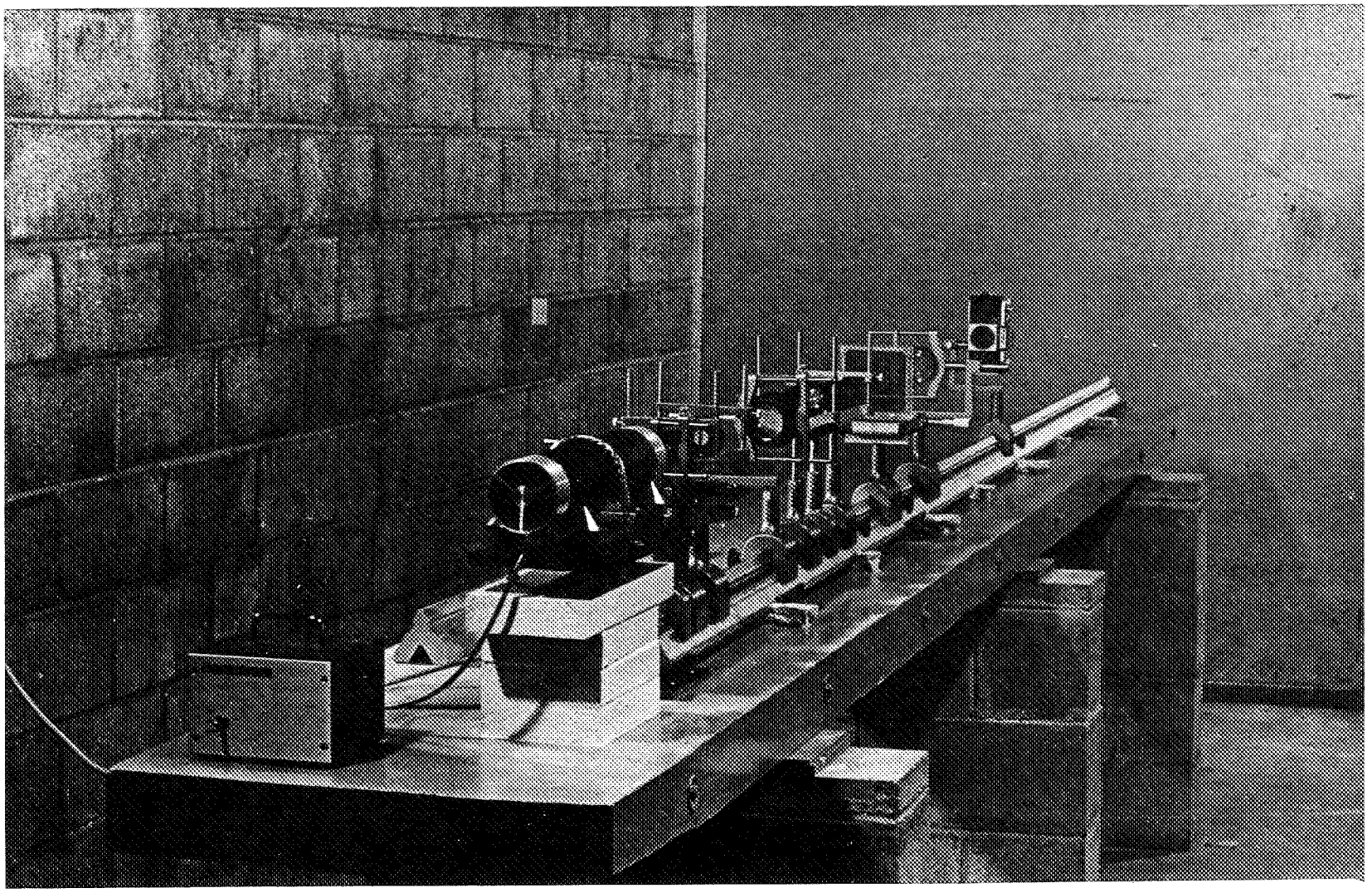

Figure 12.6 Optical computer

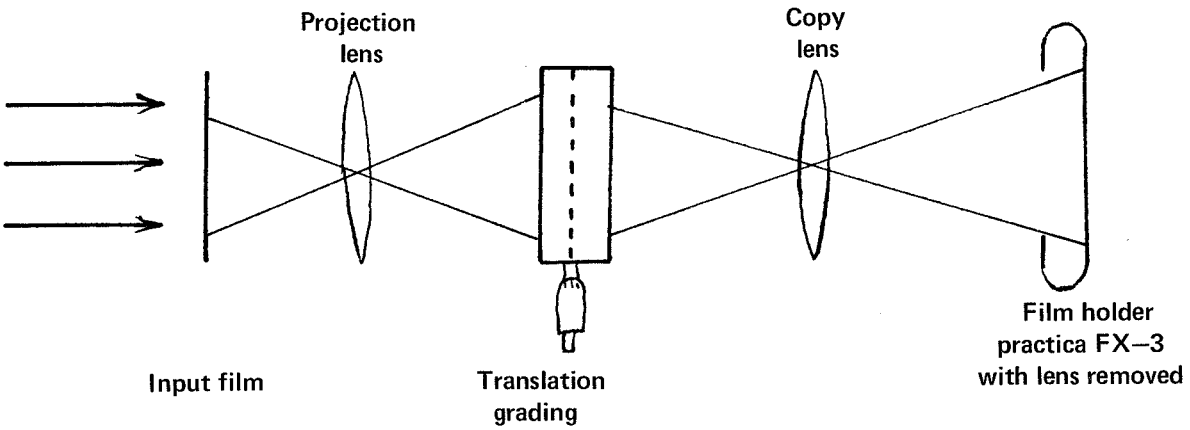

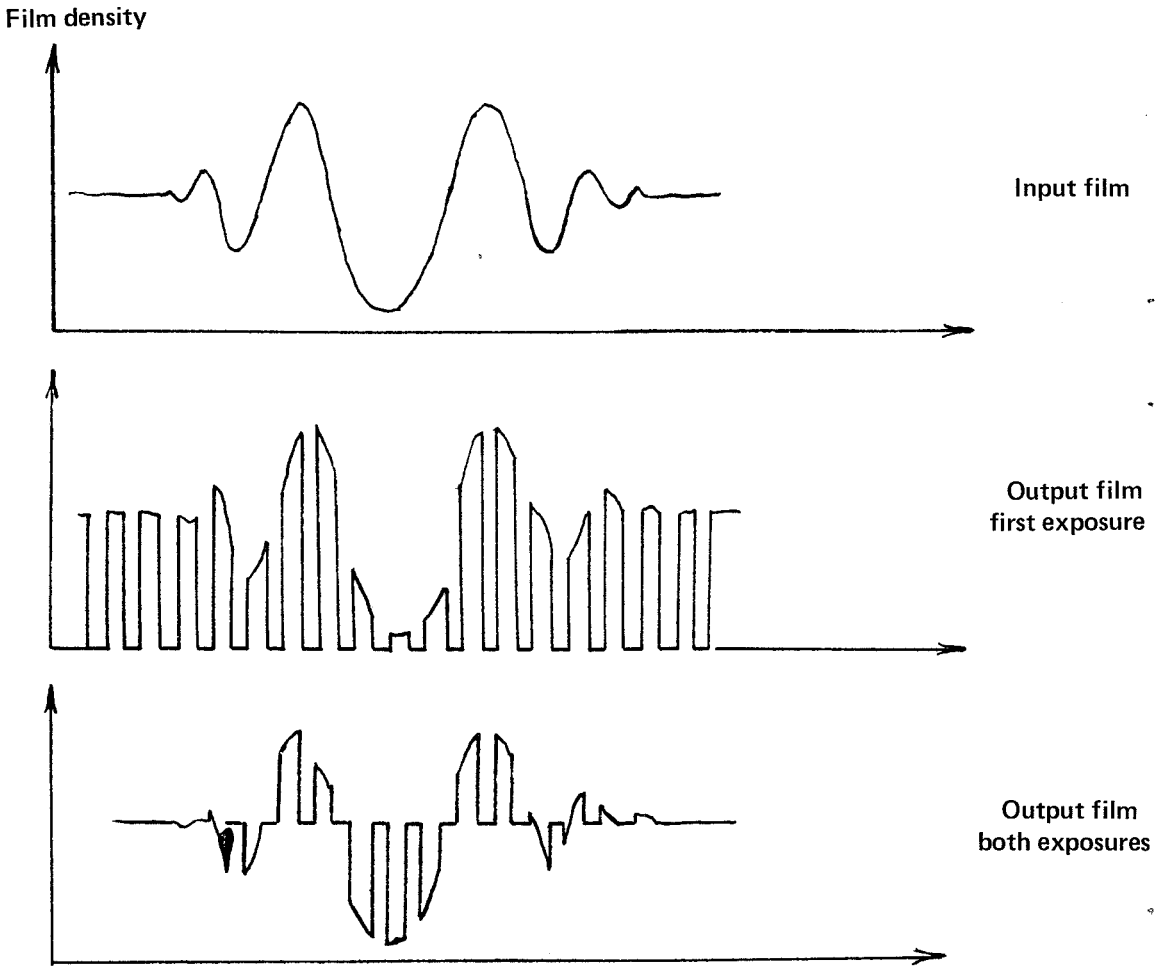

Figure 12.7 Eliminating dc offset

photographed. The new photograph will now defract the image, but it will also defract the dc terms. To avoid this, the grating is translated 180° (the width of one line) and the film exposed to its average density. This new exposure defracts the dc term 180° out of phase and hence cancels the dc term defracted by the first exposure.

A one-dimensional reconstruction is shown in figure 12.8. The two cylinders show as two lines. The contrast in the prints available for this report are lower than that of the image created by the laser beam, and some degradation will no doubt occur in printing. Most of the improvements required for this technique are in the photographic processes.

The process described above for laterally separating reflections is formally the same as light holography. There is one important difference: The plane wave illuminating the scene in optics is synthesized by scanning a point source. Many objects that would not reflect a plane wave back into the recording plane will reflect signals synthesized by the point source, thus alleviating the "perfect mirror" problem.

A series of scans with the vertical position of the scan synchronized with the x axis of the scope (fig. 12.3) yields a two-dimensional hologram capable of three-dimensional imaging. The depth axis is greatly increased in the reconstruction. This exaggerated depth provides the means for locating the third-dimension—the distance from the scanning plane—which is determined by the position of the object when it comes into focus. The process is similar to locating particles in a drop of water with a microscope. The microscope is first focused on the top of the drop, then scanned to the bottom with the focus control.

This type of hologram has limited application in NDT work. Defects in the dielectric that would escape detection in this type of hologram are those without well-defined boundaries. For example, a plane laminar separation extending over a large area would have no features on which the eye can focus. The boundary of the separation is a feature, but if the separation closed gradually, the boundary could easily be missed. A worse case is when the separation extends over the whole area inspected; it would be missed completely. This is another "perfect mirror" problem.

GENERALIZED HOLOGRAPHY

To circumvent the problem outlined above, a new type of hologram was developed. A conventional hologram is processed in one dimension of the photographic film and depth information in the other. The resulting picture is similar to that obtained with the side-looking radar, that is, a cross-sectional picture. The intermediate steps in producing the picture are considerably different.

The picture is in the cross section of the B scan in figure 12.1. The display differs from the B scan in two important respects. First, the lateral resolution is much higher. Although the transducer sends out a broad beam, the holographic processing synthesizes the resolution of a narrow-beam technique with a transducer the size of the entire distance the broad beam transducer traveled. Since it would be impractical to use such a large transducer for narrow-beam inspections, the resolution required is obtained with the scanned broad-beam technique. Second, defects need not

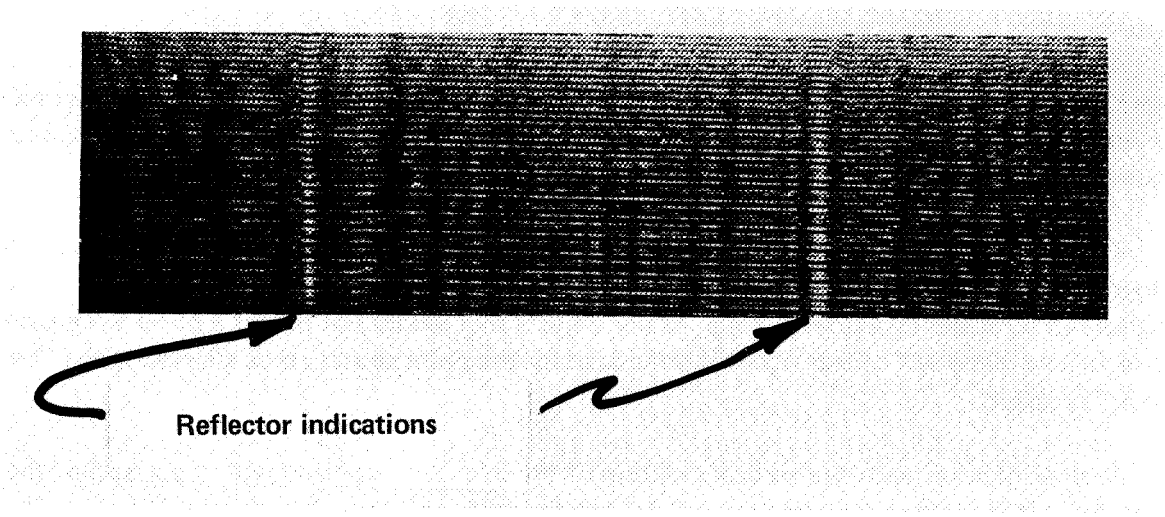

Figure 12.8 One-dimensional reconstruction

be normal to the beam to be detected. Curved and irregular surfaces will be shown. Thus, the display will have the characteristics of a picture of the cross section.

The depth information is obtained by swept-frequency rather than short-pulse technique. The swept-frequency technique requires a Fourier transform, and taking Fourier transforms is an ideal problem for the optical computer.

The signal processing for the depth information is illustrated in figure 12.9. The microwave transmitter sends a signal with a frequency linear with time. The heterodyne between the transmitted and reflected wave is used to modulate the film density. If the object is close to the transducer, it produces a low heterodyne frequency that defracts the beam through a small angle. Defects farther from the transducer produce higher frequencies, which defract the beam at a higher angle.

The model used for depth-only optical processing is shown in figure 12.10. Cardboard sheets were inserted into the sand to simulate defects. The plexiglas front matched the sand, so with no defects, only the plexiglas-to-transducer interface reflected. Figure 12.11 shows some preliminary results from a reflector 3/4 in. and 1-1/2 in. from the front surface. The final transform shows two simulated defects in the beam.

The special optical lens for two-dimensional processing was not available for these preliminary experiments. However a conventional B scan could be made. The equipment for B-scan generation and readout is shown in figure 12.12; the model used is shown in figure 12.13. Two cardboard sheets and one metal reflector were used. The hologram is printed in figure 12.14 and the processed scan in figure 12.15. Again, the printing does little justice to the results, but the front surface and three defects can be seen.

The experiments conducted to date are preliminary, and intended to demonstrate feasibility and uncover problems. The principal problems are background signals from nonlinearity in the oscilloscope x, y, and z axes and the photographic processes. In addition, aperture defraction of some parts of the optical system produce background indications. All these problems should be readily overcome with improvements in technique.

ACKNOWLEDGMENTS

The success of the project is due, in large measure, to the overall direction of the program manager, Gil Lewis at the Jet Propulsion Laboratory, and the experimental work of coworker Bill Lamb.

This project was supported by the National Aeronautics and Space Administration under contract NAS 7-759.

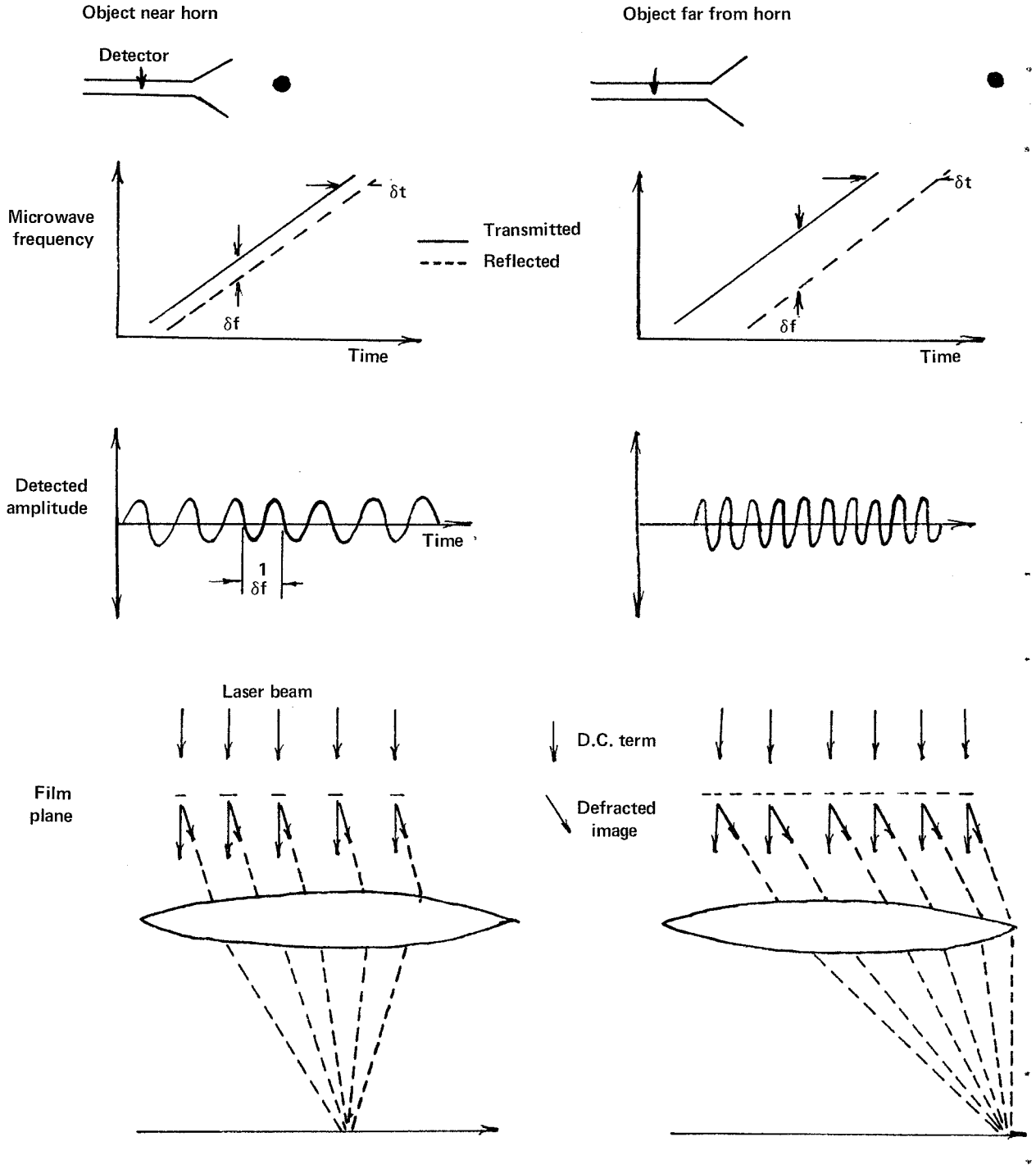

Figure 12.9 Obtaining distance with optical transforms

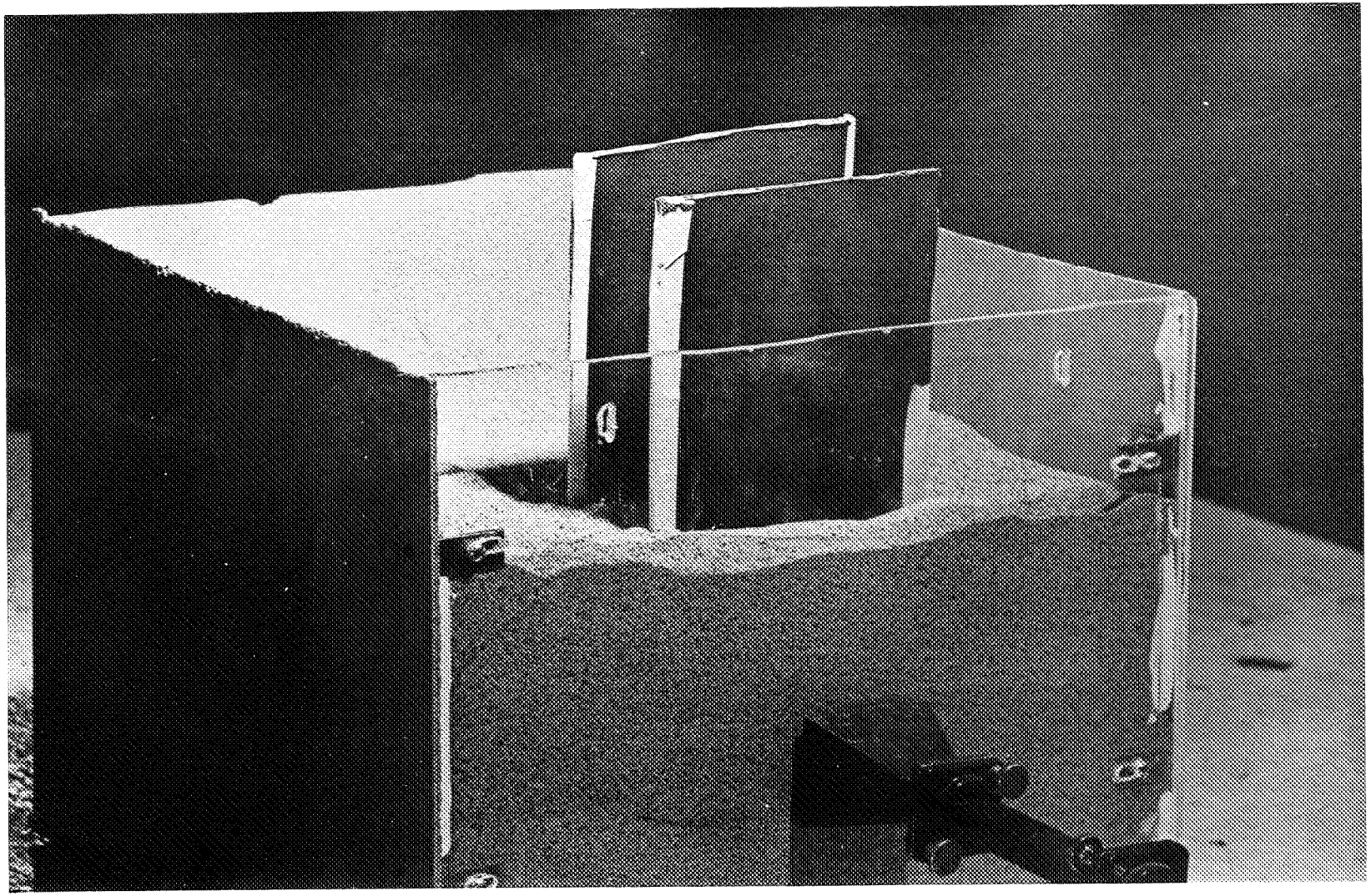

Figure 12.10 Depth-only defect model

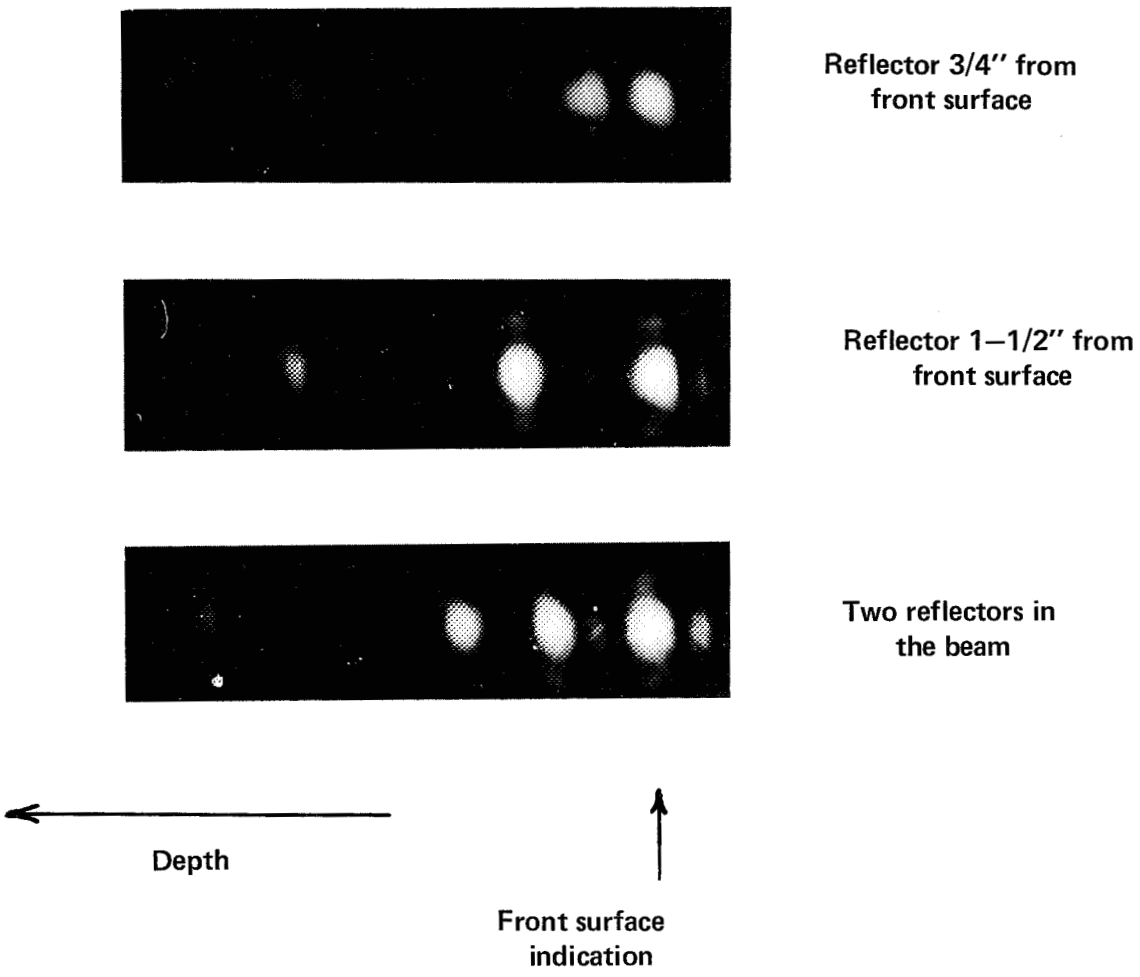

Figure 12.11 A-scan defect indications

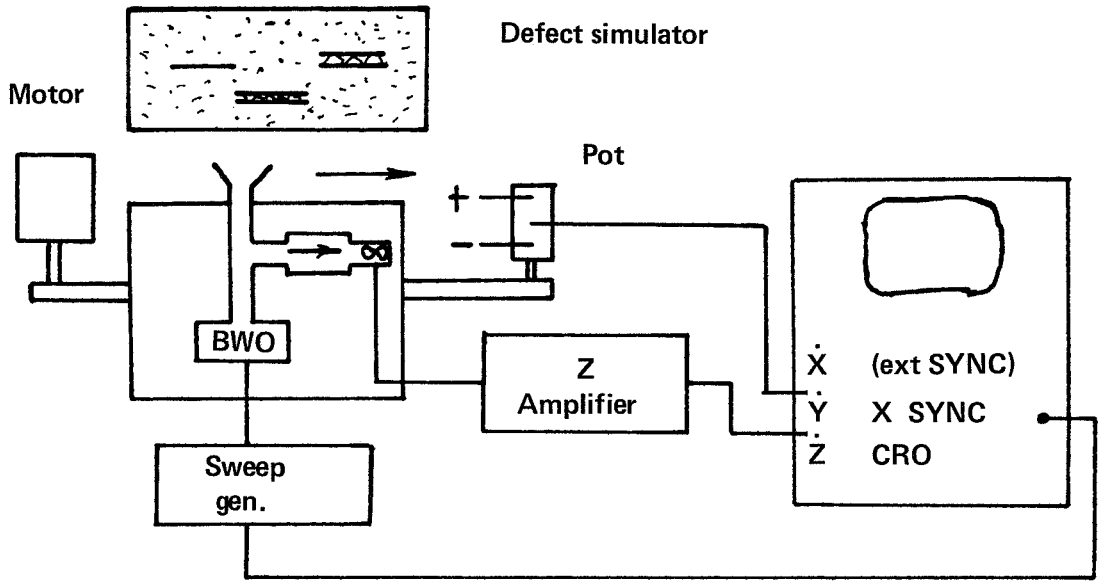

Recording B–Scan hologram with FDI

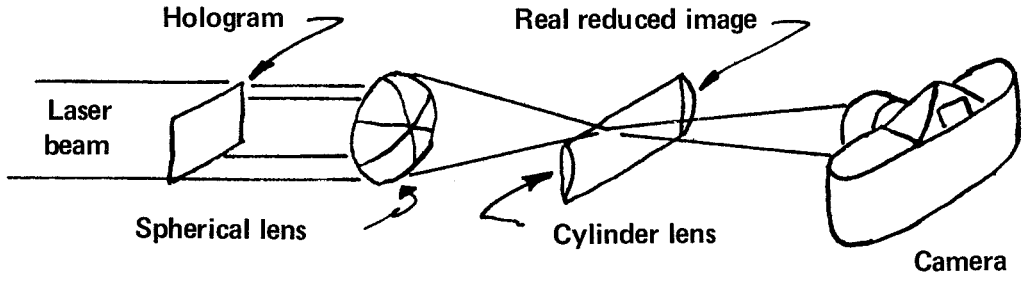

Reconstructing B–Scan image

Figure 12.12 B-scan optical equipment

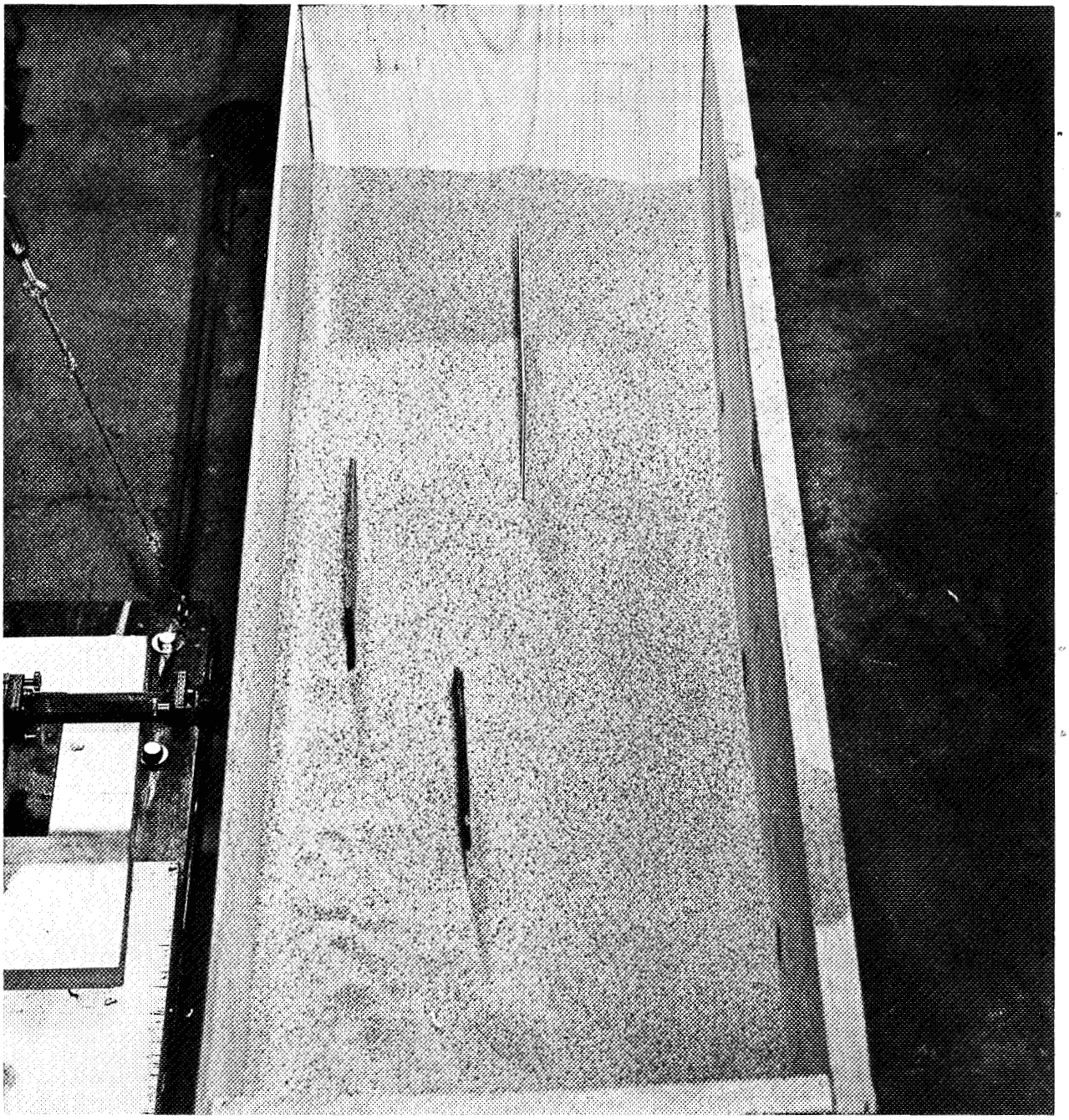

Figure 12.13 Defect model

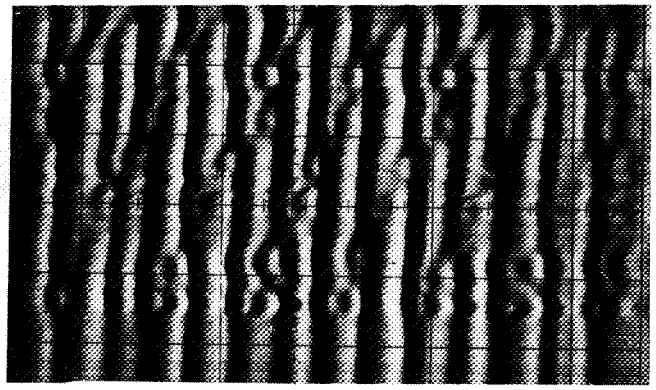

Figure 12.14 Two-dimensional hologram

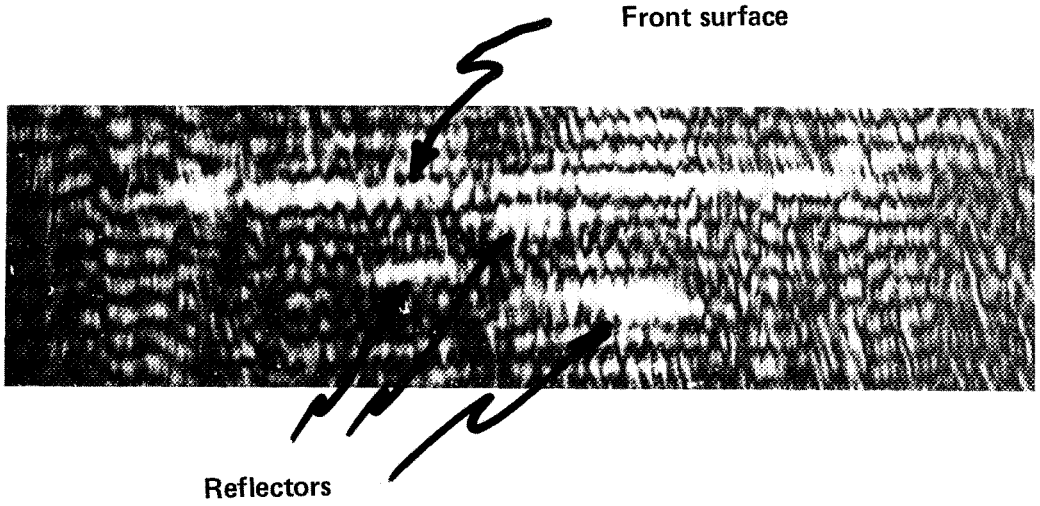

Figure 12.15 Two-dimensional reconstruction

13 HOLOGRAPHIC INTERFEROMETRY AS A MEANS OF MEASURING SMALL LINEAR AND ANGULAR DISPLACEMENTS

Barton J. Howell
Sperry Rand Corporation
Space Support Division

Responsibility for optical alinement measurements and calibration at Goddard Space Flight Center requires that methods for improving the accuracy of angular measurements be sought. Double-exposure and real-time holographic interferometry have been studied experimentally and theoretically to determine the accuracy with which displacements can be measured. Results for angular motion and lateral shifts of a diffuse target block are shown. A general theory is developed that accounts for both angular and linear motion. An error model treats the accuracy of linear and angular measurements considering the two largest sources of error: (1) measurements of fringe spacing and (2) measurements of experiment geometry.

It has been observed by many that a very slight displacement of a subject between exposures of a hologram produces a series of dark bands on the reconstructed image. The dark bands are, of course, interference fringes formed between the two coherent subjects. The same general effect can be achieved on a real-time basis by interfering a displaced subject with the reconstructed image of the subject. In the latter case, there is usually less fringe visibility than in the double-exposure case.

Since interferometry has application in the measurement of small displacements to a high accuracy, a study was made of the accuracy with which small linear and angular displacements could be measured using the techniques of holographic interferometry. Both double-exposure and real-time methods were used. The experimental work included rotation of the subject about an axis lying in its plane, and translation of the subject in its plane.

Mathematical analyses have been performed for the case of rotation about an axis lying in the plane of the subject and translation in the plane of the subject, and rotation about an axis perpendicular to the plane of the subject.

EXPERIMENTAL WORK

The arrangement of apparatus to make double-exposure holograms is shown in figures 13.1 and 13.2. The beam from a model 112 Spectra-Physics helium-neon laser is diverged through a spatial filter, folded, and directed onto a mirror and subject block, which are side by side. The portion of the beam that falls on the reference mirror is attenuated by a linear polarizer to obtain a proper balance between reference and subject beam. The subject is a block of aluminum that has been sandblasted by Black Beauty #80 grit. The block is mounted so that the axis of rotation lies in the face. Behind the subject block is a Hilger & Watts model TA-3 autocollimator, which monitors the

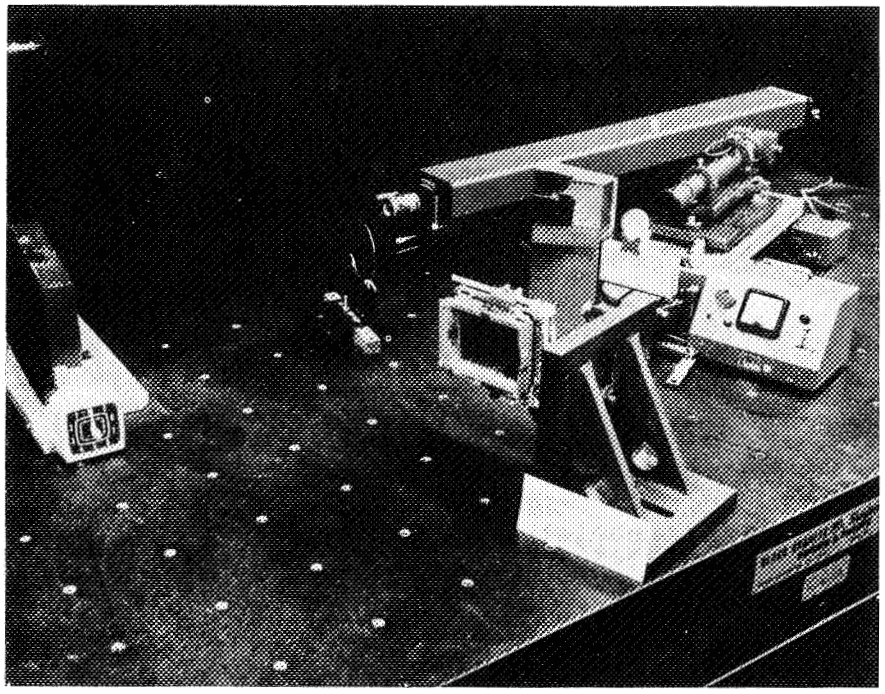

Figure 13.1 Double-exposure holography setup

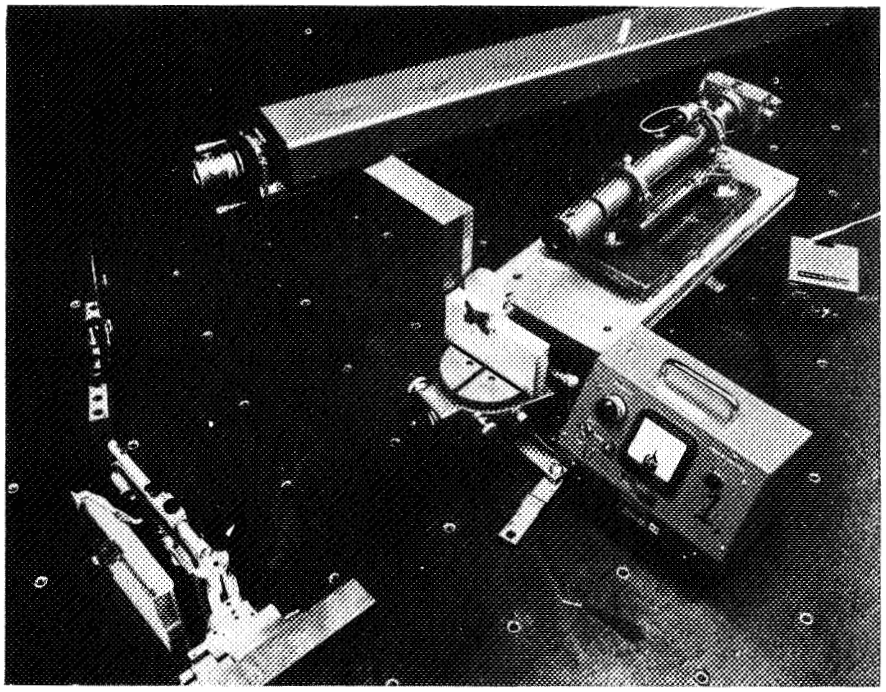

Figure 13.2 Subject block, monitoring theodolite, and plateholder in double-exposure holography setup

position of a small flat mirror mounted on top of the subject block. The photographic plate is mounted in a camera back shown in the lower left of figure 13.2.

In making the rotation measurements, the autocollimator was nulled on the flat mirror, and then offset by the desired rotation. Between exposures, the Hilger & Watts model TB-95 clinometer supporting the subject block was turned until the autocollimator was again nulled. The plate was returned to the holder after processing, and the photographs were made by photographing the reconstructed double images against a black background.

The fringes formed by a 1-arcsec rotation are shown in figure 13.3, and those formed by a 15-arcsec rotation are shown in figure 13.4. A scale is inscribed directly on the face of the subject block, and because the fringes formed by rotation about an axis that lies in the plane of the subject are also in the plane of the subject, the scale gives a direct measure of the fringe spacing without having to scale the photographs.

A real-time holographic setup was used for the lateral translation measurements (fig. 13.5). The subject block and clinometer base were mounted on a Unertl mirror mount base with the face of the subject block parallel to the ways of the base. The motion of the base was monitored by dial indicators. The real-time capability was achieved by exposing and processing the plate in the cell shown in figure 13.6. Fringe patterns formed by translations of 0.001 in. and 0.002 in. are shown in figures 13.7 and 13.8, respectively.

MATHEMATICAL MODEL

A mathematical model was developed to facilitate analysis of the accuracy of measurement of motion. The subject block is treated as an array of very many facets or minuscule mirrors, oriented in a random distribution. Therefore, in a given viewing direction, one can always find a facet oriented so that reflection directs the light from the source to the observer. When the facet is moved from one position to another through a small displacement, the result is an optical path length change, and the two sources interfere with one another in a manner dependent on the phase difference. It is important that the displacement have a lateral component (perpendicular to the line of sight) that is not sufficiently large for the two facet sources to be resolved. If they were resolved, the positions of constant phase difference would form a random pattern, rather than fringes.

Lateral Motion

The motion X of the subject plane is a vector in the plane of the subject (fig. 13.9). The vector N is a unit vector normal to the facet being considered, the angle T is the sum of the angles of incidence and reflection, and the angle S is the angle between the reflected ray and the face of the plate.

From studies of optical system tolerances (refs. 1, 2)

$$P = X \cdot N(n \cos i - n' \cos r) \qquad (1)$$

where P is the optical path difference, X is the displacement vector, N is the unit vector normal to the surface being displaced, i is the angle of incidence on the facet and r is the angle of refraction, n is the index of refraction of the space preceding the surface, and n' is the index of refraction of the space following the surface. The law of refraction implicit in equation (1) becomes the law of

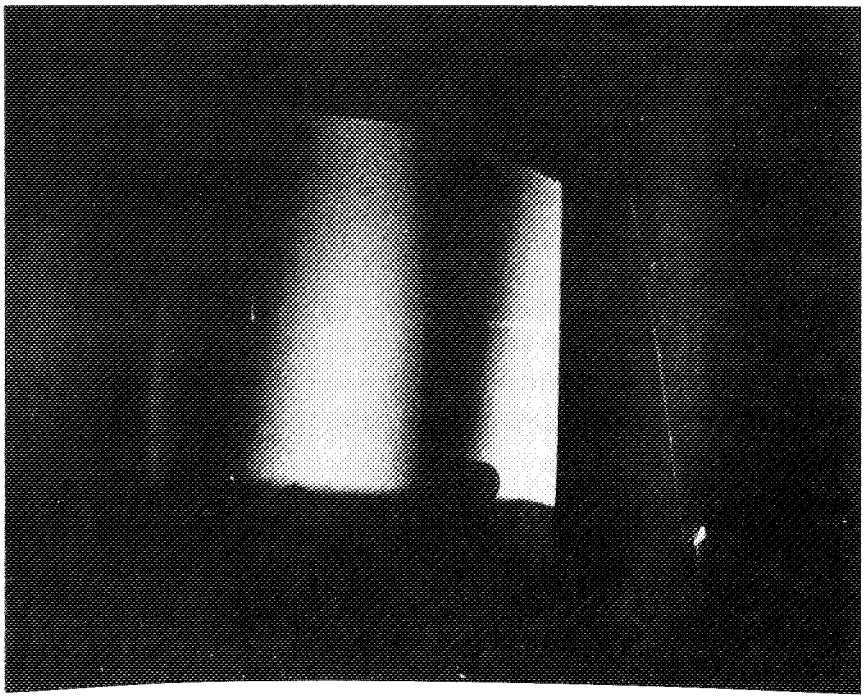

Figure 13.3 Fringe pattern formed by 1-arcsec rotation; marks are 1 cm apart

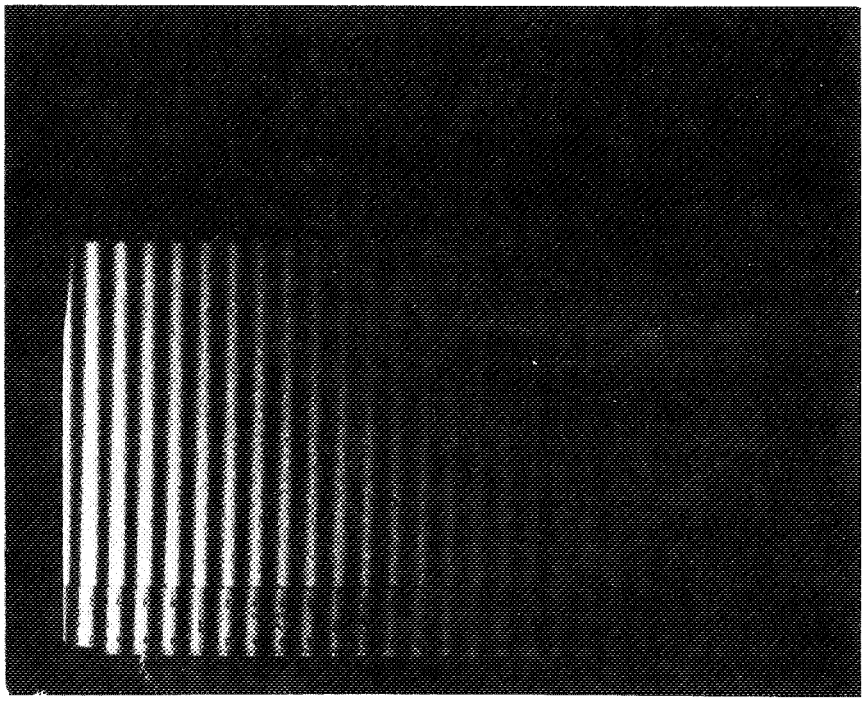

Figure 13.4 Fringe pattern formed by 15-arcsec rotation; scale is mounted on block

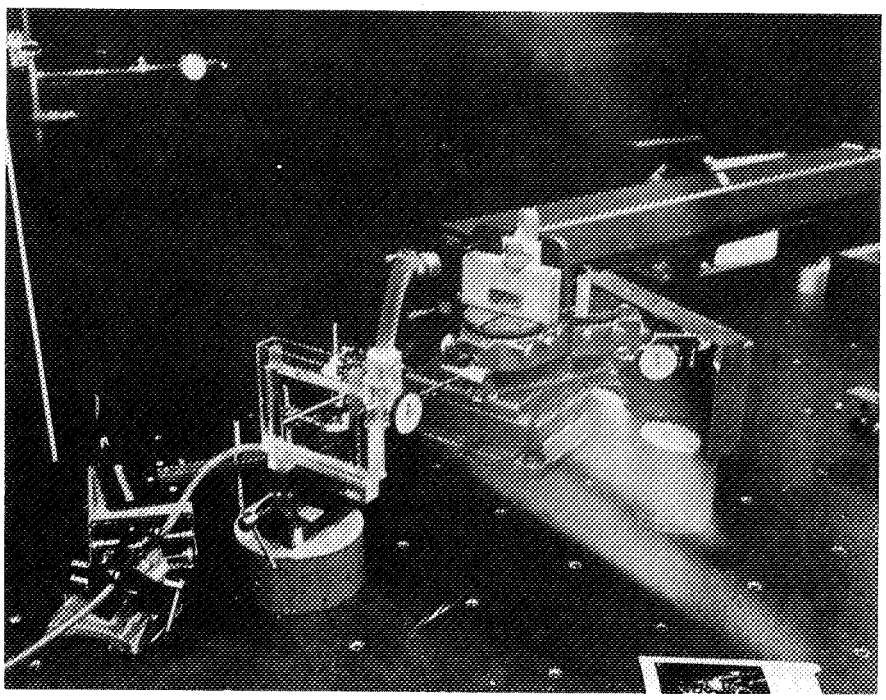

Figure 13.5 Real-time holography setup

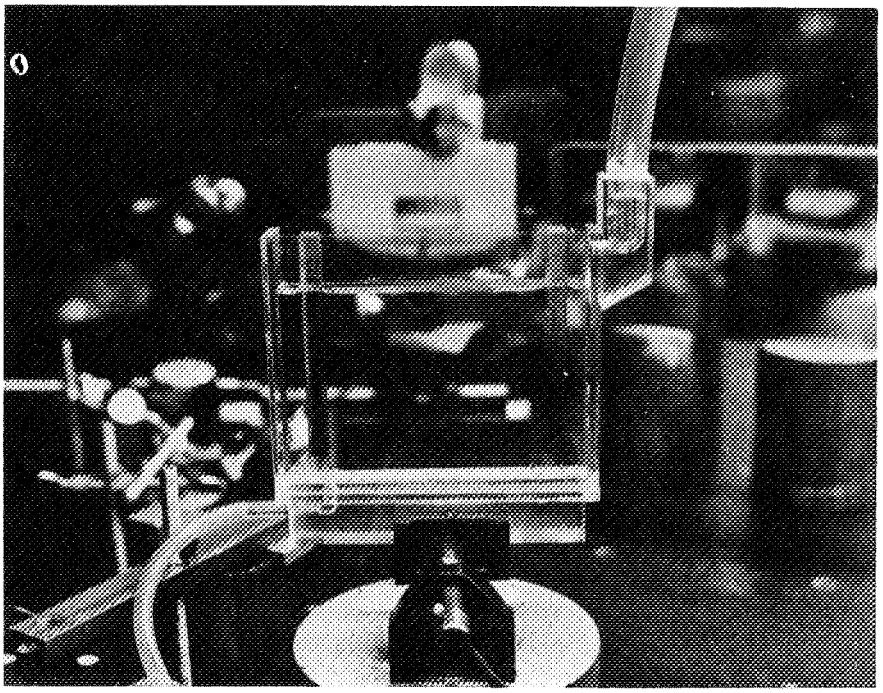

Figure 13.6 Plate cell used for exposure and processing in real-time holography

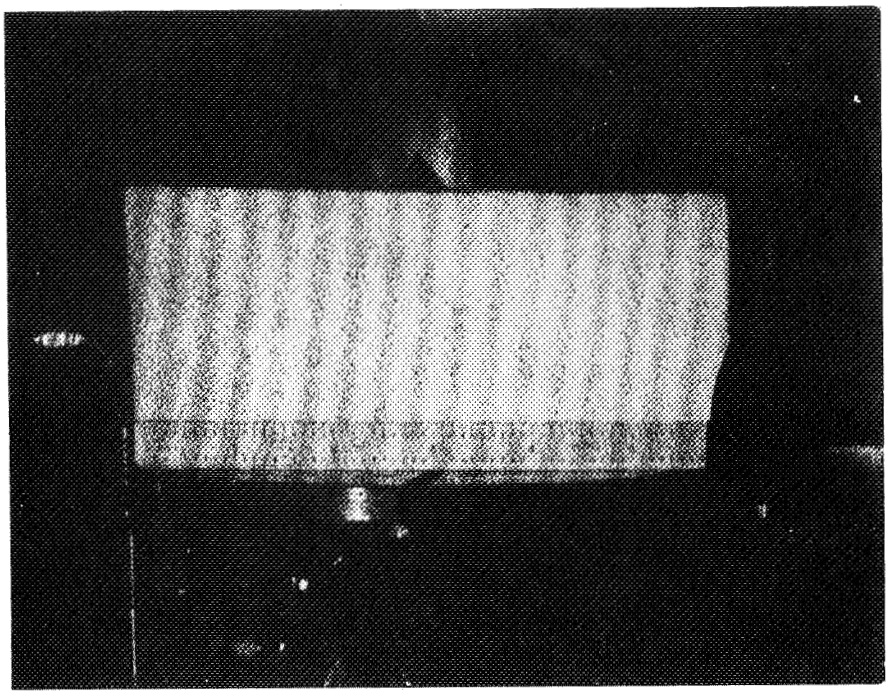

Figure 13.7 Fringe pattern formed by 25-μ lateral translation

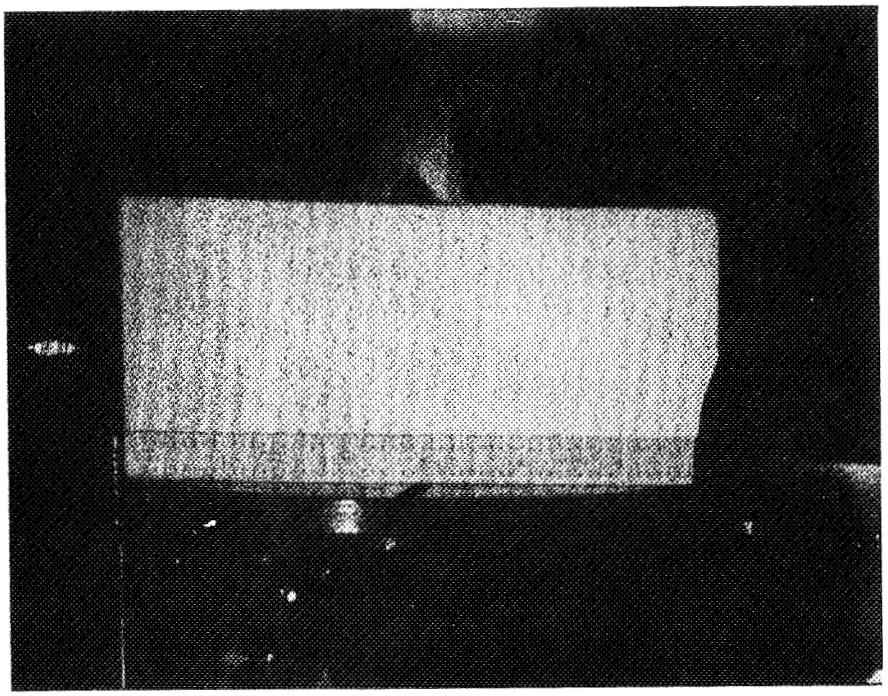

Figure 13.8 Fringe pattern formed by 50-μ lateral translation

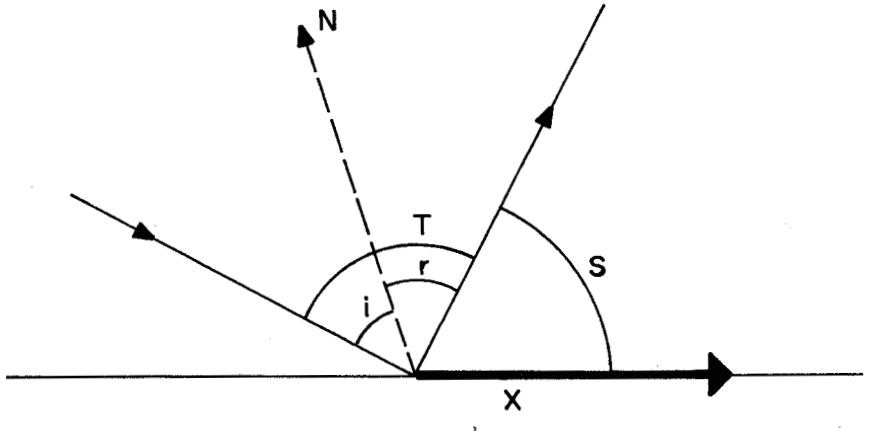

Figure 13.9 Vector relationships in effect in lateral translation

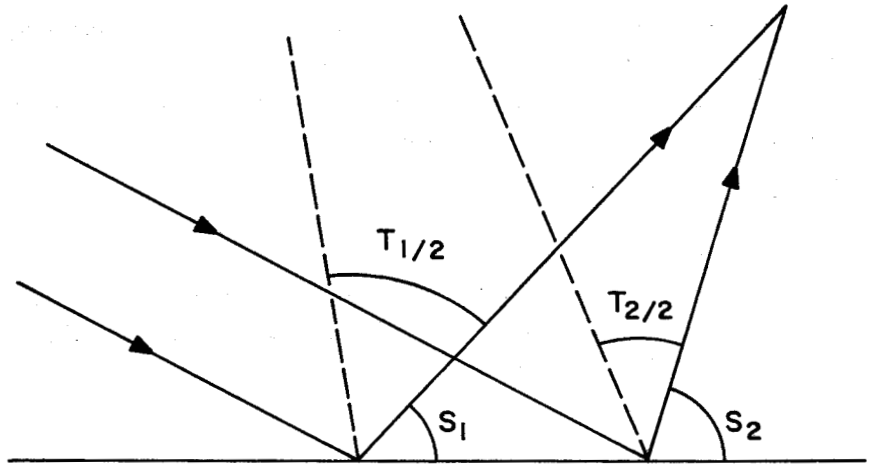

Figure 13.10 Angle relationships between two consecutive fringes in lateral translation

reflection by making the substitution $n' = -n = -1$. Since i is numerically equal to r for reflection, the expression for optical path difference becomes

$$P = X \cdot N \left(2 \cos \frac{T}{2}\right) \tag{2}$$

where

$$X \cdot N = X \cos\left(S + \frac{T}{2}\right) \tag{3}$$

Upon shifting the facet by an amount X from position 1 to position 2, a series of fringes is formed. The positions of two consecutive fringes are viewed at angles S_1 and S_2, as shown in figure 13.10.

$$P_1 = 2X \cos\left(S_1 + \frac{T_1}{2}\right) \cos \frac{T_1}{2} \tag{4}$$

$$P_2 = 2X \cos\left(S_2 + \frac{T_1}{2}\right) \cos \frac{T_2}{2} \tag{5}$$

Because the two fringes are consecutive, $P_2 - P_1 = \lambda$, the wavelength of the light used. By using the definitions

$$A = S_2 + \frac{T_2}{2}$$

$$B = \frac{T_2}{2}$$

$$C = \frac{T_2 - T_1}{2}$$

the expression for $P_2 - P_1$ becomes

$$P_2 - P_1 = 2X(\cos A \cos B - \cos (A + C) \cos (B - C)) \tag{6}$$

or

$$X = \frac{\lambda}{2(\cos A \cos B - \cos(A + C) \cos(B - C))} \tag{7}$$

The angles S and T can be measured with theodolites. To aid in these measurements, a mirror was attached to the subject block, as shown in figure 13.5. There was uncertainty in the measurement of these angles, and in the value of the wavelength of light. The larger source of error was in the measurement of the angles. Assuming a typical configuration:

$S_1 = 45°$ $S_2 = 55°$ $T_1 = 60°$ $T_2 = 50°$

$A = 80°$ $B = 25°$ $c = -5°$ $\lambda = 632.8$ nm

the displacement is found to be 4.7388 μ. Assuming various errors in each of the four terms in the denominator of equation (7), always in a direction resulting in worst-case conditions, the errors in the measured value of X are found (Table 13.1).

Table 13.1

Error in A, B, A + C, B − C	*X* (μ)	*Error in X* (μ)
0	4.7388	--
2 min	4.6606	.079
10 min	4.3710	.36
30 min	3.7835	.97

Rotary Motion

For rotation about an axis that lies in the plane of the subject, the individual facets do not all translate the same amount as in the lateral translation case, but the motion is a function of the distance from the axis to the facet, as shown in figure 13.11. Here the points K and L are located one fringe apart; the displacements X_1 and X_2 are taken as the arc formed by the product of the distance from the axis O and the angle G. The angles S and T are defined as in figure 13.10. We find the following relationships:

$$P_1 = 2X_1 \cos\left(S_1 + \frac{T_1}{2} + 90°\right) \cos\frac{T_1}{2} \tag{8}$$

$$P_2 = 2X_2 \cos\left(S_2 + \frac{T_2}{2} + 90°\right) \cos\frac{T_2}{2} \tag{9}$$

Because there is no displacement at O and therefore no fringe, and because the fringes are formed symmetrically about O, the distance OK = F/2 and KL = F, where F is the fringe spacing.

In order to determine the angle G, we note:

$$X_1 = \frac{FG}{2} \text{ and } X_2 = \frac{3FG}{2} \tag{10}$$

Subtracting equation (8) from (9), setting the difference equal to the wavelength λ, and introducing some trigonometric identities, we obtain

$$G = \frac{\lambda}{F(-3 \sin A \cos B + \sin(A + C)\cos(B - C)} \tag{11}$$

where A and B are defined as in equation (6). From the following set of values

$S_1 = 95°$ $S_2 = 85°$ $T_1 = 40°$ $T_2 = 50°$ $F = 7.62$ cm
$A = 110°$ $B = 25°$ $C = 5°$ $\lambda = 632.8$ nm

we obtain the errors in G due to worst-case combinations of errors in the measurement of angles (Table 13.2).

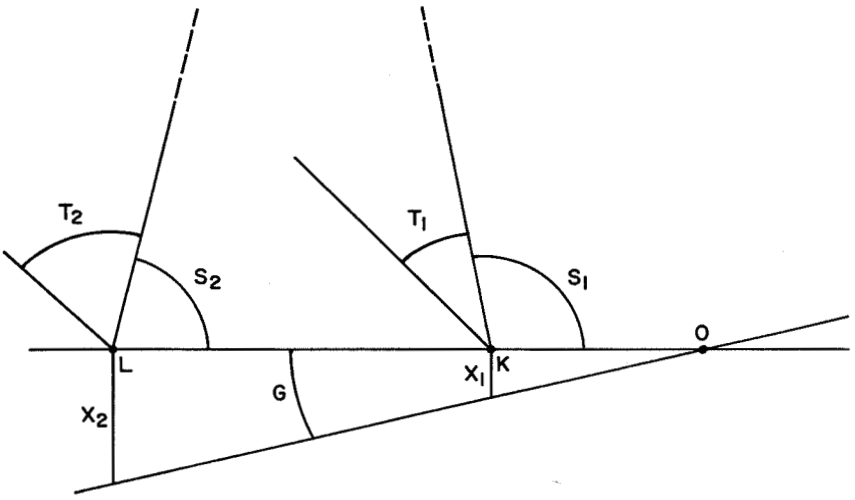

Figure 13.11 Angle and distance relationships between two consecutive fringes in rotation about an axis in the plane of the subject

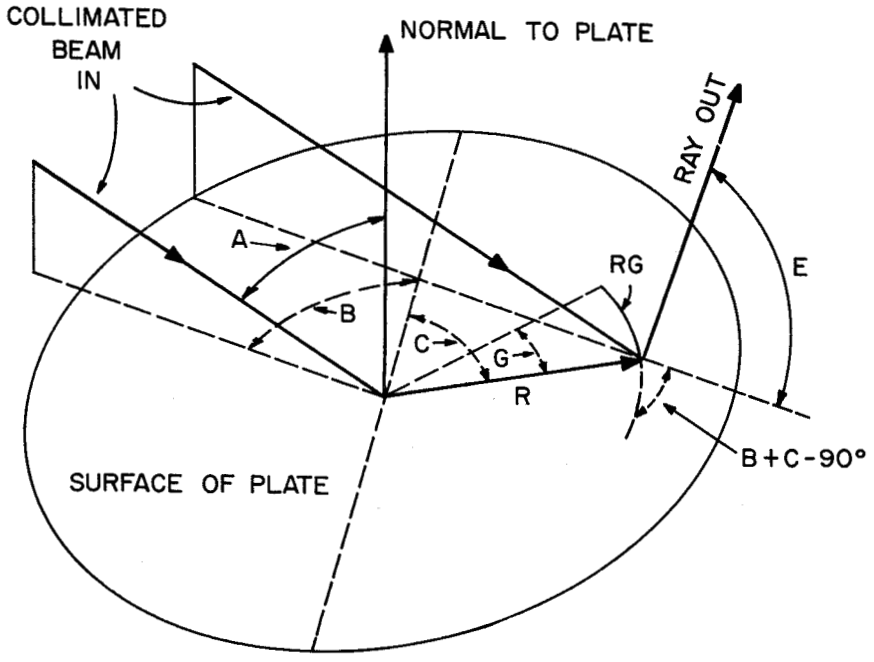

Figure 13.12 Vector and angle relationships in rotation about an axis perpendicular to the plane of the subject

Table 13.2

Error in A, B, A + C, B − C	*G (sec)*	*Error in G (sec)*
0	1.005671	--
1 sec	1.005679	0.000008
2 sec	1.005687	0.000016
5 sec	1.005712	0.000040
10 sec	1.005752	0.000081
30 sec	1.005914	0.000243
1 min	1.006157	0.000486
2 min	1.006644	0.000973
5 min	1.008108	0.002437
10 min	1.010560	0.004888
30 min	1.020524	0.014852

The standard deviation of measurement of angles in the experimental setup was ±13 min. This results in an error of the angle being measured of 0.0066 sec. The largest source of error of all those involved in the rotation measurements is the measurement of the fringe spacing F. The standard deviation of measurements of F for different values of G, and the resulting errors in the value of G are shown in Table 13.3.

Table 13.3

G (sec)	*Error in F (cm)*	*Error in G (sec)*
1	0.13900	0.01853
5	0.00539	0.01739
10	0.00390	0.05000
30	0.00821	0.94730

An interesting case with somewhat startling results is that of rotation about an axis normal to the surface of the subject plate (ref. 3). This can be explained by reference to figure 13.12. The coordinates of a point are the radius vector R and the angle C. The incoming reference beam is represented by a unit vector at an angle B with respect to the reference axis and an angle A with respect to the normal to the surface. The reflected ray is at an angle E with respect to the surface. Taking the components of motion along the rays, just as in equation (1), we have

$$P = RG \cos(B + C - 90^\circ)(\sin A + \cos E) \tag{12}$$

where P is the optical path difference, as before. Angle E is made 90° for convenience. Expanding the cosine term, we have

$$P = RG (\sin A \cos B \sin C + \sin A \sin B \cos C) \tag{13}$$

Plotting the loci of points of constant P gives a series of parallel fringes, running across the plate in the same direction B as the incoming beam. Although the fringes are formed at infinity, they may

be photographed superimposed on the plate by stopping down the camera lens. By measuring the fringe spacing perpendicular to the fringes we obtain, for that value of C, two different values of R, where the optical path difference P for each R differs by the wavelength of light λ. Because the fringes are parallel to the projection of the incoming beam on the plate, $B + C = 90^\circ$ and $\cos B = \sin C$ and $\sin B = \cos C$.

$$P_1 = R_1 \, G \sin A (\sin^2 C + \cos^2 C) \tag{14}$$

$$P_2 = R_2 \, G \sin A (\sin^2 C + \cos^2 C) \tag{15}$$

and

$$P_2 - P_1 = G \sin A \, (R_2 - R_1) = \lambda \tag{16}$$

$$G = \frac{\lambda}{\sin A \, (R_2 - R_1)} = \frac{\lambda}{F \sin A} \tag{17}$$

The largest source of error in measurement of rotation about the normal axis is the measurement of the fringe spacing F. For $A = 30^\circ$ and G = 10 sec, the fringe spacing is 2.61 cm. The error in G for various errors in fringe spacing measurements is found to be

$$\text{error in } G = 3.830741 \times \text{error in } F \tag{18}$$

and is given for some values of error in F in Table 13.4.

Table 13.4

Error in F (cm)	*Error in G (sec)*
0.13900	0.5320
0.00539	0.0206
0.00390	0.0149
0.00821	0.0315

CONCLUSIONS

Holographic interferometry provides a useful tool for making accurate measurements of static displacements, both translational and rotational.

The case of translation normal to the surface produces a fringe pattern the same as found in a Michelson interferometer, and the accuracy expected is approximately 1×10^{-5} in., the same as shown in Table 13.1 for lateral translation.

The case of rotation about an axis parallel to, but not within, the plane of the subject plate gives fringes similar in appearance to those produced by either lateral translation or rotation. This raises the important question: what does one do to interpret the fringes if the location of the axis of rotation is not known? The location of the fringes in three dimensions will give the answer to what type of motion is involved. This study has not treated the complex cases of compound motion. The objective was to assess the accuracy with which the motion of laboratory standard angle generators can be measured. In these applications, the axis of rotation is very well known.

With refined fringe-space measuring techniques, such as the use of a microdensitometer, the accuracy can be improved to a point where the method could be used to calibrate laboratory standards. By extending the theory to three dimensions, complex static displacements of components of space vehicles could be measured to a high degree of accuracy compared to present optical tooling methods.

ACKNOWLEDGMENTS

The author gratefully acknowledges the support for this work of the Test and Evaluation Division of Goddard Space Flight Center, and the contributions of R. C. Loveridge, who performed many of the laboratory experiments.

REFERENCES

1. Grey, D. S.: Tolerance Sensitivity and Optimization. Appl. Opt., vol. 9, March 1970, p. 523.
2. Rimmer, M.: Analysis of Perturbed Lens Systems. Appl. Opt., vol. 9, March 1970, p. 533.
3. Aleksandrov, E. B.; and Bonch-Bruevich, A. M.: Investigation of Surface Strains by the Hologram Technique. Soviet Physics-Technical Physics, vol. 12, Aug. 1967, p. 258.

14 NONDESTRUCTIVE TESTING BY HOLOGRAPHIC INTERFEROMETRY

John R. Williams
Marshall Space Flight Center

Numerous nondestructive testing techniques have been in use for quite some time, but there are particular test specimens that do not lend themselves to these techniques. With these problems in mind, several research efforts are being conducted by this laboratory in the field of holographic nondestructive testing.

Both real-time and double-exposure holographic techniques are being investigated. Basically, these consist of recording, in the form of holograms, the condition of the test specimen under a known load and comparing this recorded information with that obtained when the load conditions are changed. "Faults" show up in the interference patterns produced. Results using these techniques on printed circuit boards, honeycomb structures, metal welds, and deposits on optical surfaces are presented.

One of the most promising areas of holography is that of holographic interferometry. The ability to compare wavefronts interferometrically produced at two different instances in time is an extremely valuable tool. This paper deals with the application of this technique to four distinct problems: printed circuit board analyses, honeycomb structures, metal welds, and deposits on optical surfaces. Both real-time and multiple-exposure holography are being used; for the purpose of photographic presentation all of the holograms shown are multiple exposure.

HOLOGRAPHIC NONDESTRUCTIVE TESTING OF METAL WELDS

One of the most obvious test cases for holographic nondestructive testing is the metal-to-metal weld. Since a potential "flaw" in such a weld can have any one of a large number of causes, such as inclusions, fractures, poor metal-to-metal adhesion, etc., its complete analysis is not always simple and reliable.

Since the holographic interferometer measures only the surface movement, a potential problem area within the weld would have to perturb the surface enough to be measured. As this movement would normally need to be on the order of a microinch, it would appear that the thicker the sample becomes, the greater the difficulty of "seeing" an internal problem area. Investigation of numerous metal-to-metal welds substantiated this conclusion. However, since this technique is extremely test-sample dependent it cannot be completely written off for thick samples. Figure 14.1 is a normal photograph of a metal-to-metal weld between two pieces of titanium. This sample is 1/2-in. thick and the distance between numbers 1 and 2 on the photograph is 1 ft. This sample was X rayed and determined to be a perfect weld. Figure 14.2 would indicate otherwise; it is a photograph of a double-exposure hologram of the same sample. Between the exposures, the temperature of the titanium plate was increased about 1° C. This temperature change was induced at the extreme left side of the photograph and on the end of the weld itself. The closed fringe structure on the weld in the center of this photograph would

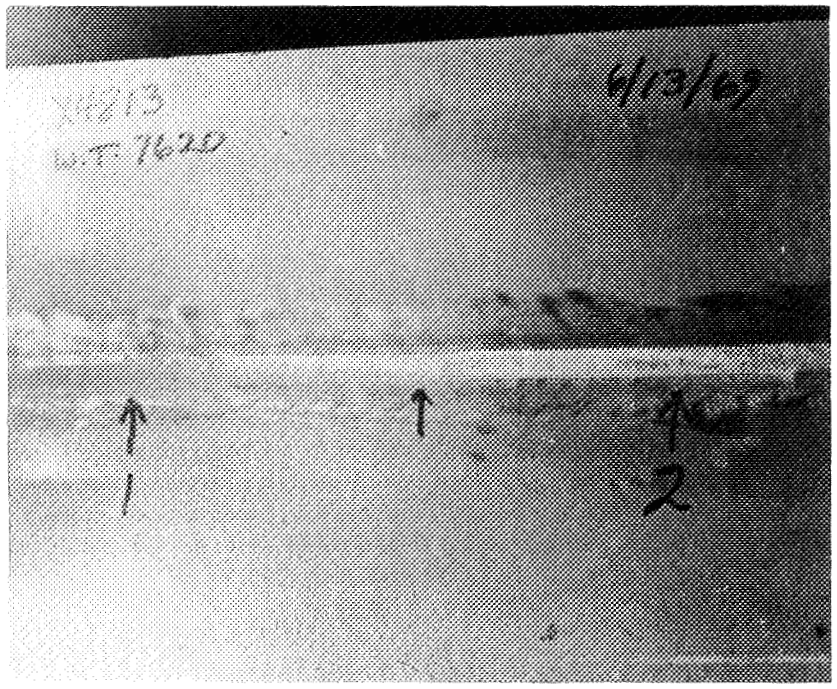

Figure 14.1 Normal photograph of titanium weld

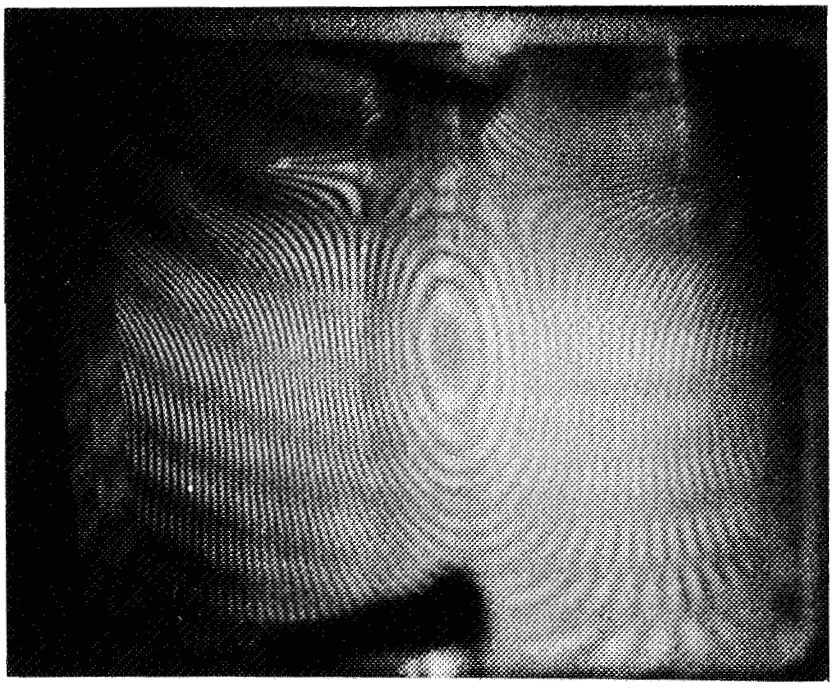

Figure 14.2 Double-exposure holographic image of titanium weld with 1° C temperature change

normally indicate a potential problem area. Further studies are being conducted to completely substantiate this finding. Other techniques, such as optical correlation, are being combined with the holographic interferometer in an effort to make this system a more useful and more reliable testing device for this type of sample.

HOLOGRAPHIC NONDESTRUCTIVE TESTING OF HONEYCOMB STRUCTURES

Honeycomb structures play a vital role in most airborne vehicles. As with other structures, there are numerous types of honeycombs, and a device or devices capable of detecting faults and prospective problem areas is badly needed. Holographic interferometry appears to provide the capability necessary to more completely analyze such structures. Work thus far indicates that this technique can identify such defects as separations between core and inner or outer skin, separations between laminate layers, separations between skin and bonded structures, cell wall separations, adhesive porosity, and debonds, between laminate layers.

Figure 14.3 is a normal photograph of the aluminum skin of a honeycomb panel. The core of this panel is nonmetallic and, therefore, would present problems for other testing techniques such as X-ray analysis. The area shown in this photograph is about 2 sq ft. Figure 14.4 is a double-exposure hologram. A small uniform temperature increase was applied between exposures. If desired, the load may be pressure, vibration, etc., rather than temperature. Most of our applied loads have been temperature changes, because temperature is (1) relatively easy to control, and (2) a prime test condition for flight qualification. Even though figure 14.4 is not a good quality reproduction of the hologram, one can still see that there is a defect in the upper center and in the center of the marked crosshairs. The closed circular fringes in the top center usually represent a lack of bonding between core and skin. This is one of the easiest and most prominent types of fault. The distortion of fringes in the crossed area usually represents a thinner than normal bond between core and skin. This represents a problem area that may show up under extended use.

Holographic interferometry is developing into one of the most powerful tools known for nondestructive testing, for it provides quick results that may be viewed real time and recorded permanently from large areas, and a variety of defects can be detected simultaneously.

HOLOGRAPHIC ANALYSIS OF PRINTED CIRCUIT BOARDS

Problems of printed circuit (pc) board failure have cost the government large sums of money each year. The increasing duration of spaceflights for both manned and unmanned vehicles places more stringent conditions on pc board lifetime, and no good technique for predicting lifetime has yet been developed. It is not too difficult to determine if a solder joint is cracked, but it is very difficult to run a small number of thermal cycles and from these test data be able to predict the solder joint lifetime. The primary objective of this effort is to develop a technique whereby the lifetime of a solder joint can be accurately predicted from a relatively small amount of test data. Of course, the ability to detect cracked or otherwise defective joints is a necessary and useful side effect.

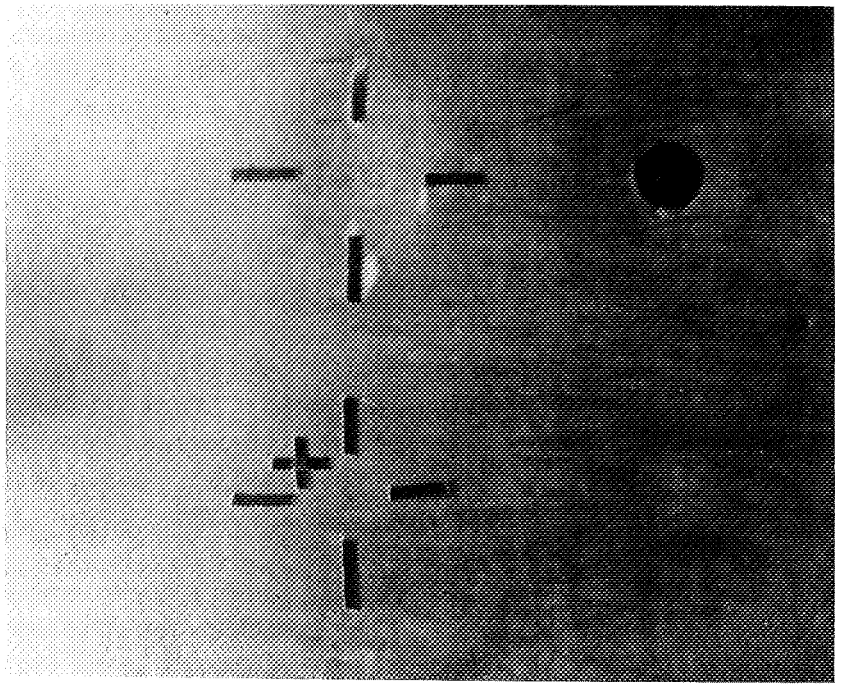

Figure 14.3 Normal photograph of aluminum honeycomb skin

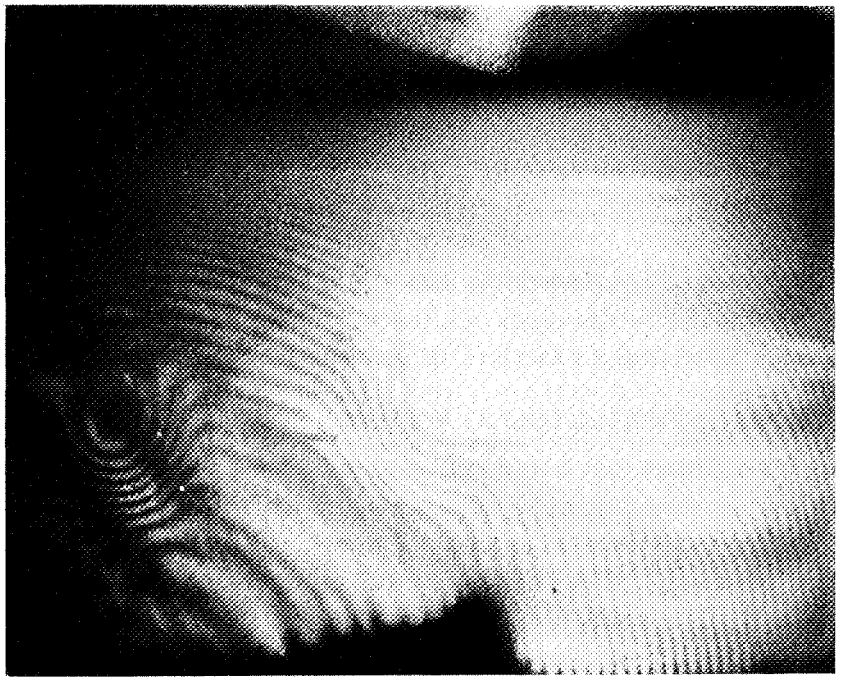

Figure 14.4 Double-exposure holographic image of aluminum honeycomb skin

In an effort to become better acquainted with our test object, high-quality holograms were made of the entire pc board. Figure 14.5 is a photograph of the reconstructed image from one of these holograms. As can be seen from this photograph, the reconstructed image can be used for analysis, instead of the real object, with very little, if any, loss in available information. Holograms of the entire pc board may not show the desired joint detail, but they can be used to demonstrate faulty joints and irregularity in material composition. Figure 14.6 is a photograph of the image from a double-exposure hologram. This sample was a flight pc board where different component spacers were inadvertently used around one joint during construction. Due to the different thermal properties, this could create problems. Also, by visual and standard inspection techniques it was impossible to determine which joint had the different spacers. As can be seen in figure 14.6, the joint was easily found by holographic interferometry. The joint F, from which the circular fringes appear to be emanating, was found to be the joint in question.

By holographing the entire pc board, several valuable pieces of data could be determined, but not enough to analyze each solder joint. Since the individual solder joint is the "bad offender," it must be analyzed to determine the lifetime of the board. One badly needed piece of information is the stress introduced in each joint by the thermal cycling. The size, complexity, and irregularity of the joint preclude standard stress measurements. Since the technique of holographic interferometry measures extremely small movements very accurately, it appears to provide a way of determining the stress in the joint. For example, consider the cross section shown in figure 14.7. A double-exposure hologram of this joint will show interference fringes indicative of the physical movement induced by the thermal cycle applied between exposures. Therefore, the fringe spacing on each constituent of the joint will indicate relative movement from which the stress can be calculated. To aid in producing and measuring this fringe parameter, the joint was enlarged by several techniques. To provide a relatively large magnification, 50X, a metallograph was incorporated in the holographic system (figs. 14.8 and 14.9). The metallograph simply enlarges the desired joint and images it on the photographic plate. This image is then used as the object wavefront for the holographic system. Several minor problems were encountered such as long exposure times (20 sec) and lack of depth of field for fringe analysis, and the system is being redesigned to correct them.

Since, for many tests, the magnification need only be from 2X to 6X, holograms using diverging beams and incorporating lenses in the object wavefront were made. By placing a simple lens in front of the pc board in a normal holographic setup, one can view various portions of the board with relatively small magnification. Figure 14.10 is a photograph of an image from a double-exposure hologram as viewed through the lens.

HOLOGRAPHIC ANALYSIS OF CONTAMINATE DEPOSITS

The Space Sciences Laboratory at MSFC has been given the primary responsibility for investigating the possible problem of contamination in space. Dr. James B. Dozier, ATM project scientist, is in charge of the entire contamination program, which is concerned with the possible problem of contamination, both as vapor and as deposits degrading scientific experiments in orbit. This contamination may be from outgassing material, waste dumps, etc. Any cloud or particulate matter around the spacecraft would produce scattering and reduce "seeing," while

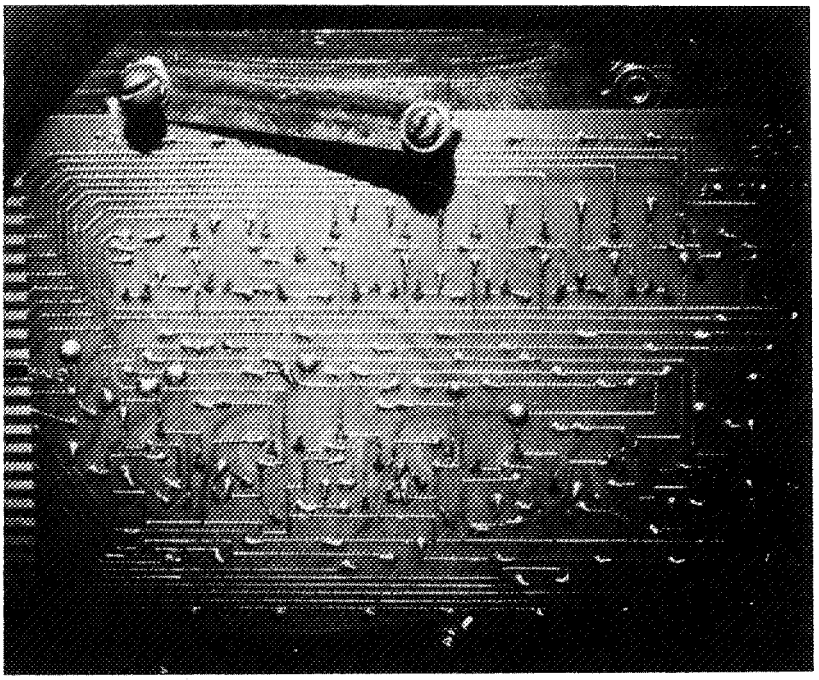

Figure 14.5 Holographic image of printed circuit board

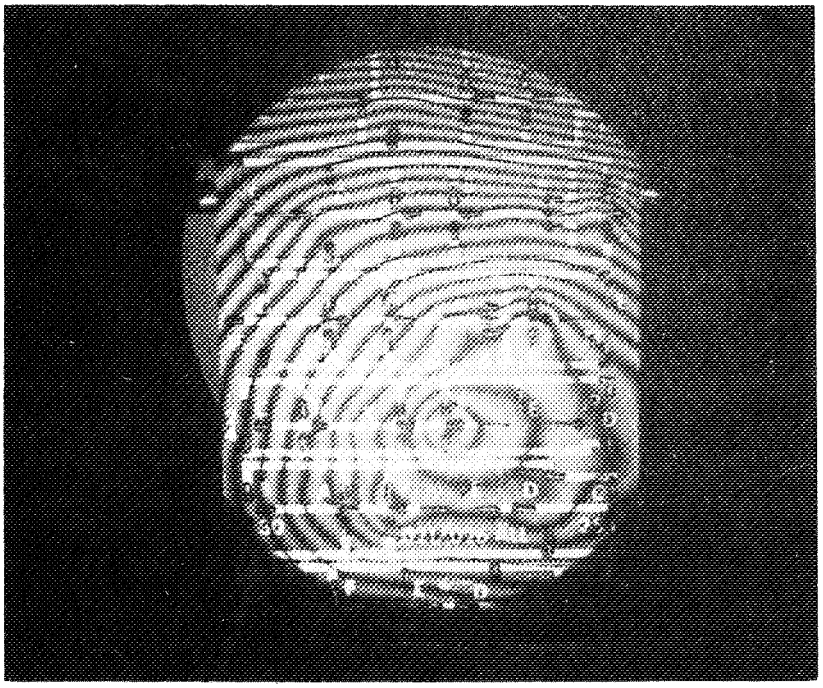

Figure 14.6 Double-exposure holographic image of printed circuit board

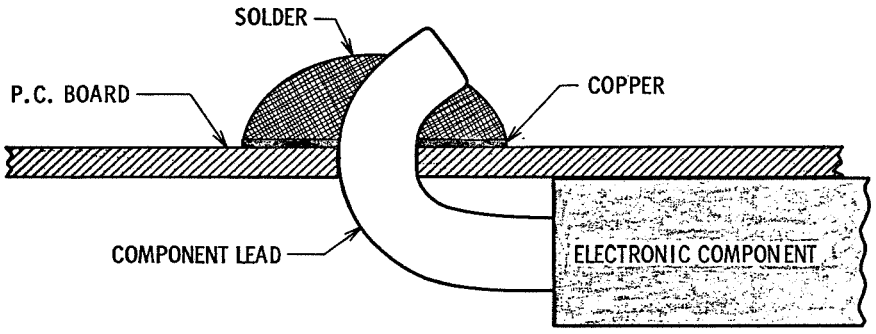

Figure 14.7 Solder joint cross section

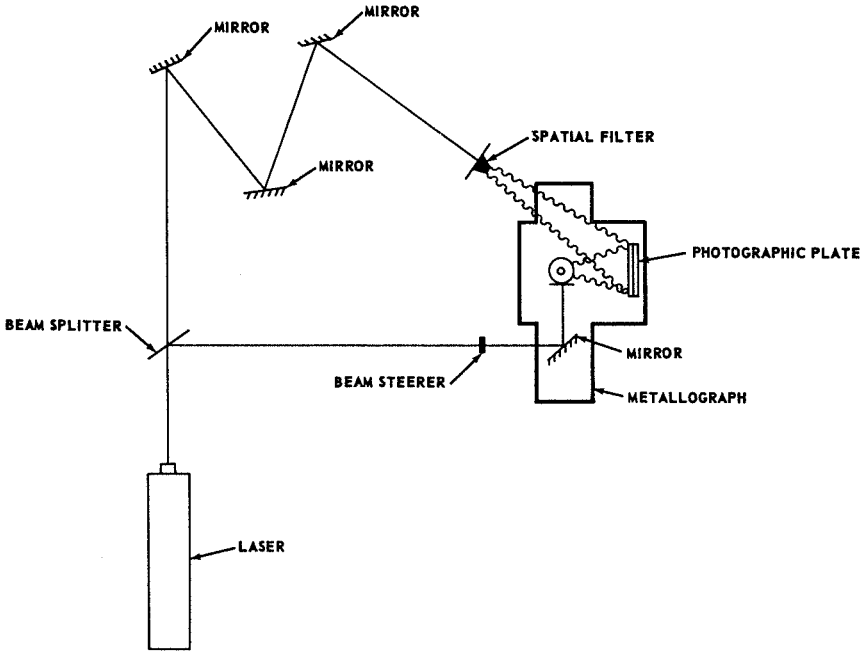

Figure 14.8 Holographic interferometer containing metallograph

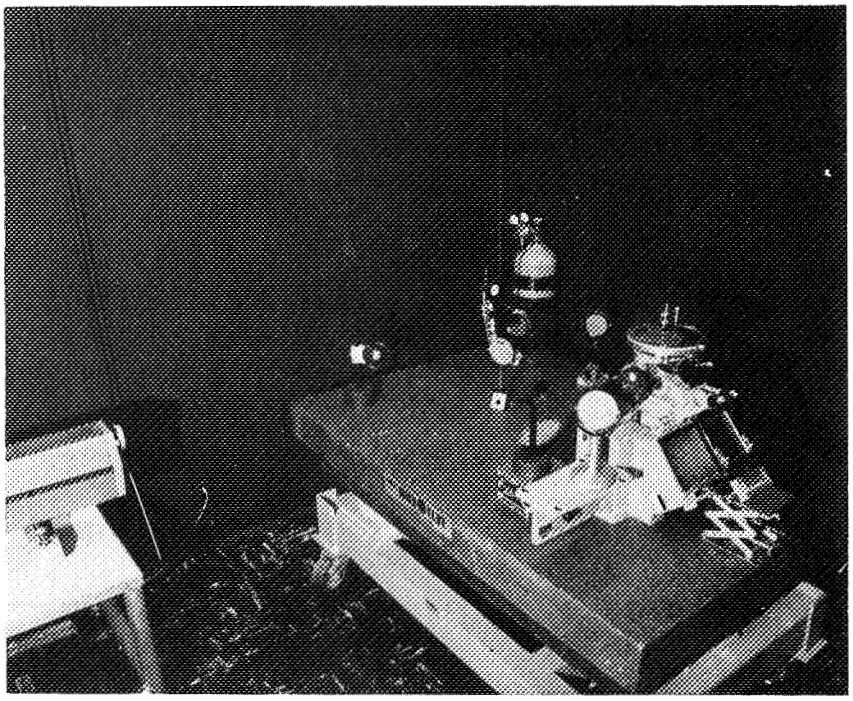

Figure 14.9 Experimental holographic interferometer utilizing metallograph

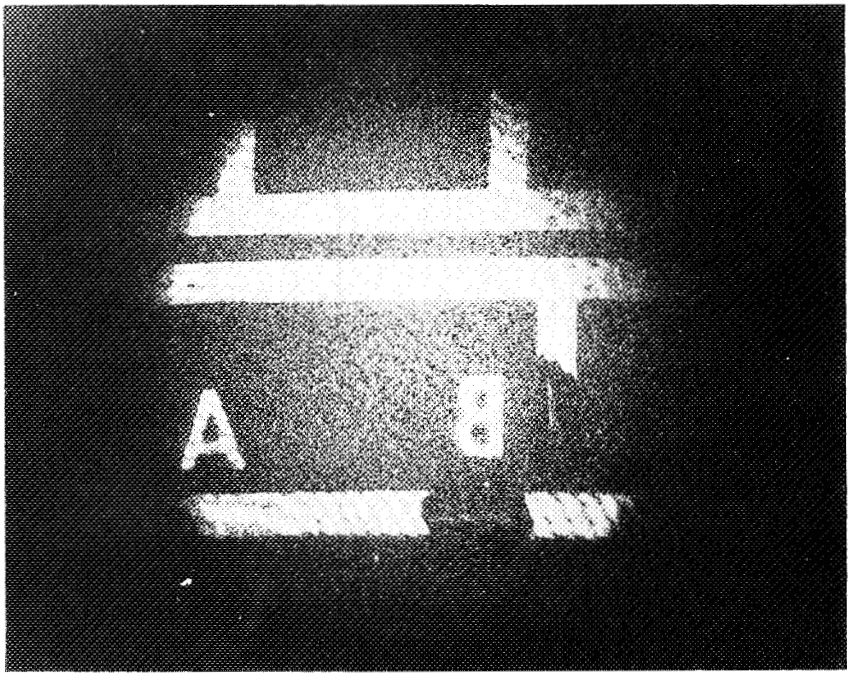

Figure 14.10 Magnified holographic image of printed circuit board

any contaminate deposit on optical surfaces would degrade the instrument. In connection with this program, we are investigating holographic interferometry as a tool for analyzing optical surfaces real time while under vacuum. Since very few simulations are as good as real-time analysis, this technique is being evaluated for future use as part of a real-time contamination monitor.

Some of the groundwork for this effort was laid in various reaction control system (RCS) engine tests. Optical flats were photographed and holographed, sent to MSC, Houston, placed in chamber A during RCS engine tests, and then returned and photographed and holographed again. Figure 14.11 is a drawing of the system used to produce dark field photographs, normal photographs, and holograms of each sample. All three pieces of data could be obtained simply by rotating the sample holder. This holder is shown in figure 14.12. With the camera to the left and the photographic plate to the right, both a photograph and a hologram were made with laser light. A comparison of a normal photographic image and a holographic image can be seen in figures 14.13 and 14.14. Figure 14.13 is a normal photograph of a contaminated optical flat, while figure 14.14 is a hologram of the same flat. These tests demonstrated the extremely good storage capabilities of the hologram in that no difference was seen between the normal photograph and the photograph of the hologram. The image on the hologram also, of course, could be reconstructed and measured directly. More information on this aspect of this effort can be found in reference 1.

In continuing the holographic analysis of contaminate deposits, an extremely simple system (fig. 14.15) was used. Figures 14.16 through 14.20 are examples of the holograms made with this system. Figure 14.16 is a double-exposure hologram where the first exposure was made without any sample in either beam and the second exposure with the 1-in. optical flat in one beam. This presents the characteristics of the optical flat just as one would get in a normal interferometer. Figure 14.17 is a triple-exposure hologram, the first exposure without a sample, the second exposure with the sample, and the third exposure with a thin film of oil on the sample. The oil film can be seen running down the center of the optical flat. This represents very gross contamination and how it would appear in a normal interferometer if, indeed, it could be seen at all. Figure 14.18 is a double-exposure hologram where the flat was present in the first exposure and the oil film applied for the second exposure. This, of course, accents the oil film and considerable fringe detail can be seen. Figure 14.19 is a photograph of an enlarged portion of the fringe structure. Figure 14.20 is a double-exposure hologram made to show a simpler fringe system. The sample in this test was a standard Perkin—Elmer 2-in. flat with an antireflection coating in the center. By making the first exposure without the flat and the second exposure with it, one can obtain the thin-film parameters.

Since the tests presented thus far represent such gross contamination, they do not produce the needed data. In order to produce contamination and allow it to deposit on an optical surface, it was necessary to incorporate a vacuum system in the holographic setup. Figures 14.21 and 14.22 are drawings of arrangements used to produce both reflectance and transmittance holograms of optical flats while under vacuum. Each technique has its advantages and disadvantages. For instance, the reflectance hologram gives more detail surface information for particulate matter, whereas the

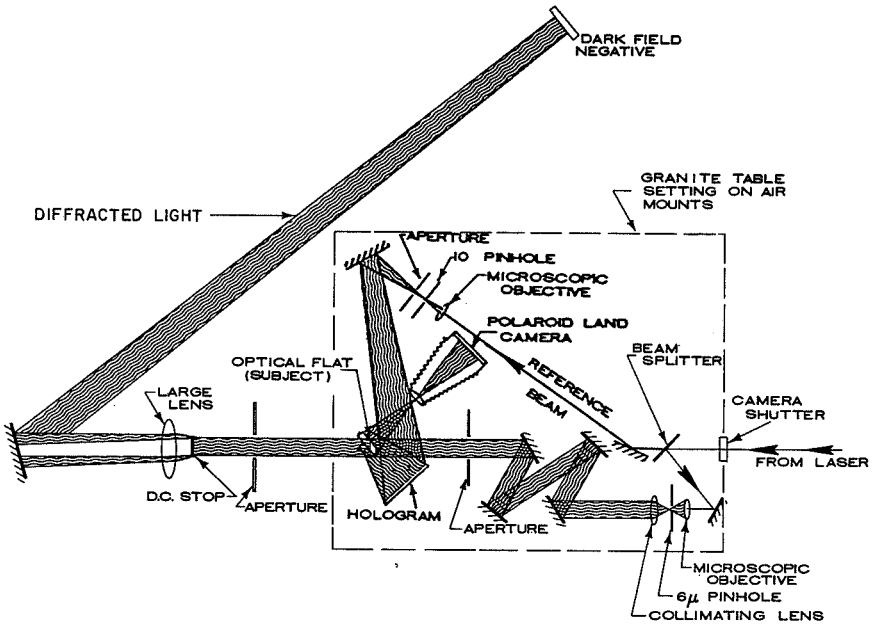

Figure 14.11 Optical layout for producing normal photographs, dark field photographs, and holograms

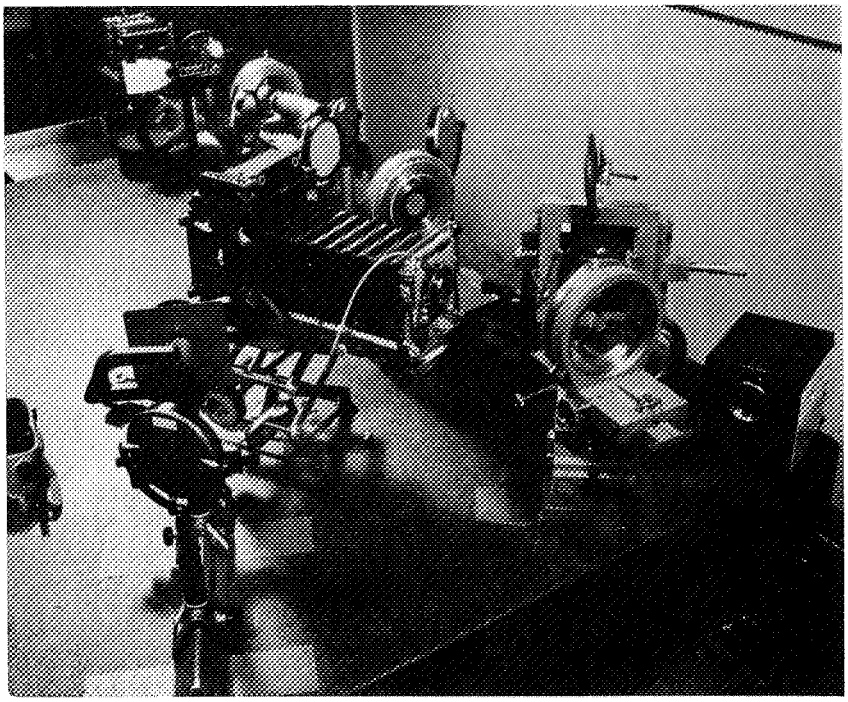

Figure 14.12 Optical sample holder and photographic equipment

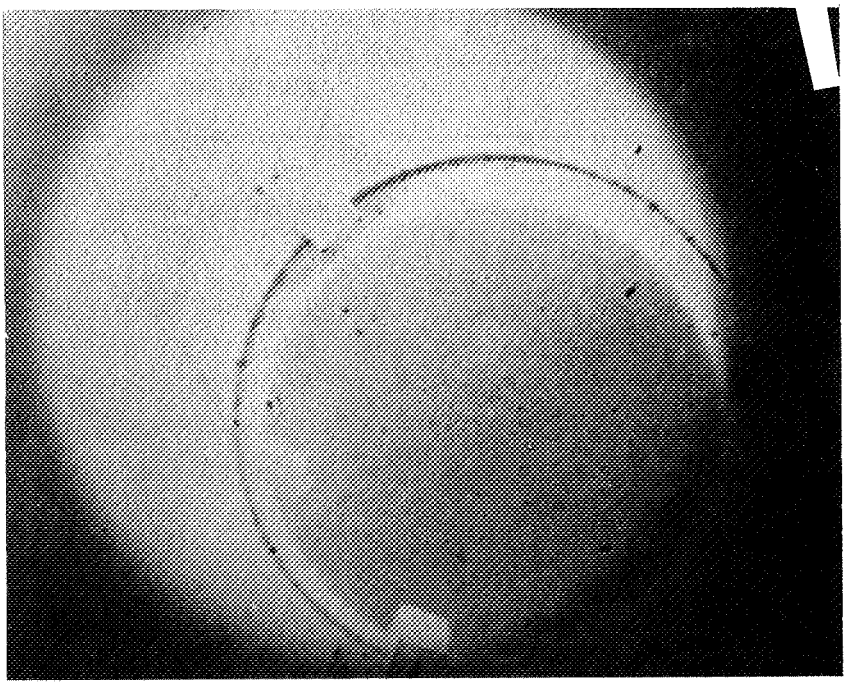

Figure 14.13 Normal photograph of contaminated optical flat

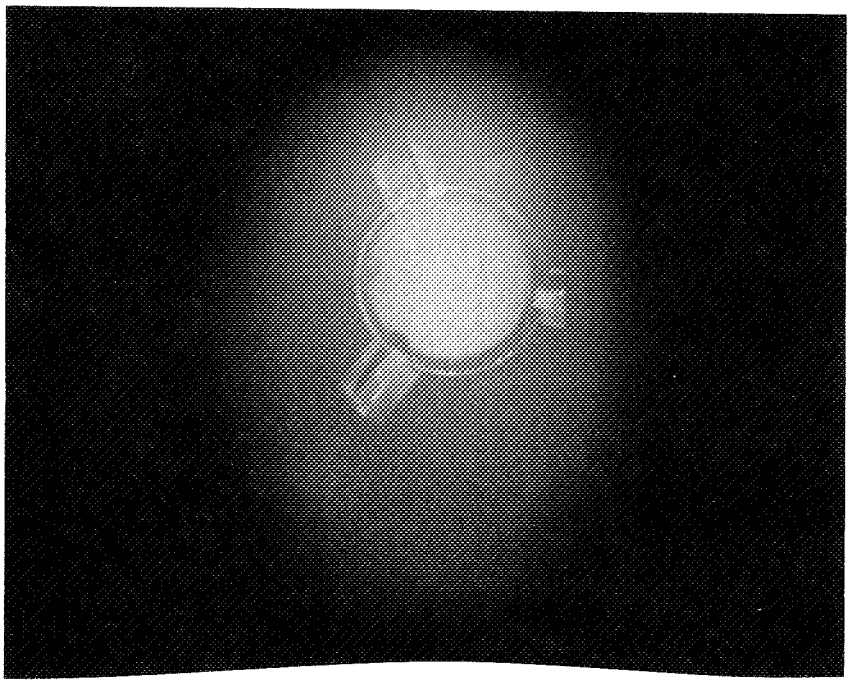

Figure 14.14 Holographic image of contaminated optical flat

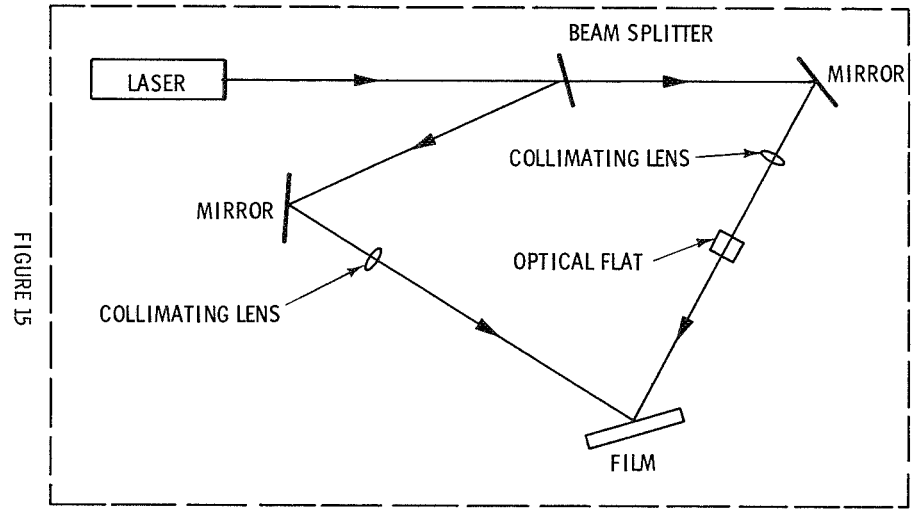

Figure 14.15 Transmission holometer

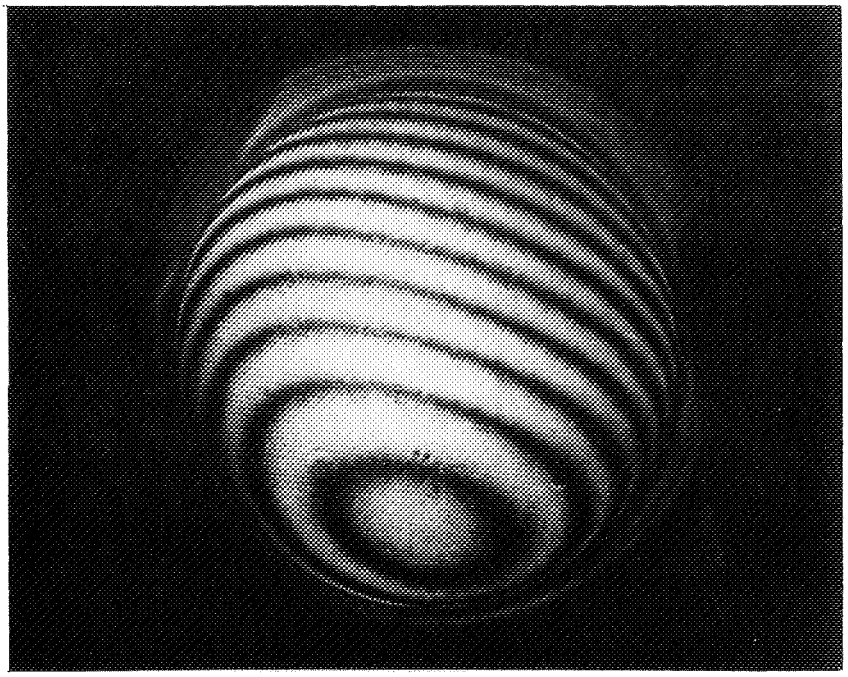

Figure 14.16 Double-exposure holographic image of clean optical flat

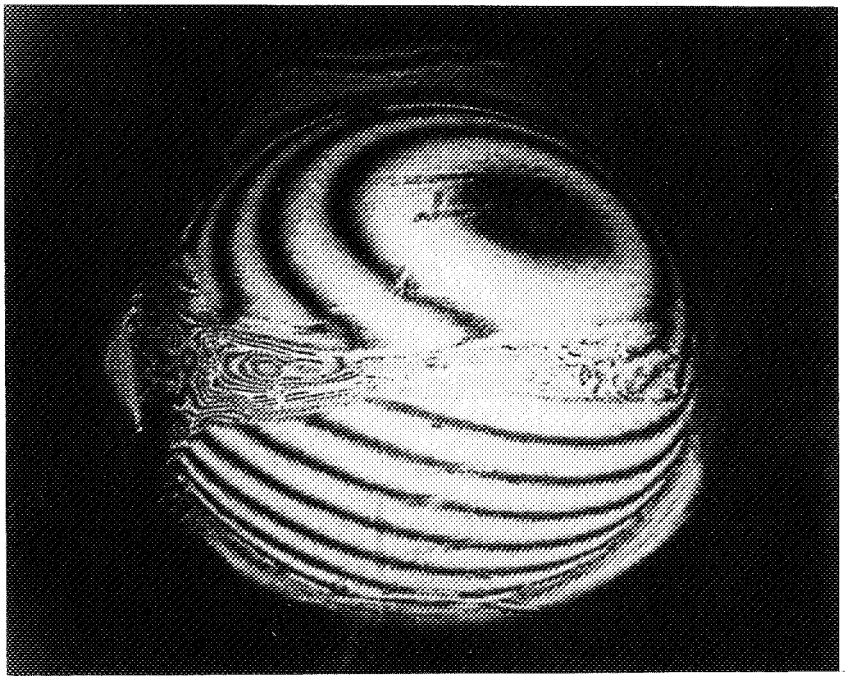

Figure 14.17 Triple-exposure holographic image of contaminated optical flat

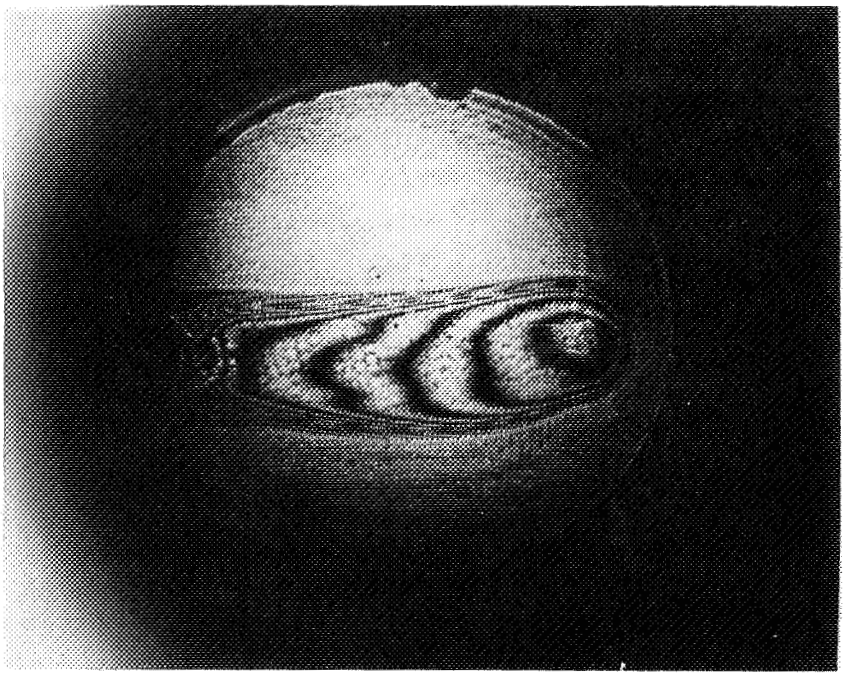

Figure 14.18 Double-exposure holographic image of contaminated optical flat

Figure 14.19 Fringe enlargement of figure 14.18

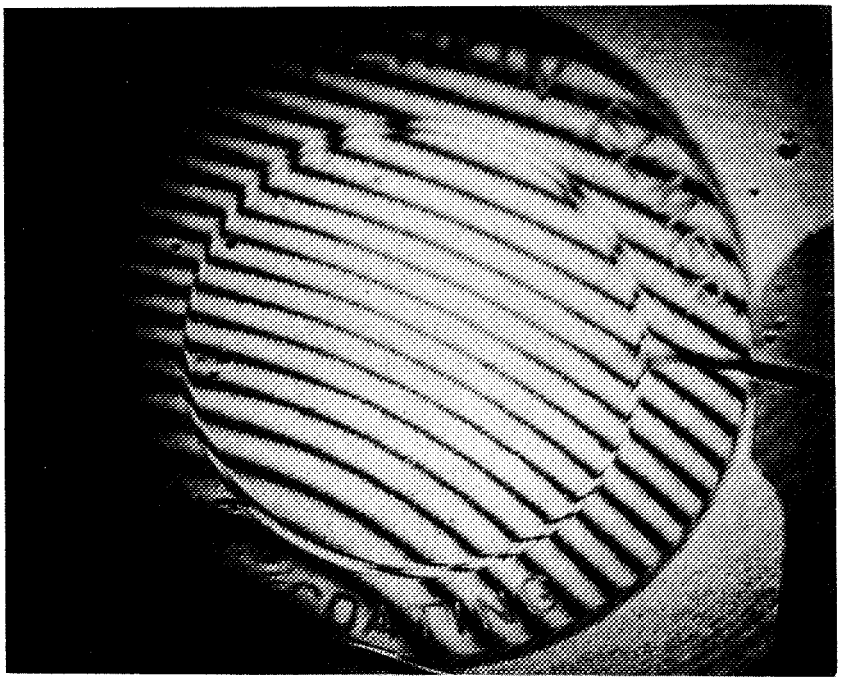

Figure 14.20 Double-exposure holographic image of thin film

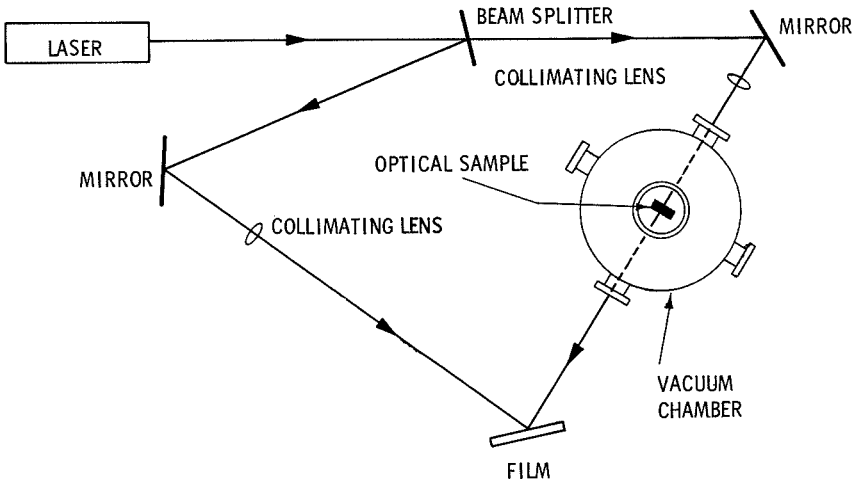

Figure 14.21 Transmission holometer

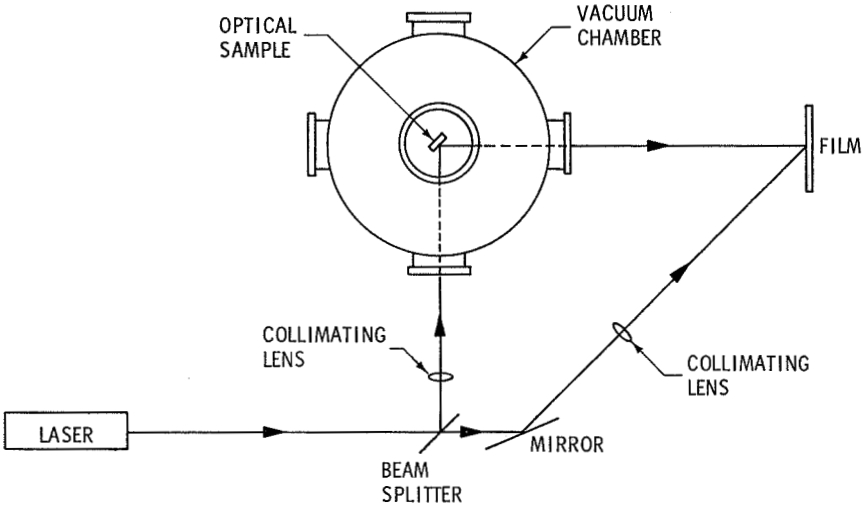

Figure 14.22 Double-exposure holographic image of thin film

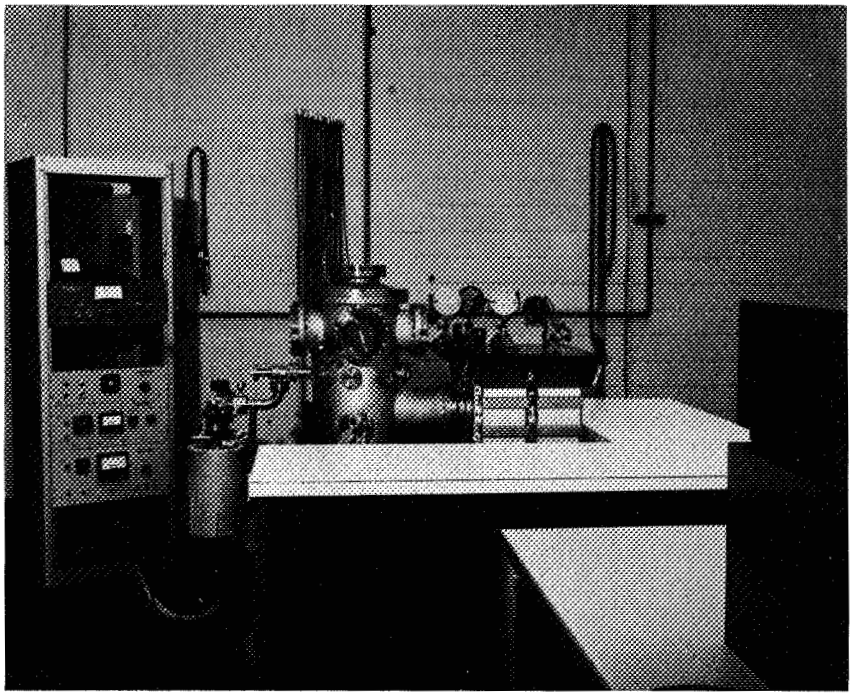

Figure 14.23 Experimental holographic interferometer

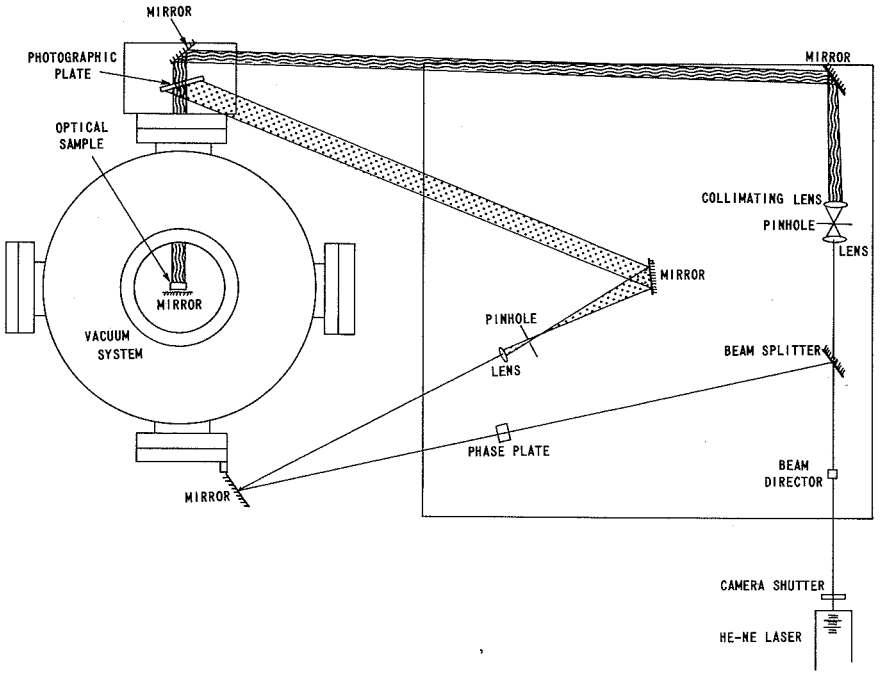

Figure 14.24 Optical layout of holographic thin film analyzer

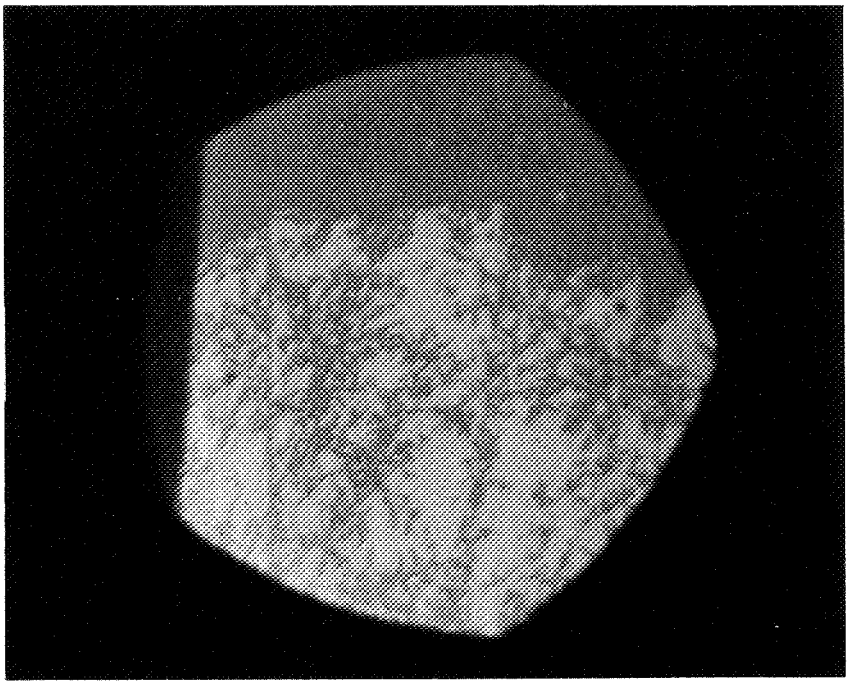

Figure 14.25 Photomicrograph of contaminate film

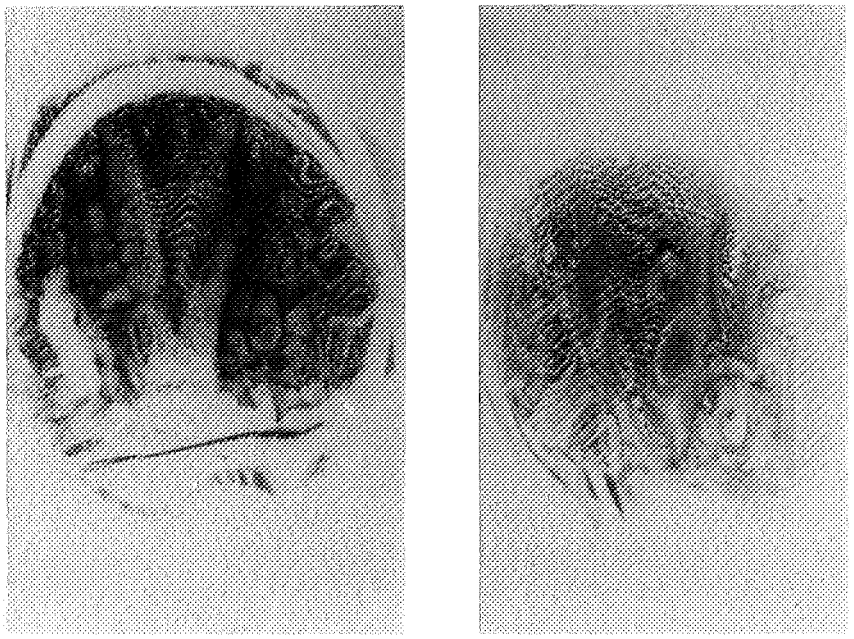

Figure 14.26 Reflectance/transmittance holographic image of contaminated optical flat

transmittance hologram gives more information about the thin film. Since it is not known exactly what the orbiting environment will produce, the ability to produce both reflectance and transmittance holograms is needed. Figure 14.23 is a photograph of the system being used. The vacuum system is a specially designed multiport chamber with an ultimate pressure less than 10^{-12} torr. Since it is advantageous to produce both reflectance and transmittance holograms, a new system was designed. As shown in figure 14.24, the object beam comes in from the back of the photographic plate and strikes the optical sample. The surface of the flat reflects part of the light back to the photographic plate, producing a reflectance hologram on a portion of the film. The rest of the light passes through the flat, strikes a mirror, and is reflected to the film. This forms a double-pass transmittance hologram on another portion of the film.

A material sample is forced to outgas by heating it with a small heater inside the vacuum system. This outgassed vapor then deposits on the optical flat. This deposit is very seldom uniform in that the material sample is not vaporized as one would do, for instance, in coating a mirror. Figure 14.25 is a photomicrograph made at 50X, of one of these outgassed deposited films. Figure 14.26 is a double-exposure hologram of a contaminated optical flat. The top photograph is a transmittance hologram, while the bottom photograph is a reflectance hologram. Both photographs were made from the same photographic plate in the system shown in figure 14.24.

All of the tests on this effort, thus far, have utilized double-exposure holography. Preparations are under way to record deposited films real time as they form. Quartz crystal microbalances will be placed in the vacuum system to produce deposited mass data to be correlated with the data obtained from the holographic interferometer. The phase of the reference beam is being rotated to increase the sensitivity of the system. This and other techniques are being used to determine just how thin a film the system will detect.

REFERENCE

1. Arnett, G. M.: Lunar Excursion Module RCS Engine Vacuum Chamber Contamination Study. NASA TM 53,859, 1969.

15 NONDESTRUCTIVE TESTING BY OPTICAL CROSS-CORRELATION

Rodney W. Jenkins
Marshall Space Flight Center

Since reliability is a crucial factor in space systems, it is desirable to be able to predict the lifetime of the components of that system under the performance environment. A newly developed technique using optical cross-correlation shows promise as a method of nondestructively testing and predicting the lifetime of printed circuit boards (and other materials) under an environment of thermal cycling.

The technique uses a Fourier transform hologram of the printed circuit board as a matched filter. Since the amplitude of the output from the matched filter is related by a cross-correlation integral to the deformation of the printed circuit board due to thermal cycling, an estimate of the lifetime of the printed circuit board under thermal cycling can be obtained.

The permanent deformation suffered by a component under repeated exposure to load (whether heat or vibration) usually is the factor that ultimately limits the lifetime of the component. For this reason, measurement of the deformation occurring, when compared with other data, can lead to an estimate of time to failure.

Holographic interferometry is one way to measure deformation occurring in materials. However, measuring the deformation quantitatively by fringe analysis is at best tedious and complicated. A more simple way to measure the deformation or change occurring is by optical cross-correlation. Instead of adding the two functions associated with the component before and after deformation, as in interferometry, the cross-correlation of the two functions is performed. The amplitude of the cross-correlation integral evaluated at the origin is a measure of the difference between the two functions.

THEORY

Figure 15.1 is a block diagram of an optical data-processing system whose output amplitude is a measure of the deformation that has occurred in the test material. The first component of the system is a light source with the necessary optics to illuminate the test material (component). A requirement of this particular system is the use of a highly coherent and relatively intense light source; for this reason, a laser is used. The wavefront backscattered off the test material is called the optical input. Its amplitude and phase can be described by a complex amplitude distribution $h(x,y)$, where the x-y plane is parallel to the face of the test material. By the use of a lens, the function $h(x,y)$ is operated on by a Fourier transformation. Then, with a matched filter, the Fourier transform of $h(x,y)$ is multiplied by the complex conjugate of the Fourier transform of the complex amplitude $s(x,y)$, where $s(x,y)$ is the value of the input when the material is unstressed. Using another lens, a Fourier transformation is performed on the product. By the cross-correlation theorem, this is equal to the cross-correlation of $h(x,y)$ and $s(x,y)$, which is described by

4

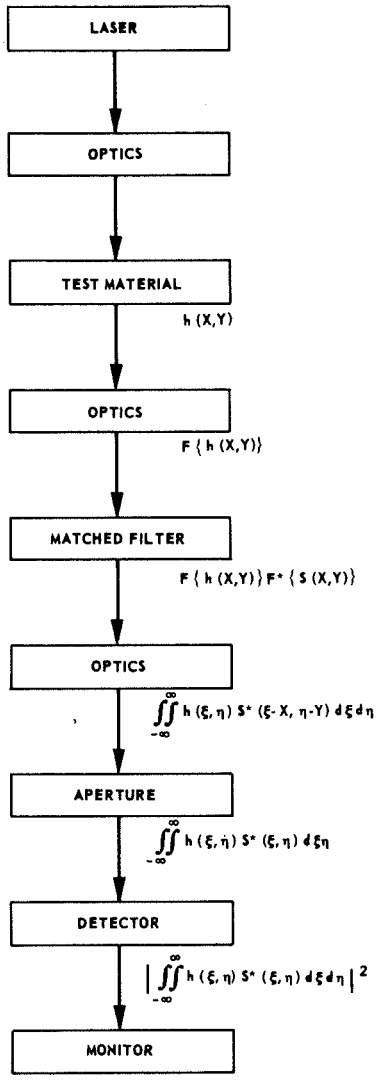

Figure 15.1 Block diagram of optical cross-correlation system

$$\int_{-\infty}^{\infty}\int h(\xi,\eta)s^*(\xi - x,\eta - y)d\xi d\eta$$

By the use of an aperture (50-μ pinhole) placed at the origin of the x-y plane (i.e., along the optical axis), the values of x and y are set at zero. This integral is the final optical output, whose properties are that it is greatest when h(x,y) is equal to s(x,y) (i.e., when the test material is unstressed), and it decreases rapidly as h(x,y) becomes increasingly different from s(x,y). The final optical output is converted into an electrical output by a detector such as a photomultiplier tube.

To realize such a system is not difficult, the greatest problem lying in the synthesis of the matched filter with the correct amplitude transmittance. This is accomplished by making a Fourier transform hologram of the unstressed test material.

MATCHED FILTER SYNTHESIS

The Fourier transform hologram is recorded using the configuration shown in figure 15.2. If the complex amplitude distribution at the photographic plate due to the reference wavefront is R(x,y) and the distribution due to the signal wavefront is the Fourier transform of s(x,y), then the intensity, I(x,y), at the plate will be

$$I(x,y) = \left|R(x,y) + F\left\{s(x,y)\right\}\right|^2$$

$$= \left|R(x,y)\right|^2 + \left|F\left\{s(x,y)\right\}\right|^2 + R^*(x,y)F\left\{s(x,y)\right\}$$

$$+ R(x,y)F^*\left\{s(x,y)\right\}$$

If the emulsion is to respond linearly to the amplitude distribution of the signal wavefront, $\left|F\left\{s(x,y)\right\}\right|$ must be much less than $\left|R(x,y)\right|$ and $\left|R(x,y)\right|$ must be such that

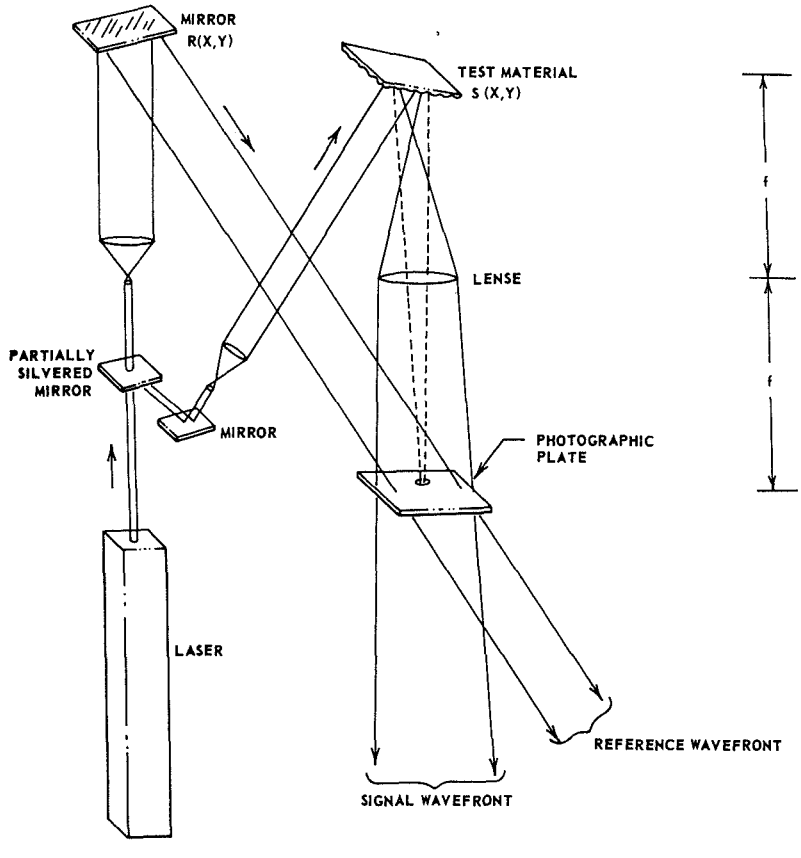

Figure 15.2 Configuration for recording the Fourier transform hologram

$$|R(x,y)|^2 + |F\{s(x,y)\}|^2 = \frac{E_o}{t}$$

where (E_o, T_o) is a point that falls in the middle of the linear section of the amplitude transmittance versus exposure curve of the emulsion (E_o being the mean exposure). In this case, the transmittance modulation will be linearly proportional to the intensity modulation. Therefore, the amplitude transmittance, $T_a(x,y)$, of the plate can be written

$$T_a(x,y) = T_o + Bt\left[R^*(x,y)F\{s(x,y)\} + R(x,y)F\{s(x,y)\}\right]$$

where B is the slope of the curve at (E_o, T_o), and t is the exposure time.

If the plate is illuminated with the complex amplitude distribution $F\{h(x,y)\}$ (fig. 15.3), the transmitted amplitude can be written $F\{h(x,y)\}\, T_a(x,y)$. If the reference wavefront is a plane-parallel beam of constant amplitude inclined at an angle θ with respect to the optical axis, it can be written

$$R(x,y) = A \exp - i2\pi \sin\left(\frac{\theta y}{\lambda}\right)$$

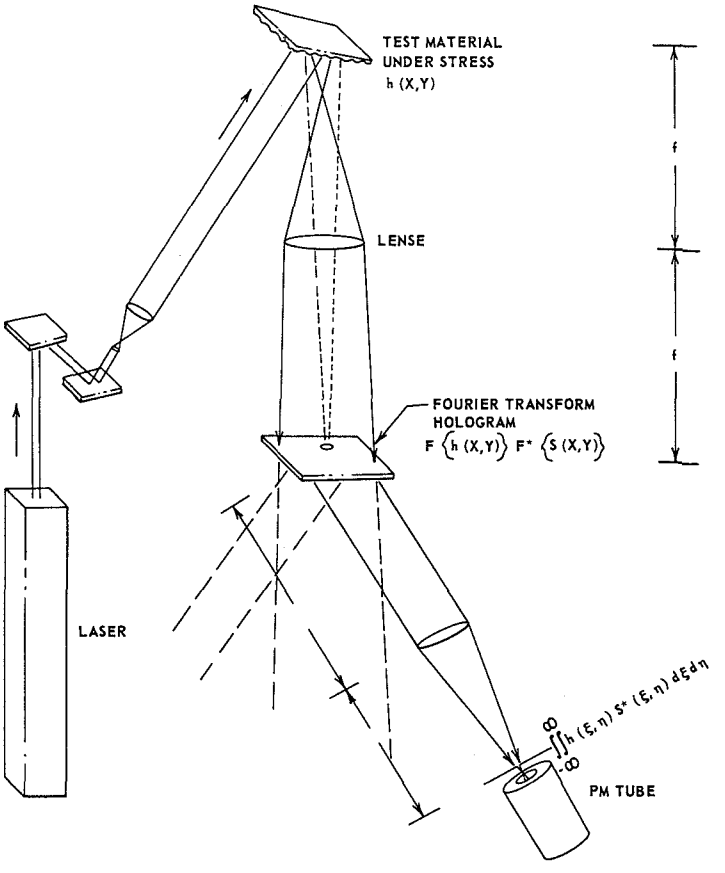

Figure 15.3 Configuration for measuring the deformation

Then, the transmitted amplitude will be

$$F\left\{h(x,y)\right\} T_a(x,y) = BtAF\left\{h(x,y)\right\} F^*\left\{s(x,y)\right\} \exp - i2\pi \sin\left(\frac{\theta y}{\lambda}\right) + \cdots$$

where the other terms are separated by angle from the first term because the exp $[-i2\pi \sin(\theta y/\lambda)]$ term serves to incline the desired transmitted amplitude off axis. Dropping the exponential term and the constants, the (off axis) transmitted amplitude is written

$$F\left\{h(x,y)\right\} T_a(x,y) = F\left\{h(x,y)\right\} F^*\left\{s(x,y)\right\}$$

Effectively, the amplitude transmittance of the developed photographic plate (hologram-matched filter) is $F^*\left\{s(x,y)\right\}$, which is the desired value.

EXPERIMENTAL RESULTS

Some preliminary work has been done to predict the lifetime of printed circuit (pc) boards using the cross-correlation technique. In the case of pc boards, failure is usually due to joule heating. Different types of solder joints have different life spans (time to failure) depending on the materials and configuration used. A typical solder joint configuration is shown in figure 15.4.

To test the cross-correlation technique, an experiment was set up to monitor three solder joints, each of a different type. The purpose was to predict which solder joints would fail first in normal use. The solder joint whose cross-correlation amplitude dropped fastest when plotted versus thermal cycles would be said to be undergoing the greatest permanent deformation and therefore be likely to fail before the others.

The experiment was performed using a cold cathode 70-mW HeNe laser. The laser was allowed to stabilize 1 hr before any exposures or tests were made. The entire setup was mounted on a heavy granite table supported by three large airmounts to stop most of the building vibration (fig. 15.5). The photographic plate (Agfa 8E70) was held by a precision plate holder with $\lambda/10$ x-y adjustment. The plate holder was also mounted such that it could be given a coarser x-y adjustment. The laser beam directed toward the pc board was split into three separate beams, each directed to one of the

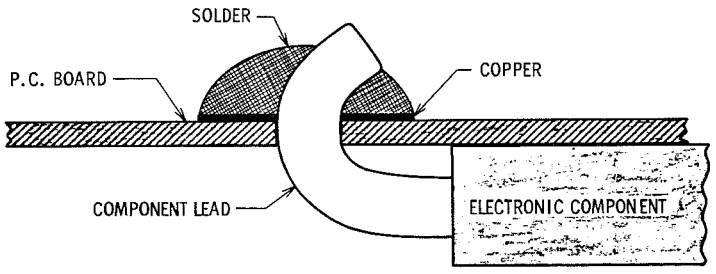

Figure 15.4 Cross section of typical solder joint configuration

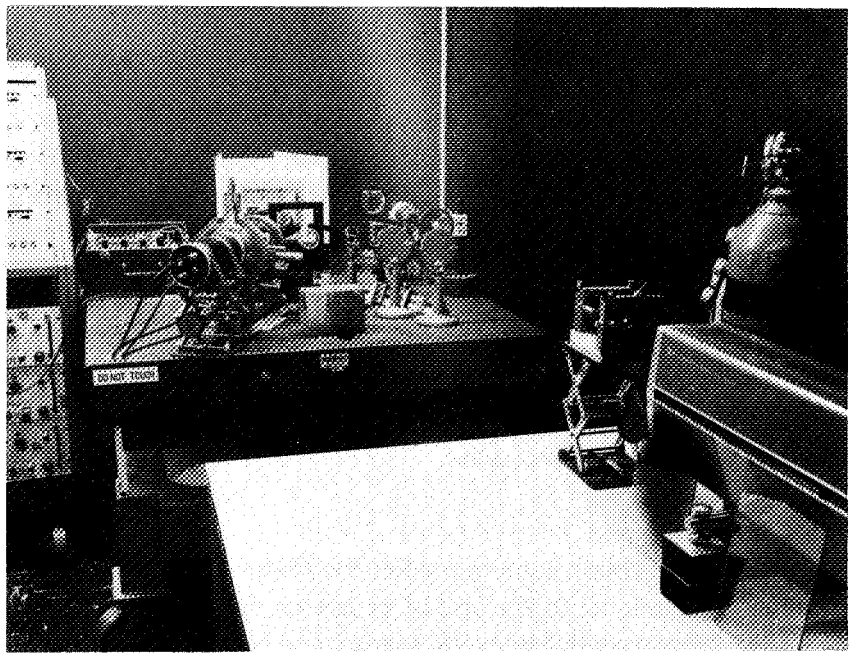

Figure 15.5 Photograph of laboratory setup

three solder joints being tested. One Fourier transform hologram was recorded for all three solder joints. After placing the developed plate back in its original position, the reference beam was blocked and the plate was adjusted for maximum autocorrelation intensity. Then, by blocking two of the three beams illuminating the pc board, the cross-correlation for each solder joint could be recorded and plotted versus the number of thermal cycles undergone by the pc board. The thermal cycling of the pc board was done without moving the pc board. Using a heat lamp, the temperature was raised from 24° C to 39° C and then allowed to cool down to 24° C each cycle. To obtain repeatable and meaningful results, the hologram and the 50-μ pinhole aperture were adjusted for a maximum detector output for each reading.

Typical results obtained from this procedure are plotted in figure 15.6. The type B solder joint had the steepest slope, and the type A joint had the least decrease in cross-correlation amplitude. Therefore, it was postulated that type B was the worst of the three and type A was the best. These predictions were found to agree with results obtained from destructive testing of the same type joints.

The destructive testing procedure was to cycle the pc boards from –50° to 80° C and back to –50° C many times, counting the number of joints that showed effects of strain, suffered simple cracks, or contained an isolated crack. (An "isolated crack" is defined to be a 360° C crack about the lead; this is a case of complete failure.) The results of these tests are shown in figure 15.7. It was found that, as was predicted by the cross-correlation measurements, type B solder joints were by far the worst type of the three joints; this type of joint was the only one that went to isolated cracking. Also in agreement with prediction, type A solder joints were the best of the three. (While the destructive testing procedure does not duplicate the thermal cycling due to joule heating,

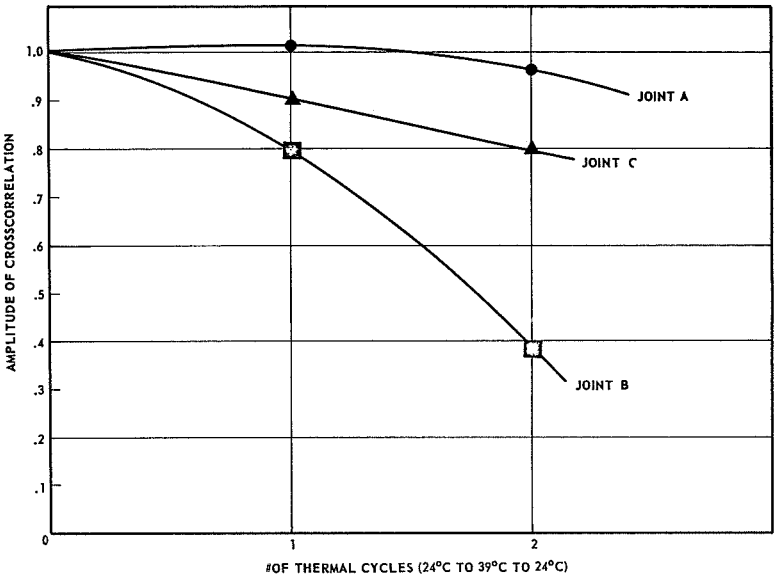

Figure 15.6 Results from nondestructive testing

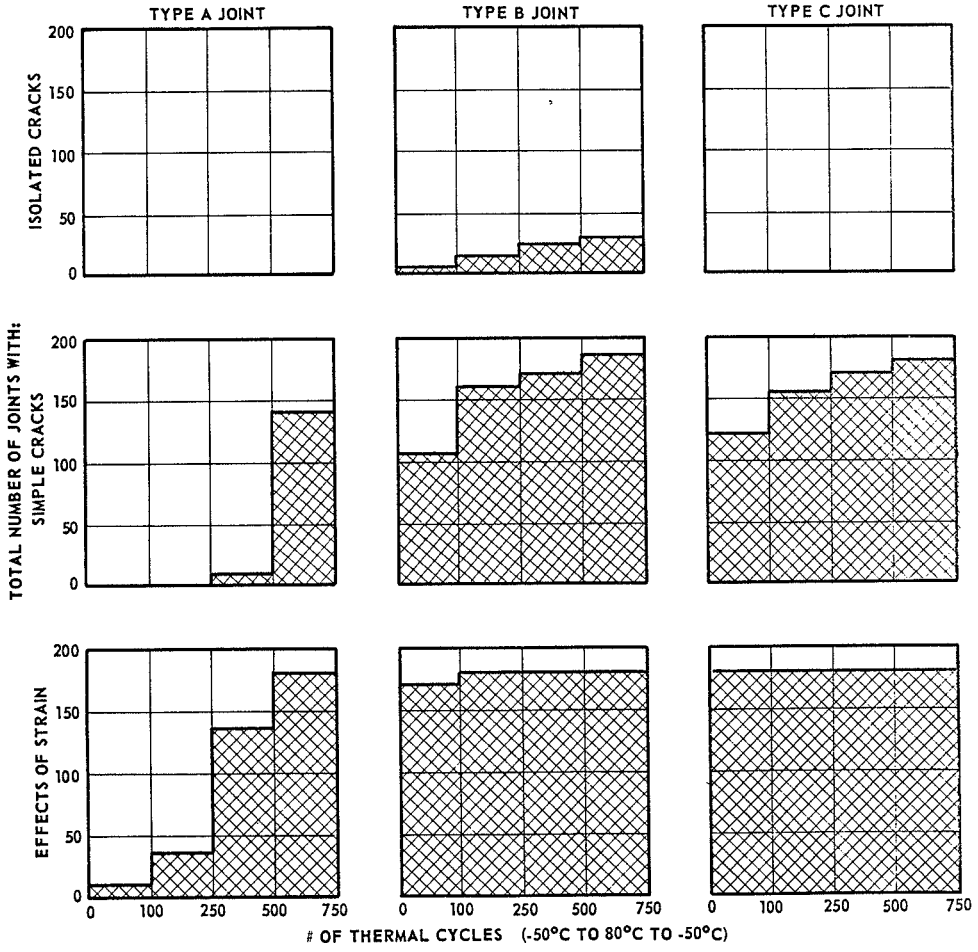

Figure 15.7 Results from destructive testing

results from extensive destructive testing were found to agree with data from solder joint failure in actual use.)

CONCLUSION

The experiment shows that it may be feasible to nondestructively test pc boards for bad solder joints and to assign lifetime predictions based on the slope of the cross-correlation versus thermal cycles curve.

The limitations of the cross-correlation technique relate to the stability required for recording the matched filter and for obtaining the cross-correlation measurement. The system must be isolated from vibration and the test material must be rigid. Materials that are too large and flexible will deform under their own weight, making the cross-correlation measurement almost meaningless.

For rigid materials, however, there are several advantages. In most other nondestructive testing, the faults must be fairly large before they can be detected. In this sytem, the faults are detected before they occur, and the material needs to be only barely stressed to detect material fatigue. Thereby, the integrity of the material is maintained.

16 ONBOARD OPTICAL PROCESSING

James P. Strong, III
Goddard Space Flight Center

As spacecraft experiments get more complex, onboard data processing becomes increasingly important. For example, such processing will be required for outer planet missions, where there simply are not enough bits to send back all the data. Onboard processing allows one to extract parameters from raw data and send back parameters, effecting a large bit saving. Optical processing is a very efficient way of doing the complicated mathematical operations necessary to extract parameters from both scientific and pictorial data using a computer with a very low "parts count."

ONBOARD OPTICAL PROCESSING

As spacecraft ranges and the quantities of experimental data increase, onboard processing techniques must be utilized to reduce the amount of data telemetered back. Optics can handle large quantities of two-dimensional data far faster and easier than digital computers. For example, at GFSC, electromagnetic whistlers have been detected and classified using optics. Cloud-cover pictures have been classified as overcast, broken, or as containing frontal patterns. We also have developed a unique sensor that detects radius and angle information from the Fourier transform plane and have used it in the cloud-cover analysis. Plans for an onboard spacecraft data system consist of an optical system complemented with a digital computer. To connect the optical system with the digital system, interface devices must be evolved.

Basically, there are two techniques for optical processing. The first, where the Fourier transform of an image is analyzed, can detect such parameters as curvature of lines, slopes of straight lines, average size of objects, and the existence of parallel-line structure. It can also give a statistical analysis of the gray levels in the image. The second type of processing, where the image is reconstructed through a spatial filter, can pick out regions containing particular spatial frequencies. (Broken cloud regions in cloud-cover pictures have been detected using band-pass filters.) If the spatial filter happens to be the Fourier transform of another picture, the reconstructed image will be the cross-correlation of the two images.

An onboard system that can do optical processing and analysis is shown in figure 16.1. The first lens takes the Fourier transform of the input made by an image generator. In the Fourier transform plane, a detector can extract parameters about the Fourier transform and can input these data to the digital computer for digital processing. The digital computer might then change the image for further analysis. If a spatial filter is placed in the Fourier transform plane, the second lens will take the inverse Fourier transform, forming a filtered image in the reconstructed plane. A detector in this plane can input the reconstructed image to the computer, allowing feedback from the input to the output. As an example of how this feedback might be used, consider the

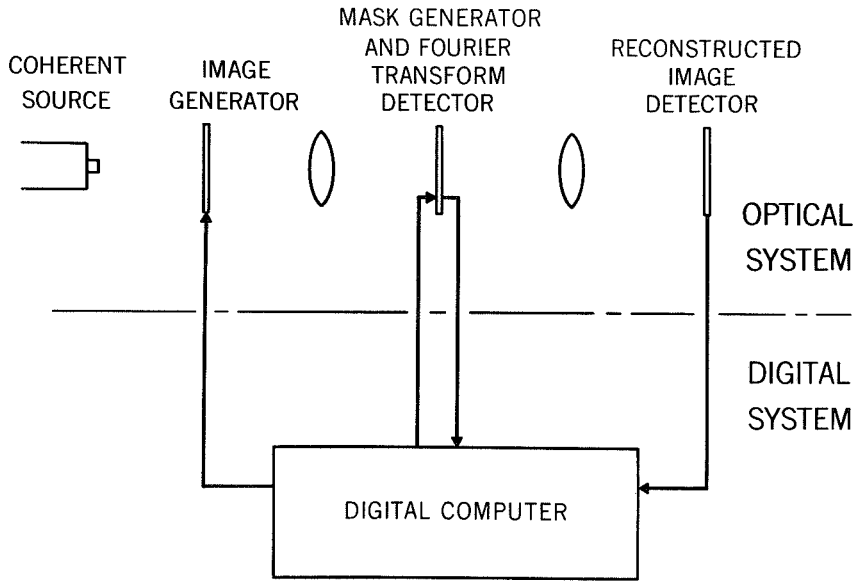

Figure 16.1 Onboard coherent optical processing system

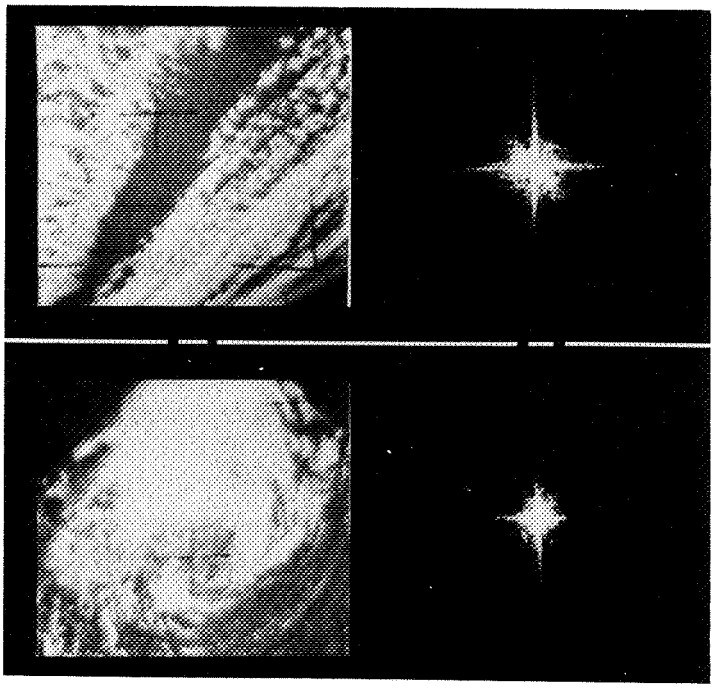

Figure 16.2 Two cloud-cover pictures and their Fourier transforms

cloud-cover picture where spatial filtering detected the broken regions. The computer could blank out all other regions in the input image, and an analysis could be made of only the broken regions.

The development of this spacecraft system at GSFC is proceeding along two channels. First, a detector in the Fourier transform plane has been developed; and second, an image generator has been planned and a contract will soon be let to construct one.

To see how a detector in the Fourier transform plane can detect useful parameters about an image, consider figure 16.2. Here are two cloud-cover pictures and their Fourier transforms. By measuring the distance at which information lies from the center of the Fourier transform, one can tell whether a picture is made up mostly of small scattered clouds or mostly of large clouds. Small scattered clouds have Fourier transforms that are more spread out than the Fourier transforms of large cloud masses, which are more concentrated toward the center. Pictures having frontal patterns, such as the top picture, produce information concentrated along a line in its Fourier transform. Figure 16.3 shows a graphic type of image. Here are two spectrum analyses of electromagnetic whistlers. Information in the Fourier transforms of these curves lies primarily along lines perpendicular to the curves. The Fourier transform of the top whistler contains a component at about 45°, corresponding to the bottom of the whistler curve. The last two graphs of figure 16.3 show the amount of light lying in a 10° angle rotated around the Fourier transform plane. The top curve is different from the bottom curve, indicating the information at 45° in the top Fourier transform. The digital computer could distinguish between the top and bottom curves, and a simple "0" or "1" distinguishing the two could be sent back. Thus, a detector that can detect radius information in the Fourier transform and can detect angles along which information is concentrated can tell a great deal about the original picture. Some detectors designed for this purpose are shown in figure 16.4; they were etched in a silicon solar cell. An example of their outputs is shown in figure 16.5. On top are the two pictures used. One is mostly small scattered clouds, and the second is mostly overcast with frontal patterns. The angle detector output corresponding to the picture with frontal patterns is more peaked than the one corresponding to the small scattered clouds. The output of the radius detector corresponding to the scattered clouds is higher at the outer radii than the output corresponding to the overcast picture, indicating the high spatial frequencies of the small clouds. The output of these detectors showed that the patterns could detect the parameters in the Fourier transform plane. However, they would not give a true indication of the total amount of light falling on each area. Yale University is currently working on materials for detectors with a more linear response.

The image generator, the "front end" of the optical processor, has been a rather elusive item because of the necessary high contrast, high resolution, and the need for memory (since the entire image must be present at any one time to get the Fourier transform). A contract is under negotiation for an image generator utilizing Kerr rotation. This device will be a matrix of 64 X 64 elements with just black and white intensity levels.

To ensure the usefulness of such a device, some tests were made, as illustrated in figure 16.6. At the top is the gray level picture with its Fourier transform; at the bottom is the 64 X 64 binary level equivalent picture with its Fourier transform. The Fourier transforms are very similar. One

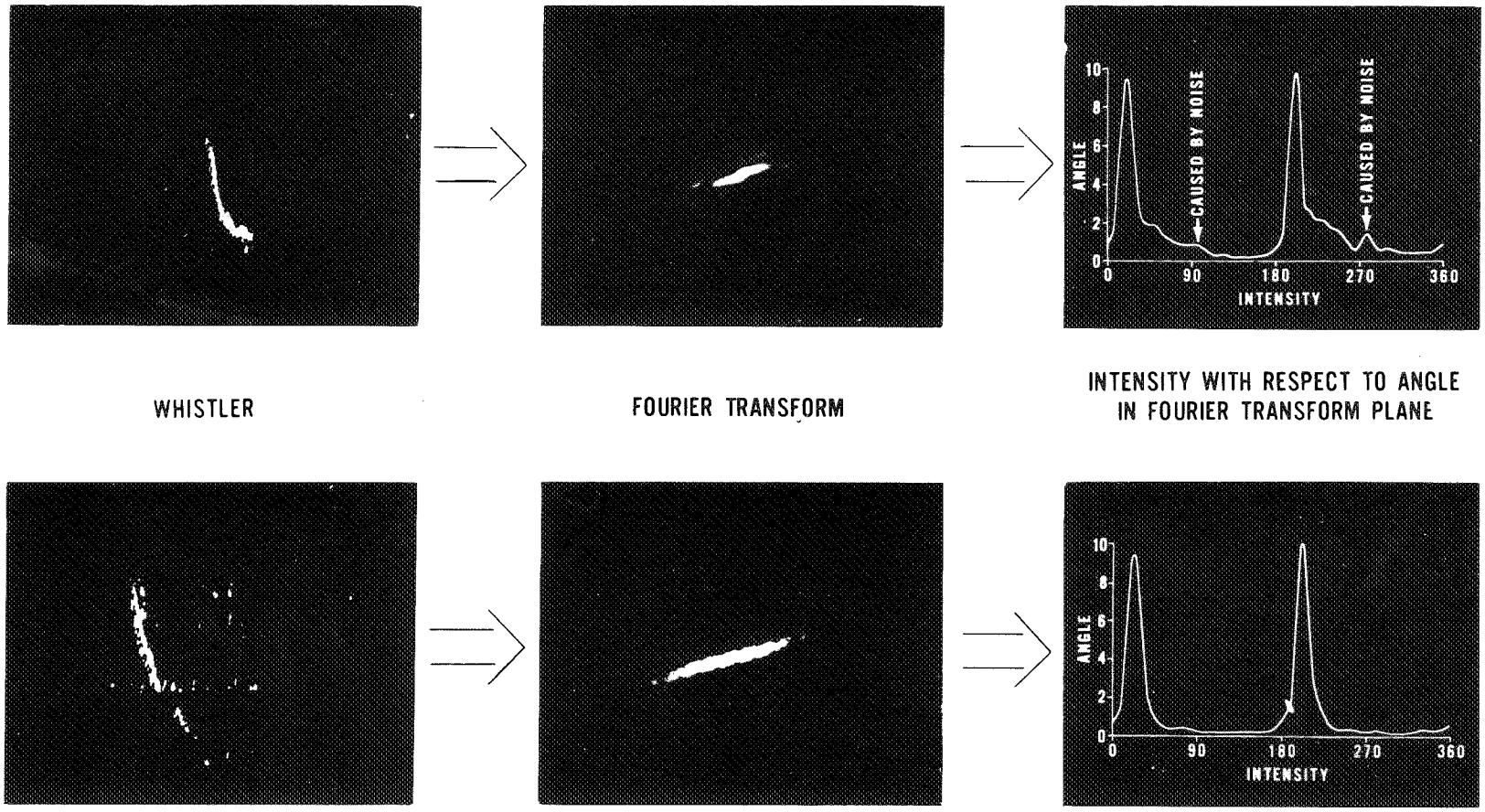

Figure 16.3 Detection and classification of "whistlers" with coherent optics

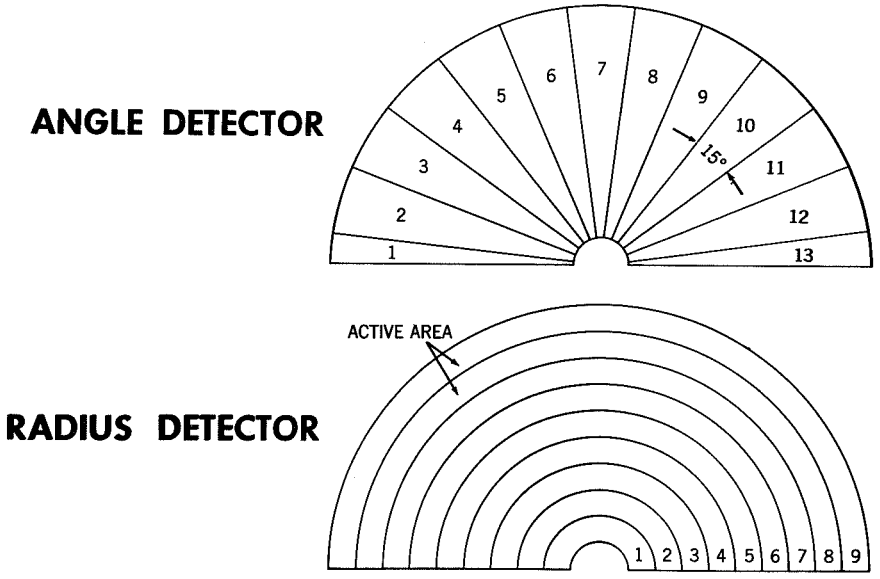

Figure 16.4 Radius and angle detectors

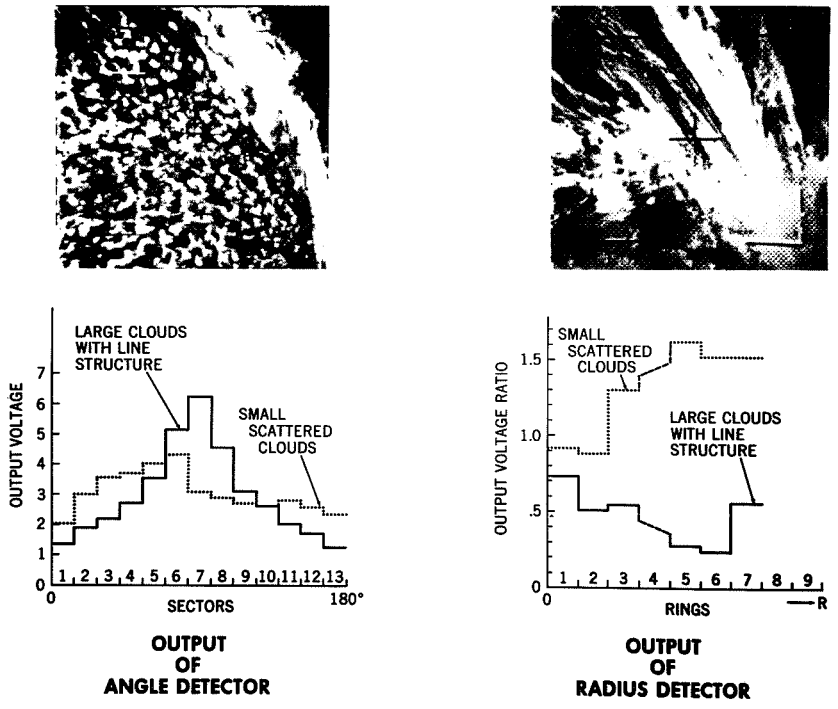

Figure 16.5 Output of radius and angle detectors

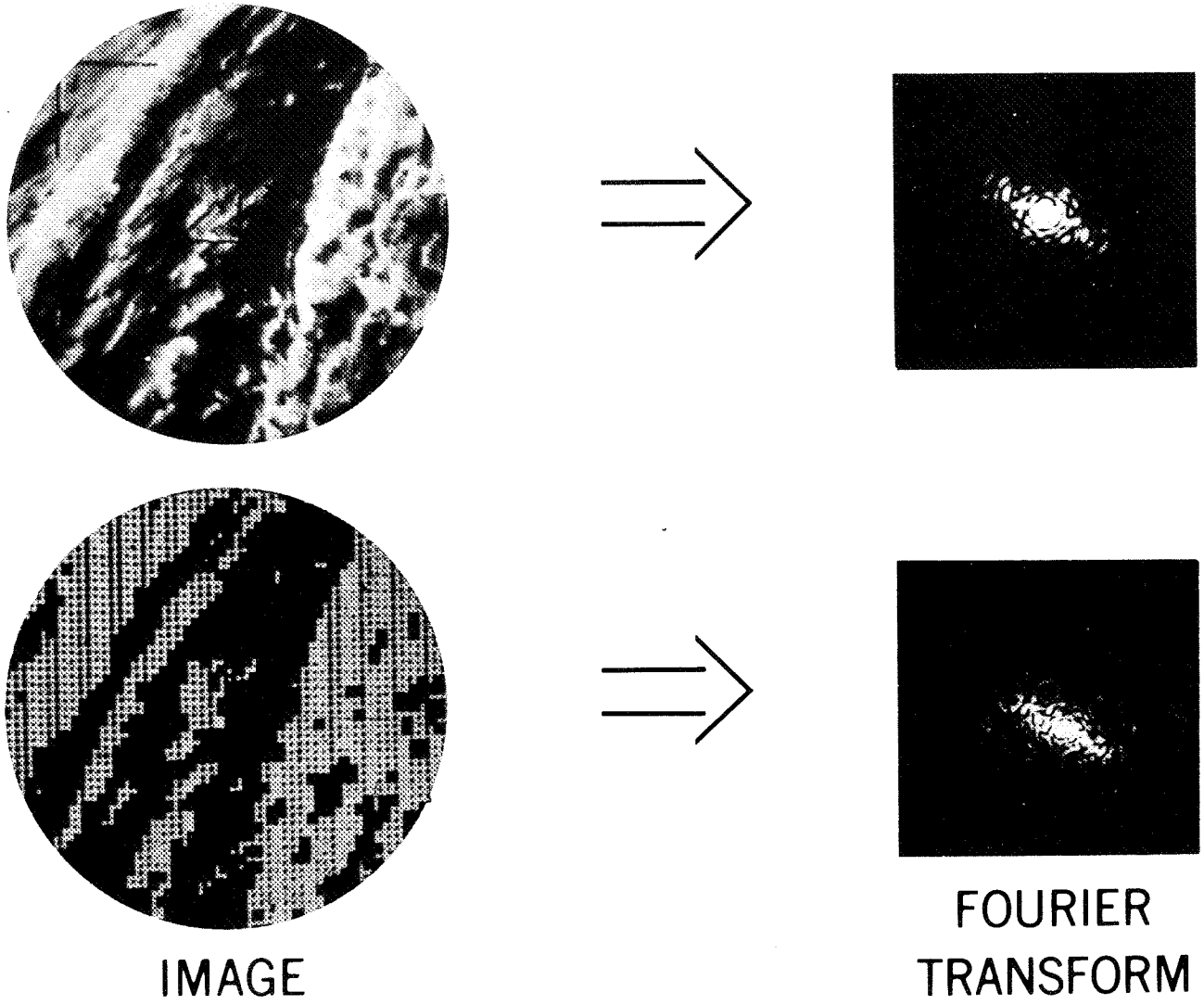

Figure 16.6 Image-generator tests

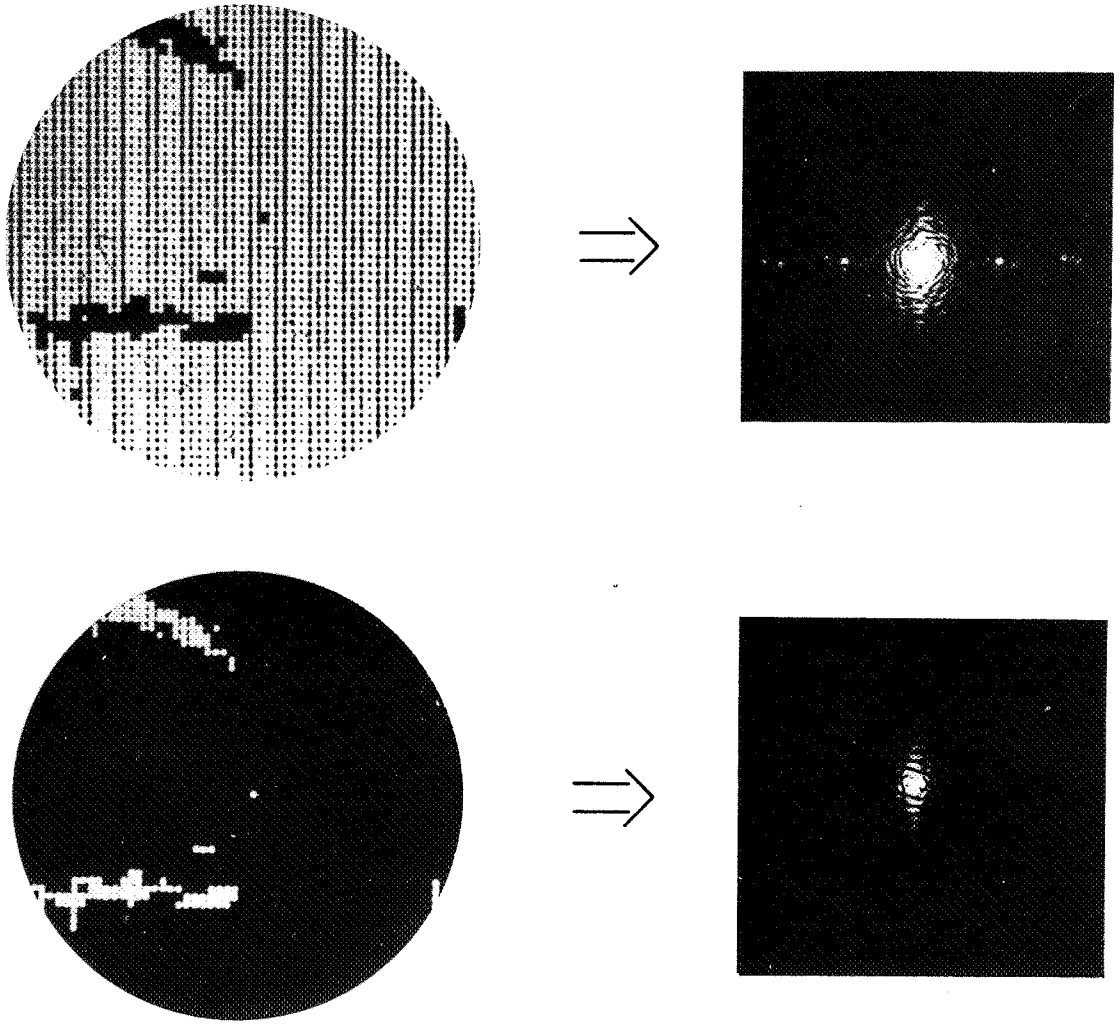

Figure 16.7 Image-generator tests with white image area

problem occurred when the image was of a large white area, illustrated in figure 16.7. The dark areas in the top picture are of interest; the Fourier transform of this image, however, is obscured by the effects of the large white area. A solution to this is to use the negative of the image as shown at the bottom of figure 16.7. Here the Fourier transform is far more apparent. Generating the negative will be easy with the computer-controlled image generator. When the image generator is completed, it will be connected to a computer to begin simulation of an onboard system.

CONCLUSIONS

Optical data processing can be used to extract parameters, which can be transmitted back to Earth to provide useful information about the spacecraft data. With the image generator and the Fourier transform plane detector, a spacecraft optical processing system can be simulated. Such a system will allow the experiments necessary for developing an optical-digital computing system.

17 FRINGE STABILIZATION FOR HOLOGRAPHY

Richard M. Brown
Ames Research Center

Motion of the standing interference fringe pattern during exposure of a hologram is known to degrade the brightness of the holographic reconstruction. Sinusoidal motion is more damaging than linear motion in this respect. A device has been built that stabilizes the fringe pattern in a holographic system in the presence of component vibration and drift. Some design considerations are discussed and the experimental results explained. The system is shown to compensate for large path-length changes at frequencies up to several hundred Hz and to operate down to dc. This system, when applied to holography, makes it competitive in many cases with pulsed laser holography.

When making holograms with low-power, continuous-wave lasers, a prime requirement for success is that the interference fringe pattern remain stable during the time necessary to properly expose the hologram. The stability of the fringe pattern can be determined by observing the holographic reconstruction. A bright reconstruction will be indicative of a stable fringe pattern and a dim one will indicate motion of the pattern, all other parameters being equal. Generally, people try to stabilize the fringe pattern by preventing all motion-inducing disturbances from affecting the holography system. This requirement for isolation generally limits the usefulness of the holographic process to projects that can be done "on the granite slab"—that is, under strict laboratory conditions. However, to expand its applicability, the process must be freed from dependence on the massive optical supports generally used. The purpose of the fringe stabilization system described here is to prevent motion of the fringes and therefore provide good holograms, even in cases where some of the optical components are not completely immobile.

SOURCES OF FRINGE MOTION

Fringe motion can be generated by several sources. One of the least troublesome is a shift in the wavelength of the laser, but even this small effect can become significant if the path-length difference between the signal and reference beams becomes appreciable. For example, the representative of one major manufacturer of argon ion lasers states that his laser, when operated with an intracavity etalon, will stay in a particular mode for periods greater than 5 min (private communication from Richard Fohr, Coherent Radiation Laboratories). The mode hop, when it occurs, is a jump of 108 MHz. The manufacturer also quotes (ref. 1) coherence lengths "in excess of 10 yards." Now, if a holographic setup using this laser with a 1-m path-length difference were to mode hop half-way through the exposure, the fringes would shift by about 0.5 times their spacing! This motion would almost completely destroy the hologram.

In similar ways, small changes in the air density caused by pressure or temperature shifts will also affect the location of the fringes, if the optical paths are of different lengths. Of course, any

change in the air density in one path that is not compensated by a similar change in the other will have the same effect, even if the path lengths are equal. This might come about as a result of convection currents or wind caused by air conditioners or by motion of people.

Probably the main cause of fringe motion can be traced to mechanical changes in the structure holding the optical components. Thermal drift is a common problem. Another, the cold flow of stressed or soft material, is sometimes overlooked. The major cause of mechanical motion, however, is the vibration of components excited through their supports or through the air. It is this problem, more than any other, that leads to the heavy granite tables and pneumatic supports that are so typical of holography labs.

While all the above problems can be alleviated by various methods, the usual result is a system too awkward or bulky to take out of the laboratory and put into the real world. There are two possible exceptions to this: either the hologram can be made using a Q-switched laser so that there is essentially no motion during the exposure time, or the system can be actively servostabilized so that problems of component motion may be ignored.

In choosing between these possibilities, several factors must be considered. The prime consideration, of course, is the nature of the subject. If it is transient, such as the shock wave from a detonation, the pulsed laser is mandatory. If a time-averaged hologram of a slowly moving panel is desired, the CW laser is required. Of course, there is a wide range of objects that could be recorded by either method. In this case, other parameters must be considered, for example, the equipment available or the economics of the system. The question to be answered in this latter case is: Is it better to buy an expensive pulsed laser and pay little attention to system stabilization, or to buy a less expensive gas laser and put some effort and money into the stabilization of the structure?

FRINGE MOTION EFFECTS

To see how well a holography system must be stabilized, consider figure 17.1. This is a plot of the relative diffraction efficiency of a hologram as a function of the visibility of the fringe pattern recorded on it. Diffraction efficiency can be considered a measure of the brightness of the holographic reconstruction. These curves show the effect of linear fringe motion—that is, fringe motion with constant velocity—on the efficiency. These data are calculated (ref. 2) and assume that the recording medium has a linear relationship between the exposure and the amplitude transmittance. For visibilities up to about 0.5, these calculations correlate well with experimental data (ref. 2).

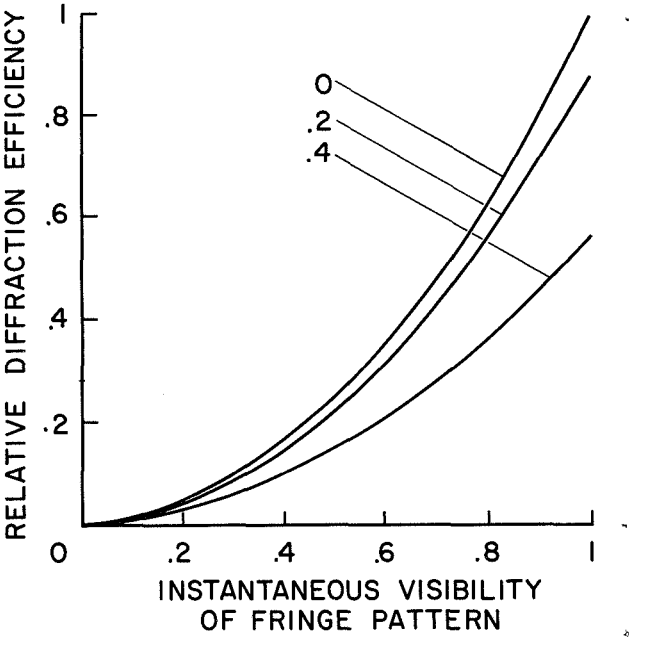

Figure 17.1 Relative reconstruction efficiency of holograms. The parameter indicates the fractional wavelength linear motion of the fringe pattern during the exposure

The ratio of the efficiencies of motion-blurred holograms to static fringe holograms depends on the type of motion involved. If the fringe system is moving at a constant velocity, the visibility of the recorded pattern is degraded by a factor of $\text{sinc}(\pi f)$, where f is the fraction of a fringe spacing traversed during the exposure. Since the curve in figure 17.1 shows a quadratic relationship between efficiency and fringe visibility, the efficiency in the case of linear motion will go as $\text{sinc}^2(\pi f)$. In the case of sinusoidal motion of the fringe pattern, however, the efficiency will go as $Jo^2(2\pi f)$, where Jo is the zeroth order Bessel function, and f is the peak-to-peak motion of the fringe pattern measured in units of the fringe spacing (ref. 3). The relative diffraction efficiencies for the cases of linear and sinusoidal motion are shown in figure 17.2. This curve indicates that for small motions, sinusoidal fringe motion is more troublesome than linear motion. Since the servocontrol system described below has a sinusoidal residual error, the curve of sinusoidal motion in figure 17.2 is of particular interest.

Criteria must be established for determining when a vibration compensation system is performing adequately. Looking at figure 17.2, we see that if the peak-to-peak residual motion of the fringes is less than 0.1, corresponding to an optical path difference change of 0.1 wavelength peak to peak, the efficiency of the hologram will be better than 80 percent of the case where the fringe pattern is steady. Therefore, a success criterion will be chosen stating that residual fringe motion is less than 0.1 wave.

FRINGE MONITORING

Figure 17.3 shows one form of the fringe position monitor. In this case, the fringe monitor is behind the photographic plate, sampling the light that passes through the semitransparent holographic emulsion. The beam combiner in figure 17.3 superimposes the point source in the upper beam with the one in the lower beam. Because the path lengths are matched in this system and

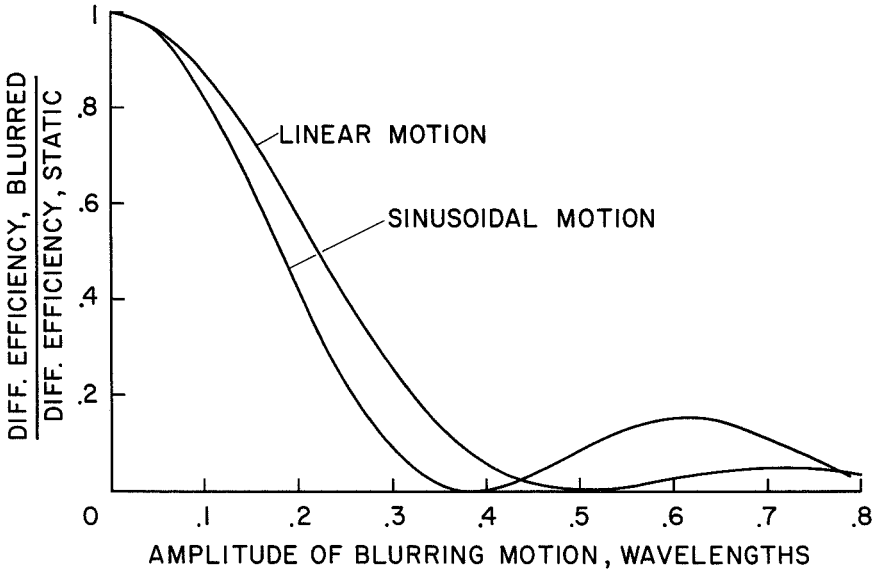

Figure 17.2 Effect of fringe motion on reconstruction efficiency

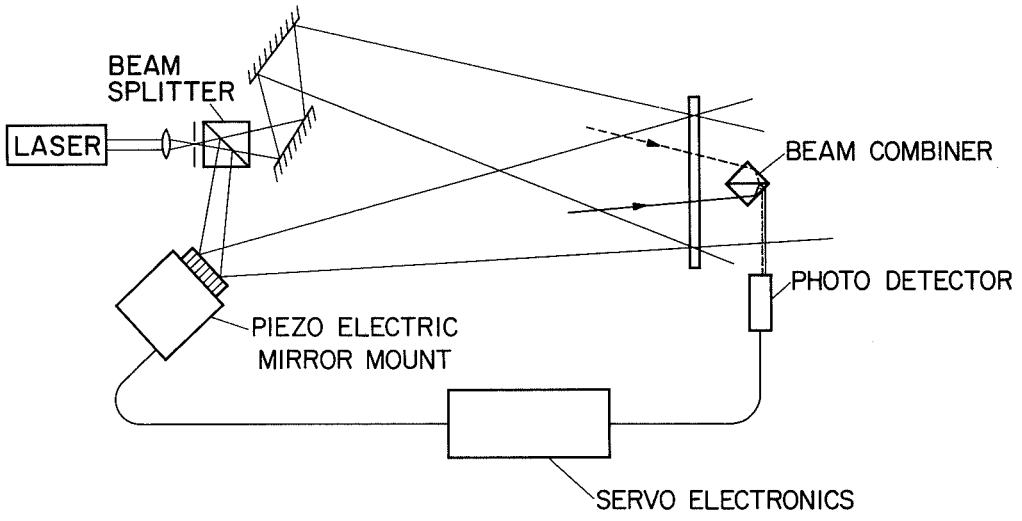

Figure 17.3 Servosystem showing fringe monitor

because each beam is coherent with the other, a fringe pattern will be formed at the detector plane. The large fringe spacing at this location allows us to sample a small fraction of a fringe. Therefore, the output of the photodetector can be related to the position of the maxima and minima in the fringe pattern.

Because all the components used in the holography system are also used in the fringe monitoring interferometer, motion that affects the fringes forming the hologram will also affect the fringes being observed. Except for a single optical element, the beam combiner, the converse is also true. Therefore, if this component can be fixed in place, stabilization of the fringe pattern being monitored will ensure stabilization of the pattern forming the hologram.

FRINGE STABILIZATION

Fringe stabilization is accomplished by the use of a piezoelectric crystal in one leg of the holography system. Charge is placed on the crystal to change its length and hence the length of the beam reflecting from the face of the piezoelectric crystal.

The electronics package is designed to affect the crystal in a manner such that the active path of the interferometer will change to match the path-length changes in the other (or passive) path. Still in its early stages of development, the servoelectronics subsystem (fig. 17.4) uses operational amplifiers. The

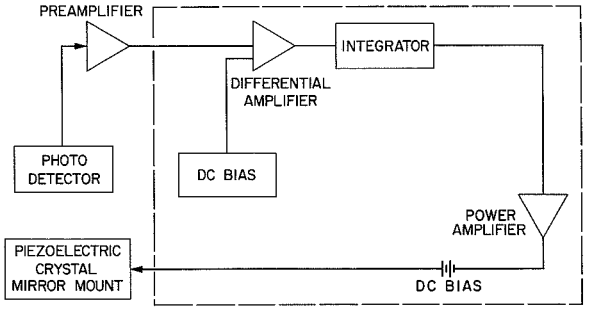

Figure 17.4 Servoelectronics diagram

input signal from the photodetector is amplified, and a bias signal equivalent to the average intensity of the fringes is subtracted from it in a differential amplifier. The output of this amplifier is inserted into an operational integrator, followed by a high-voltage operational amplifier, which drives the piezoelectric crystal. Motion of this crystal will change the relative path-length difference between the legs of the interferometer, and hence, the location of the fringes, thus closing the loop. Because of the nature of the interference pattern, the system will always be operating with negative feedback; therefore, the path change will be in a direction to drive the output of the differential amplifier to zero. The net effect is to stabilize the fringe pattern at the photodetector location.

The extent of stabilization depends on the nature of the motion to be compensated. Linear motion can be compensated equally across the whole field, while rotational motion is stabilized exactly only at the photodetector location. Positions away from this point are stabilized to a degree dependent on the distance from the stabilized point.

EXPERIMENTAL RESULTS

The amount of stabilization depends on the amplitude and frequency of the disturbing motion. With the system presently in use, stabilization at very low frequencies (less than 10Hz) to about 1/60 of a wavelength has been demonstrated for unwanted path-motion (noise) amplitudes greater than 1 wavelength. Figure 17.5 shows the results of a recent measurement of the system response. It shows that, using the 0.1-wavelength criterion for success, 1-λ noises can be stabilized with frequencies up to 200 Hz.

Motions greater than 4 wavelengths peak to peak can be successfully stabilized at frequencies up to 60 Hz. Figure 17.6 shows motion of a fringe pattern with a disturbance magnitude of 4.25 waves peak to peak. On the left side, the servoloop is not in operation. A hologram made with this magnitude of vibration would have only 0.0475 the efficiency of the static case. On the right side, the servoloop has been activated, and the system is stabilizing the fringes to 1/10 of a wave. The brightness of the hologram resulting from this motion will be 0.95 of the reconstruction brightness

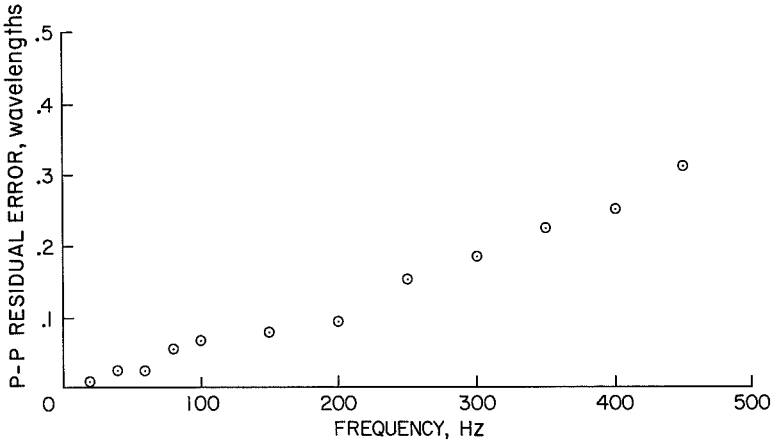

Figure 17.5 Compensation for 1-wavelength noise

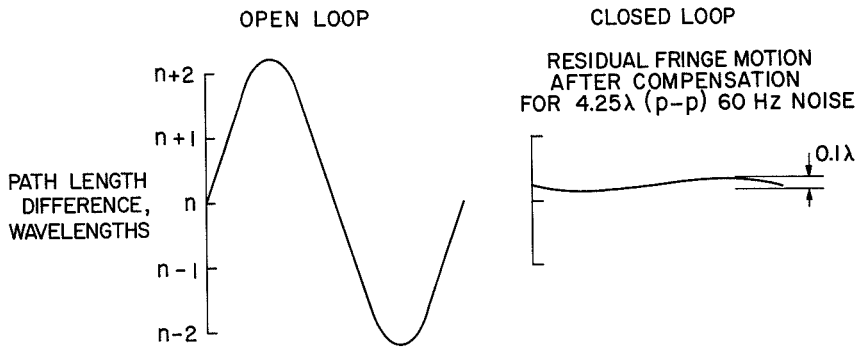

Figure 17.6 Control of large amplitude 60-Hz vibration

that a static fringe pattern would provide. Therefore, for this vibration input, the servosystem gives a 20-fold increase in brightness.

Of course, as the amplitude and frequency of the disturbance increase, the servoaction becomes less efficient. Figure 12.7 shows the effects of stabilization at 60 Hz and 250 Hz for different disturbance amplitudes. A linear relation is seen, as expected. In its present form, the system cannot continuously stabilize for excursions larger than about 6 wavelengths, but it is hoped that modifications to the present design will remove all limitations on the maximum excursion that can be stabilized.

CONCLUSIONS

The results shown here indicate that active fringe stabilization is a useful complement to vibration-isolation systems when attempting to improve holographic systems employing CW lasers. The vibration-isolation technique works best at high frequencies, while the servotechnique is most effective at low frequencies. Changes made to the system described here will improve its performance, and I feel that servo-stabilized holography using a low-power gas laser must be seriously

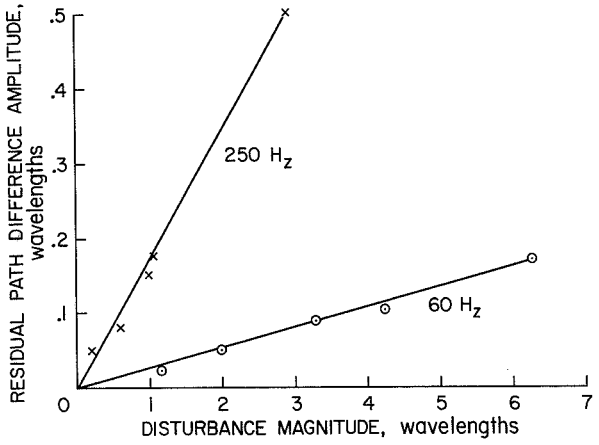

Figure 17.7 The effect of noise amplitude on servoaction

considered as an economical alternative to pulsed laser holography when attempting to apply holographic techniques under difficult ambient conditions.

REFERENCES

1. Fohr, R.: Coherent Radiation Laboratories Newsletter dated 12/31/69.
2. Friesem, A. A.; Kozma, A.; and Adams, G. G.: Recording Parameters of Spatially Modulated Coherent Wavefronts. Appl. Opt., vol. 6, 1967, p. 851.
3. Powell, R. L.; and Stetson, K. A.: Interferometric Vibration Analysis by Wavefront Reconstruction. J. Opt. Soc. Am., vol. 55, 1965, p. 1593.

18 FLASH HOLOGRAPHY APPLIED TO FLUID HEAT-TRANSFER PHENOMENA

Charles G. Miller and James B. Stephens
Jet Propulsion Laboratory

JPL is conducting a program of studies concerning fluid heat transfer at the anode of a high power xenon compact-arc lamp. Flash holograms of the hot-gas paths around the outside surface of the anode indicate the particular anode shapes that give turbulent or laminar flow when used in developmental arc lamps at JPL.

Another aspect is the nucleate boiling of the water-cooling medium in the inner surface of the anodes. Flash holograms will be made of the inside of an anode surface to study the development of nucleate boiling processes in relation to surface material and condition.

A program of studies is under way at JPL in connection with the environmental testing of spacecraft and testing of major spacecraft systems concerning two areas: fluid flow phenomena, and surface deformation due to imposed stresses.

Among the fluid flow interests are fluid heat-transfer phenomena, which deal with convective gas paths and surface turbulence in a flowing gas; bubble formation in incipient nucleate boiling at water-cooled surfaces, where cooling is by liquid-to-gas phase change; and the design of a suitable expansion throat for a high-power pulsed CW CO_2 laser. Surface deformation studies of interest involve measurements of physical displacements of a surface due to metal creep and detailed examination of surface deformation as gas is sorbed and diffused into a cryogenic pumping surface. All of these problems are capable of being studied by means of double-exposure holographic interferometry.

HEAT TRANSFER STUDIES

Our earliest application of flash holography has been to studies of fluid heat transfer in xenon compact-arc lamps. These are dc-arc lamps used as light sources for simulating solar heat loads on spacecraft. They are contained in quartz bulbs, in which the gas pressure is 180 psi and the lamp current of 450 amp is maintained by a potential difference of 45 V. For highest luminous output and brightness, the lamps are operated near the materials and structural physical limits, so it is necessary to cool them by fluid heat transfer. The fluids involved are the pressurized xenon gas, which transfers heat convectively, and water flow, which cools the interior of the cathode and anode of the lamp. Heat fluxes at the anode of an operating lamp are high, up to several times 10^7 Btu/hr-F-ft^2. Such high rates can be permitted only with knowledge of the mode of action of gasious conventive cooling and of liquid heat transfer inside the water-cooled elements of the lamp.

Figure 18.1 shows the lamp whose operation is under study. The holocamera has been partially disassembled for this picture. Figure 18.2 shows the anode of the lamp in more detail. The point under study is the nature of the convective flow of gas over the anode during operation, particularly the relationship of the shape of the tip of the anode to laminar or to turbulent flow and efficiency of heat transfer. A holographic interferogram of the area around the anode tip will disclose the fringe shifts in the gas layers adjacent to the anode surface that are clues to the nature of the gas flow. Figure 18.3 is a drawing of the complete holocamera in place; figures 18.4 and 18.5 are photographs of the camera in place.

The experimental difficulty is that we wish to see the gas-flow pattern during operation of the lamp in spite of the bright emission from the arc discharge. The problem of high background light interference is unique here because of the high luminance of the arc stream—a luminance equal to that of a black body at over 5000° K. This problem is being handled by the use of especially narrow-band interference filters, heavy Wratten filters for the wings of the spectrum, and the use of a large leaf shutter and a focal plane shutter in combination as a capping shutter. Figure 18.6 shows a representative holographic interferogram of the gas-flow pattern in an operating high current arc. The pointed cathode and the rounded anode show no signs of turbulent flow under the operating conditions.

In order to study the cooling processes on the inside of the anode and cathode structures, we intend to make flash holograms of the development of nucleate boiling on the anode surface. Since this cannot be done in the operating lamp, it will be necessary to simulate the incident heat load.

Besides the above studies, we are examining the potential of flash holography for the visualization of other types of plasma flow to get a better understanding of them. For example, another plasma-flow problem to which this technique is applicable is the study of coaxial free streams of gases in which only the inner stream is active in the arc process. Examination of the boundary between these streams might give some insight into the process of heat transfer across the boundary and therefore shed light into the usefulness of cooling gases. Such streams are presently being studied by simulating the process using coaxial streams of acetylene and oxygen and examining the turbulence apparent at the burning interface. The usefulness of such simulations is limited, however, by the relatively low temperature of the oxyacetylene flame, and flash holography is expected to enable a better interpretation of the actual gas-flow conditions.

OTHER FLUID FLOW STUDIES

Flash holography appears to have application to other areas of fluid dynamics. We are studying the possibility of its use in examination of the expansion throat of a CO_2 gas-dynamic laser, flow visualization of hypersonic free-flight ballistic models, and studies of nonthermionic cathodes such as that in an ignitron. In this latter case, the high brightness and random motion of the cathode spot in a pool of mercury have hampered investigation of the processes involved. The techniques perfected for looking at high-luminance xenon arcs should be applicable here.

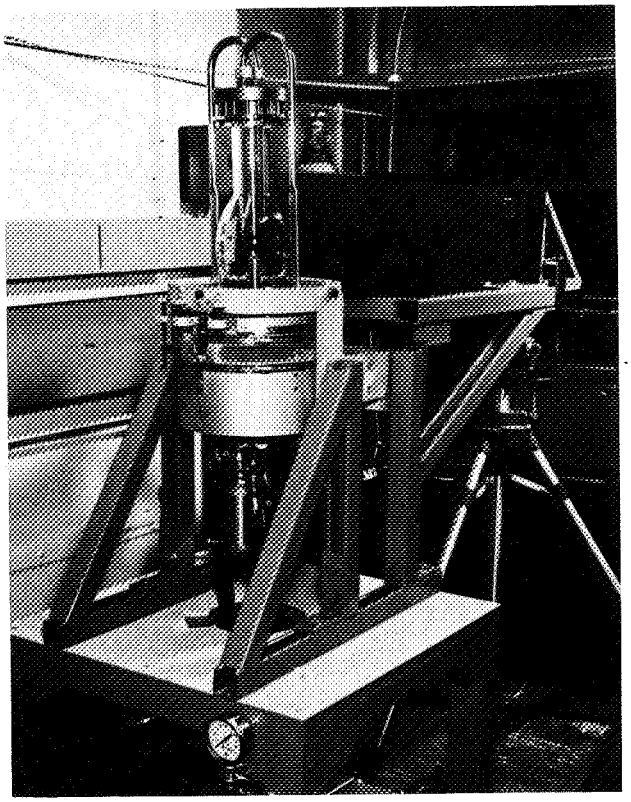

Figure 18.1 Compact-arc lamp and holocamera

Figure 18.2 Compact-arc lamp showing electrode arrangement

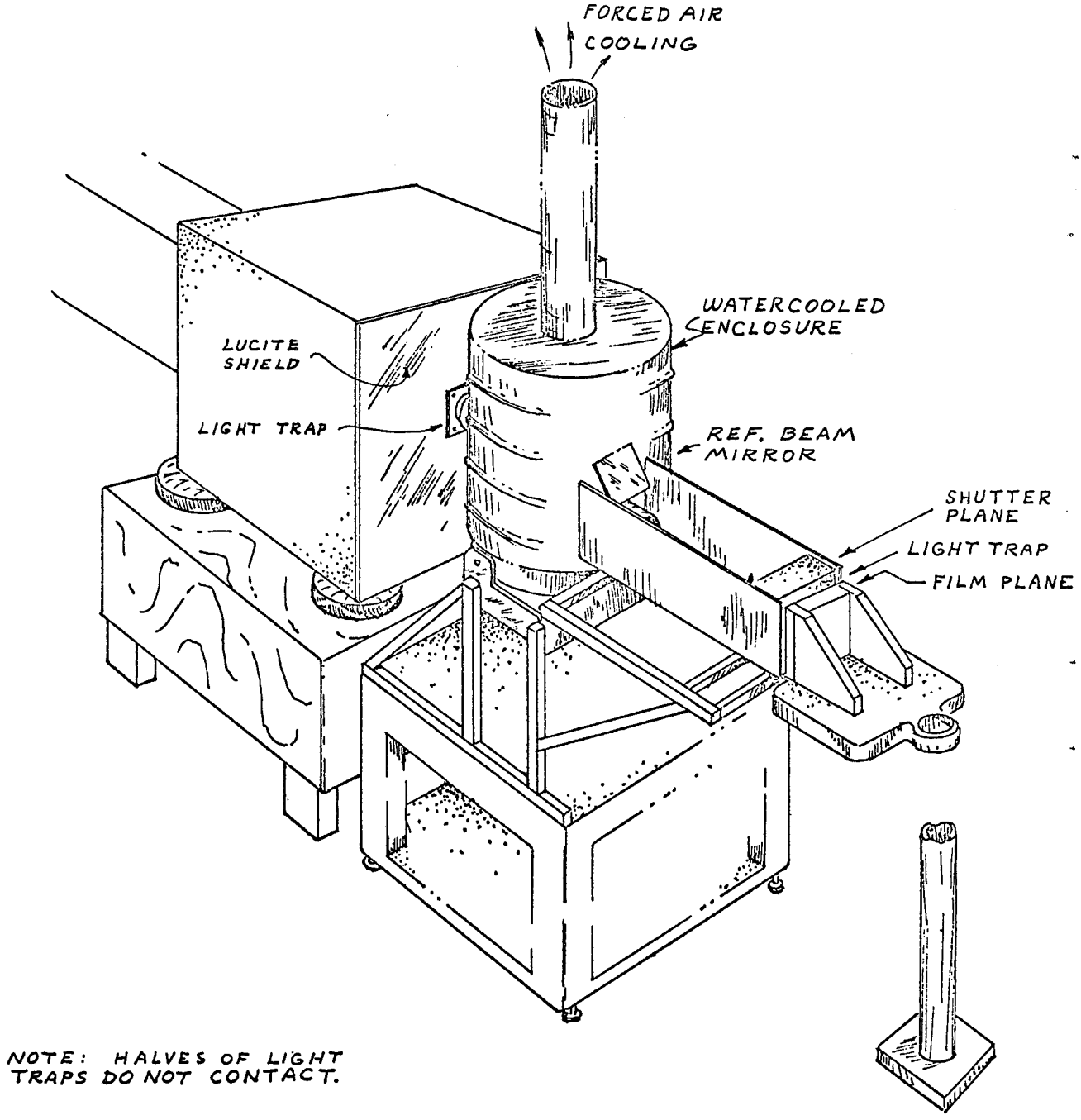

Figure 18.3 Holocamera arrangement

Figure 18.4 Lamp with protective enclosure in place

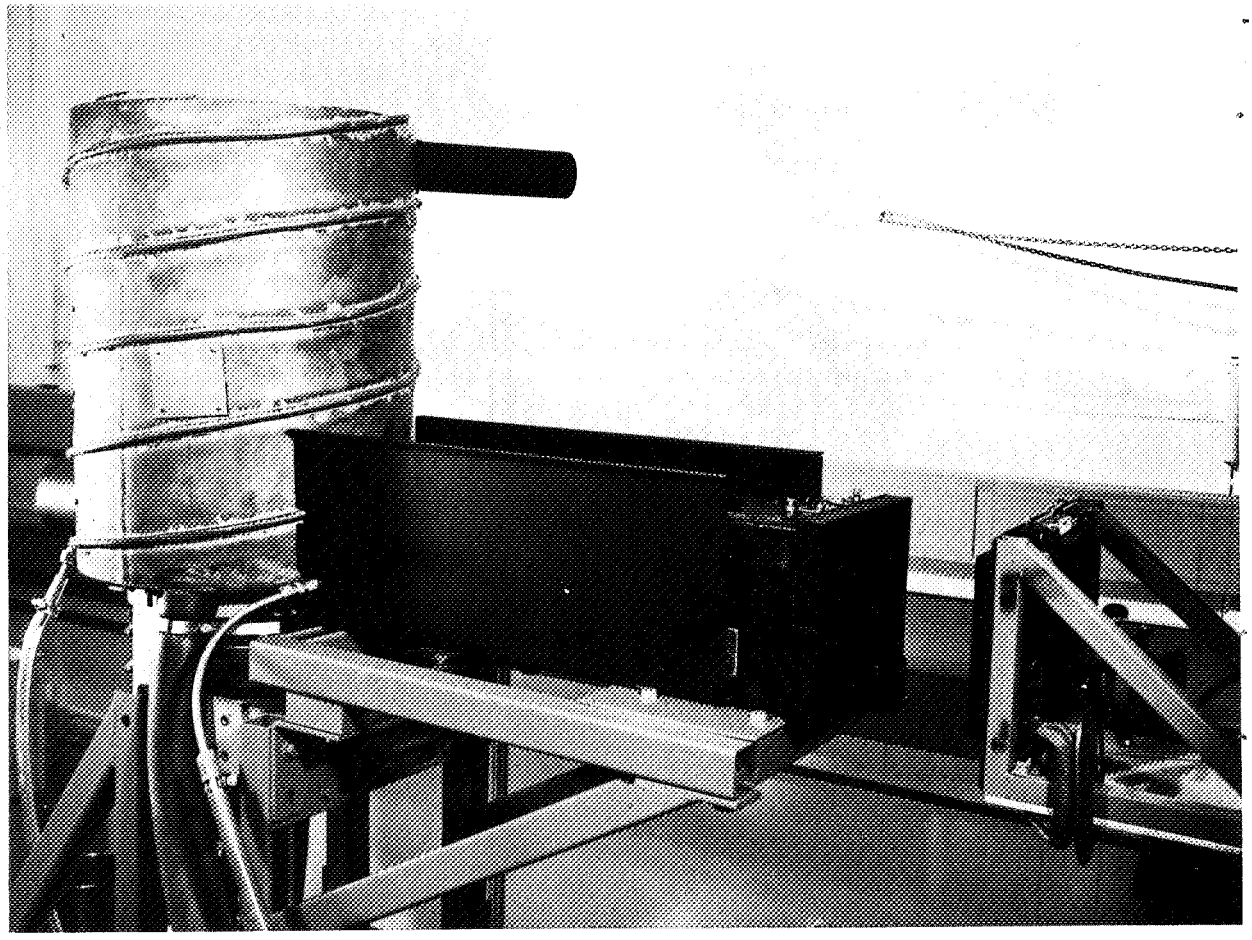

Figure 18.5 Isolated filmholder and capping shutter

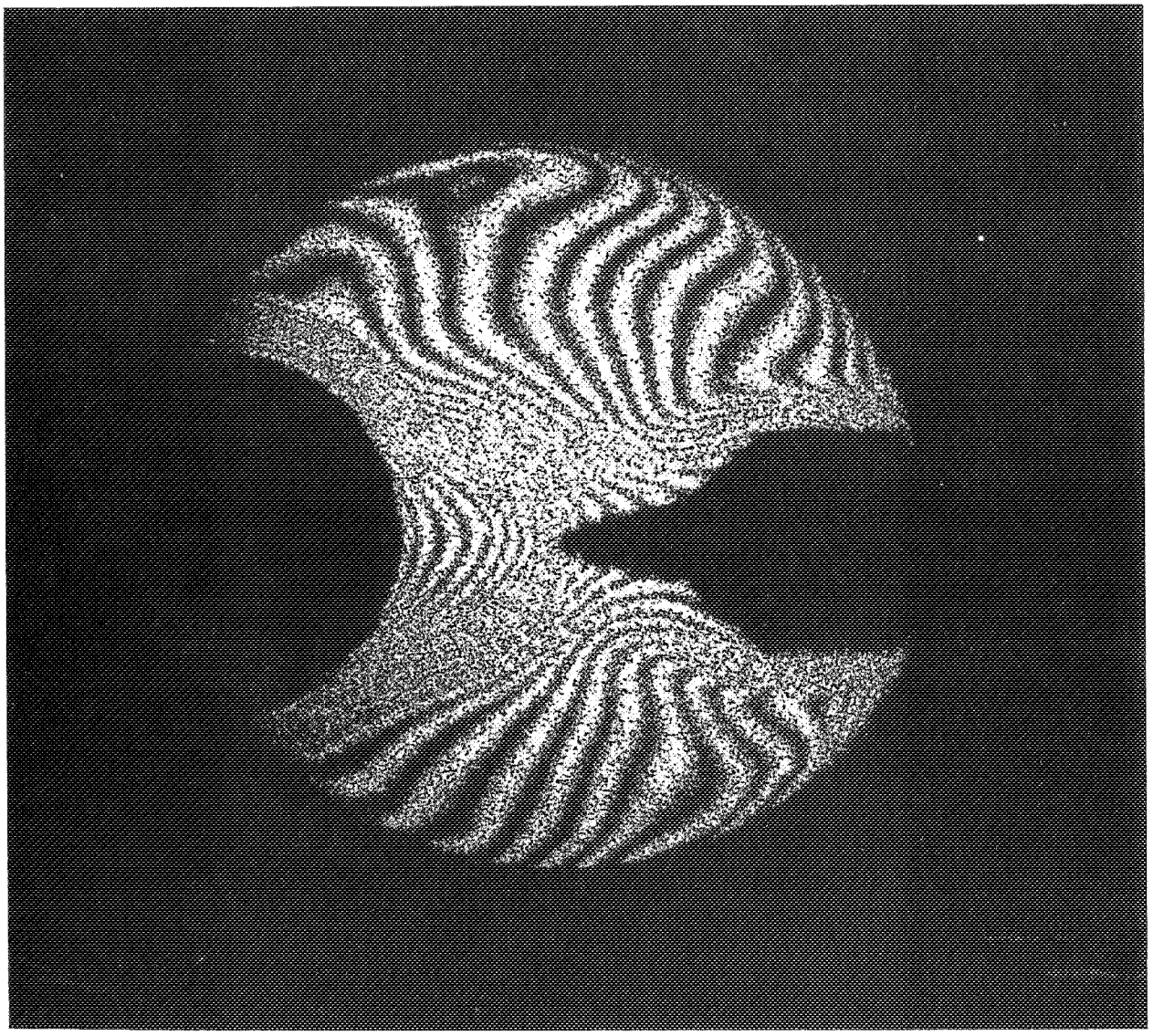

Figure 18.6 Representative holographic interferogram reconstruction of arc during operation

CRYOGENIC STUDIES

Interests other than those concerning fluid flow are being pursued in our laboratory. Other applications of flash holography under study include the physical sag of a vertical face of solid metal and the detailed mode of action of the cryopumping process. Mr. A. H. Wilson of JPL is interested in the application of holography to the study of metals collected on a cryogenic surface. Of particular interest are the type II metals such as mercury, tin, or bismuth, which are candidates for tests of ion engines for space use. In free space, these ions are discharged from the spacecraft and have no further interaction. In laboratory tests, however, such ions must be captured on cryogenic walls and frozen into massive metal. If the metal sheets sag due to creep, measurements might be affected, so the laboratory experimenter must be prepared to accommodate such action. The holographic tests would determine the degree of creep.

The cryopumping of gases is being studied in connection with a similar problem. The pumps in the vacuum chambers used to simulate the space environment must maintain a vacuum in the 10^{-11}-Torr range, even while gas is being discharged into the volume from small rockets (hot gas) or compressed gas storage (cold gas). The aspect of the cryopumping action being studied is the surface change as a titanium- or CO_2-covered surface absorbs gas. To be useful, the titanium or other absorbing material must absorb the incident gas into its interior. The relative contributions of bulk diffusion, compared to diffusion along channels and microcracks, can be studied by holographic interferometry and provide useful design information on cryopumping surfaces.

19 A HOLOGRAPHIC FLOW VISUALIZATION SYSTEM

Richard M. Brown
Ames Research Center

There have been many attempts to apply holographic interferometry to the examination of fluid flow fields. To investigate the application of holography to airflow studies of particular interest to Ames Research Center, a system is being built that can be used to make holograms in an extremely noisy wind tunnel environment. Details and features of the system are examined; for example, the advantages and disadvantages of diffusers are discussed. A variable ratio beamsplitter is described that makes efficient use of the laser light.

The use of holographic interferometry as a practical technique began when a group at TRW Systems accidentally[1] produced a double-exposure hologram while attempting to holograph a .22-caliber bullet. Their pulsed ruby laser fired twice, once when the projectile was in the field of view and once when it was not. The holographic reconstruction showed a pattern of fringes surrounding the slug that proved to be an interferometric map of the flow pattern. This experiment started a deluge of work in interferometry. The fact remains, however, that flow visualization must be considered the classic use of double-exposure holographic interferometry.

After the TRW Systems group had published (ref. 1), our interest grew in holographic interferometry for flow visualization at Ames Research Center. The earlier work of Horman (ref. 2) had suggested that holographic flow visualization had possibilities, but the technique he proposed appeared to have some serious difficulties in practice. The double-exposure holographic form of interferometry seemed to solve most of the practical problems, so a second look was in order.

Early experiments at Ames Research Center using CW lasers to examine the flow patterns of small free jets and supersonic nozzles were described in a previous paper reviewing the holographic activities of Ames (ref. 3). Double-exposure holograms, with exposures on the order of 0.5 sec, were made under laboratory conditions. The reconstructions of these holograms are shown in figures 19.1 and 19.2. The holographically determined pressure ratios in the throat of the nozzle in figure 19.2 matched the theoretical values very closely, providing strong encouragement to the hypothesis that CW flow field holography was feasible. Therefore, an instrument system was designed to work reliably in a full-size wind tunnel and produce useful data concerning aerodynamic flow.

TUNNEL CONDITIONS

The only readily available and convenient tunnel at Ames with the proper flow regime is a small blowdown tunnel, which is a part of the Unitary facilities. The tunnel works at a reasonably

[1] R. F. Wuerker, private communication.

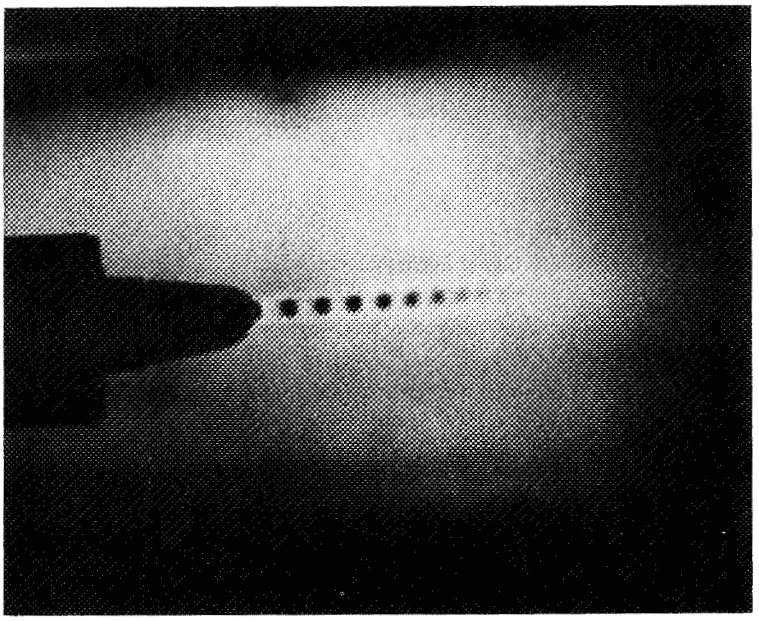

Figure 19.1 Double-exposure holographic interferogram of airflow from a free jet

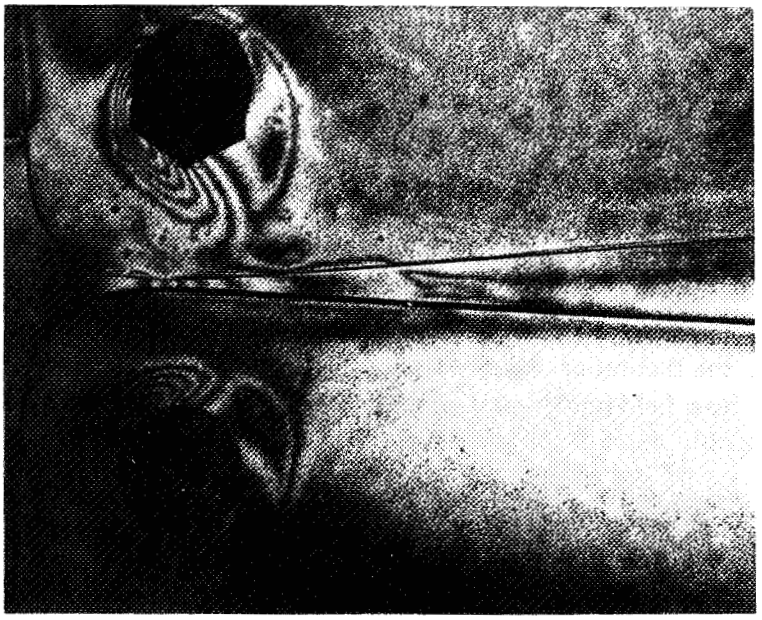

Figure 19.2 Interferogram of airflow in a supersonic nozzle

high density, with Mach numbers from 2.5 to 4 and atmospheric exhaust. The test area cross section is 8 in. square. This size is convenient for two reasons. First, it is small enough that the optical path length change due to shocks and other flow details is a convenient number of fringes in depth, thus facilitating fringe interpretation. Second, tunnel size and available room make design of the mechanical structure for the holographic optics convenient. The main disadvantage with this tunnel is its very severe vibration environment—both structure-borne and acoustic—which will provide a stringent test of the concept of CW holographic instrumentation in wind tunnels.

OPTICAL SYSTEM FOR FLOW FIELD HOLOGRAPHY

The basic optical system for holographic flow visualization is shown in figure 19.3. The system has two features not generally found in holography systems. The first, a servocontrol system, described in Section 1, is used to stabilize the holographic fringe pattern. The second innovation is the use of a variable ratio beam splitter that is highly efficient in its use of light. This device, a combination of a Rochon prism and a half-wave plate, can be used to provide beam intensity ratios from about 10^{-4} to 10^{4} using the normal output light from a helium-neon laser.

After being split into the signal and reference beams, the light is passed through the test section. The signal beam passes through a Porro prism for spatial matching and then through a polarization rotator, which changes the polarization of the signal beam light to the same plane as that of the reference beam. A standard telescope arrangement is used to enlarge the beam diameter to about 13 cm. This beam then passes through the test section and, after being refocused, impinges on the hologram plane.

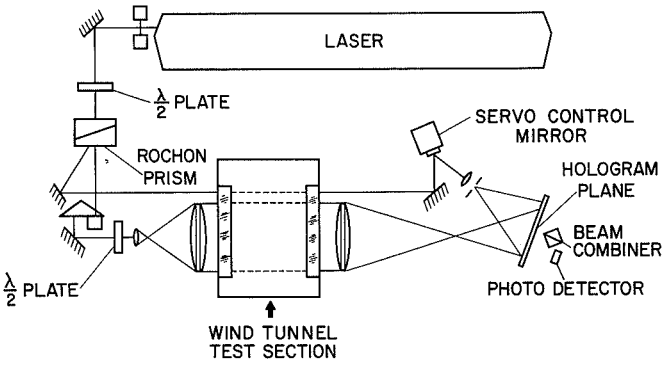

Figure 19.3 Optical schematic of holographic flow visualization system

At the same time, the other beam is passed through the test section above the airflow disturbances. After reflection from a piezoelectric servocontrol mirror, it passes through a spatial filter and becomes the reference beam. Because of the particular nature of the beam combiner used for fringe stabilization, it is important that the distance to the beam combiner from the focal points of both the signal and reference beam be approximately equal. The use of the beam combiner and piezoelectric mirror for fringe stabilization was described in Section 17.

MECHANICAL STRUCTURE

Because of the severe vibration environment to be encountered, special attention was given to the design of the mechanical support structure. The main structure fits over the top of the tunnel in a "U" or "C"-like shape as shown in figure 19.4. It has the appearance of a bridge in that the structure is made of 2-in. box beams, with much cross-bracing. The triangular cross section of the structure increases stiffness and stability in the horizontal plane. The bridgework elements are kept short to keep their resonant frequency high and there are no large panels, which would act as drum heads and resonate under acoustic loadings. The basic consideration has been to design a structure

with maximum stiffness and stability, and the smallest possible interaction with the acoustic and structure-borne vibration that would tend to destroy the holograms being made. Isolation from the vibration environment is accomplished by a spring-mass support system; the open structure limits the cross section for acoustic excitation; and the stiffness of the members keeps motion at levels that the servocontrol system can compensate. The optical supports have a low profile in that their centerline is only 2 in. above the optical bench. This avoids the cantilevered arrangement, which tends to introduce mechanical vibration.

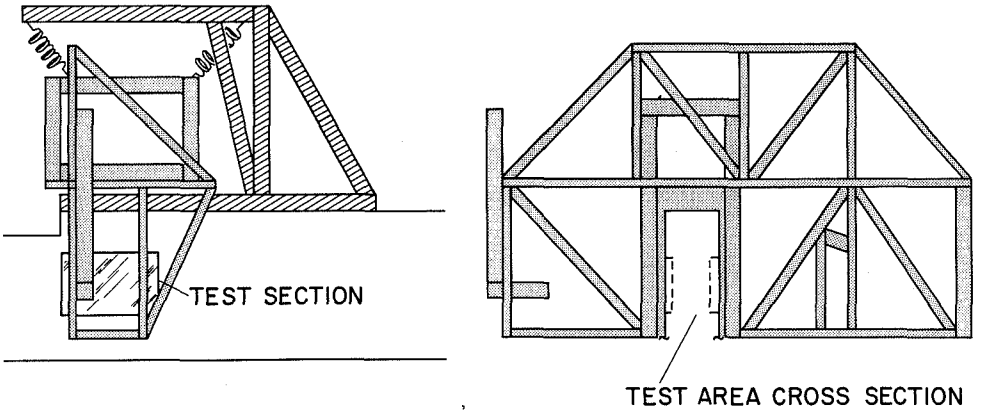

Figure 19.4 Support structure for holographic flow visualization system

VARIABLE RATIO BEAMSPLITTER

Because this system is designed to be used with a low-power gas laser, and because of the problem of vibration, every effort must be made to conserve the available light and thus provide the shortest possible exposure time. The experimental nature of the equipment dictates a variety of beam-intensity ratios, and due to the stringency of the energy conservation requirement, the use of attenuators was considered to be ill-advised. Therefore, a birefringent device, which has very low attenuation and a continuous range of available beam ratios, has been incorporated into the design. As mentioned above, it consists of a combination of a half-wave plate and a Rochon prism. The linearly polarized light emitted by the laser is separated into orthogonally polarized components by the Rochon prism (fig. 19.5). Rotation of the half-wave plate about the optical axis rotates the plane of polarization of the light incident to the prism. Since the horizontally polarized component of the light wave amplitude is passed straight through the prism, while the vertical

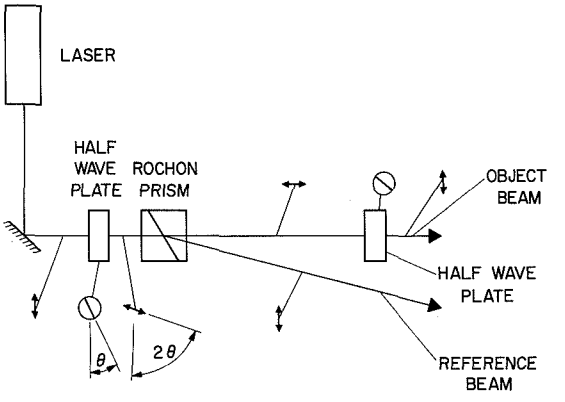

Figure 19.5 Variable ratio beam splitter

component is refracted downward, the position of the half-wave plate can be used to control the amount of light entering either beam. Except for the small amount of light lost through surface reflections, all the light enters one or the other beam. This accounts for the high total transmittance of the birefringent beamsplitter.

Although the beam-intensity ratio is now controllable, and the beams can be independently manipulated, one more element is necessary when using this device for making holograms. As shown in figure 19.5, the subject and reference beams are orthogonally polarized, while beams of the same polarization are required to obtain the interference effects necessary for holography. This is provided by the introduction of a polarization rotator, a half-wave plate with axis at 45° to the plane of the incident light, which turns the plane of polarization of the light by 90°.

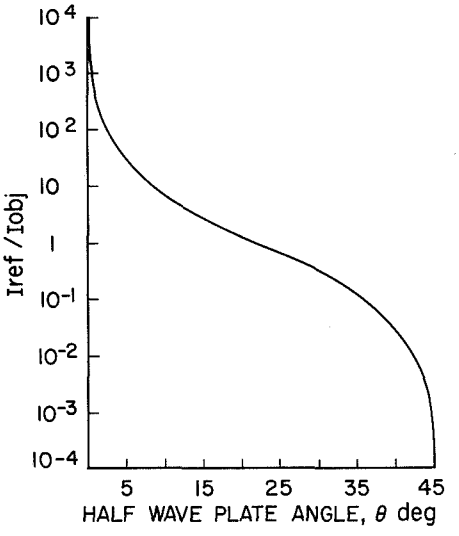

Figure 19.6 Range of beam ratios available

Figure 19.6 shows the results obtainable with this beamsplitter arrangement. Rotation of the light control half-wave plate by 45° provides a beam ratio range extending almost eight orders of magnitude. The predictions shown here have been confirmed experimentally. An interesting point is that although no external polarizer was used to ensure that the incoming light from the laser was truly polarized, measured beam ratio ranges extended from over 5×10^3 to less than 2×10^{-4}.

SYSTEM CONFIGURATIONS

While a wide range of beam ratios generally is not needed in a holography system, it is convenient in this case because of the variety of system configurations desired, and because of the light problem. For example, in some cases it will be desirable to use a ground-glass diffuser in the signal beam. In this case, most of the light should be in the signal beam to compensate for the large light losses introduced by this scatter. On the other hand, there will be times when no diffuser is used, and most of the light should then go into the reference beam. Figure 19.7 shows how the system would look with no diffusers in the path. There are several advantages to this type of operation. First, the hologram itself resembles a shadowgraph, so that one can look directly at the hologram and see the model and some flow details without need for reconstruction. This is often convenient. A second advantage is that the reconstructed real image can be used for schlieren work, although the generally poor optical properties of the emulsion and glass substrate cause some real problems here. The third advantage is that the light economics of this system are much better than in any system using diffusers, since no light is being thrown away. This means that the exposure time is shortest, and problems of flow instability during exposure are minimized. This arrangement, however, also has some shortcomings. For example, it is quite difficult to view the reconstructed image. An auxiliary optical system with an aperture of 3- or 4-in. diameter is required to see the whole

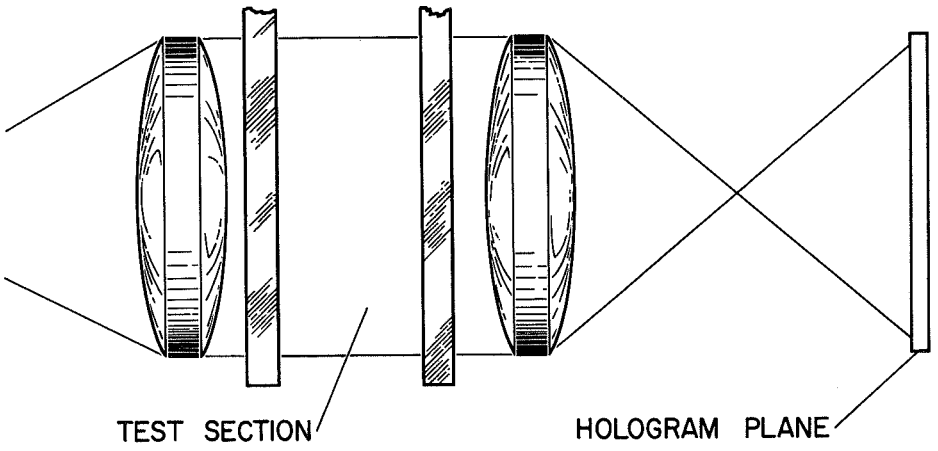

Figure 19.7 Flow visualization with a clear beam

field. A second problem is that the viewing direction is restricted to the original beam direction, thus precluding parallax viewing and the determination of the three-dimensional properties of the flow.

The standard way of avoiding these problems is to use a diffuser in the signal beam, as shown in figure 19.8. Use of a prediffuser lying beyond the test area as seen from the hologram avoids the two main objections to the clear-beam operation. The entire test section may be observed with the bare eye, and various viewing directions, with resulting parallax, are available. With this arrangement, however, all flow visualization must be via interferometry. If the test model is not axisymmetric, the interference lines may not be located in the same plane as the model, thus making the field hard to photograph.

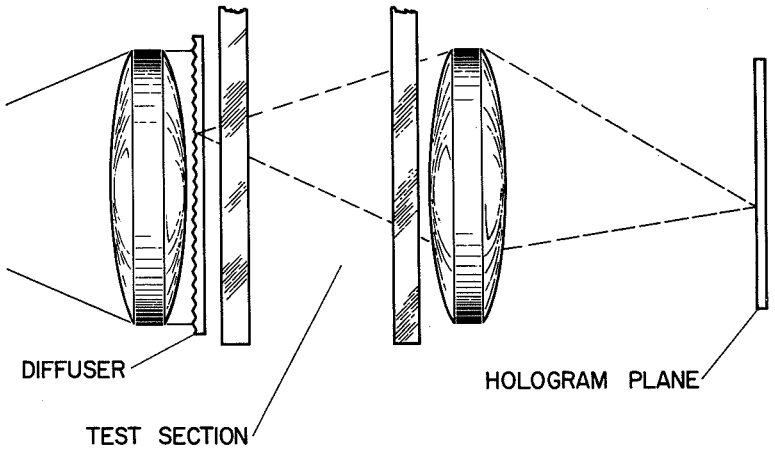

Figure 19.8 Flow visualization with a prediffuser

To avoid this problem we can use the postdiffuser arrangement shown in figure 19.9. In this case, the ground glass is interposed between the tunnel and the hologram plane. No view of the test section is now possible, but a shadow of the test area, including a shadowgram of the flow, can be seen on the ground glass. Interferometry may also be used, and the fringes are located on the plane of the model shadow. Because the light passes undiffused through the tunnel, no parallax is possible, and the quality of the tunnel windows must be at least of shadowgraph quality.

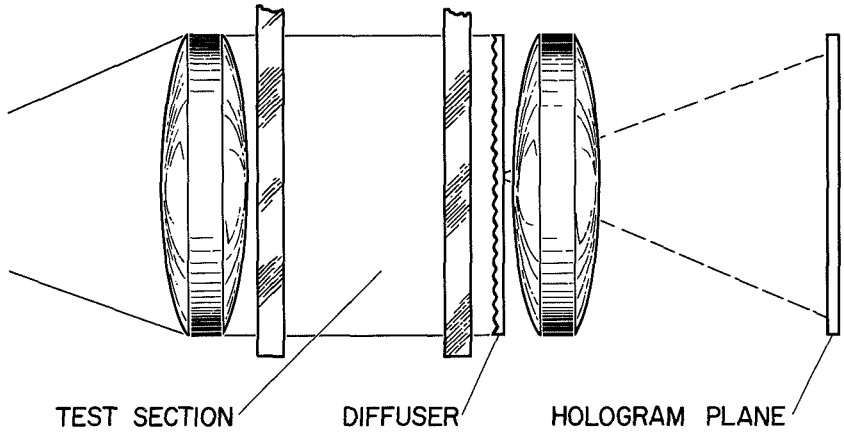

Figure 19.9 Flow visualization with a postdiffuser

In studying the flow fields around supersonic models, any or all of the above techniques may be required. The device described here can accomplish all of these, with minor modifications, and is expected to be a good first step toward a useful, reasonably inexpensive, flow visualization system.

REFERENCES

1. Heflinger, L. O.; Wuerker, R. F.; and Brooks, R. E.: Holographic Interferometry. J. Appl. Phys., vol. 37, 1966, p. 642.
2. Horman, M. H.: An Application of Wavefront Reconstruction to Interferometry. Appl. Opt., vol. 4, 1965, p. 333.

20 INTERIM TESTS ON A HOLOGRAPHIC TECHNIQUE FOR PHOTOGRAPHING HIGH-SPEED MIL-SIZE PARTICLES

Don M. Robinson
Langley Research Center

A Pockel-cell Q-switched ruby laser was used to obtain single-beam, far-field holograms of 100- to 200-μ-diameter particles, which were accelerated to a velocity of approximately 2.5 km/sec. Both collimated and diverging illumination of the particles was used; however, due to the physical constraints of the test apparatus, the best results were obtained by forming the holograms at a magnification of 2. The reconstruction of the far-field holograms was accomplished with a helium-neon laser and a television camera/monitor type readout. This type of reconstruction enhances the signal-to-noise ratio of the process by the use of brightness and contrast control in the readout.

The use of small, high-speed particles to simulate micrometeoroid impact has been in progress for several years at Langley Research Center. Attempts to extend impact damage data to the mil-size (25 μ), hypervelocity (20 km/sec) range have encountered instrumentation problems in determining such parameters as particle velocity and integrity (size) prior to impact. Conventional techniques (such as light reflection from the particles or conventional type photography) for determining these parameters are inadequate because of unreliability or other limitations (for example, depth of field). One technique under investigation at Langley is the use of Fraunhofer or far-field holography to photograph these particles. Preliminary work on this technique for both static-particle distributions and low-velocity applications indicates feasibility from the standpoint of simplicity and reliability within the tolerances desired.

The experiment described in this paper represents the first attempt to apply this technique to a dynamic sizing problem at the Langley impact and projectile range. Tungsten and glass particles from 100 to 250 μ in diameter were accelerated by a 220-caliber rifle/sabot mechanism down an evacuated tube at a velocity of approximately 2.5 km/sec. Before target impact, the particles passed through a test chamber where a single-beam, far-field hologram was made of the projectiles with a Pockel-cell Q-switched ruby laser. The holograms were later reconstructed with a helium-neon laser from which the particle distribution in the test chamber was determined.

EXPERIMENTAL PROCEDURE

Synchronization

Even though the particle velocity used in this experiment was much less than the ultimate goal of 20 km/sec, a synchronization procedure was required to time the laser pulse properly relative to the particle's position. The technique used for this test is shown in figure 20.1. Signals from the two SGD-100 photodiodes indicate the particle's position at the start and just before entering the test chamber. These signals are fed into a system of scopes and preset time delays so that the Pockel

cell is triggered at the desired time. An example of the scope trace for this procedure is shown in figure 20.2. This trace indicates the particle position just before entering the test chamber (diaphragm), the laser pulse while particles are in the field of view, and the target impact downrange.

Optical Technique

The optical geometries used for single-beam Fraunhofer holography are generally either the collimating or magnifying type, depending primarily on the physical constraints of the experiment. A common method for recording the holograms at a known magnification is shown in figure 20.3. The particles or objects to be holographed are defocused a distance z from the focused position, which satisfies the far-field condition ($z > d^2/\lambda$, where d = mean particle diameter and λ is wavelength of illumination). The far-field diffraction pattern is then imaged on the photographic plate at a known magnification. Reconstruction of holograms taken with this geometry is obtained by using this geometry in reverse, as is shown in figure 20.4. If the same wavelength is used for both the recording and reconstruction, the system represented by figures 20.3 and 20.4 is symmetric (for minimizing aberrations in the process). Figure 20.5 shows a hologram and reconstruction of a calibration reticle having 100-μ divisions; figure 20.6 shows a distribution of opaque particles placed on a glass flat. The reticle spacing is 100 μ. The holograms and reconstructions shown in both figures 20.5 and 20.6 were made with a helium-neon laser.

The initial optical arrangement used for the test range experiment was somewhat different from that shown in figure 20.4. This system, shown in figure 20.7, used a collimated illumination scheme for both the recording and reconstruction. Such a geometry is simple to set up and gives good results, provided film resolution is not a factor and the film can be place sufficiently close to the objects being holographed. For very small particles, however, the physical constraints of the system may force the film plate to be placed at too great a distance from the particles to ensure that good fringe contrast is obtained on the hologram. This is especially important for lasers of limited spatial coherence. To date, we have obtained our best results by recording the holograms at a distance of from 1 to 3 far fields (1 far-field distance is d^2/λ). Such a figure has also been indicated in the literature. Hence, for the reasons outlined above, a magnifying geometry was used so that a defocusing of slightly more than 1 far-field distance would be achieved for the particles closest to the film in the test chamber and about 3 far fields for particles farthest from the film (hence, about a 2 far-field depth of field was used. This is approximately 5 cm for 100-μ-diameter particles). The setup is shown in figure 20.8. With this particular optical geometry, the holograms of particles in the test chamber were formed at a magnification of 2 with about a 5-cm field of view.

In order to determine what quality one might expect for a hologram formed through the test section with the Pockel-cell Q-switch ruby laser, a static distribution of particles placed on a calibration reticle was used as the object. The results of this (fig. 20.9) indicate both relatively poor spatial coherence and a high level of background noise in the system. This latter difficulty can be alleviated, however, by using a TV vidicon/monitor type readout of the reconstruction to suppress the background noise, as shown in figure 20.10. In all these examples, the holograms were recorded on Agfa-Gavaert 10E75 glass plate and reconstructed on Polaroid type 55PN using a helium-neon laser.

Dynamic Tests

The techniques just described were then applied to photograph the 2.5-km/sec particles (both tungsten and glass spheres). Results, however, were somewhat difficult to obtain due to several problems. Since the technique previously described made no velocity calculation for each shot (until after the event), any variation in the powder charge used to accelerate the sabot containing the particles produced an uncertainty in the velocity and, therefore, each shot became a "hit-or-miss" arrangement. Second, such a powder-gun type accelerating mechanism produces "dirty" shots, which create considerable background noise in the test chamber. This makes the hologram recording difficult and also can make interpretation of the reconstruction uncertain if the background level is too high. A further problem encountered in these tests is shown in figure 20.11. This example is a TV vidicon/monitor type reconstruction taken with a helium-neon laser of the particles as they passed through the test section. Results of this type were obtained on several other shots and indicated that the particles were grouping together to form a large fiberlike object. This could be due to either a natural tendency for the particles to "bunch" or some adhesive contaminant in the firing process (for example, the vacuum grease or cotton sabot-packing material used). Because of this grouping characteristic, sizing of individual particles was not possible. However, one alternative test was conducted that did produce a particle distribution from which sizing information could be obtained. In this case, the sabot struck an aluminum target at a velocity of 2.5km/sec. From the impact, a large volume of particle "spray" was produced which individual particle fragments could be identified. An example of the hologram and reconstruction obtained from this technique is shown in figure 20.12. Here, two individual particles were chosen on the hologram from the entire array recorded. These particles were sized at about 100-μ mean diameter.

CONCLUSIONS

The static and dynamic results of this experiment and previous particle sizing experiments indicate that sizing by the technique described can be performed to within the designed tolerances. Other related problems, however, necessitate further testing before this system can perform in the hypervelocity range. For example, there is always the problem of synchronizing the laser pulse to the particle velocity. At present, it appears that this difficulty can be solved through the use of suitable particle-detection stations and an automatic time-delay system; this remains to be confirmed through actual tests. However, one of the main problems involves the laser. In addition to having the laser operate as cleanly as possible to produce good holograms, there is also the requirement that the laser pulse fast enough to "stop" the particle's motion to a sufficient degree. A relatively clean laser pulse can be obtained by use of suitable mode-control procedures; however, the pulse-duration requirement remains somewhat in doubt. At present there are two ways of producing the ultrashort pulse requirement. First is a mode-locking technique, which has received considerable attention in the literature. This technique, however, is extremely difficult to reproduce reliably under lab conditions, much less in the environment in which these tests will eventually be made. For this reason, a second approach is under consideration that will produce pulses of a somewhat longer duration than the mode-locked case, but which is, hopefully, more reliable. This technique is the reverse-pumped Raman laser, which can generate pulses of about 0.3-nsec duration at high brightness. At this pulse duration, the particles should still be sufficiently "stopped" for adequate holograms to be obtained.

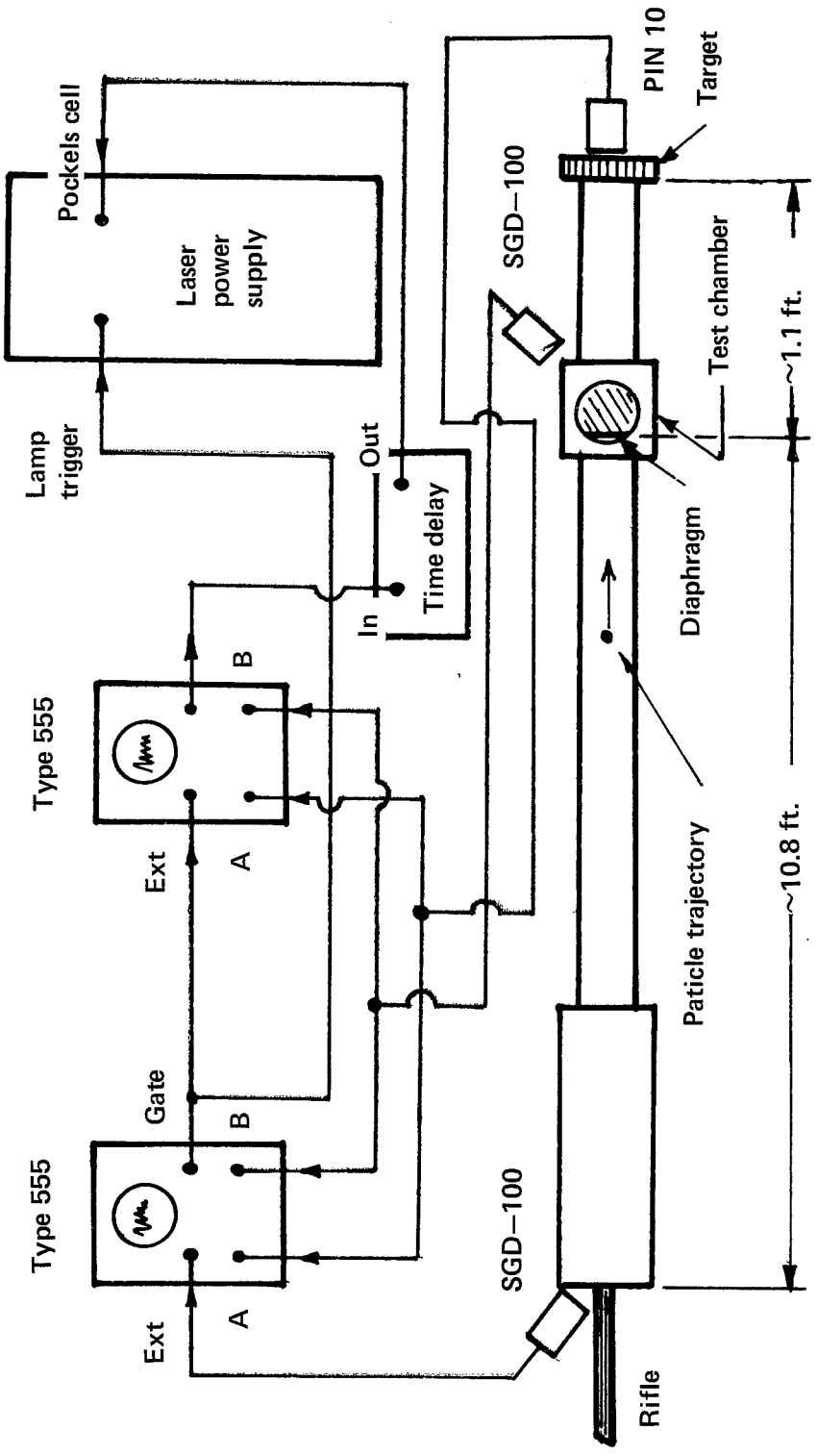

Figure 20.1 Diagram of technique used to synchronize particle position to laser pulse; maximum particle velocity is about 2.4 km/sec

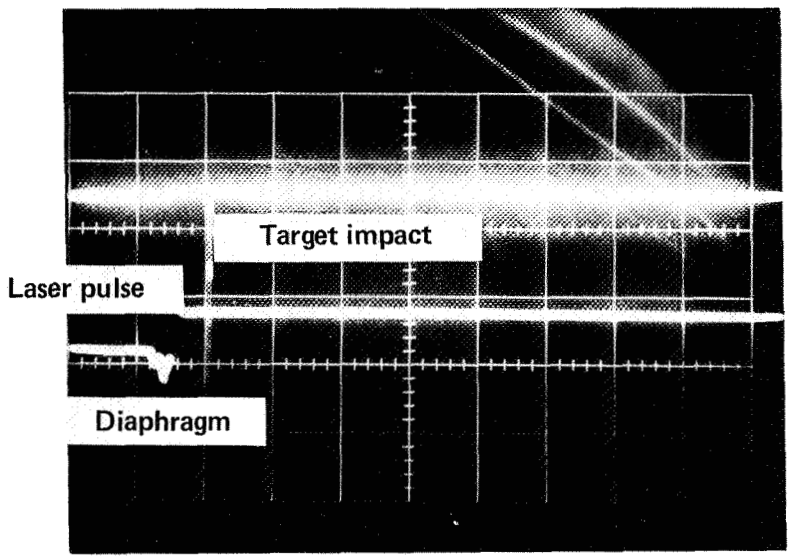

Figure 20.2 Scope trace showing the diaphragm penetration, laser pulse, and target impact; sweep speed on both traces is 20 μsec/cm

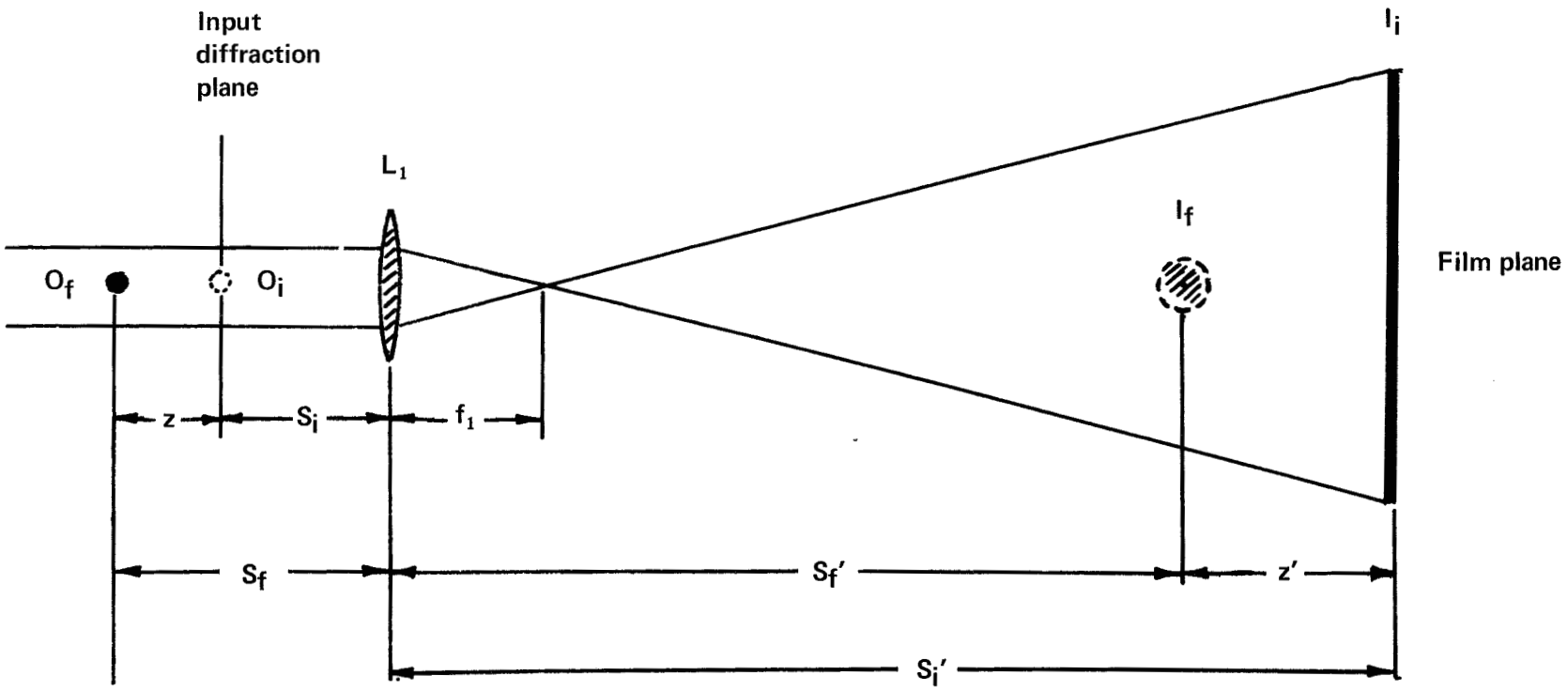

Figure 20.3 A technique for magnifying the interference pattern. Lens L_1 focuses object O_i in film plane at a magnification m; O_i is then defocused a distance z to position O_f producing image I_f; the interference pattern in the film plane is magnified m times

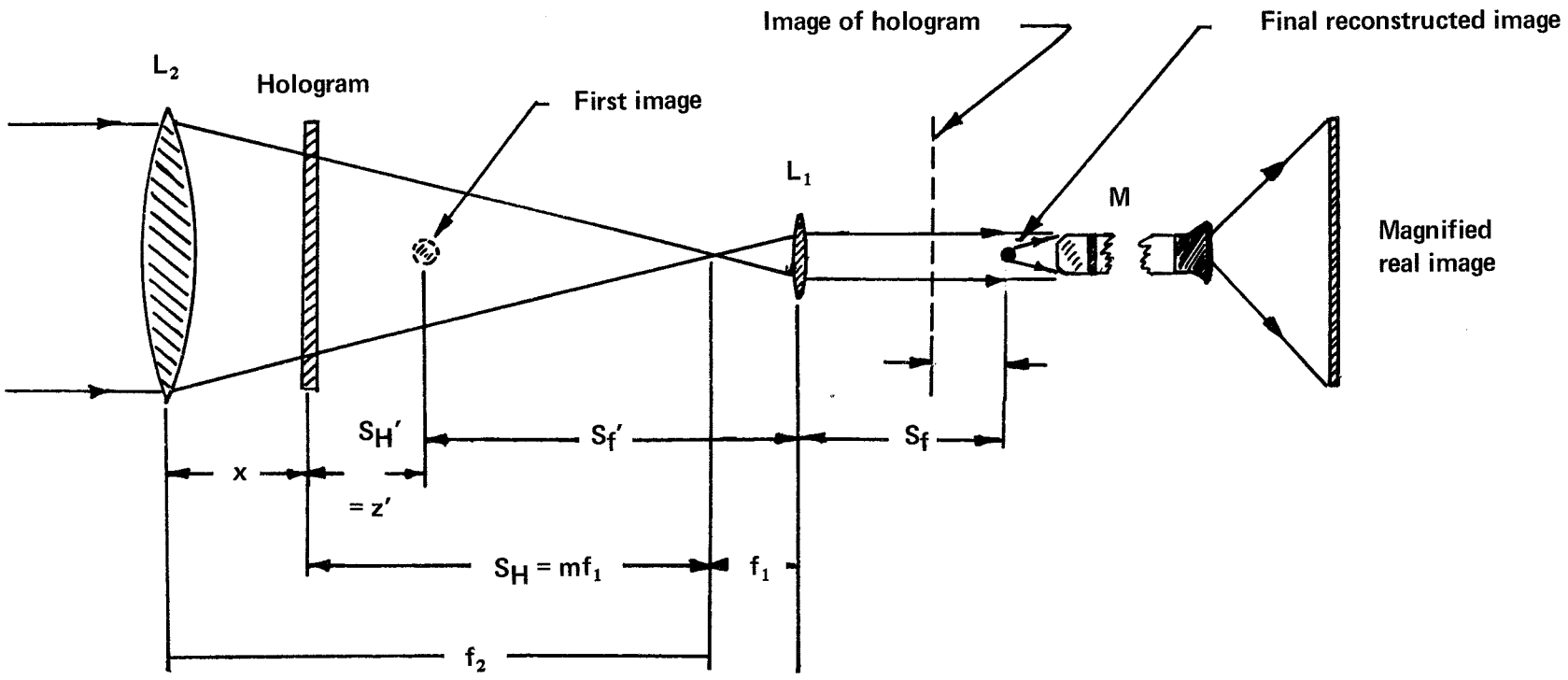

Figure 20.4 Reconstruction geometry using a reverse path. Lens L_1 is the same lens used in the formation; L_2 is a long focal length lens. The postions of the lenses and hologram result in an overall magnification of unity in the reconstruction; a magnified view of the real image is achieved by microscope M

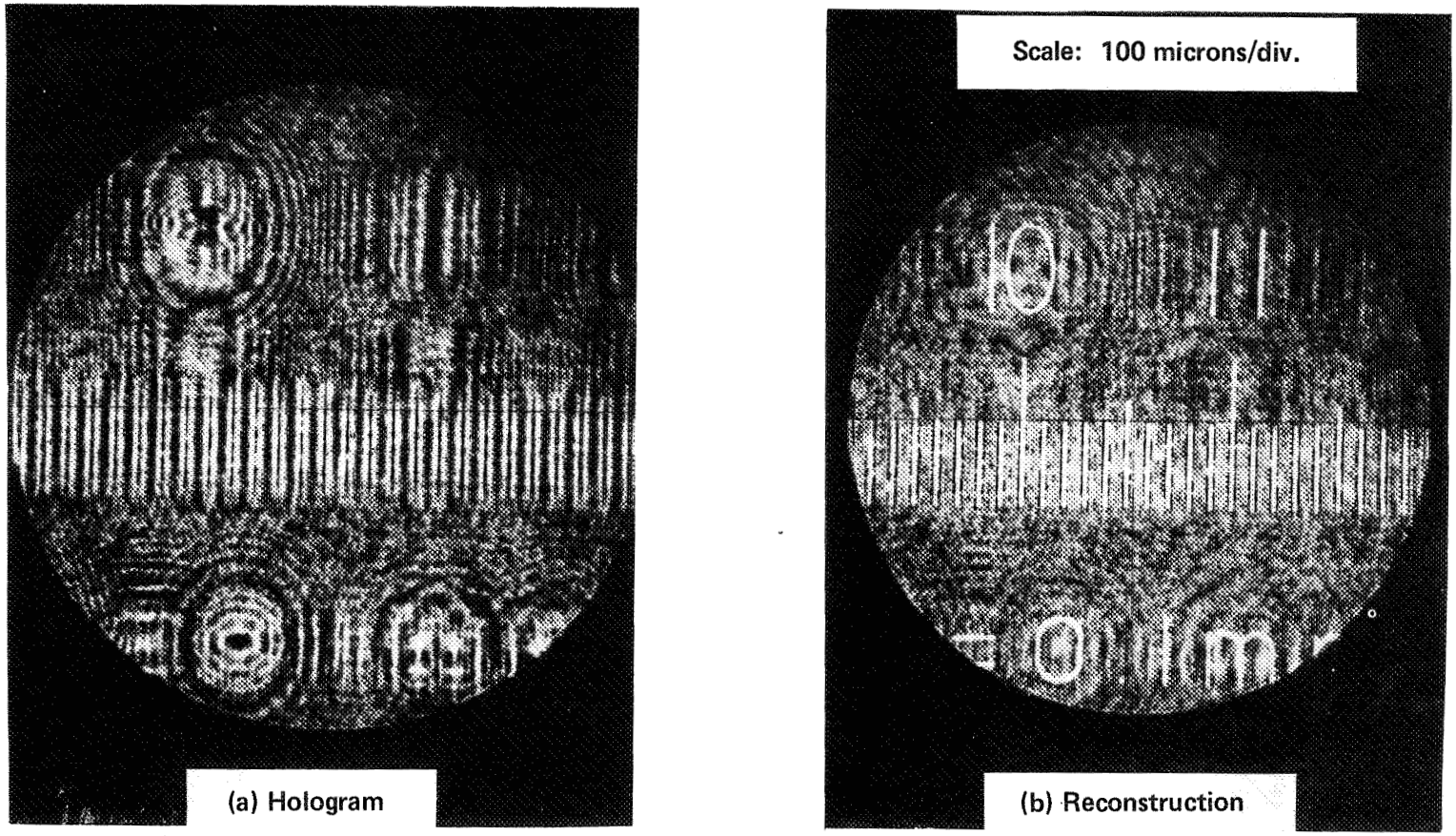

Figure 20.5 Same as in fig. 20.6, except that the defocused distance z = 2.0 cm and far-field condition is satisfied; magnification in the photograph is approximately 30X

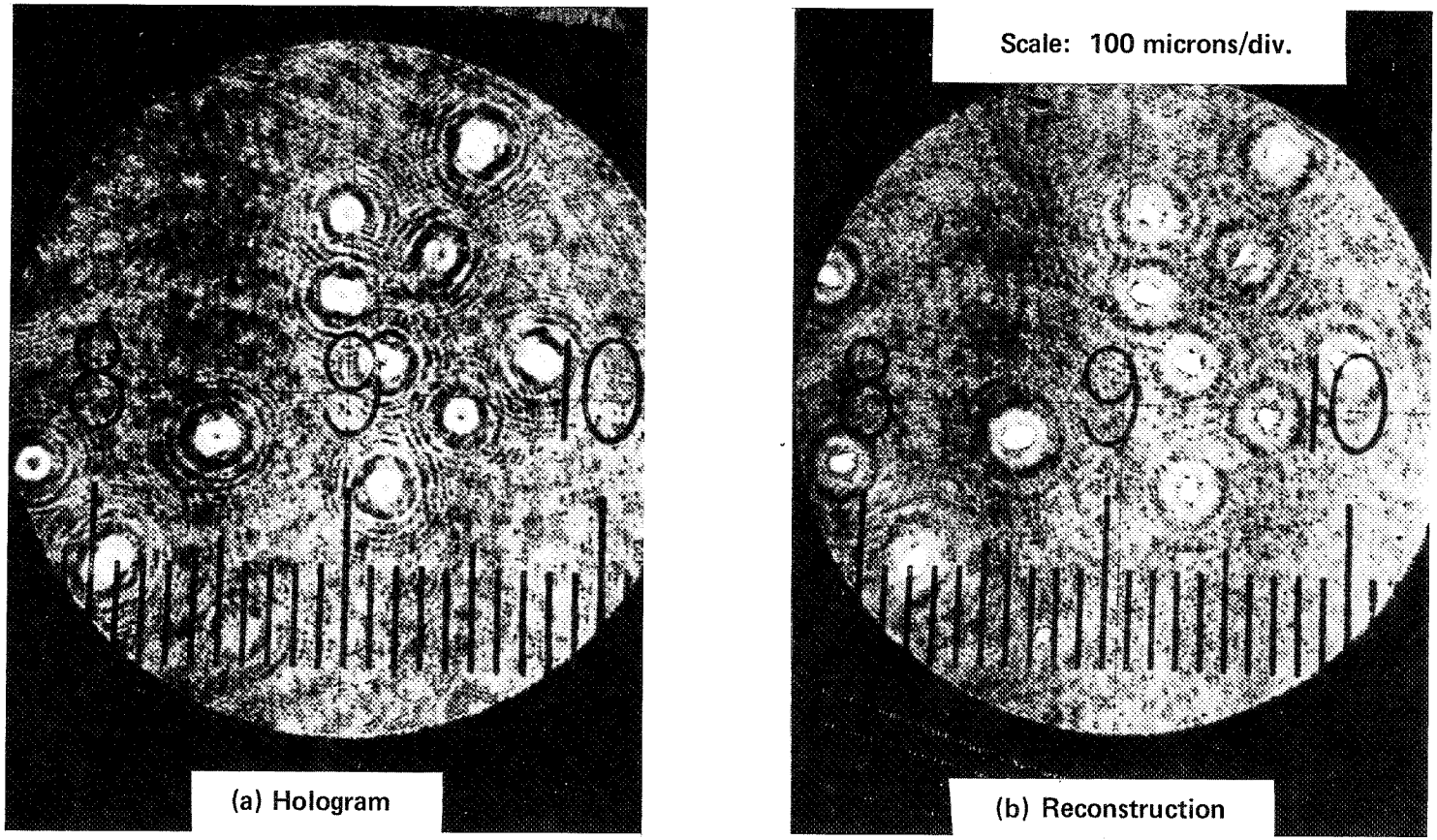

Figure 20.6 Hologram and reconstruction of 100- to 150-μ-diameter particles in a single plane; z is about 1.5 cm or 1 FFD; magnification is 33X (scale is superimposed on the photograph to indicate size)

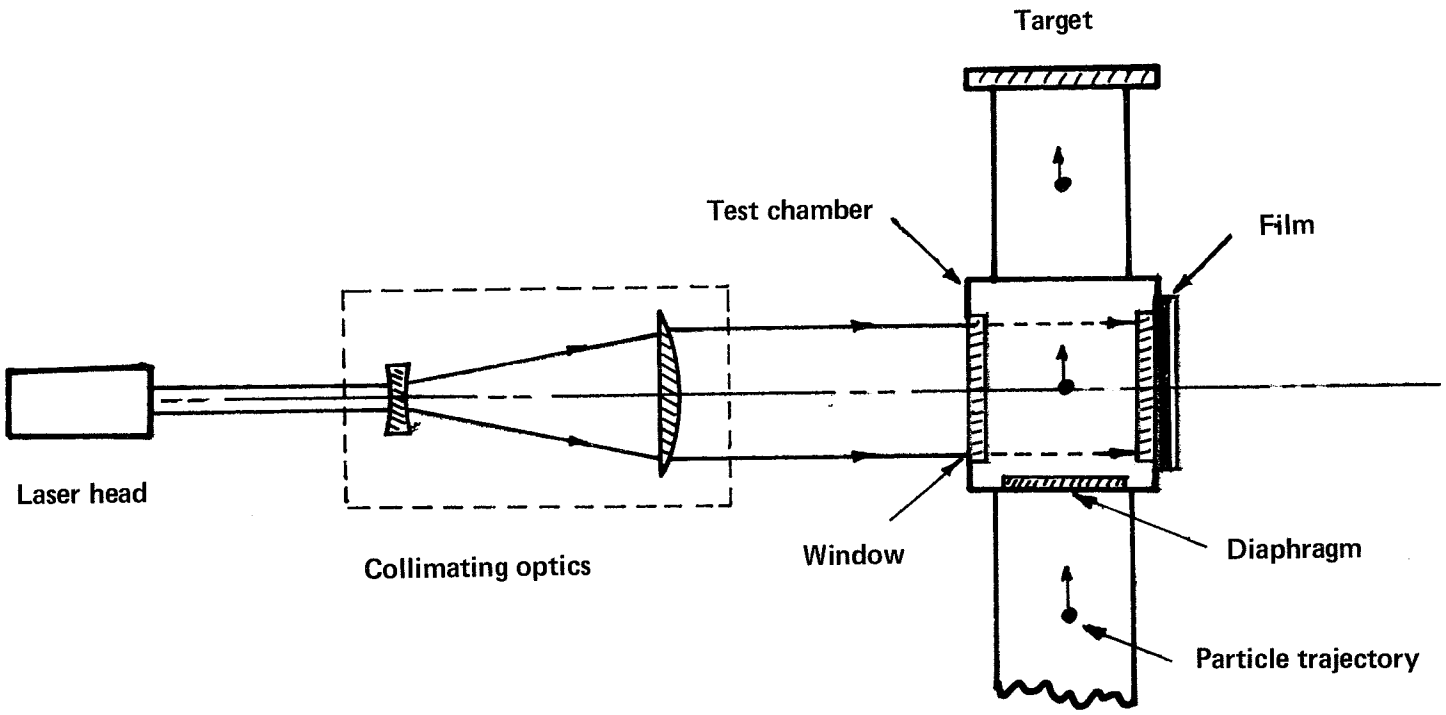

Figure 20.7 Collimated illumination optics. Input beam is expanded to a 3-in. field at the test chamber, and the laser pulse is Q switched to produce a 20-nsec pulse of approximately 50 MW

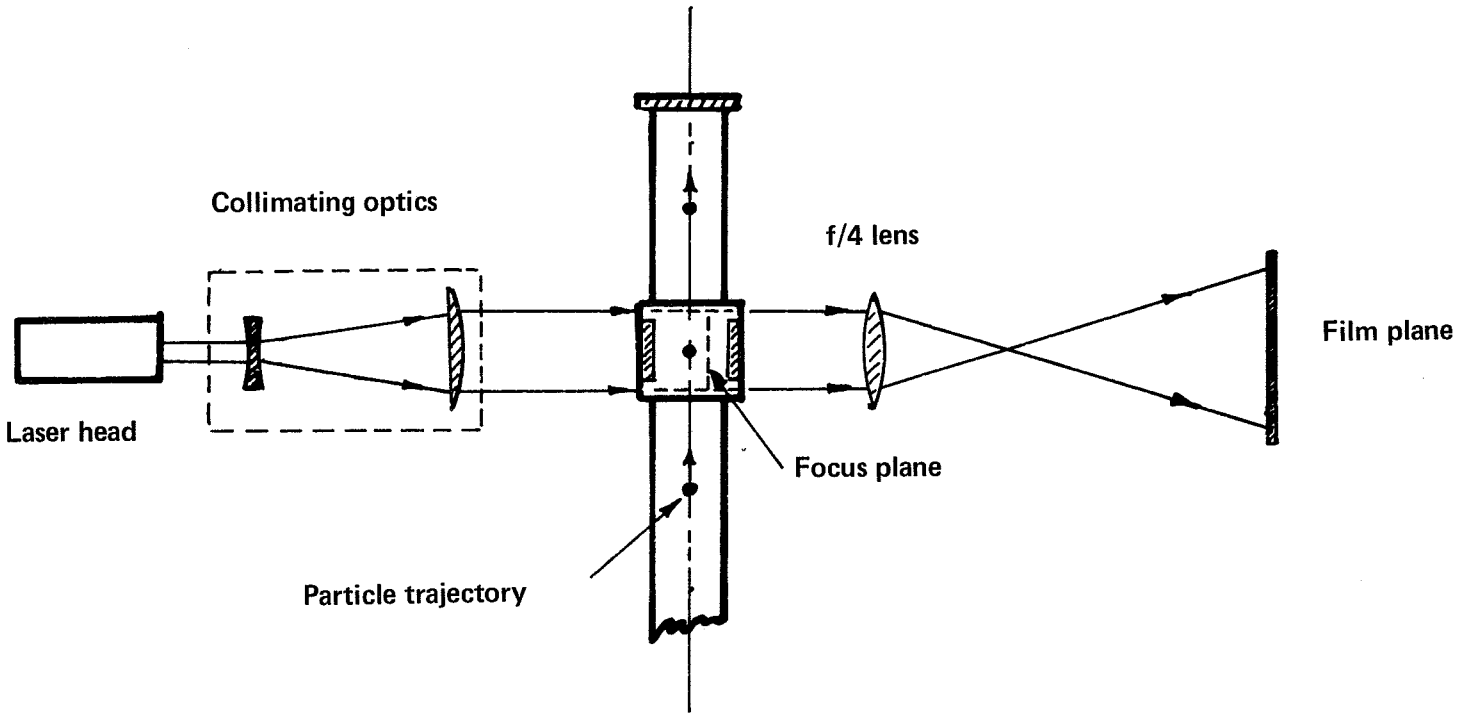

Figure 20.8 Magnifying optics. The addition of the lens magnifies diffraction pattern of the particles by 2X. Particles 2.0 cm toward lens side of chamber are in focus at the film plane; particles that are accelerated down the center of that tube therefore are defocused between 1 and 2 FFD

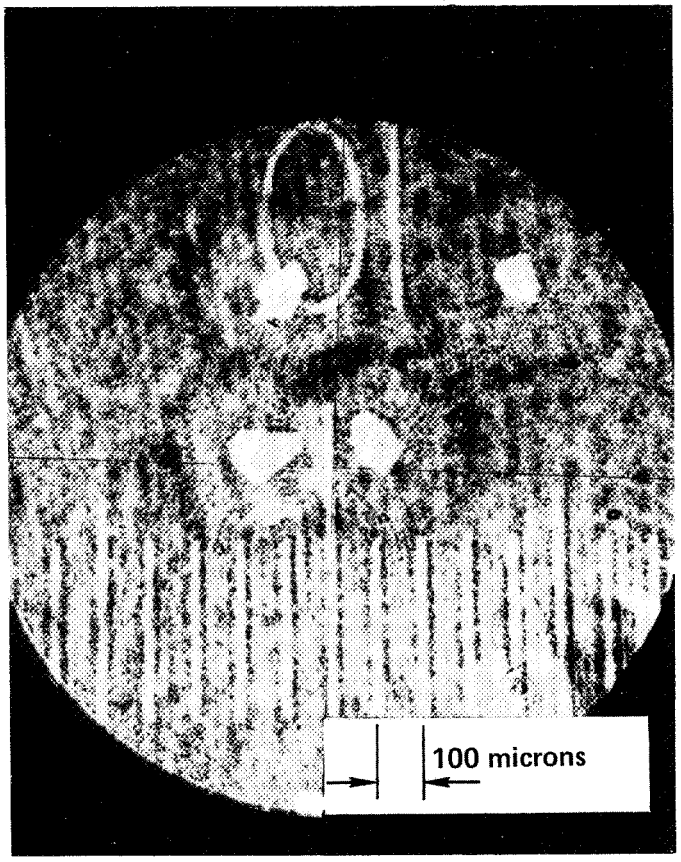

Figure 20.9 Reconstruction of a hologram of 100- to 200-μ particles placed in a reticle located in the test chamber. Magnification shown here is about 60X; the reticle spacing is 100 μ per division. The reconstruction was taken on Polaroid type 55P/N film using a helium-neon laser

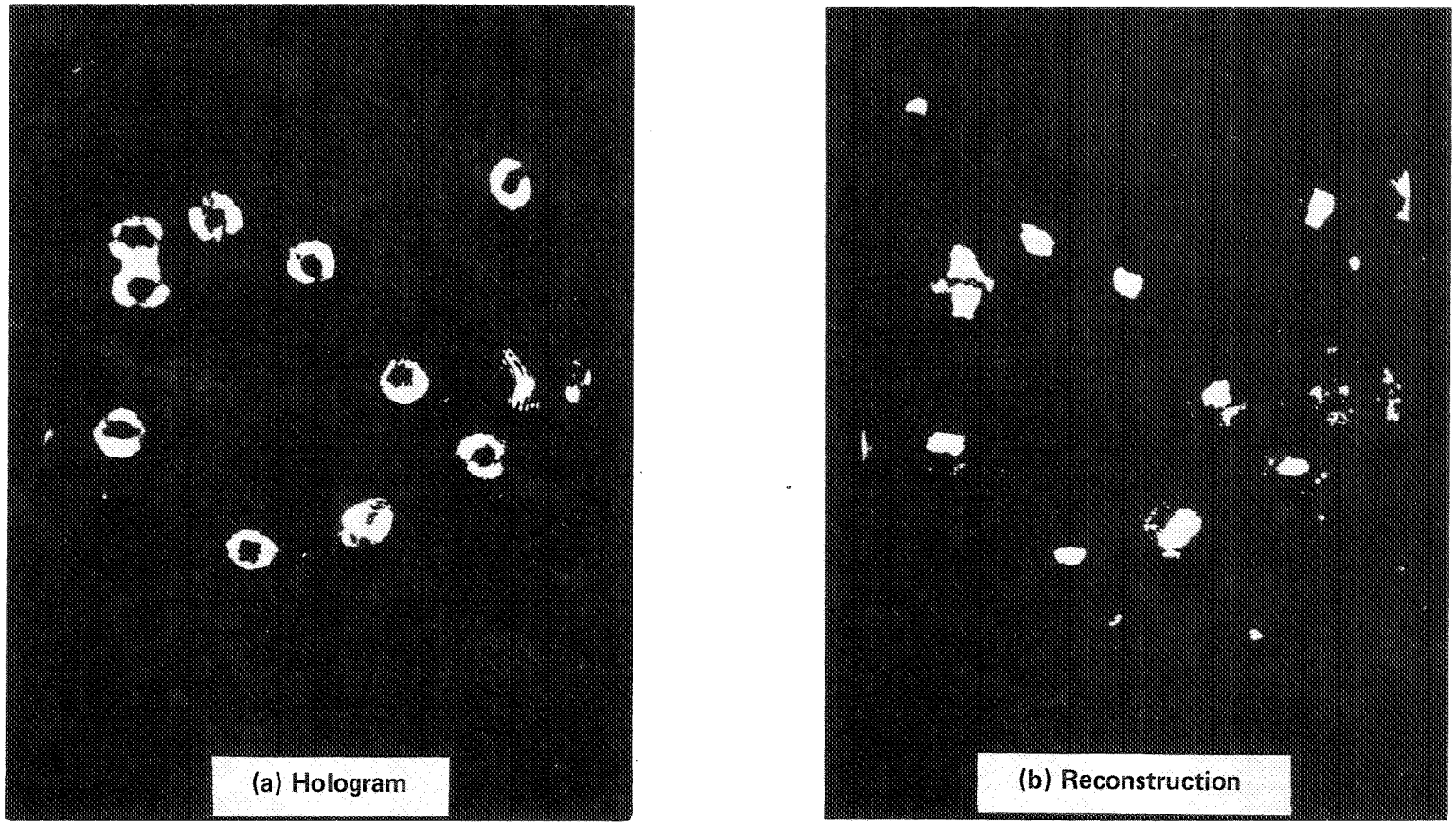

Figure 20.10 Hologram and TV reconstruction of a static distribution of 100- to 200-μ particles. These particles are reconstructed from same hologram as fig. 20.7; magnification is 35X

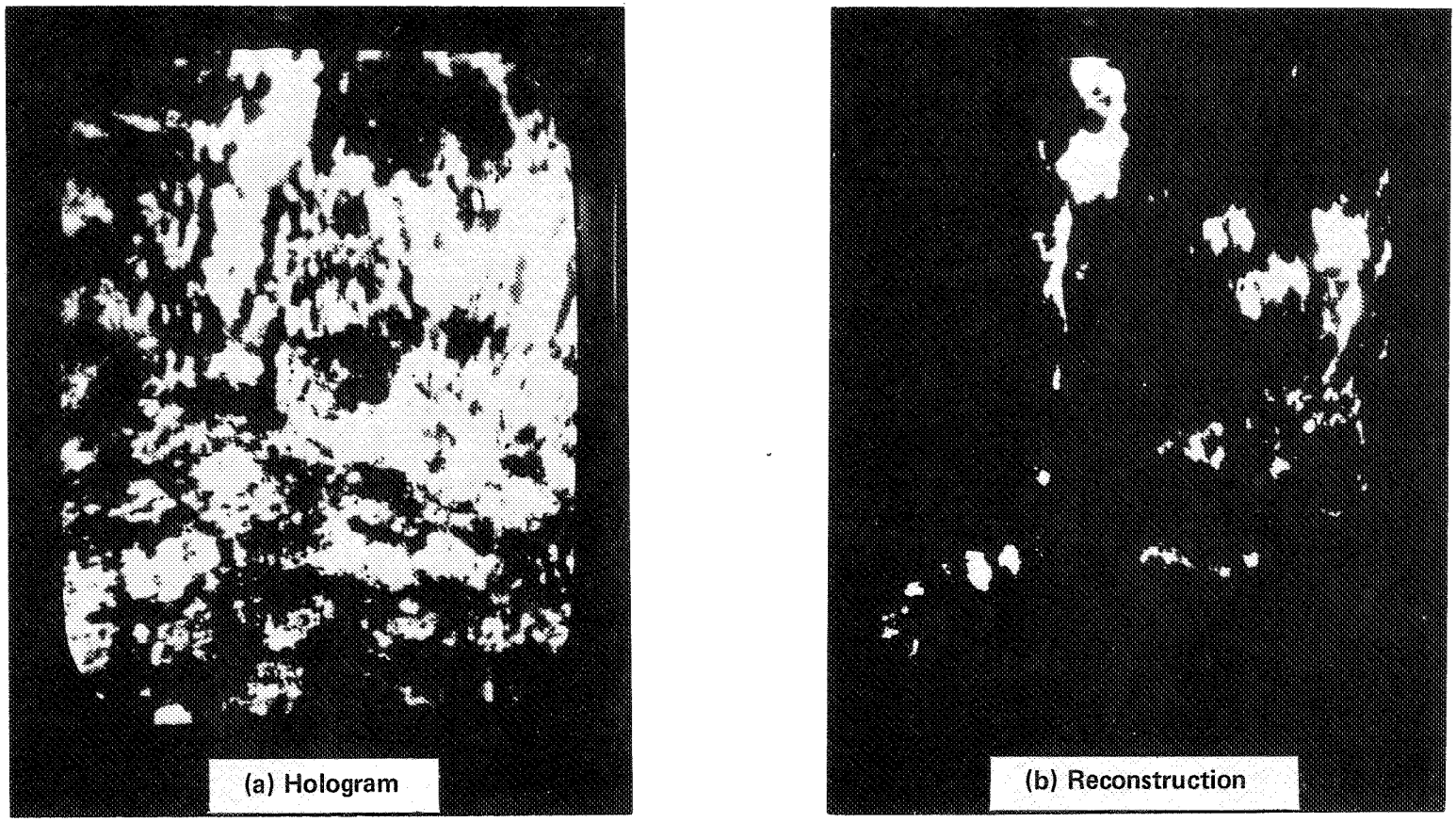

Figure 20.11 TV reconstruction of "object" moving through chamber at about 8000 fps. Fiberlike character of the reconstruction indicates the object may be grease or cotton strands; magnification is 35X

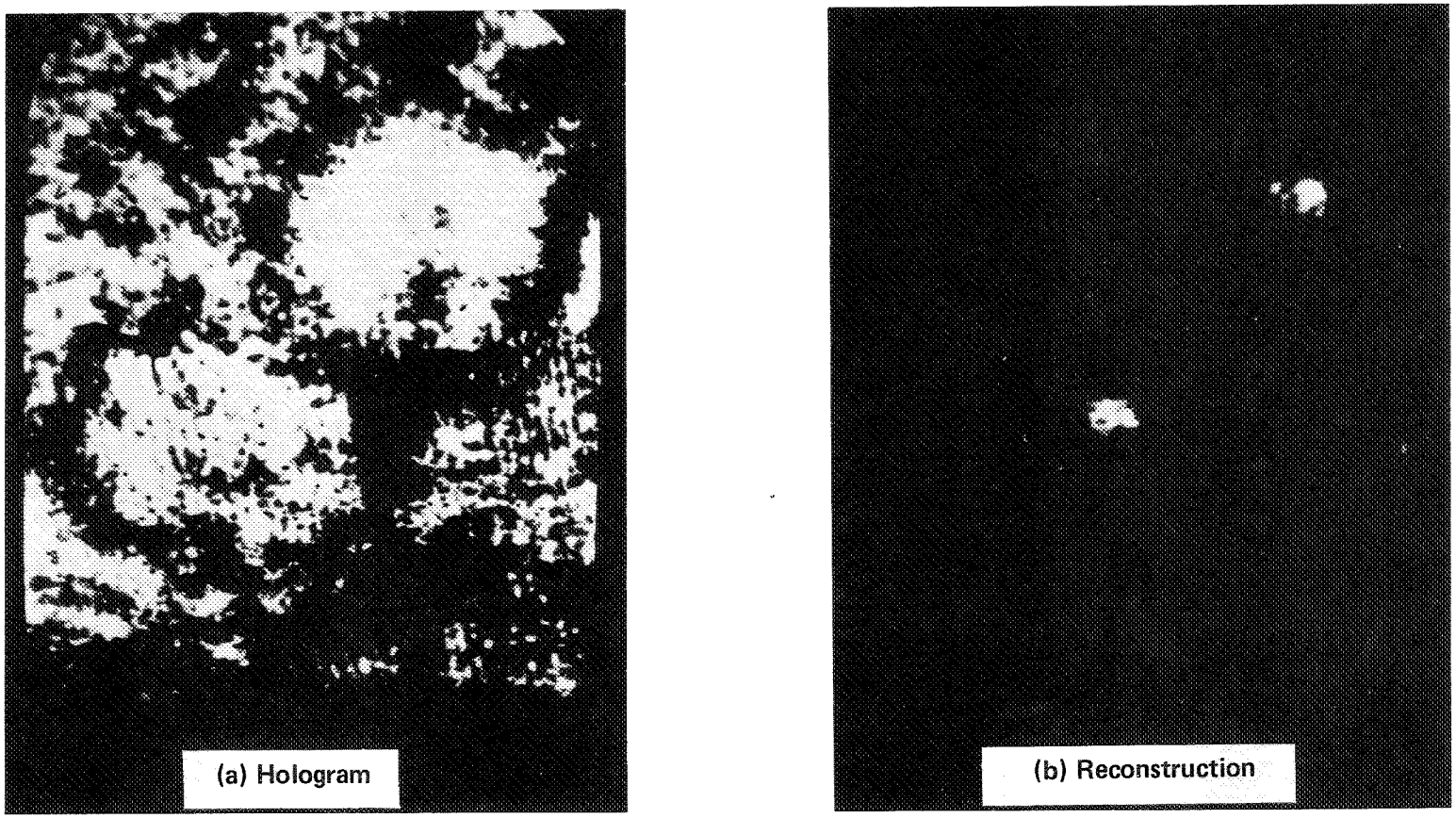

Figure 20.12 Holograms and reconstructions of the spray from a sabot penetrating a 1/32-in.-thick aluminum target; both hologram and reconstruction are photographed on the TV monitor

21 OPTICAL DATA PROCESSING

Arnold R. Shulman
Goddard Space Flight Center

Present and proposed satellites and space probes are sending back much more data than can be processed by electronic computers. For that reason, optical data processing appears to have important applications in the near future. A program has been under way for several years to examine the possibilities and limitations of this technique. A large amount of effort has been invested in a critical study of the whole photographic process and its relation to data processing. This has centered in two areas: photographic sensors and electro-optical devices. The physical properties of a gelatin emulsion have been carefully observed, including the effect of shrinkage associated with an image. Techniques for retarding the shrinkage, including tanning the emulsion and swelling the untanned gelatin with triethanolamine, have been perfected. The development process has been closely examined to determine the best techniques for extending the range, changing the contrast, and improving the sensitivity of standard emulsions. The annealing process, in which the emulsion is moistened and dried several times to relieve internal strains, has been found to reduce the scattered light that appears as "noise" in holography.

Another major area of concern is the development of electro-optical transducers to interface electronic devices with optical computers. A system employing a photochromic storage tube has been developed to serve as an input device for an optical computer. Systems using this tube are being developed for other NASA centers.

22 REVIEW OF HOLOGRAPHIC INSTRUMENTATION AT WALLOPS STATION

Frank E. Hoge
Range Engineering Division
Wallops Station

The interests and activities at Wallops Station in the realm of holography and applications have thus far centered on the allied field of coherent optical processing. For our earth resources and geodetic altimetry work, it is important that the "ground truth" be accurately known. To this end, we plan to apply the theory and techniques developed by Stilwell (ref. 1) for determining the surface wave energy spectra from photographs. One of Wallops station's aircraft has been fitted with the proper cameras and preliminary arrangements have been made to have the initial data reduced by the Naval Research Laboratory, Washington, D.C. These initial investigations, along with further planned studies, will help to more fully delineate the role of holography and optical processing at Wallops Station.

REFERENCE

1. Stilwell, Denzil; Journal of Geophysical Research, vol. 74, no. 8, April 15, 1969, pp. 1974–1986.

23 THE EFFECT OF OBJECT MOTION IN FRAUNHOFER HOLOGRAPHY WITH APPLICATION TO VELOCITY MEASUREMENTS

William P. Dotson
Flight Support Division
Manned Spacecraft Center

The in-line Fraunhofer hologram is analyzed under the assumption that the object moves a significant distance during the observation time. An equation is derived which predicts the effect object velocity has on the recorded fringe pattern. An analysis of the fringe pattern recorded on the film will consequently yield the object velocity. It is also possible to reconstruct the resultant hologram with the result that the path the object traveled during the exposure is reproduced; this knowledge, coupled with the exposure time, yields the desired measurement of velocity. This work has been published as NASA TN D-5515 under the above title.

NASA-Langley, 1970 —— 14 A-3643

"The aeronautical and space activities of the United States shall be conducted so as to contribute . . . to the expansion of human knowledge of phenomena in the atmosphere and space. The Administration shall provide for the widest practicable and appropriate dissemination of information concerning its activities and the results thereof."

—NATIONAL AERONAUTICS AND SPACE ACT OF 1958

NASA SCIENTIFIC AND TECHNICAL PUBLICATIONS

TECHNICAL REPORTS: Scientific and technical information considered important, complete, and a lasting contribution to existing knowledge.

TECHNICAL NOTES: Information less broad in scope but nevertheless of importance as a contribution to existing knowledge.

TECHNICAL MEMORANDUMS: Information receiving limited distribution because of preliminary data, security classification, or other reasons.

CONTRACTOR REPORTS: Scientific and technical information generated under a NASA contract or grant and considered an important contribution to existing knowledge.

TECHNICAL TRANSLATIONS: Information published in a foreign language considered to merit NASA distribution in English.

SPECIAL PUBLICATIONS: Information derived from or of value to NASA activities. Publications include conference proceedings, monographs, data compilations, handbooks, sourcebooks, and special bibliographies.

TECHNOLOGY UTILIZATION PUBLICATIONS: Information on technology used by NASA that may be of particular interest in commercial and other non-aerospace applications. Publications include Tech Briefs, Technology Utilization Reports and Technology Surveys.

Details on the availability of these publications may be obtained from:

SCIENTIFIC AND TECHNICAL INFORMATION DIVISION
NATIONAL AERONAUTICS AND SPACE ADMINISTRATION
Washington, D.C. 20546